

STUDIES OF ACTIVITY IN LATE TYPE STARS

A Thesis

*Submitted For The Degree Of
Doctor Of Philosophy In The Faculty Of Science
BANGALORE UNIVERSITY*

By

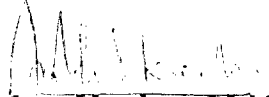
MATHEW VARGHESE MEKKADEN

**INDIAN INSTITUTE OF ASTROPHYSICS
BANGALORE 560 034
INDIA**

APRIL 1996

Declaration

I hereby declare that the matter contained in this thesis is the result of the investigations carried out by me at the Indian Institute of Astrophysics, Bangalore, under the supervision of Professor N. Kameswara Rao. This work has not been submitted for the award of any degree, diploma, associateship, fellowship, etc. of any university or Institute.

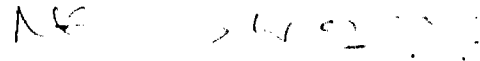


Mathew Varghese Mekkaden
(Candidate)

Bangalore 560034
1996 April 23

Certificate

This is to certify that the thesis entitled 'Studies of Activity in Late Type Stars' submitted to the Bangalore University by Mr. Mathew Varghese Mekkaden for the award of the degree of Doctor of Philosophy in the faculty of Science, is based on the results of the investigations carried out by him under my supervision and guidance, at the Indian Institute of Astrophysics. This thesis has not been submitted for the award of any degree, diploma, associateship, fellowship, etc. of any university or institute.


Professor N. Kameswara Rao
(Supervisor)

Bangalore 560034
23 April 1996

Acknowledgements

I am extremely grateful to Prof. N. Kameswara Rao for suggesting the topic, for his guidance and encouragement through out the work. I am also thankful to Prof. C. Raghavendra Rao, Dr. A. R. Hanumanthappa and Prof. Ram Sagar for the keen interest shown by them in the progress of the work.

My sincere thanks are due to late Prof. M. K. V. Bappu, who initiated me to the field of observational astronomy.

I am grateful to Director, Indian Institute of Astrophysics, for providing the necessary facilities.

I thank Prof. M. R. Deshpande, and Dr. U. C. Joshi for allowing me to use their polarimeter. The generous allotment of observing time at ESO, Chile, greatly helped me in this work and I express my sincere gratitude to the ESO management. I am also thankful to Dr. H. W. Duerbeck, Dr. C. Sinachopoulous, Dr. C. Sterken, and the ESO Long Term Photometry of Variables group for helping me in obtaining part of the observational data.

It gives me immense pleasure to thank my friends Raveendran, Mohin and Baba Varghese for their invaluable help at various stages in the preparation of the thesis. Mr. Gajendra Pandey helped in the data reductions and Mr. S. Muthukrishnan prepared some of the line drawings. I acknowledge their sincere help. Finally I am grateful to all my friends who have helped me during the course of this work.

Summary

Photometric and spectroscopic variability of late type stars are usually interpreted as evidence for magnetic activity. The present picture of stellar activity, evolved largely based on solar analogy, includes cool dark spots with enhanced photospheric magnetic fields, which is manifested in the light variation due to rotational modulation, and the associated chromospheric emissions. The domain of stellar activity encompasses the T Tauri stars, young late type stars, and the evolved binary systems like the RS CVn, W UMa, Algol and FK Com type objects. While the weak emission T Tauri stars, young late type stars and the RS CVn systems show evidences for the presence of cool spots, the active classical T Tauri stars indicate the presence of hot spots that are supposed to be produced by an entirely different mechanism.

The present investigation was started with the goal of studying the nature of activity in a selected sample of RS CVn systems, young active-chromosphere objects and T Tauri stars, and also to examine the observed differences in the levels of activity exhibited by them. For this purpose we have carried out extensive multi-band photometry of all the objects under investigation. We have also carried out near-simultaneous photometry, spectroscopy and polarimetry of T Tauri stars that are included in the present study.

The present study includes two RS CVn systems, two young active-chromosphere stars, two classical T Tauri stars and two weak emission T Tauri stars.

The thesis has been divided into eight chapters. The first chapter contains a general introduction to RS CVn systems, young active-chromosphere

stars and T Tauri stars listing out their main observational characteristics. The objectives of the present study are also given. The second chapter describes the method of observations and data reduction techniques.

Chapter 3 deals with the spot model developed by us to solve the observed light curves for the spot parameters. This model employs the method of least squares using differential correction to the parameters. An investigation of the synthetic light curves for various combination of spot parameters is also made. The computer program developed by us is fairly general; there is no restriction either on the nature of spots or on their location.

The analysis of *UBVRI* and *uvby* photometry of the RS CVn systems HD 81410 and HD 127535 is presented in chapter 4. The most significant finding from the analysis of the photometry of HD 81410 is that the star has two preferred longitudes about which the spots are generally formed. The modeling of the light curves indicates a large range in spot temperature (~ 1000 K). In the case of HD 127535 the photometric period is found to be almost the same as the orbital period. There is also an indication of an activity cycle of about 10 years for HD 127535.

Chapter 5 deals with the analysis of the photometry of the young active-chromosphere stars HD 139084 and HD 155555. It is noticed that the amplitudes of light variation in both these stars are comparatively smaller than that usually observed in RS CVn systems. The brightness at light maximum observed any two different epochs were not the same. We attribute this phenomenon to a large longitudinal spread of spot groups. The analysis of light curves of HD 155555 gives evidences for the presence of short-lived photospheric plages. It is found that the observed light variability is mainly due to the brighter and hotter component.

The observation and analysis of the weak emission T Tauri stars FK Ser and V410 Tau are the subject of chapter 6. We have detected periodic light variation in FK Ser and also the presence of hot plages co-existing with cool spots on its surface. The $H\alpha$ observations also give evidence for the presence of cool spots. In V410 Tau the large amplitude light variation and the corresponding $H\alpha$ emission strength variation have given conclusive evidence for the cool spot hypothesis. The linear polarization measurements

exhibit a periodic behaviour which is in anticorrelation with light variation and hence in agreement with the cool spot phenomenon.

The observations and analysis of the classical T Tauri stars TW Hya and V4046 Sgr are discussed in chapter 7. We have derived the photometric periods of these stars. The wavelength dependence of amplitude observed in the light curves of TW Hya shows that the modulation of the light is caused by hot spots. Apart from periodic light variations, TW Hya also show sudden brightening that last for one or two days. The light variation in V4046 Sgr has very low amplitudes which is interpreted as due to the low inclination and magnetically controlled flow from the accretion disc. The $H\alpha$ emission strength in TW Hya does not show any indication of periodicity, while in V4046 Sgr there is an indication for the same. Both TW Hya and V4046 Sgr show variable linear polarization.

In chapter 8 the results of the present study are summarized and the further investigations needed to answer some of the related problems are discussed. The tables and figures are numbered sequentially in each chapter and the corresponding chapter number is prefixed whenever a reference is made to them. The references, which are listed in the alphabetical order, are given at the end.

Contents

	<i>Acknowledgements</i>	i
	<i>Summary</i>	ii
1	INTRODUCTION	1
	1.1. RS Canum Venaticorum objects	2
	1.2. Young active-chromosphere objects	5
	1.3. T Tauri stars	7
	1.4. Present study	10
2	OBSERVATIONAL TECHNIQUES	13
	2.1. Photometry	13
	(a). <i>Observations</i>	13
	(b). <i>Data reduction</i>	15
	2.2. Polarimetry	19
	2.3. Spectroscopy	23
	2.4. Period determination	24
3	SPOT MODELING	27
	3.1. Introduction	27
	3.2. Mathematical formulation	28
	3.3. The direct problem	30
	3.4. The inverse problem	44

4	RS CANUM VENATICORUM OBJECTS	53
	4.1. HD 81410	53
	4.1.1. Introduction	53
	4.1.2. Orbital elements	54
	4.1.3. Photometry	56
	4.1.4. Light curves	66
	4.1.5. The brightness at light maximum and minimum	82
	4.1.6. Phase of light minimum	83
	4.1.7. Amplitude of light variation	85
	4.1.8. Results of spot modeling	85
	4.2. HD 127535	92
	4.2.1. Introduction	92
	4.2.2. Photometry	93
	4.2.3. Photometric period	93
	4.2.4. Light curves	97
	4.2.5. The brightness at light maximum and minimum	107
	4.2.6. Phase of light minimum	109
	4.2.7. Amplitude of light variation	111
5	YOUNG ACTIVE-CHROMOSPHERE OBJECTS	113
	5.1. HD 139084	113
	5.1.1. Introduction	113
	5.1.2. Photometry	114
	5.1.3. Photometric period	115
	5.1.4. Light curves	119
	5.1.5. The brightness at light maximum and minimum	123
	5.1.6. Phase of light minimum	125
	5.2. HD 155555	131
	5.2.1. Introduction	131
	5.2.2. Photometry	132
	5.2.3. Light curves	137
	5.2.4. $U - B$ variation	141

5.2.5.	Broad band colours of the components	142
5.2.6.	Amplitude and phase of light minimum	152
6	WEAK EMISSION T TAURI STARS	155
6.1.	FK Serpentis	155
6.1.1.	Introduction	155
6.1.2.	Photometry	157
6.1.3.	Light variation	161
6.1.4.	$H\alpha$ & $Li I$ lines	167
6.1.5.	Linear polarization	170
6.2.	V410 Tauri	175
6.2.1.	Introduction	175
6.2.2.	Photometry	176
6.2.3.	$H\alpha$ & $Li I$ lines	178
6.2.4.	Linear polarization	179
6.3.	Summary	186
7	CLASSICAL T TAURI STARS	187
7.1.	TW Hydrae	187
7.1.1.	Introduction	187
7.1.2.	Photometry	189
7.1.3.	Light variation	191
7.1.4.	$H\alpha$ & $Li I$ lines	201
7.1.5.	Linear polarization	203
7.2.	V4046 Sagittarii	212
7.2.1.	Introduction	212
7.2.2.	Photometry	213
7.2.3.	Light variation	214
7.2.4.	$H\alpha$ & $Li I$ lines	223
7.2.5.	Linear polarization	226
7.3.	Summary	230

8	CONCLUSIONS	231
8.1.	Results of the present work	231
8.1.1.	Photometric study	231
8.1.2.	Spot modeling	236
8.1.3.	Spectroscopic observations	237
8.1.4.	Polarimetric Study	239
8.2.	Future prospects	241
	References	244

1

INTRODUCTION

Stellar activity encompasses those phenomena that occur when locally strong magnetic fields modify the local momentum and energy balance in stellar atmospheres to produce observational effects. This astrophysical phenomenon has been observed as sunspots for the last few centuries. The simplest manifestation of the existence of solar magnetic fields is the sunspots. Since magnetic fields control the structure and energy balance of the outer solar atmospheres, an increase in the solar magnetic activity is manifested as an increase in the number of spots and active regions, plages and flares. Till recently only the sun's activity could be studied intensively. The advent of sensitive electronic detectors has helped to increase the range and quality of stellar data, especially of late type stars that show enhanced solar-type activity.

As mentioned above large concentrations of magnetic flux can modify the photospheric energy balance to produce relatively dark structures, spots, the main indicator of stellar activity. The degree of sun's activity is very small when compared to active stars of late spectral types. Even during the epochs of maximum activity sunspots cover less than 0.2% of the solar surface, whereas the analogous starspots in RS Canum Venaticorum systems, young active main sequence stars and T Tauri stars cover up to 10–30% of the stellar surface. Another observational aspect of stellar activity is the

enhancement of chromospheric $Ca II H \& K$, and $H\alpha$ emissions due to the large heating rates associated with the conversion of magnetic energy into heat by the dissipation of shocks or acceleration of electrons that become thermalized.

The late type active stars include pre-main sequence stars (T Tauri), young active main sequence stars of spectral types G and K, and the slightly evolved RS Canum Venaticorum systems. Moderate amplitude, regular or semi regular light variations due to the stellar rotational modulation of spots have been observed in these objects. Strong and variable emission lines of chromospheric origin are also observed indicating variations in stellar activity. The observed variations in the activity indicators result either due to intrinsic variations in the plasma or due to stellar rotation that brings in and out of view of the relatively long-lived features having large brightness contrast relative to the mean atmosphere.

1.1. RS Canum Venaticorum objects

RS CVn objects are binaries and their classification is based on the following observational criteria suggested by Hall (1976): (i) Orbital periods range from 1-14 days, (ii) strong $Ca II H \& K$ emissions, and (iii) the hotter component is of spectral type F or G and luminosity class V or IV. The cooler component, which usually causes the activity, is of spectral type late G or early K and luminosity class III-IV. It is now known that a number of these systems are single-lined spectroscopic binaries (eg., II Peg, DM UMa, HD 81410, HD 127535) where the nature of the secondary is not known. Stars with periods longer than 14 days have also been identified. We can distinguish an RS CVn system from the rest of the variable stars if it has the following observational characteristics (Fekel et al. 1986): (i) Binary with a late-type giant-subgiant component, (ii) variable light curves arising from the rotational modulation of one of the components, (usually the component with later spectral type), not attributable to pulsation, eclipses or ellipticity, and (iii) variable and enhanced chromospheric activity.

RS CVn stars have attracted much attention due to their peculiarities at wide wavelength regions. Apart from the presence of strong $Ca II H$

& *K* emissions in the optical region, they also show intense coronal X-ray emissions and very strong radio flares (Spangler et al. 1977; Linsky 1988).

X-Ray spectroscopy of the active RS CVn stars shows multi-temperature spectra indicating that the emission originates from two physically distinct regions, one of which is at a typical solar coronal temperature while the other is at a considerably higher temperature. The line emission is consistent with solar abundances of heavy elements. Observations of X-ray flares from V711 Tau, DM UMa and II Peg suggest extremely energetic events with peak soft X-ray luminosities ranging from 6×10^{30} to $10^{33} \text{ erg s}^{-1}$. Similar flare events have been detected as enhanced ultraviolet emission line fluxes in several systems (Weiler et al. 1978; Buzasi et al. 1987; Simon & Sonneborn 1987)

The IUE spectra of RS CVn Stars have provided important information. Due to the stars' rotation, the active regions modulate the fluxes in the emission lines arising from the high temperature transition regions. This modulation, which shows the connection between the photospheric active regions and the associated active regions in the upper atmosphere, became clear only with the IUE observations. Simultaneous optical photometry and coordinated IUE observations of several RS CVn objects revealed that the emission line flux shows correlation with photometric phase. The strengths of emission lines such as *C II* (λ 1335), *C IV* ($\lambda\lambda$ 1530, 1548) and *Si IV* ($\lambda\lambda$ 1394, 1403) originating in the transition region are 30%-50% higher than that at light maximum (Marstad et al. 1982; Rodono et al. 1987).

Many RS CVn stars exhibit strong and variable radio emission on time scales of minutes to several days. The flare luminosities observed in some of these stars exceed even 10^5 times that of a typical solar radio flare. The main radio properties of RS CVn systems are explained by Bookbinder (1988). Slee et al. (1987) have reported the detection of 25 systems out of 37 at 8.4 GHz in a survey of southern objects. The radio emission is often circularly polarized, and its apparent correlation with the observed luminosity and orbital inclination suggests the existence of large-scale magnetic field structure (Mutel et al. 1987). Using VLBI techniques the sizes of the radio emitting regions have been measured for several systems. These sources are often resolved at milliarc sec level and have brightness temperatures of the order of a few

10^{10} K. The structures revealed by these observations also indicate that there are two characteristic sizes: (i) an optically thin emission component, with moderate polarization, that has a size comparable to the binary separation and (ii) an unresolved, unpolarized core. The combination of high brightness temperature and moderate degree of circular polarization suggests that the radiation is probably due to gyro-synchrotron emission from MeV electrons in a magnetic field between 10 and 100 Gauss.

The *Ca II H & K* emission lines are the signatures of the stellar chromosphere. It is generally accepted that non-radiative heating is responsible to a large extent for the existence of the solar chromosphere. It is in this region that the emission lines of neutral and singly ionized atoms originate (Linsky 1980). The stars with different luminosities and masses that have temperatures comparable to that of the Sun display features indicative of stellar activity similar to solar activity, but on a very large scale. Because the stellar surfaces are unresolved we are unable to have spatially resolved observations as in the case of the Sun. So the existence of chromosphere and its activity in cool stars is usually derived from a study of *Ca II H & K* lines. The search for *Ca II H & K* emission variability in RS CVn stars by Weiler (1978) indicated a correlation between emission intensity and orbital phase in UX Ari, RS CVn and Z Her. Observations of λ And had shown that the relative flux at *Ca II H & K* is larger at light minimum by 25-100% than at light maximum. Bopp (1990) suggested that $H\alpha$ is also an important indicator of chromospheric activity in RS CVn systems. The observations by Bopp et al. (1990) had shown that $H\alpha$ line exhibits complex temporal behaviour. In a few RS CVn systems $H\alpha$ is always seen in emission.

Evolutionary studies have shown that RS CVn systems consist of evolved stars, both components having evolved from the main-sequence through processes not entirely different from normal single-star evolution. Studies based on stellar evolution calculations of binaries with periods in the range 1-30 days have shown that the evolutionary status of components of RS CVn binaries is consistent with the normal nuclear evolution (Morgan & Eggleton 1979).

The most important characteristic of late type active stars in the optical

region is the variable light curve arising from the rotational modulation of spotted areas on the stellar surface. The spot hypothesis was first introduced by Kron (1947, 1952) to explain the light variations of AR Lac and YY Gem. It did not receive much attention then due to the limited observational data available. Hall (1972) re-introduced the starspot model to explain the peculiar nature of the light variability noticed in the light curves of the prototype RS CVn. Co-ordinated multi-wavelength observations supported the model of a star with starspots and the associated active regions (Bopp 1983, 1990; Linsky, 1988; Ramsey 1990). Simultaneous IUE and optical photometry of II Peg showed a clear enhancement of chromospheric and transition region lines during light minimum (Rodono et al. 1987). Since the bulk of the radiation from late type stars emerges from the photosphere and appears in the optical and infra-red, the ability to detect star spots and flares against the bright background requires that the brightness contrast relative to the photosphere be large. Analysis of the photometric light variability of RS CVn systems by several investigators (Mekkaden et al. 1982; Rodono et al. 1986; Cutispoto 1993; Mohin & Raveendran 1993, 1994) have shown that starspots will have to cover an appreciable area of the stellar surface to explain the *V* band peak to peak amplitudes of 0.60 mag, and the spot temperatures are typically 1500 K less than the photospheric temperature. The maximum degree of spottedness yet proposed for any star is 54-64% of one hemisphere of II Peg in October 1989 (Neff et al. 1995). Changes occur in light curves even during time scales as short as a few orbital periods. Slow changes in the phase of light curves are attributed to the differential rotation of the active star in the binary. The light curves obtained during different seasons show changes in amplitude, phases of the light maxima and minima, mean light level and brightness at the light maximum and minimum. Availability of light curves over an extended period of time would help in modeling these variations, and hence it would be possible to investigate the physical characteristics and evolution of spot groups and eventually spot cycles.

1.2. Young active-chromosphere objects

Recently a new group of young late type stars have been identified that are

presumably passing through a short-lived evolutionary phase following core contraction during their approach to the main sequence. They are usually members of young clusters like Pleiades. Light variations up to several percent are observed in the case of lower main sequence stars in the Pleiades and Hyades (Robinson & Kraft 1974; Radick et al. 1982) and even up to 10% in the case of chromospherically active K type dwarfs in the Pleiades (van Leeuwen & Alphenaar 1982). Rotational modulation with variations up to 6% in b light has been reported in the case of dwarf stars of late spectral type in Hyades (Radick et al. 1983). Stauffer et al. (1987) have found that several of the late type dwarfs in the Pleiades cluster are light variables with periods of several hours to several days. Innis et al (1986) have shown that the rapidly rotating late type stars AB Dor and PZ Tel have space velocities identical with the Pleiades moving group and hence they are in their final stages of their approach to the main sequence, like the rapidly rotating Pleiades cluster dwarfs. Fekel et al. (1986) found that the active, Lithium strong single star HD 82558 is likely a very young disc population star. From the derived rotational velocities, space motions and Lithium abundances Anders et al. (1991) suggested that the stars HD 102077 and HD 139084 are members of the Pleiades Super cluster. Pasquini et al. (1991) have argued on the basis of several spectroscopic evidences, including the presence of strong Lithium, that the binary system HD 155555 is a pre-main sequence object rather than an evolved RS CVn binary. Recently Eggen (1995) discussed the membership probability of the stars in the Pleiades Super Cluster using astrometric and photometric data. He included HD 139084 and HD 155555 as members of this Super Cluster. The $Li\ I$ abundances in these two stars suggest that they are younger than Pleiades. Based on the proper motion measurements and $Li\ I$ abundance, Martin & Brandner (1995) argued that HD 155555 is in an evolutionary stage intermediate between T Tauri stars and Pleiades low mass stars.

The photometric observations of young active-chromosphere stars have shown the peculiar nature of the light variations (Cutispoto 1993; Anders 1991). Changes in the shape and amplitude of light curves take place faster than that usually observed in RS CVn stars. The light variability generally

have amplitudes smaller than that of RS CVn systems. While RS CVn systems are binaries, the active chromosphere stars can be either single (HD 139084) or binary stars (HD 155555).

1.3. T Tauri stars

T Tauri stars were identified as a separate class of objects because of their light variability (Joy 1945, 1949). It was largely due to the work of Herbig (1962) they were recognized as pre-main sequence stars. The late type T Tauri stars have masses about one solar mass and ages about a few million years and display a wide variety of phenomena. In the stellar evolutionary sequence they represent an important phase that lies between the low luminosity sources, which are deeply embedded in dust which can be studied only at IR (and some also in radio) wavelengths, and solar type stars.

T Tauri stars show uv and IR excesses and strong emissions in the optical, uv , and X-ray regions. Since the T Tauri stars rotate faster than the normal dwarfs, their X-ray emission is considerably higher. Several of the known T Tauri stars of the near-by Taurus-Auriga association have emissions at 1.3 mm (Chini 1989; Beckwith et al 1989).

T Tauri stars are broadly classified in to three groups according to their spectra and level of activity. They are: (i) Weak emission T Tauri stars (WTTS), (ii) Classical T Tauri stars (CTTS), and (iii) early type T Tauri stars. The WTTS include mostly weak emission pre-main sequence stars of spectral types later than K0 and $H\alpha$ emission equivalent width less than 10 \AA (Herbig & Bell 1988). Walter et al. (1988) from their X-ray study, defined a WTT star as an X-ray source with an optical counterpart showing pre-main sequence characteristics.

The CTTS that match Herbig's (1962) definition have the following spectroscopic characteristics: (a) Strong Hydrogen Balmer lines and $Ca II H$ & K emissions, (b) anomalous emission of $Fe I \lambda\lambda 4063, 4132$, (c) $Li I \lambda 6708$ absorption is very strong, and (d) forbidden emissions of $O I$ and $S II$ are usually strong. Recent papers classify CTTS as pre-main sequence stars with spectral types later than K0 and $H\alpha$ emission equivalent width greater than 10 \AA (Herbst et al. 1994).

A large amount of observational work has been devoted in the last two decades to study the physical cause of the light variations of T Tauri stars; but still there remains a great deal of uncertainty. These stars sometimes show drastic light variations on time scales of hours to months and also *uv* flaring (Rydgren & Vrba 1983). The variations on time-scales of 2 to 10 days are much more regular. These variations are apparently due to the rotational modulation of hot or cool surface features, and hence allow the rotation periods for these stars to be determined. Periodic light variation caused by the rotational modulation of a star with inhomogeneous distribution of cool spots on its surface are usually present in WTTS. The cool spots in the WTT star V410 Tau cover up to 40% of the surface which are comparable to that seen in RS CVn stars. In some T Tauri stars, like DN Tau, there is evidence for the presence of hot and cool spots (Vrba et al. 1986). The light variations in CTTS are attributed to the presence of hot spots or zones resulting from the impact zones of an accretion flow on the stellar surface from the active accretion disk. The presence of the boundary layer between the star and accretion disk produces veiling of the continuum and changes in the veiling also produce light variations. The accretion and the associated changes are responsible for the large light variations observed in CTTS (Herbst et al. 1994). The CTTS sometimes show large amplitude variations (> 0.80 mag in *V*). The main difference between the CTTS and the WTTS is believed to be the presence or absence of an accretion disk (Bertout 1989).

The chromospheric non-radiative losses as measured by $H\alpha$ appear qualitatively similar in WTTS and other late type active stars, but they can be up to 100 times larger in CTTS. The $H\alpha$ in WTTS can be accounted as entirely of chromospheric origin, and hence possibly arises from magneto-hydrodynamic wave dissipation. Accretion disks are currently the standard way to interpret the properties of CTTS (Basri & Bertout 1993; Valenti et al. 1993). In this model a circumstellar disk produces the near infra-red emission, and a narrow boundary layer between the disk and the central star emits optical and ultra violet radiation. Kenyon et al. (1994) invoked a magnetic accretion model to explain the spectral energy distribution of DR Tau; this model assumes that a dipole magnetic field truncates the disk

several stellar radii above the stellar photosphere. This field channels the accretion flow into the bright spot which they approximate as a narrow ring symmetric about the magnetic pole, and it is this luminous ring that causes the strong $H\alpha$ emission. The photometric and spectroscopic observations of CTTS by Vrba et al. (1993) have shown a strong correlation between the amplitudes of $H\alpha$ EW variation and light variability. They also found that the long-lived cool spots are responsible for most of the light variability found in WTTS while temporal hot spots are primarily responsible for that observed in CTTS.

The CTTS and WTTS usually have $Li\ I\ 6708\ \text{\AA}$ EW of the order of $0.50\ \text{\AA}$. Paterrer et al. (1993) have observed a few WTTS to examine the effects of magnetic activity on the $Li\ I$ EW and line profile. They detected $Li\ I$ variability in two WTTS and also noticed $Li\ I$ profile variations in V410 Tau.

The general properties of polarization in T Tauri stars were first surveyed by Bastien (1982, 1985). In the optical region the linear polarization P% is typically 0.3-2.0%. HL Tau has P% around 10%, which is the highest polarization observed in a T Tauri star. There exists no standard polarization curve, P% vs λ , for T Tauri stars. In about 30% of the stars in Bastien's (1985) study, P% decreases while for about 20% the polarization increases with increasing wavelength, and for the remaining objects the curve is almost flat. He has also found that the amount of P% of T Tauri stars is correlated with their IR excesses.

The work by Menard (1986), Dissen et al. (1989) have shown that 85% of the T Tauri stars that have several polarization measurements, are polarimetric variables. Menard & Bastien (1992) extended the polarization survey of T Tauri stars down to 15 mag.

Many CTTS are intrinsically polarized at optical and infra-red wavelengths (Shulte-Ladbeck 1982; Bastien 1985) and exhibit polarimetric variations up to 2% on time scales of a few days (Menard & Bastien 1992). From a survey of the polarimetric properties of T Tauri stars, Bastien (1988) has concluded that the polarization observed in young stars is due to scattering by dust grains of radiation from the stars and their extended emission

regions; the dust is usually outside the emission region. The observations have not indicated the presence of aligned non-spherical grains around these stars. Usually in T Tauri stars we observe two types of polarization variability; the polarization outbursts and small amplitude variations. The small amplitude variability may be due to the presence of inhomogeneities in the circumstellar environment of the star. The small amplitude variation may also be produced by the spots on the stellar surface. If the variation is due to the spots then a periodic behaviour is expected (Menard & Bastien 1992). Periodic polarization variability has been detected in RY Lup (Bastien et al. 1992) and RU Lup. The presence of accretion disk can also explain the variable polarization observed in CTTS. Recently Wood et al. (1996) has investigated the polarimetric variability of a magnetic accretion model for CTT stars. This model predicts periodic polarimetric variations. The irregular variations are explained on the basis of rapid changes in spot size and temperature and also the accretion rate.

The reviews by Appenzellar & Mundt (1989) and Bertout (1989) give detailed description of the general properties of T Tauri stars. The first catalogue of T Tauri stars by Herbig (1962) has 126 entries and the second by Herbig & Rao (1972) has 323. The catalogue by Herbig & Bell (1988) has 742 T Tauri stars listed.

1.4. Present study

RS CVn objects, young active-chromosphere stars and T Tauri stars have been studied as individual groups, both photometrically and spectroscopically, by many investigators. But a comprehensive study of these objects that show enhanced solar-type activity, which are at different stages of stellar evolution, has not been made so far. The principal goal of the present research is to study in detail the various aspects of stellar activity exhibited by these objects. As mentioned earlier in this chapter, the activity exhibited by the RS CVn objects, young active-chromosphere stars and WTT stars are mainly due to solar type dynamo-driven process while the activity observed in CTT star implies the presence of short-lived hot spots formed by the accretion flow from the active circumstellar disc to the star. The present

investigation is aimed at examining the nature and similarities in the activity in these objects which are at different evolutionary stages.

The stellar activity signatures that are observable in the optical region are the photospheric surface inhomogeneities and chromospheric emissions. For a proper understanding of these stars it is necessary to carry out photometric observations extended over a long interval of time.

The stars that are observed in the present investigation include two RS CVn systems (HD 81410 and HD 127535), two young active-chromosphere stars (HD 139084 and HD 155555), two classical T Tauri stars (TW Hya and V4046 Sgr), and two weak emission T Tauri stars (FK Ser and V410 Tau). The two CTT stars TW Hya, V4046 Sgr and the WTT star FK Ser stand apart from the other T Tauri stars due to their location in space; they are not associated with any star forming regions or dark clouds. Broadband *UBVRI* and intermediate-band *uvby* (Stromgren) photometry were carried out mostly at ESO, Chile, where the observing conditions are excellent.

We could include HD 81410 and HD 127535 in the ESO LTPV (Long Term Photometry of Variables) project, and hence we could collect a large amount of data over several seasons. Though HD 81410 is one of the most active RS CVn systems, very few observations are reported in the literature. Earlier observations of HD 127535 (Mekkadon & Geyer 1988) have shown that the object is also very active with sudden changes in the nature of light variation. The long-term photometry and the analysis of the light curves would definitely help to study the different aspects of activity. We have also done photometry of HD 139084, HD 155555, TW Hya, V4046 Sgr and FK Ser over several seasons to investigate the nature of light variability and possible periodicity. HD 139084 and HD 155555 are in an earlier stage of stellar evolution when compared to the RS CVn systems and the photometric study of these objects would show the differences in the level of activity between these groups. We have analyzed our photometric data along with those published to study the long-term nature of activity and also modeled the light curves numerically to derive the physical characteristics of spots.

The strong emissions observed in CTT stars have contributions from both the chromosphere and the active circumstellar accretion disk while in

WTT stars the emission lines originate from the chromosphere. We have carried out quasi-simultaneous photometry and low resolution spectroscopy of the programme T Tauri stars to examine the correlation of $H\alpha$ emission strength and $Li\ I$ absorption strength against light variation. The spectra were obtained using the 102 cm telescope and the quasi-simultaneous photometry using the 75 cm telescope of Kavalur Observatory.

Polarimetry of T Tauri stars would help us in investigating the circumstellar environment. We have carried out long-term as well as short-term broadband polarimetric observations of T Tauri stars near-simultaneously with photometric observations. The photometric, spectroscopic and polarimetric observations were done simultaneously whenever possible, so that a consistent picture of the nature of activity of these stars can be obtained. Searching for periodic variations in linear polarization in T Tauri stars which show periodic light variability would enable us to obtain information on the distribution of spots and on the characteristics of dust around them.

2

OBSERVATIONAL TECHNIQUES

2.1. Photometry

(a) *Observations*

$UBV(RI)_c$ observations of the programme stars were carried out at the European Southern Observatory (ESO), LaSilla, Chile, during April 1987 and May 1988 using the 50 cm ESO Cassegrain telescope. A single channel photometer equipped with a thermo-electrically cooled RCA 31034 GaAs photomultiplier tube and standard filters matching the $UBV(RI)_c$ system and operating in the photon counting mode was used for the observations. A 21 arc sec diaphragm was used through out the observations. The integration time was set to 1 sec and the integrations were continued until either the desired standard deviation in the total photon counts registered was achieved, or the maximum number of integrations already specified was reached. The maximum number of integrations were fixed typically at 60 and 20 for the star and sky measurements and the standard deviations were set, respectively, at 0.5% and 5.0%. Typically, a standard deviation less than 0.5% was achieved within thirty integrations for a star of $V = 12$ mag in all bands except U where due to the low available flux it required a larger number of integrations. About 15–20 photometric standards in the Cousin system,

available in the E - region (Vogt et al. 1981) were observed each night in order to determine the atmospheric extinction coefficients as well as the system transformation coefficients.

BV measurements of T Tau stars were made during March 1993 using the 75 cm telescope of Vainu Bappu Observatory (VBO), Kavalur, simultaneously with the spectroscopic and polarimetric observations of those objects. A single channel photometer equipped with a thermo-electrically cooled EMI 9658R tube and operating in the photon counting mode was used for this purpose. The integration time was set to 5 sec and the integrations were repeated for a sufficient number of times so as to reduce the error due to photon statistics.

Stromgren *uvby* photometry of the programme stars were obtained with the 50 cm ESO telescope during four seasons, June 1988, August 1989, January 1990 and July 1990. On some occasions observations were made only in *b* and *y* bands due to the intrinsic low photon flux of the programme stars in *u* and *v*. The observations during June 1988 were carried out using a thermo-electrically cooled EMI 6256 photomultiplier tube and during the other three seasons a dry ice cooled EMI 9658A tube was used. A 15 arc sec diaphragm was used through out for the observations. About 15 to 30 standard stars taken from the list of Perry et al. (1987) were observed each night of programme star observations.

In order to study the photometric behaviour of the programme stars in detail, observations spanning over several years are required. This is a rather difficult task to perform due to several factors, like, the heavy demand for telescope time and bad weather conditions. The Long Term Photometry of Variable stars project (LTPV) of ESO (Sterken, Manfroid, Mekkaden et al. 1993) was started solely to build up data base for objects which need high quality and uninterrupted data over several seasons. The above project exploits fully the best observing conditions prevailing at LaSilla. Only two of the stars (HD 81410 and HD 127535) could be included in the project for obtaining observations spread over several seasons because of the heavy demand for the telescope time. The LTPV programme uses the Stromgren *uvby* photometric system and the observations are carried out either with

the Stromgren Automatic Telescope (SAT, the Danish 50 cm telescope), or with the ESO 50 cm telescope, both at ESO, La Silla. The SAT, which is mostly used to carry out the LTPV programme, is equipped with a six channel instrument consisting of a *uvby* spectrograph–photometer and a two channel $H\beta$ photometer, all combined in one box. All the passbands are defined by interference filters placed in front of each of the six photomultiplier tubes and a six channel photon counting system is used to record the data simultaneously (Gray & Olsen 1991). However, for the LTPV programme only the *uvby* bands are used.

The LTPV observations were mostly carried out in blocks of one month duration. Multiple observations obtained for a star in a single night were averaged to give one single observation for that night. A sufficient number of standard stars taken from the catalogue of Olsen (1983) were also observed each night for the purpose of atmospheric extinction correction and transformation of instrumental quantities to standard quantities.

In all the above cases mentioned a typical sequence of observation in each filter consists of the observations of the comparison, variable and check star, in that order. The comparison and check stars chosen were always located close to the variable and were similar in spectral types so that the differential magnitudes were almost free from any uncertainty in the determination of the extinction and system transformation coefficients. The sky measurements were taken immediately after the observations of each star.

(b) *Data reduction*

The data reduction involves two steps, correction for the atmospheric extinction and the transformation of the instrumental magnitudes and colours thus obtained to the magnitude and colours in a standard system. Both these steps are performed using the observations of standard stars in the natural system and the magnitudes and colours available in the standard system.

If m is the magnitude observed through an airmass X , the extinction corrected magnitude m' , can be written as

$$m' = m + kX,$$

where k is the extinction coefficient. The extinction corrected colours can also be written in a similar way. The effect of second order terms in the extinction can be neglected because of the differential approach adopted in the photometric observations. The airmass is calculated from the known α and δ of the object and the time of observation.

The colour transformation coefficients are defined by the following equations (Hardie 1962):

$$\begin{aligned} V &= V' + \psi_1(B - V)', \\ B - V &= \psi_2(B - V)', \\ U - B &= \psi_3(B - V)' + \psi_4(U - B)', \\ V - R &= \psi_5(V - R)' \end{aligned}$$

and

$$V - I = \psi_6(V - I)',$$

where the primed indicates the extinction corrected instrumental magnitudes and colours and the unprimed the standard magnitudes and colours. The ψ 's are the system transformation coefficients.

The $UBV(RI)_c$ observations obtained at ESO were reduced using the VAX version of SNOBY, the photometric reduction program available at ESO, La Silla. The extinction and colour transformation coefficients were computed by an iterative procedure until a stable solution was reached. Table 1 gives the mean extinction, and the magnitude and colour transformation coefficients used for the reduction of the observations obtained during 1987 and 1988. The standard deviations (σ) estimated from the observations of the standard and comparison stars during these two observing runs are also listed in Table 1

The reduction of the BV observations obtained at VBO were made using photometric reduction programme developed by us. Mean extinction coefficients and system transformation coefficients derived for the entire season were used in the reduction of the data.

The Stromgren $uvby$ observations obtained at ESO were also transformed to the standard system using the ESO photometric reduction program SNOBY. The Stromgren system is basically a system of colour indices

(Manfroid & Sterken 1987). The instrumental y magnitudes are usually transformed to the Johnsons' V magnitudes since no standards were initially established for the Stromgren y magnitudes. For the transformation of the instrumental y to V magnitudes the standards were taken from the catalogue of Olson (1983).

Table 1. Broadband data: mean extinction and colour transformation coefficients, and standard deviations in the observations in magnitude.

Parameter	April 1987	May 1988
k_U	0.476 ± 0.011	0.500 ± 0.016
k_B	0.259 ± 0.008	0.247 ± 0.008
k_V	0.138 ± 0.011	0.147 ± 0.009
k_R	0.107 ± 0.008	0.106 ± 0.009
k_I	0.064 ± 0.012	0.042 ± 0.105
ψ_1	-0.057 ± 0.005	-0.074 ± 0.003
ψ_2	1.121 ± 0.003	1.165 ± 0.003
ψ_3	-0.164 ± 0.011	-0.157 ± 0.016
ψ_4	1.091 ± 0.010	1.065 ± 0.014
ψ_5	1.028 ± 0.007	1.027 ± 0.008
ψ_6	0.914 ± 0.005	0.908 ± 0.003
σ_V	0.010	0.020
σ_{B-V}	0.010	0.020
σ_{U-B}	0.015	0.030
σ_{V-R}	0.010	0.010
σ_{V-I}	0.010	0.010

A detailed description of the procedure followed for the reduction of the data collected under the LTPV programme is given in Manfroid et. al (1991) and Sterken & Manfroid (1992). The algorithm uses every measurement of

every constant and standard star. The equations for transformation of the quantities from the natural system to a standard system is written as

$$U_s = MU_o + K,$$

where U is the vector indices

$$U = \begin{pmatrix} b - y \\ y \\ m_1 \\ c_1 \end{pmatrix}$$

The suffixes s and o denote the standard and instrumental quantities respectively. K is the column vector of zero points in the respective quantities.

The colour transformation matrix M is written as

$$M = \begin{pmatrix} m_{11} & 0 & 0 & 0 \\ m_{21} & 1 & 0 & 0 \\ m_{31} & 0 & m_{33} & 0 \\ m_{41} & 0 & 0 & m_{44} \end{pmatrix}$$

The instrumental setup and the final m_{ij} values for each instrumental configuration are given in Table 2. The m_1 and c_1 indices are converted back to u and v using

$$c_1 = (u - v) - (v - b)$$

$$m_1 = (v - b) - (b - y).$$

Table 2. Intermediate band data: colour transformation coefficients.

PMT	m_{11}	m_{33}	m_{44}	m_{21}	m_{31}	m_{41}	Ref
EMI6256S	1.0706	1.0781	1.0534	0.0205	-0.1449	0.3028	1
EMI9789QA	„	„	„	„	„	„	„
EMI19789QB	1.0232	0.8935	1.0032	0.0122	0.0290	0.1632	2
EMI9789QB	1.0686	1.0747	0.9816	0.0431	-0.1412	-0.3040	1
EMI9658RA	„	„	„	„	„	„	„

References: (1) Danks 1982; (2) Florentin Nielsen 1983

2.2. Polarimetry

The state of polarization of a beam of light, particularly in scattering problems, can be described conveniently by the use of the four Stokes parameters defined as

$$I = \langle E_{0x}^2 \rangle + \langle E_{0y}^2 \rangle,$$

$$Q = \langle E_{0x}^2 \rangle - \langle E_{0y}^2 \rangle,$$

$$U = \langle 2E_{0x}E_{0y} \cos \delta \rangle$$

and

$$V = \langle 2E_{0x}E_{0y} \sin \delta \rangle,$$

where E_{0x} and E_{0y} are the amplitudes of the components of electric vector E_0 in two orthogonal planes XZ and YZ and δ is the phase difference between the x- and y-vibrations. If E_0 makes an angle θ (usually, called the position angle of polarization) with x-axis, then

$$E_{0x} = E_0 \cos \theta$$

and

$$E_{0y} = E_0 \sin \theta.$$

The Stokes parameters can be re-written as

$$I = \langle E_{0x}^2 \rangle + \langle E_{0y}^2 \rangle = \langle E_0^2 \rangle,$$

$$Q = I \langle \cos 2\theta \rangle,$$

$$U = I \langle \sin 2\theta \cos \delta \rangle$$

and

$$V = I \langle \sin 2\theta \sin \delta \rangle.$$

The most general form of polarization is partially elliptical polarization which can also be described in terms of the ellipsometric parameters, handedness, ellipticity, azimuth and intensity. The Stokes parameters are related to the ellipsometric parameters by

$$I = a^2 + b^2 = E_0^2,$$

$$Q = I \langle \cos 2\chi \cos 2\beta \rangle,$$

$$U = I \langle \sin 2\chi \cos 2\beta \rangle$$

and

$$V = I \langle \sin 2\beta \rangle .$$

where a and b are the semi-major and minor axes and $\tan\beta$ is the handedness, left or right. The ellipticity ϵ is given by

$$\epsilon = |\tan \beta| = \frac{a}{b}$$

and χ is the angle between the major axis of the ellipse traced by the end point of electric vector and the x-axis of the coordinate system, defined as the azimuth.

From the above equations it is obvious that for any beam of light, the parameters Q and U take particular values according to the chosen reference axes, whereas the other two remain independent. In other words, the quantities I , $(Q^2 + U^2)$, V and are invariant under a rotation of the reference axes. For a celestial object the equatorial coordinate system provides a convenient system of reference axes, with the x-axis in the direction of north, y- in the direction of east and z- in the direction of the line of sight. The direction of vibration of the electric vector (position angle θ) is measured eastward from the direction of north, and the degree of polarization is given by

$$p = \frac{(Q^2 + U^2 + V^2)^{\frac{1}{2}}}{I}.$$

The Stokes' parameters can be written in terms of the degree of linear polarization p , position angle θ , and the degree of circular polarization q as

$$I(\text{intensity}),$$

$$Q = Ip \cos 2\theta,$$

$$U = Ip \sin 2\theta$$

and

$$V = Iq,$$

with $p = (Q^2 + V^2)^{1/2}/I$ and $q = V/I$. For partially plane polarized light, $V = 0$.

Linear polarization measurements of the T Tauri stars were made using the PRL- polarimeter (Deshpande et al. 1985). In astronomical polarimetry the main sources of error are of atmospheric origin, the scintillation and seeing. A Wollaston prism is used as the analyzer and so the two beams with mutually perpendicular planes of polarization can be measured simultaneously. The scintillation noise pattern is same for all planes of polarization because air is not birefringent and hence by taking the ratio of the two beams it can be essentially eliminated. This procedure also helps to reduce the errors caused by any variation in atmospheric transparency (Hiltner 1962). The simultaneous measurement of the two beams ensures that the incident radiation is fully utilized, thereby reducing the observation time required to build up the desired signal to noise ratio.

The imperfections in the telescope guiding and the nonuniform sensitivity across the surface of photocathodes tend to reduce the polarimetric accuracy. The errors caused by these two sources can be minimized by the use of Fabry lenses in front of detectors (Cox & Sinnott 1977). Young (Serkowski 1974) has shown that the errors of atmospheric origin can be reduced by a sinusoidal modulation of the light with a frequency that is larger than a critical value which depends on the telescope aperture. This principle is applied in the PRL polarimeter and the rapid modulation of the signal is achieved by the rotation of a super achromatic half-wave plate. The main disadvantage of using such a plate, made by cementing three achromatic plates of quartz and magnesium fluoride (Pancharatnam 1955), is the wavelength dependence of position angle of its effective optical axis and hence an accurate determination of position angle becomes difficult since when wide spectral bands are used corrections that depend on the spectral energy distribution of the observed object must be applied to the measured position angle. This problem can be avoided by introducing another stationary identical Pancharatnam plate between the rotating plate and analyzer (Frecker & Serkowski 1976). The intensity (I') of the transmitted light by two half-wave plates followed by the analyzer depends only on the Stokes parameters I , Q and U of the

incident light and the angle (Ψ) between the effective optical axes of the two half wave plates, and is given by (Serkowski 1974)

$$I' = \frac{1}{2}(I \pm Q \cos 4\Psi \pm \sin 4\Psi).$$

The upper signs represent the case with the principal plane of analyzer at position angle θ° and the lower signs with that at 90° . The rotation frequency of the first half wave plate is 10.41 Hz and because of the 4Ψ factor the actual modulation frequency is four times this value. The Glan-Taylor prism, which can be inserted in the beam of light, is for the purpose of checking the instrument for 100% polarization. The acquisition and on-line processing of the data are done using a PC.

The T Tauri stars were observed during 1990, 1991, 1992 and 1993 seasons with the 236 cm Vainu Bappu Telescope of VBO. During 1990, 1991 and 1992 seasons only a few sets of observations could be collected because of the limited telescope time available. Nevertheless, these observations serve the purpose of detecting the presence of any variation in the linear polarization exhibited by these stars. During March 1993 the T Tauri objects could be observed continuously on 9 nights, making it possible to carry out a detailed study of the variability of polarization with respect to the rotation period of these stars. The observations were done mostly in *V* band and occasionally in *B* and *R* bands.

The observing procedure with the PRL polarimeter is as follows. After selecting the desired filter, the sky background adjacent to the programme star is first measured by integrating for a pre-specified time interval (typically, 60 sec), depending on the sky conditions and the brightness of the object in the wavelength band considered. The measurements are then repeated on the required object after centering it in the diaphragm. The data reduction program is automatically activated at the end of integration and the computer calculates and prints out the time of observation, percentage of linear polarization (P%), its probable error (ϵ_p), position angle of polarization (θ°) and the magnitude (m). The sky background is subtracted before a least square solution for the Stokes parameters is made. The parameter *I* is essentially the brightness of the source, and hence it is converted into magnitude which is printed. The above procedure is repeated several times

(typically 15 to 20 times) to bring down the errors due to the photon statistics to a desired level. The probable error in the computed position angle is estimated using (Treanor 1962)

$$\epsilon_{\theta} = 28.5^{\circ} \epsilon_p P^{-1}.$$

Several zero polarization standard stars from the list of Serkowski (1975) were observed each night to determine the instrumental polarization which was found to be significant. Since the Stokes vectors linearly add at low polarization levels, we have

$$Q_{observed} = Q_{star} + Q_{instrumental}$$

and

$$U_{observed} = U_{star} + U_{instrumental}.$$

The intrinsic linear polarization and position angle of the object are given by

$$p_{star} = (Q_{star}^2 + U_{star}^2)^{1/2}$$

and

$$\theta = \frac{1}{2} \tan^{-1} \frac{Q_{star}}{U_{star}}.$$

The Stokes parameters Q and U are calculated from the observed values of p and θ . The observations of zero polarization standards directly give the instrumental Q and U. Several polarization standards, were also observed to correct the the zero point error in the observed position angle. These objects were also chosen from the list of Serkowski (1975).

2.3. Spectroscopy

Spectroscopic observations of the T Tauri stars were made with the Universal Astronomical Grating Spectrograph (UAGS) attached to the 102 cm telescope of the VBO. A grating of 651 *lines mm*⁻¹ blazed at 5000 Å was used in the first order, and a 384×576 Thomson–CSF TH 7882 CCD chip mounted in a liquid nitrogen cooled dewar as the detector. The data acquisition was done through the CCD System supplied by Photometrics Ltd.,

USA. The UAGS setup with a 250 mm Schmidt camera gives a resolution around 1.38 \AA per pixel in the red region. The wavelength calibrations were done using a Fe-Ne hollow cathode. The $H\alpha$ and the $Li I 6708 \text{ \AA}$ lines were obtained in a single exposure. The spectroscopic data were analyzed with a Sun Work Station using the Image Reduction and Analysis Facility (IRAF). The extraction of the spectrum from the two dimensional raw image involves the correction for the electronic bias, dark current, sky background subtraction, and flat fielding. Several bias and dark frames were obtained each night and the mean bias and dark values of each night were subtracted out from the raw image data. Though CCD has a good linearity, there still exists pixel to pixel variations in sensitivity. To correct for this variations a few flat field images were taken each night using a specially made white screen fixed in the dome and illuminated by a tungsten lamp. The dark and bias-corrected images were divided with the flat field images. The extracted stellar spectrum was then wavelength calibrated. The standard deviation of the polynomial fit to the wavelength position in the comparison spectra was found to be around 0.02 \AA . The spectra were normalized to the continuum and the equivalent width of $H\alpha$ and $Li I$ lines were measured. The resolution employed in the present observations is not adequate for a detailed profile analysis, and hence only the equivalent width of the lines were measured.

2.4. Period determination

In the literature, for some of the programme stars photometric periods are not available. To derive the same, a computer program, developed by us, based on an algorithm similar to the one described by Bopp et al. (1970), has been used. The period finding algorithm is based on the principle that the observations when folded with the correct period show a minimum scatter in the magnitude-phase diagram.

For each trial period the photometric phases are computed from the time of observations using an arbitrary initial epoch, and all the observations are ordered in phase. Then the quantity Q , taken as the measure of scatter in

the magnitude-phase diagram, is calculated from

$$Q = \sum_{i=1}^{N-1} |m_i - m_{i+1}| + |m_N - m_1|$$

where m_i is the i^{th} magnitude after the ordering in phase. If there are no observational errors and the light curve shows a single maximum the value of Q will be exactly twice the total range in the observed magnitudes. Because of the observational errors in a real case, however, the value of Q will be several times the total range, especially when the amplitude of light variation is small.

If T_1 and T_N are the times corresponding to the first and last observations, and P is the trial period the number of cycles covered during the interval $T_N - T_1$ is given by

$$\phi = \frac{T_N - T_1}{P}$$

A change dP in P will cause a change $d\phi$ in ϕ given by

$$d\phi = \frac{T_N - T_1}{P^2} dP.$$

Apart from the minimum and maximum periods to be tried, the input to the program includes a value for $d\phi$ also. The incremental period is calculated from

$$dP = \frac{P^2}{T_N - T_1} d\phi.$$

A typical value for $d\phi$ is 0.02. If the observations span over a large time interval and a large range in period has to be tried a higher value of $d\phi$ can be used initially to derive a preliminary period, and then the program is re-run around this period with a smaller value for $d\phi$.

The final print out includes printer plots of (i) the light curve folded with the period which gives the minimum value for Q and (ii) the values of Q against the trial period. All the trial periods and the corresponding Q are not stored in the computer memory, only a limited number, usually 300 pairs, is stored. Once the number of trial periods exceeds this limit, each time the highest value of Q stored and the corresponding period P are replaced by

the current values if the current value of Q is smaller, otherwise the stored quantities are left as they are.

The program displays the total number of periods to be tried and the number of periods already tried which is continuously updated. If sufficient observations are available, there will be no difficulty in identifying the real period because there will be only a single deep minimum. A typical plot of Q , the measure of scatter in the magnitude-phase diagram, against the trial period, which was obtained in the present analysis, is shown in Figure 18 of § 4.2.3.

3

SPOT MODELING

3.1. Introduction

The large amount of observational data on RS CVn stars, young active chromosphere stars, and T Tauri stars at wide wavelength ranges from X-ray to radio collected over the last two decades provide evidences for the existence of starspots analogous to sunspots on the surface of the stars. The starspot hypothesis was first introduced by Kron to explain the distortions in the light curves of AR Lac and YY Gem (Kron 1947; Kron 1952). Bopp & Evans (1973) and Torres & Ferraz Mello (1973) were the first to introduce quantitative formulations of spot models with a single spot. Since then several investigators have developed models to reproduce the light curves of rotating variables, especially those belonging to RS CVn and BY Dra groups of objects, assuming that cool starspots to be responsible for the observed light variation (Eaton & Hall 1979; Kimble et al. 1981; Dorren & Guinan 1982; Vogt 1983; Rodono et al. 1986; Bouvier & Bertout 1989; Zeilik et al. 1990; Mohin & Raveendran 1992; Eker 1994)

There are two basically different approaches that have been followed to reproduce the light curves using the spot model: (i) a continuous distribution of small spots in an equatorial belt (Eaton & Hall 1979; Kimble et al. 1981), and (ii) one or two large spots, usually at higher stellar latitudes (Dorren &

Guinan 1982; Poe & Eaton 1985; Zeilik et al. 1990). The high latitude spots which have no solar analogue suggests that the magnetic activity on active chromosphere stars can be qualitatively different from that seen on the sun (Vogt 1988).

The main problem usually encountered in light curve modeling is the non-uniqueness of the spot parameters derived. The solutions of Doppler imaging technique (Vogt & Penrod 1983; Vogt, Penrod & Hatzes 1987) using high resolution spectra of rapidly rotating stars claim to resolve some of the ambiguities in the derived starspot parameters. This technique applies the principle of reconstruction of the surface brightness distribution of a rapidly rotating star by analyzing the distortions in the line profile. Most of the Doppler images of the rapidly rotating stars suggest the presence of long-lived polar spots. The main drawback of this technique is that it can be applied only to rapidly rotating stars (periods around two days) and it needs very high resolution and very high S/N spectra, and hence limits the number of objects that can be studied. Though some authors (Strassmeier 1988; Hatzes 1993) claim uniqueness in the solution using this technique along with photometric light curve models, Budding & Zeilik (1990) caution that the Doppler imaging technique is also expected to share similar ambiguities which exist in the light curve modeling using starspots.

In view of the inherent uncertainty in the derived spot parameters, modeling a single light curve of a rotating variable may not be of much significance. However, modeling a series of light curves of the same star obtained during several successive seasons would be of immense help in investigating the spot characteristics and spot evolution. With this in mind spot models have been developed both (i) for the direct problem of light curve synthesis from given spot parameters, and (ii) for the inverse problem of obtaining spot parameters from a given light curve.

3.2. Mathematical formulation

The following assumptions were made in the spot modeling: (i) The spotted star is spherical, (ii) both the undisturbed and spotted regions radiate like blackbodies and (iii) limb-darkenings in the two regions follow quadratic

laws. The monochromatic luminosity of the undisturbed star is then given by (Friedemann & Gurtler 1975),

$$L_\lambda = B_\lambda(T_p) \int \{1 - A_p(1 - \cos \theta) - B_p(1 - \cos \theta)^2\} \cos \theta dA,$$

where T_p is the effective unspotted photospheric temperature, $B_\lambda(T_p)$ the Planck function, A_p and B_p are the quadratic limb-darkening coefficients, dA is an element of surface area, and θ is the angle between the line of sight and the radius along dA ; the integration is carried over the visible hemisphere. The change in luminosity due to the presence of a spot of effective temperature T_s is given by

$$\begin{aligned} \Delta L_\lambda = & B_\lambda(T_p) \int \{1 - A_p(1 - \cos \theta) - B_p(1 - \cos \theta)^2\} \cos \theta dA \\ & - B_\lambda(T_s) \int \{1 - A_s(1 - \cos \theta) - B_s(1 - \cos \theta)^2\} \cos \theta dA, \end{aligned}$$

where A_s and B_s are the limb-darkening coefficients of the spotted region, and T_s is the effective temperature of the starspot; the integrations are over the visible spot area. If several discrete spots are present, the total change in luminosity is obtained using

$$\Delta L_\lambda^T = \sum_{spots} \Delta L_\lambda.$$

The magnitude of the star at photometric phase ϕ is given by

$$m_\lambda(\phi) = -2.5 \log \frac{L_\lambda - \Delta L_\lambda^T(\phi)}{L_\lambda} + M_\lambda, \quad (1)$$

where M_λ is the unspotted magnitude of the star. In the case of light contribution by a nearby companion, L_λ in equation (1) should be replaced by $L_\lambda(1 + R_\lambda)$, R_λ being the luminosity ratio of the components at λ .

The above considerations are general to the extent that no assumptions are made either on the shape or nature, whether cool or hot, of spots.

The above equations show that the modeling of light curves involves integration of the intensity, which has a different value due to spots and limb darkening, over the visible hemisphere for the different rotational phases. Some authors prefer numerical integration (Bopp & Evans 1973; Strassmeier

1988; Strassmeier & Bopp 1992; Mohin & Raveendran 1993) while others use analytical integration (Budding 1977; Dorren 1987; Eker 1994). Accuracy of the numerical method depends on the number of grid points involved in the integration and with sufficient number of grid points this method gives better results compared to the analytical integration technique. The main advantage of the numerical integration technique is the possibility of including spots of any shape in the light curve modeling, whereas the analytical approach requires circular spots.

3.3. The direct problem

(a) *Computer program*

The synthesis of light curve from a set of given spot parameters is a direct problem, and hence can be easily accomplished. It provides a lot of clues on how and to what degree the various parameters, like, latitude, area and temperature, which describe a starspot, affect the general characteristics of a light curve, and these clues in turn will be helpful in interpreting the observed light curve in terms of the spot parameters, at least qualitatively. Based on the above mathematical formulation, a computer program in Fortran was developed to compute the light curves of rotating variables wherein the modulation in the observed flux results from their surface brightness inhomogeneities.

The computer program is fairly general. The integration of the intensity of radiation at the effective wavelength across the visible hemisphere is done numerically; the effective wavelengths of *UBVRI* bands are taken as 0.36μ , 0.44μ , 0.55μ , 0.64μ and 0.79μ . The starspots can be either circular or bounded by latitudes and longitudes. If circular in shape, an overlapping of the spots is also allowed so that an elongated spot can be specified as segments of several circular spots. Since the temperature of each segment can be specified independently the light curve resulting from a two component spot, with a circular umbra and penumbra, can also be computed. The limb-darkening coefficients can be different for the photospheric and spotted regions. There is no limit on the number of spots that can be included in the computation of the light curve.

The execution of the program is done interactively. Each time a light curve is generated from a set of given spot parameters the monitor displays a plot of the computed curve along with the observations, if available. When the observational errors are appreciable, to have a better visual judgement, the data can be displayed after smoothing. The standard deviation of the fit is also calculated and displayed so as to have a quantitative assessment of the fit to the observations. The results can be stored if the fit is acceptable, or the computation of another light curve from a new set of spot parameters can be initiated.

(b) *Numerical results*

Figure 1 shows the synthetic light curve in V due to a circular spot of radius 30° present at different polar distances (θ_P), with the pole above the sky plane taken as the reference. The rotational axis of the variable was assumed to make an angle $i = 90^\circ$ with the line of sight. The various parameters which were assumed for the computation of the light curve are indicated in the figure. Limb-darkening coefficients were assumed to be linear and the same for both the spotted and unspotted regions. About 5000 surface area elements were taken for the numerical integration of the intensity. Figures 2 and 3 are similar to Figure 1, but for the cases $i = 60^\circ$ and $i = 40^\circ$. From the figures it is clear that the faintest magnitude (~ 0.3) for the hemisphere visible at light minimum is same for all inclinations and it occurs when the spot centre coincides with the central latitude, *i.e.*, when the polar distance is the same as the inclination of the rotational axis.

The light curve shows a flat light maximum for all values of polar distances when $i = 90^\circ$ because the spots disappear completely from the field of view for a substantial fraction of the rotational period. Even when the edge of the spot coincides with the circumpolar boundary (Figure 2, for the case $i = 60^\circ$, $\theta_P = 60^\circ$), the light curve appears flat-topped. Only when a substantial fraction (\sim half) extends over the circumpolar region the circular spot gives rise to a continuously varying light curve. This indicates that a continuously varying light curve would result only if the radius of the spot extends over the entire range of longitude on the hemisphere visible at light minimum.

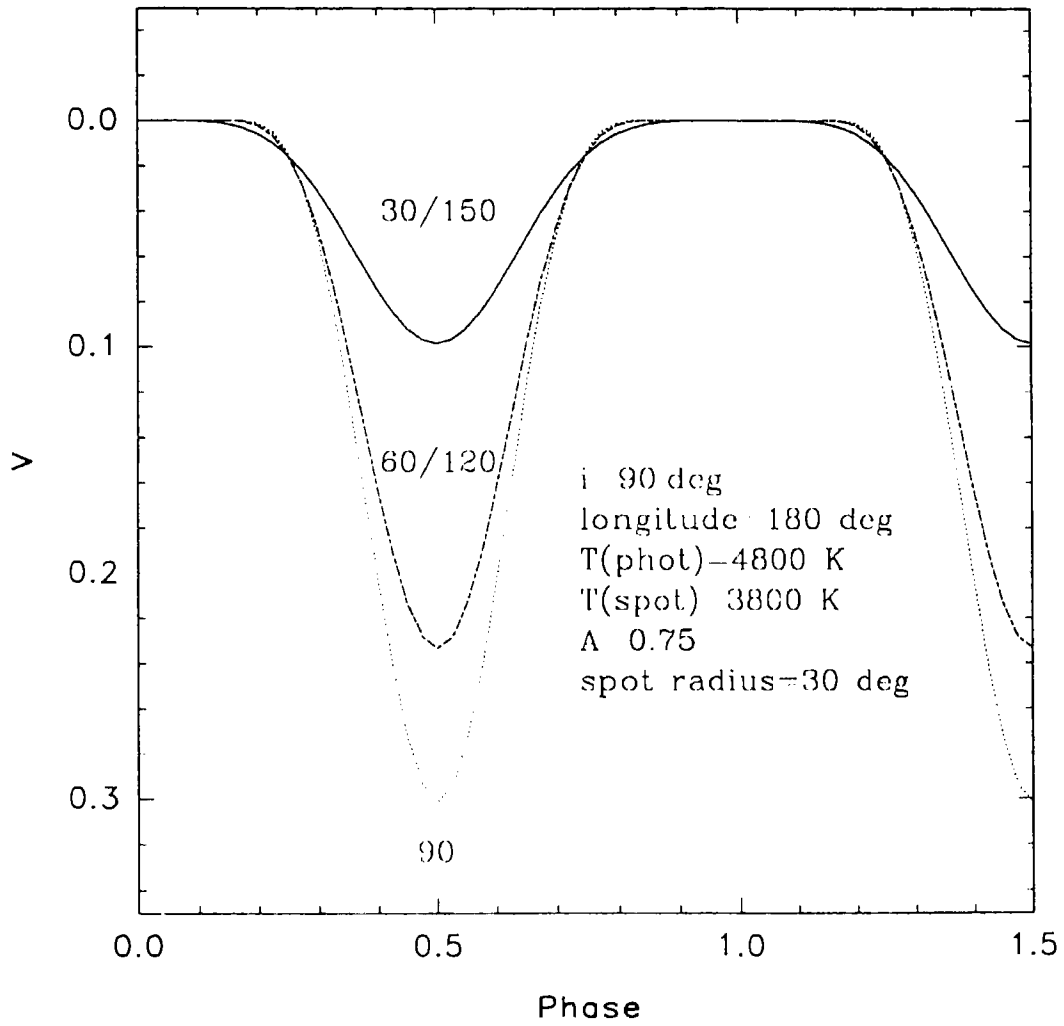


Fig. 1. light curves produced by a circular spot at different polar distances as it moves across the visible hemisphere due to rotation

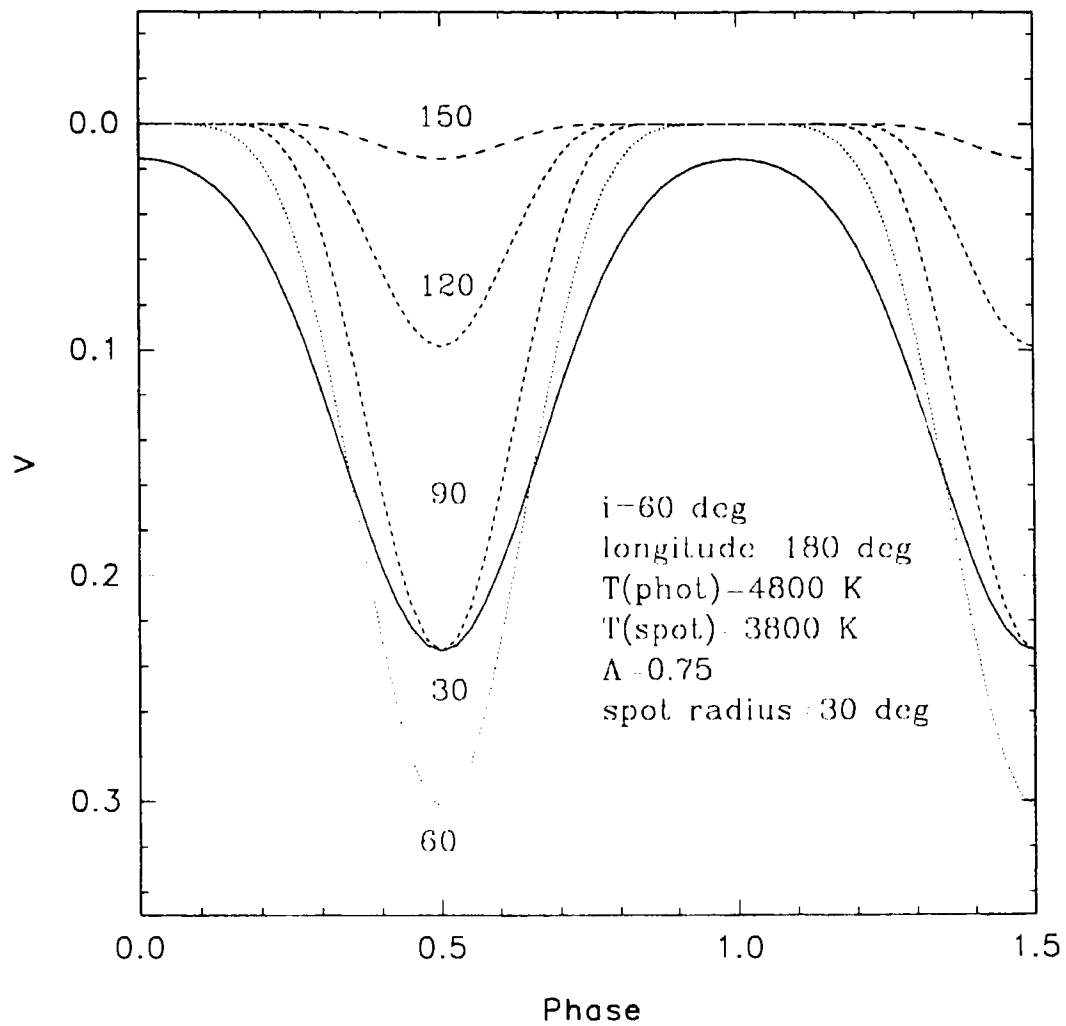


Fig. 2. Light curves produced by a circular spot at different polar distances as it moves across the visible hemisphere due to rotation

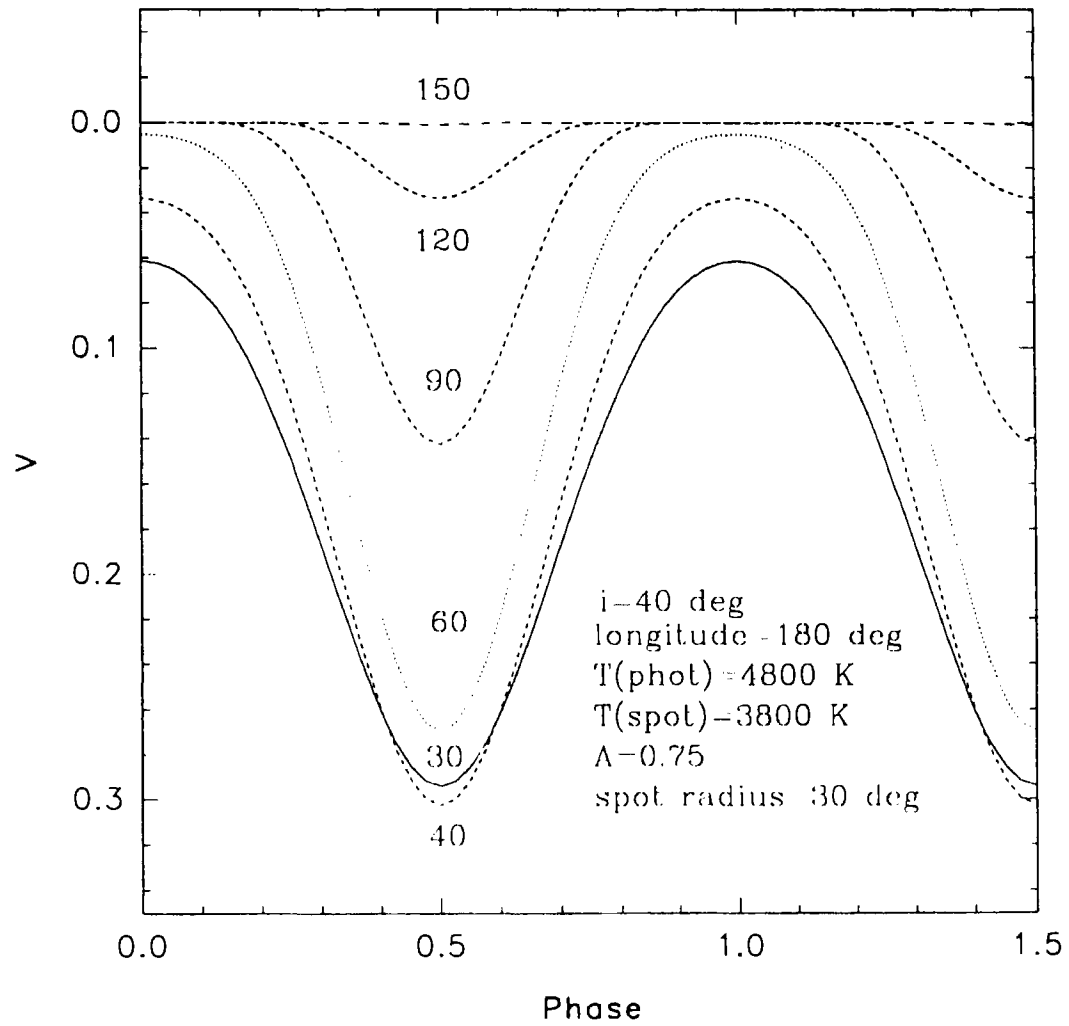


Fig. 3. Light curves produced by a circular spot at different polar distances as it moves across the visible hemisphere due to rotation

If the rotational axis of the variable makes an angle i with the line of sight, the light modulation is produced only by the starspots confined to an equatorial band defined by the latitude limits $\pm i$. If the pole of the star seen above the sky plane is taken as the north pole, spots above the latitude $+i$ will appear through out the rotational period and those below $-i$ will not be seen at all, and hence both groups will not contribute to the amplitude of light variation. In the case of the Sun the spots are confined mostly to within $\pm 30^\circ$ of the equator during sunspot maximum. Extending the solar analogy that spots occur with equal probability in both the northern and southern hemispheres, a limit on the latitudinal spread of starspots can be put from the largest observed amplitude of the light curve if the angle i that the rotational axis makes with the line of sight is known.

Figure 4 shows the variation of brightness at light minimum in V with the width of the equatorial bands for different orbital inclinations; the spots were assumed to cover the entire latitudinal belt which is symmetrical about the equator, and extend in longitude over the entire hemisphere visible at light minimum. The temperatures of the photosphere and spot were taken as 4800 K and 3800 K. Limb-darkening coefficients were assumed to be linear, and the same for both the spotted and unspotted regions. About 10000 area elements were taken for the numerical integration. For the largest equatorial band considered the change in magnitude was found to be only 0.001 mag when the grid points were increased from 5000 to 10000.

If the corresponding equatorial band in the opposite hemisphere is devoid of any spots, the brightness at light minimum plotted in Figure 4 gives essentially the amplitude of light variation. For example, for an orbital inclination $i = 50^\circ$, if spots are restricted to within $\pm 30^\circ$ of the equator as in the case of the Sun, the maximum possible amplitude for the assumed photosphere-spot temperature difference of 1000 K is around 0.45 mag. The assumption that the spot coverage over the entire equatorial band is full is rather idealistic. In a real situation the coverage could be very much smaller than this. For a 50% coverage the maximum possible amplitude is only ~ 0.20 mag. A reduction in the amplitude of light variation would occur for the same spot coverage on the hemisphere visible at light minimum, if spots

are present in the opposite hemisphere, *i.e.*, if the brightness at light maximum V_{max} is less than the unspotted magnitude. For a case corresponding to V_{max} fainter than the unspotted brightness by 0.2 mag, the maximum possible amplitudes for 100% and 50% spot coverages are around 0.25 and 0.12 mag, respectively.

Figures 5 and 6 are similar to Figure 4, but for spot temperatures 3300 K and 0 K, respectively. For the same spot coverage, cooler spots give fainter magnitudes at light minimum, and hence larger amplitudes of light variation. The maximum possible amplitudes for 100% and 50% coverages for a spot temperature of 3300 K against a photospheric temperature of 4800 K are 0.55 mag and 0.24 mag. The corresponding figures are 0.65 mag and 0.28 mag when the spot temperature is 0 K which, of course, represents an extreme case.

The theoretical light curve modeling shows that the effect of wavelength dependence of limb-darkening on the colour variation over the rotational period could be significantly larger, especially at shorter wavelengths, than the effect of the temperature difference between the spot and photosphere. All the spot models that demonstrate such an effect assume circular and equatorial starspots on a rotating variable seen at an inclination $i = 90^\circ$ (Eaton & Poe 1985; Eker 1994). The light curves corresponding to the above case would be flat-topped since the spots would disappear from the field of view over a considerable fraction of the rotational period. In general, the observed light curves are continuously variable over the photometric cycle and hence it follows that the spots have a large longitudinal extent. The light and colour curves due to a rectangular spot bounded by the latitudes $\pm 20^\circ$ and extending over the full range in longitude on the hemisphere visible at light minimum are plotted in Figure 7. The angle between the rotational axis and line of sight was assumed to be 60° . The spot was assumed to be 1000 K cooler than the photosphere. The calculations were done for both (i) no limb-darkening (dashed line) and (ii) linear limb-darkening (solid line). The linear limb-darkening coefficients in $UBVRI$ given in Strassmeier & Olah (1992) and Eker (1994), namely 0.96, 0.88, 0.75, 0.61 and 0.50, respectively, were used in the computations. Both the photospheric and spotted regions

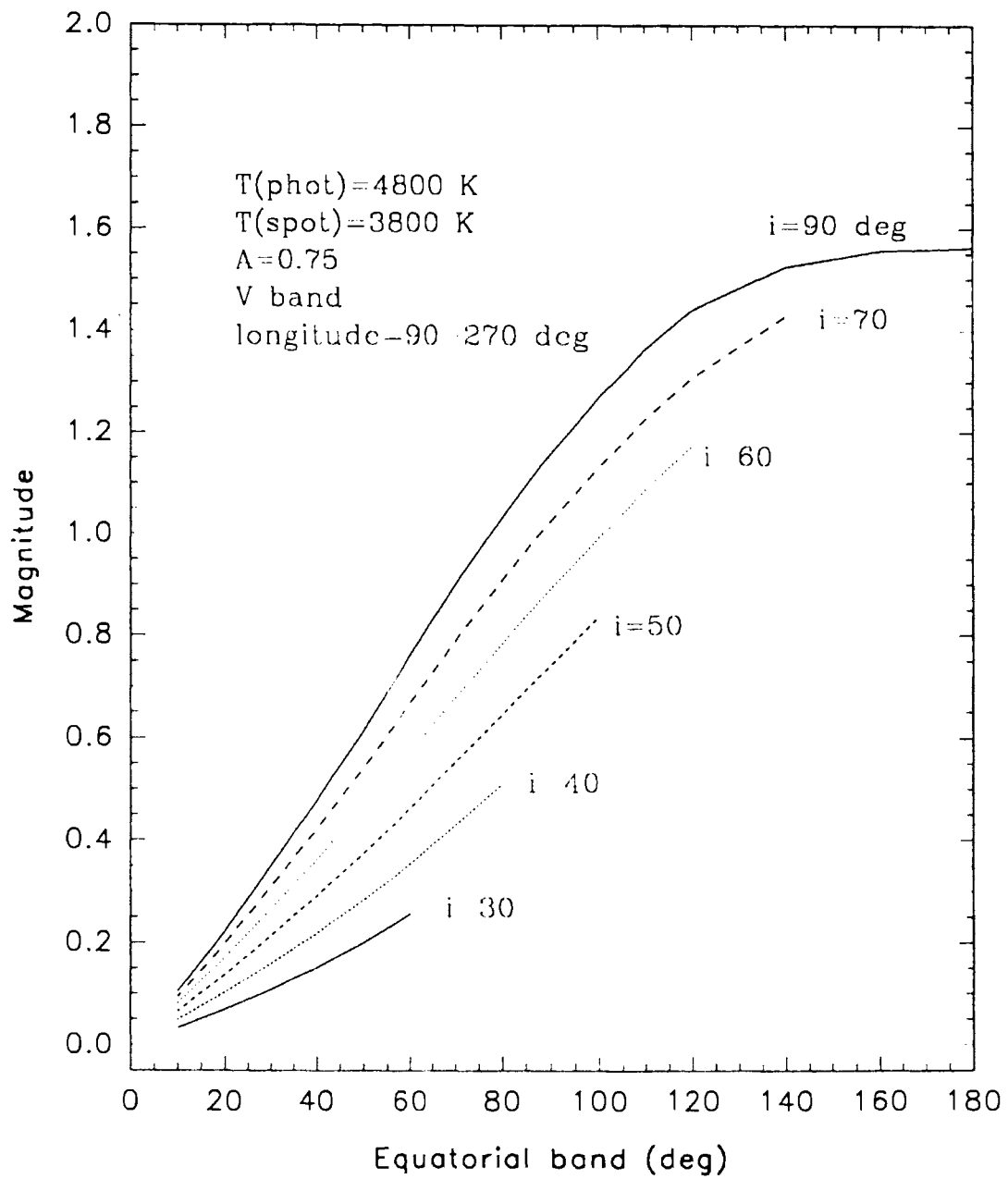


Fig. 4. Plots of the magnitude at light minimum against the equatorial band for different orbital inclinations. The spot is assumed to cover the entire band

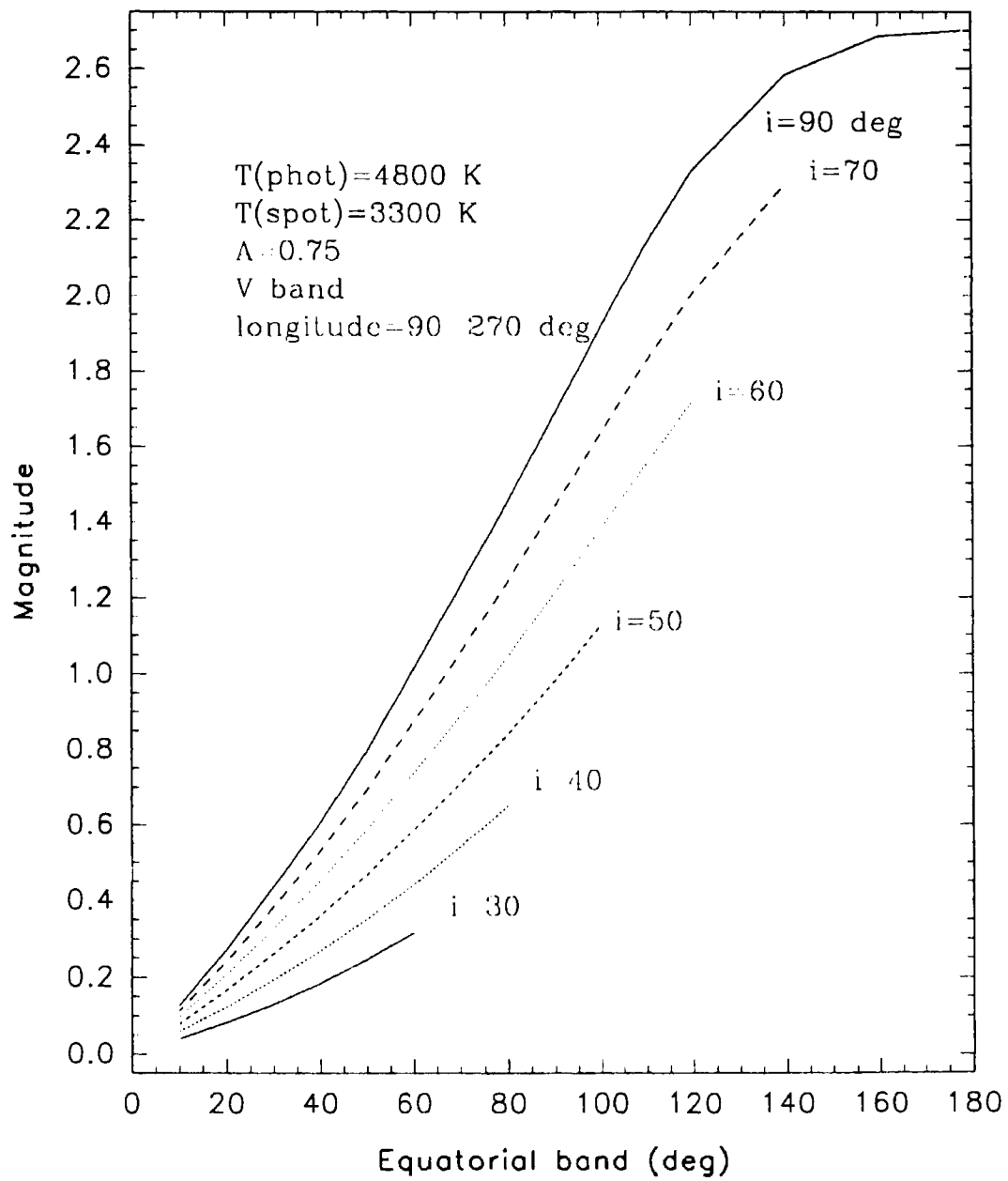


Fig. 5. Plot of the magnitude at light minimum against the equatorial band for different orbital inclinations. The spot is assumed to cover the entire band

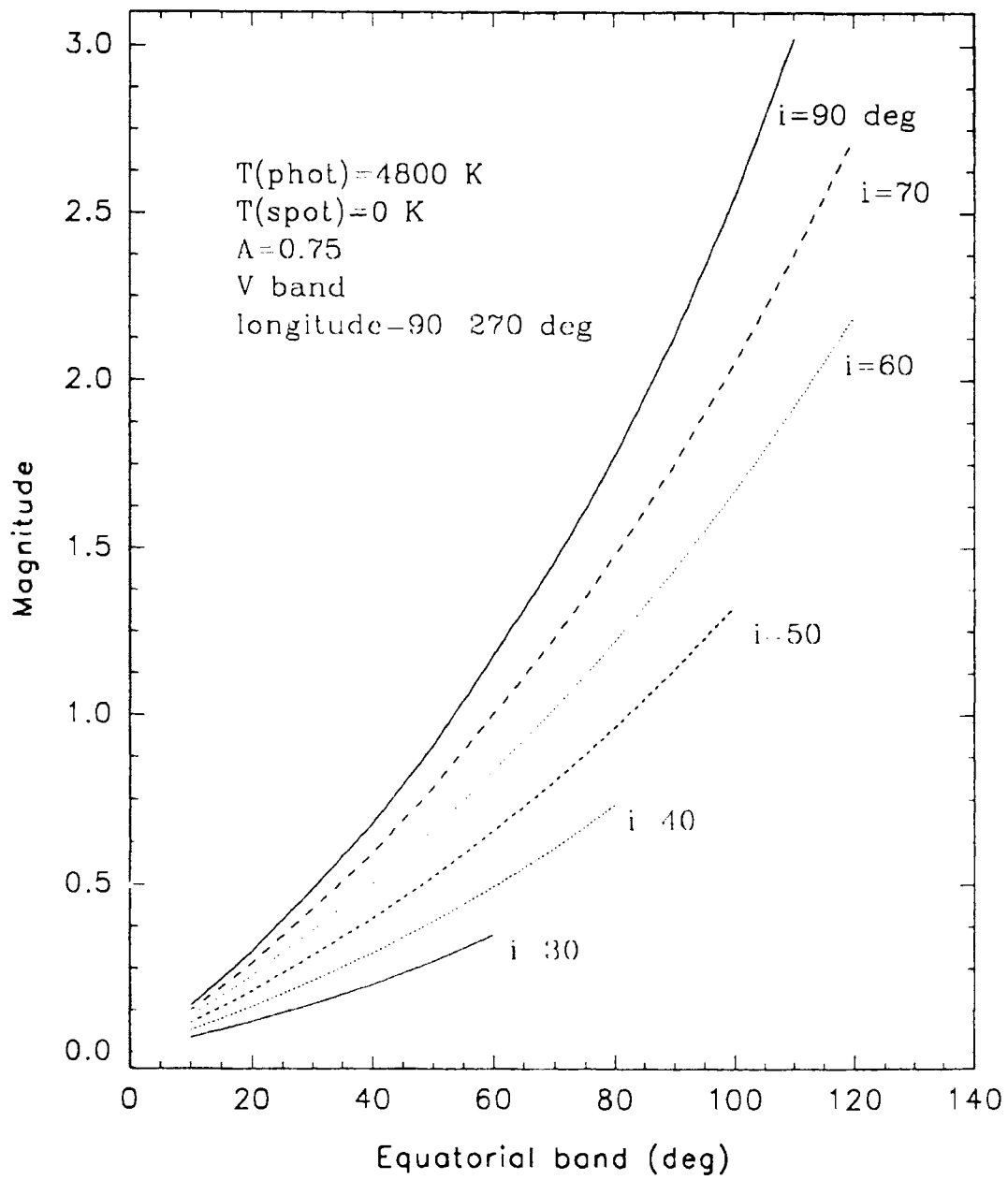


Fig. 6. Plot of the magnitude at light minimum against the equatorial band for different orbital inclinations. The spot is assumed to cover the entire band

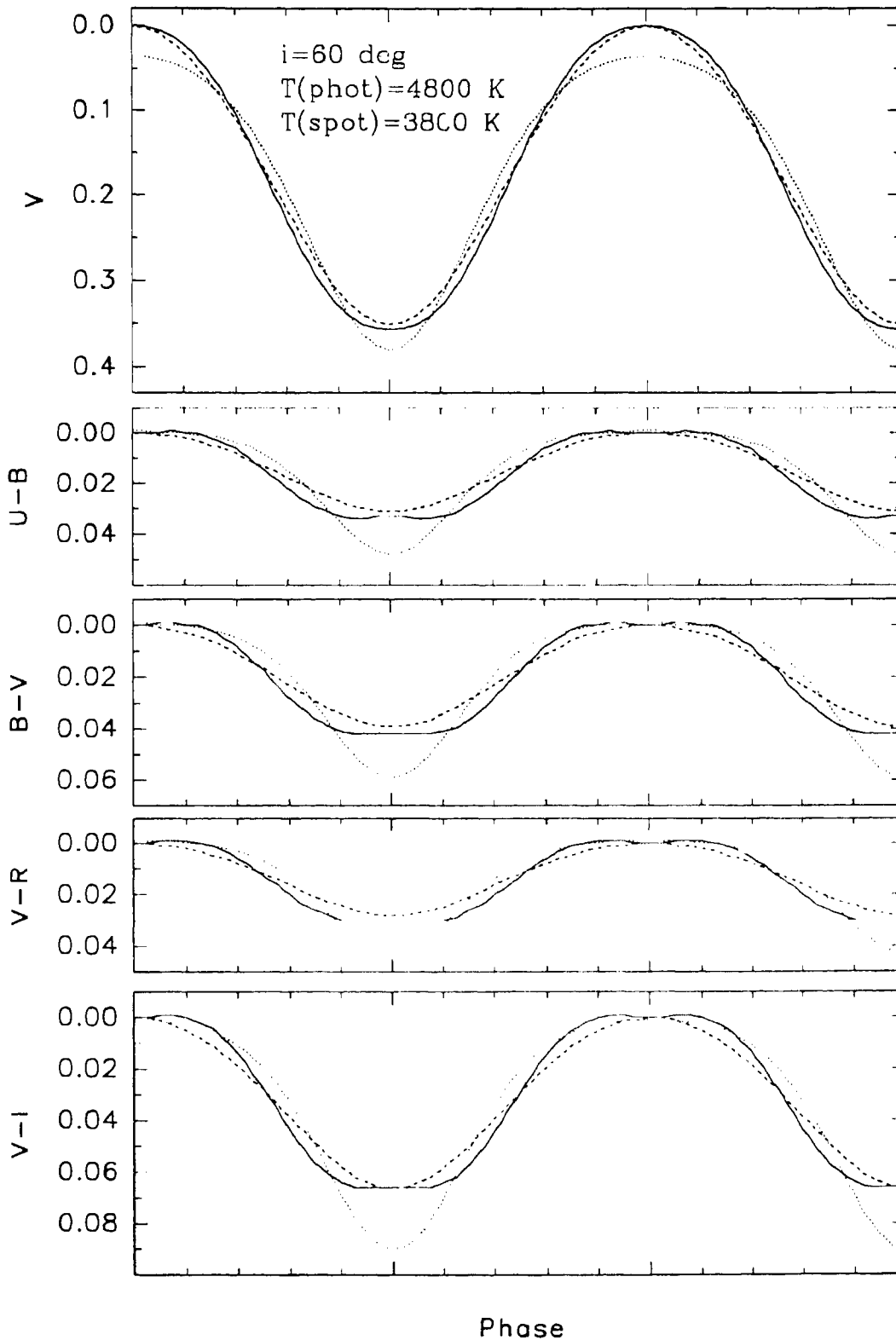


Fig. 7. Light and colour curves of an equatorial band of spot and a circular spot. solid line: equatorial band with linear limb darkening (LD), dashed line: same without LD and dotted: circular spot with linear LD.

were assumed to follow the same limb-darkening law; any difference in the two would produce only marginal differences in the resulting light curves (Mohin & Raveendran 1992). From Figure 7 it is clear that the light and colour curves differ only marginally indicating that the colour variations are caused by the temperature effects rather than the limb-darkening effects. The amplitudes in both cases are nearly same. The difference is only in their shapes, with the colour curves with limb-darkening showing nearly flat maximum and minimum. The limb-darkening law alters the intensity distribution across the projected visible disc of the star; it essentially assigns higher intensities towards the centre. The net effect produced by the limb-darkening depends on the exact distribution of spots on the stellar surface.

A circular spot of 39° radius at a polar distance of 30° also produces a continuous light curve with an amplitude and shape similar to that of the rectangular spot considered above. Figure 7 also shows the colour and light curves due to such a circular spot. The limb-darkening was assumed to be linear and the same as those quoted above. It is clear from the figure that the colour curves due a circular spot differs significantly, both in amplitude and shape, from that due to an extended rectangular spot. The former curves are flatter at maximum and show deeper minimum than the latter curves. The amplitudes of all colour curves due to the circular spot are larger than those due to the rectangular spot by more than 50%. The distribution of surface intensity is altered by the limb-darkening which assigns a higher intensity towards the centre. The centres of the rectangular and the circular spots from the projected stellar disc are nearly the same (see Figure 9). The first one has a large longitudinal extent where as the second has large spread in both latitude and longitude. Therefore, apart from the photosphere-spot temperature difference the colour curves also depend to a large extent on the exact distribution of spots on the stellar surface because of the limb darkening effects.

(c) *The implications of observations*

Almost all RS CVn systems, for that matter all rotating variables, usually exhibit continuously varying light curves; flat-topped light curves are seldom observed. Even in the case of eclipsing RS CVn variables the outside eclipse

variation arising from the spotted nature of the active star is nearly sinusoidal. This implies that the spots which modulate the observed flux have a large longitudinal spread $\sim 180^\circ$; the individual spots may be compact as in the case of the Sun, but there may be several of them spread over a substantial range of longitudes to cause the continuously varying light curve observed.

It is known that in all well-observed RS CVn objects both the amplitude of light variation and brightness at light maximum are variable. In the case of single-lined binaries the entire observed light variation is due to the intrinsic variation of the active primary, whereas in double-lined systems the observed light variation would be much less than the actual intrinsic variation of the active star because of the substantial light contribution by its companion. In most cases it is rather difficult to evaluate the intrinsic light variation of the active star because of the difficulty in the estimation of the exact light contribution by the other component. The orbital inclination is unknown if the binary is noneclipsing, and it is more difficult to estimate the same in the case of single-lined systems. However, reasonable limits can be put in most of the cases from a knowledge of the luminosity class and rotational broadening of spectral lines of the visible primary.

Some of the implications of the observations are discussed below in the context of one of the well-observed RS CVn systems. DM UMa is a single-lined RS CVn binary, and has been observed almost every season for the last 15 years (Mohin & Raveendran 1994). The orbital inclination of DM UMa is most likely close to 40° , and the maximum amplitude in V so far observed is 0.32 mag (Crampton et al. 1979; Mohin & Raveendran 1994). From Figure 4 it is clear that nearly 100% coverage is required to produce an amplitude of this order if spots are restricted to only within $\pm 30^\circ$ of the equator and if they are cooler than the surrounding photosphere by 1000 K. If spots are 1500 K cooler than the photosphere, Figure 5 indicates that the maximum possible amplitude for 100% coverage over a $\pm 30^\circ$ latitude belt is only 0.45 mag, and therefore an amplitude of 0.32 mag would require a spot coverage of approximately 75%. In the extreme case of 0 K for the spot temperature it is seen from Figure 6 that the corresponding value is

0.50, and hence the required spot coverage would be 70%. The brightness at light maximum was 0.17 mag below the brightest V_{max} so far observed at the time of maximum amplitude. This could happen either due to (i) the presence of spots in the equatorial belt on the hemisphere visible at light maximum, or (ii) the presence of spots at latitudes higher than $+40^\circ$, *i.e.*, in the circumpolar region. In the former case for a photosphere-spot temperature difference of 1000 K an amplitude of 0.32 mag in V would result only if spots cover the entire latitudinal belt within $\pm 40^\circ$ of the equator because the hemisphere visible at light minimum should be at least 0.50 mag below the unspotted brightness. In the latter case the maximum possible amplitude is 0.50 mag and hence the required spot coverage within the same belt would be only around 70%. Further, in the computations presented in Figure 4, it was assumed that spots cover the full range in longitude across the visible hemisphere. Therefore, for a reasonable level of spot coverage it is essential that spots should extend beyond $\pm 40^\circ$ in latitude and the photosphere-spot temperature difference should be more than 1000 K.

A lower limit on the latitudinal extent for the occurrence of starspots can also be put from the total range in V observed, *i.e.*, $V_{max}(\text{brightest}) - V_{min}(\text{faintest})$ for a rotating variable. In the case of DM UMa the above quantity is 0.52 mag. Assuming that $V_{max}(\text{brightest})$ corresponds to the unspotted magnitude and spots are cooler than the surrounding photosphere by 1000 K, it is seen from Figure 4 even for 100% coverage spots should extend well beyond $\pm 40^\circ$ in latitude in the hemisphere visible at light minimum; for a lower percentage of coverage and smaller longitudinal extent, starspots should be present at latitudes higher than 40° and photosphere-spot temperature difference should be more than 1000 K, as already concluded from a consideration of the maximum amplitude of light variation and the brightness at light maximum observed at that epoch.

II Peg is another well-observed RS CVn binary, and the maximum amplitude in V so far observed is 0.5 mag (Mohin & Raveendran 1993). HD 81410 which is the subject of § 4.1, also shows a similar amplitude of light variation. The highest amplitude in V so far reported for an RS CVn object is 0.6 mag, and that is in the case of HD 12545 (Nolthenius 1991). The

observed light variations in the case of these binaries are entirely due to the active component in the corresponding systems because all are single-lined binaries. All these systems are noneclipsing, and hence the orbital inclinations are unknown.

If i is the orbital inclination then, spots present in the entire $\pm i^\circ$ belt would contribute to the rotational modulation. From Figures 4-6 it is seen that the maximum possible amplitude increases drastically with the orbital inclination. For example, even for a spot-photosphere temperature of 1000 K an increase in i from 40° to 60° increases the maximum possible amplitude from 0.5 to 1.2 mag, a range of about 0.7 mag. For temperature difference of 1500 K the range would be more than 1 mag. However, the range in the maximum observed amplitudes for the above four stars is only around 0.2 mag. If spots are confined to $\pm 40^\circ$ latitude, it is seen from Figure 4 that the increase in amplitude when seen at $i = 60^\circ$ instead of $i = 40^\circ$ is about 0.2 mag. The corresponding increase is around 0.3 mag if the spots are cooler than the photosphere by 1500 K (Figure 5). Hence it is tempting to conclude that spots are mostly restricted to around $\pm 40^\circ$ in latitude at least at the epochs of large amplitude of light variation. High latitude spots could be present, but their contribution to the light modulation may not be appreciable, especially at large amplitude phases.

The above conclusion is based on the assumption that the orbital inclination of all the four systems are different and they show at least a range of about 20° . It is highly unlikely that they are the same. A study of a larger sample of similar objects for which photometry is available over extended time intervals is highly desirable in this context.

3.4. The inverse problem

The determination of spot parameters from the observed light curve is essentially an inverse problem. The uncertainties in the several parameters, like, the spot distribution on the stellar surface, the unspotted photospheric magnitude, etc., make the exact determination of the spot characteristics a nearly impossible task. In the case of single stars and noneclipsing systems an additional problem arises from the unknown inclination of the rotational

axis. However, as indicated earlier the modeling of several light curves of an object would give meaningful information on the spot parameters, including the surface distribution.

Most of the existing models estimate spot parameters by trial and error until the desired accuracy of the fit is achieved. This, in essence, is a direct approach because several synthetic light curves are generated for the assumed, plausible spot parameters and then compared with the observed light curve. There are many sources of difficulties even in such an approach in modeling the observed light curves. The most important parameter in the spot modeling is the brightness of the unspotted hemisphere. It is rather not easy to assign the unspotted magnitude of an active star because observationally it is extremely difficult to rule out the presence of spots on the visible hemisphere. Under-estimation of the unspotted magnitude changes the generated spot models considerably. In a photometric study of BY Dra and RS CVn systems, Rodono et al. (1986) noted that the unspotted magnitudes of their programme stars were always brighter than the highest observed magnitude at light maximum. They suspected that this could be due to anyone or more of the following reasons: (i) high latitude, or nearly polar spots, (ii) small, nearly equatorial spots suitably distributed over a wide range of longitudes, and (iii) a uniform distribution of small spots over the stellar surface.

In the above approach the spot parameters are derived by varying systematically the different parameters involved until acceptable approximation to the observations is obtained. A limited number of spots, usually two or three, are assumed to produce the observed light variation. In most cases the spot temperature is fixed initially and only a single wavelength data is made use of (Rodono et al. 1986; Zeilik et al. 1988). Zeilik et al. (1990) have determined the spot temperature using multiband photometry. They used the *V* band data to determine the size of the spot (assuming $T = 0$ K) and then adjusted the ratio of the flux of the spot to that of the photosphere at *B*, *R* and *I* bands to derive the spot temperature.

A computer program in Fortran was developed by us to model the light curves of spotted stars. It employs the method of least squares using dif-

ferential correction to the parameters to arrive simultaneously at the best fit value for the various parameters, including the temperature, assuming that the light variation is caused by a limited number of large spots. The presence of a minimum in the sum of the squares of the deviations in the multidimensional parameter space is indicated by the absolute convergence of the solution on iteration. The problem of choosing the final parameters from a set of possible values does not arise in this method because all the spot parameters are optimized simultaneously. This method also allows the simultaneous determination of the spot temperature when observations are available in more than one wavelength band. In this respect the present method is better than the other spot modeling methods available in the literature.

The spots are assumed to be circular in shape so that a spot is completely described by the four parameters, spot radius (θ_R), polar distance (θ_P), measured from the pole above the sky plane, longitude (θ_L) and temperature (T_s). The assumptions are, of course, simplistic. The fact that there is always a clear rotational modulation, in most cases with well defined one or two minima, indicates that the light variation is due to prominent spots or spot groups extended over the stellar surface. There may additional spots or spot groups scattered over the surface contributing negligibly to the overall light modulation. An irregular, extended spot, or spot group can be replaced by an 'equivalent' circular spot, and the spot parameters thus determined would refer to this equivalent spot.

The observed magnitude is a function of ΔL_λ^T which in turn is a function of the above parameters of the various spots. If we denote these parameters by θ_i ($i = 1, n$ where n is four times the number of spots) equation (1) can be written in the functional form as

$$m_\lambda = m_\lambda(\phi, \theta_i, \dots). \quad (2)$$

For a least square solution of the spot parameters, the iterative procedure used for a nonlinear function as outlined in Scarborough (1964) was used. Expanding equation (2) about the initial guess values for the spot parameters

θ'_i , using Taylor's theorem, we obtain

$$m_\lambda = m_\lambda(\phi, \theta'_i, \dots) + \left(\frac{\partial m_\lambda}{\partial \theta_i}\right)_0 \delta\theta_i + \dots \quad (3)$$

The derivatives $\left(\frac{\partial m_\lambda}{\partial \theta_i}\right)_0$, etc. are obtained at $\theta_i = \theta'_i$. Equation (3) is linear in $\delta\theta_i$ and using observational data the normal equations which are equations of condition to minimize the sum of the squares of residuals are derived. Here $\delta\theta_i$ are the corrections to the initial guess values, and the procedure is repeated by replacing θ'_i by $\theta'_i + \delta\theta_i$ until convergence is reached. The various derivatives are numerically evaluated using

$$\left(\frac{\partial m_\lambda}{\partial \theta_i}\right)_0 = \frac{m_\lambda(\phi, \theta'_i + \Delta\theta_i, \dots) - m_\lambda(\phi, \theta'_i - \Delta\theta_i, \dots)}{2\Delta\theta_i}.$$

The monochromatic luminosities at the effective wavelengths of observation were numerically evaluated by taking about 500 surface area elements, and a similar number of area elements were taken inside the region of a spot to compute ΔL_λ . On doubling these numbers the changes in the derived spot parameters were found to be less than the uncertainties in their determination. To compute the derivatives, typically, we used a value of 2° for $\Delta\theta_R$, $\Delta\theta_P$ and $\Delta\theta_L$, and a value of 20 K for ΔT . The resulting normal equations were solved using the Cracovian matrix method (Kopal 1959), since along with the coefficients it gives the uncertainties involved in their evaluation. The derivatives can also be derived using these uncertainties for $\Delta\theta_R$, $\Delta\theta_P$, etc. after the first iteration onwards, but no additional advantage was noticed; the convergence was reached faster, but the computation time increased since after each iteration the standard deviation of fit had to be calculated for the evaluation of the uncertainties.

The computer program in Fortran developed by us is fairly general; there is no restriction either on the number of discrete spots or on their latitudes or longitudes. An overlapping of the circular spots is also allowed so that an elongated spot can be taken care of. If there are two or more spots, all of them can be of the same radius or of different radii. Further, the temperature of the spots may be treated as either known or unknown, in which case it may be either the same for all the spots or different for different spots. The

determinancy of the spot parameters is indicated by their absolute convergence on iteration from the starting initial guess values; otherwise divergence occurs with the spot area or temperature finally becoming negative.

The trials with synthetic data using circular spots indicate that the choice of the initial guess values are not critical for achieving the convergence of the solution. Even in the case of overlapping spots the initial parameters could be always retrieved. Here it may be noted that synthetic data provide ideal conditions for the solution of the spot parameters — accurate values at closely and evenly distributed over the entire photometric cycle.

Table 1. Circular spot parameters derived for the synthetic light curve due to an equatorial band of spot.

No. of spots	Polar distance (deg)	Longitude (deg)	Radius (deg)	Frac. area	Temp. (K)	σ (mag)
1	29.1±0.4	180.2±0.5	38.0±0.4	0.10	3702±38	0.0259
2	63.4±0.7 63.6±0.7	134.9±0.5 225.5±0.5	26.9±0.1 26.9±0.1	0.10	3622±5	0.0032
3	84.5±0.4 84.0±0.6 84.5±0.4	119.0±0.2 180.2±0.4 241.4±0.2	25.3±0.1 26.1±0.2 25.3±0.1	0.14	3741±5	0.0009
4	89.9±0.1 90.1±0.1 90.1±0.1 89.9±0.1	110.7±0.1 156.0±0.3 204.4±0.3 249.1±0.1	22.9±0.1 24.4±0.1 24.4±0.1 22.9±0.1	0.16	3799±1	0.0001

In order to test the convergence of the above iterative technique in the case of an extended spot and also to see how accurately the resulting equiv-

alent spots reproduce the light curve being solved, the synthetic curves in *UBVRI* due to an equatorial band described above and plotted in Figure 7 was also subjected to an analysis. A spot extended longitudinally instead of latitudinally was considered because the continuously varying light curve over the photometric phase indicate a large longitudinal spread for the spots.

Four different trials, corresponding to the cases of a single, two, three and four spots, were made, and in all cases the convergence of the solutions could be obtained. The temperatures of the spots were assumed to be the same for all the spots in the cases where the number of spots assumed were more than one. As before the initial starting values for the iteration were not at all critical for obtaining convergence. The final parameters for the four cases are given in Table 1, and the resulting light and colour curves along with the corresponding synthetic curves are plotted in Figure 8. The equatorial band of spot and the equivalent spots as they would appear on the hemisphere visible at light minimum are shown in Figure 9. It is clear from Figure 8 and also from the standard deviation of fit (σ) given in Table 1 that the single-spot assumption gives a poor approximation to the light and colour curves while the two-spot assumption gives an acceptable fit to the synthetic data. The light and colour curves corresponding to three- and four-spot assumptions are mutually indistinguishable and they excellently reproduce the data.

Since the light curve continuously vary, the single-spot solution gives a large radius and high latitude for the spot; half of the spot lies in the circumpolar region and therefore the light at maximum is slightly lower than that given. As the number of spots assumed is increased their sizes become smaller and they shift towards the equator where the spot is assumed to be present while synthesizing the data; when their number becomes four the spots slightly overlap and produce an equatorial band with nearly uniform width. The area occupied by the spots as a fraction of the total area of the stellar surface is also given in Table 1. The fractional area of the equatorial spot is 0.16. Both the single- and two-spot assumptions give the fractional area as 0.10, about 50% smaller, where as three-spot assumption gives almost the correct value. The spot temperature was assumed to be 3800 K, cooler

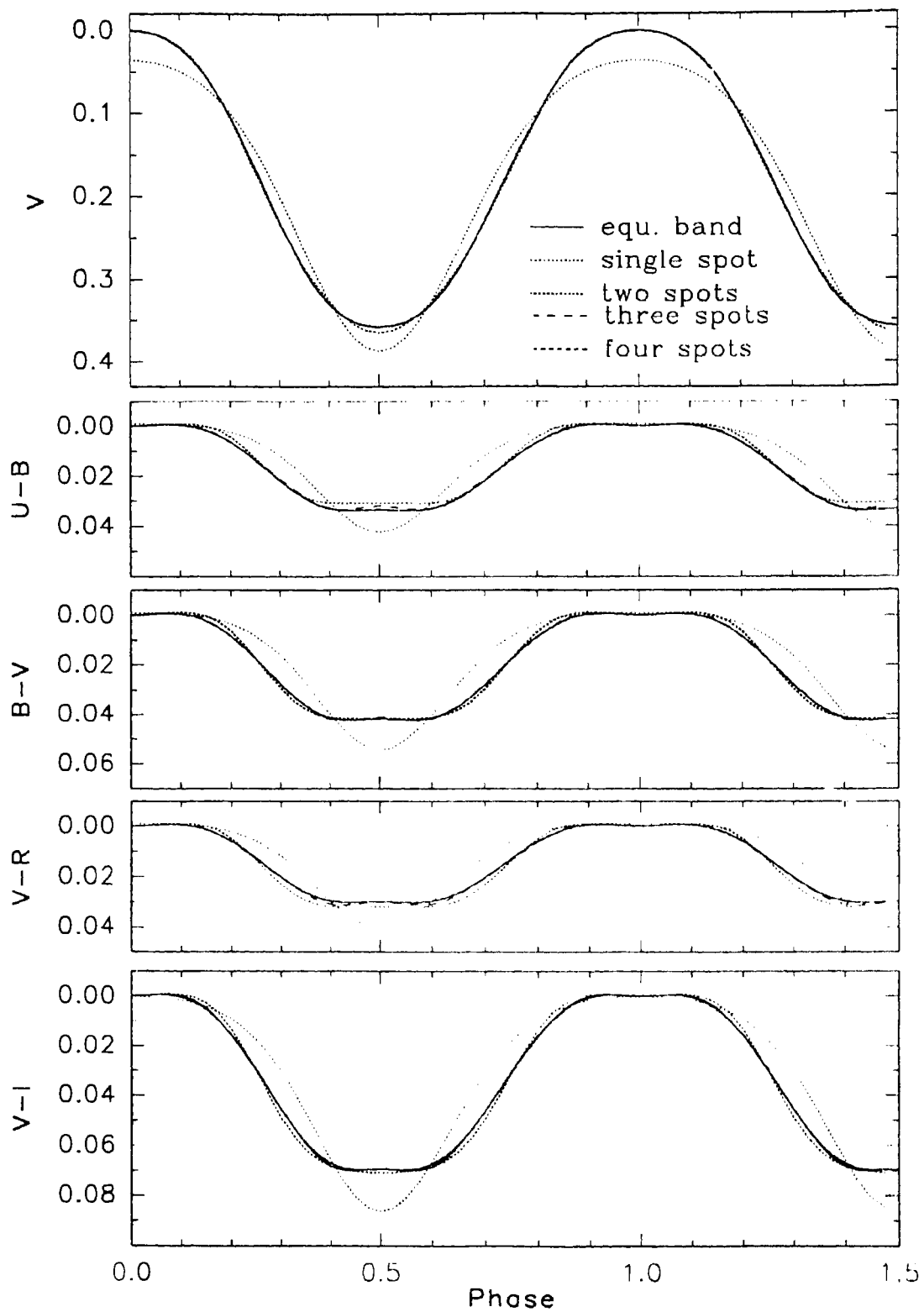


Fig. 8. Light and colour curves of an equatorial band of spot and equivalent single, two, three and four spots. The curves for three and four spots merge with those of the equatorial band of spot.

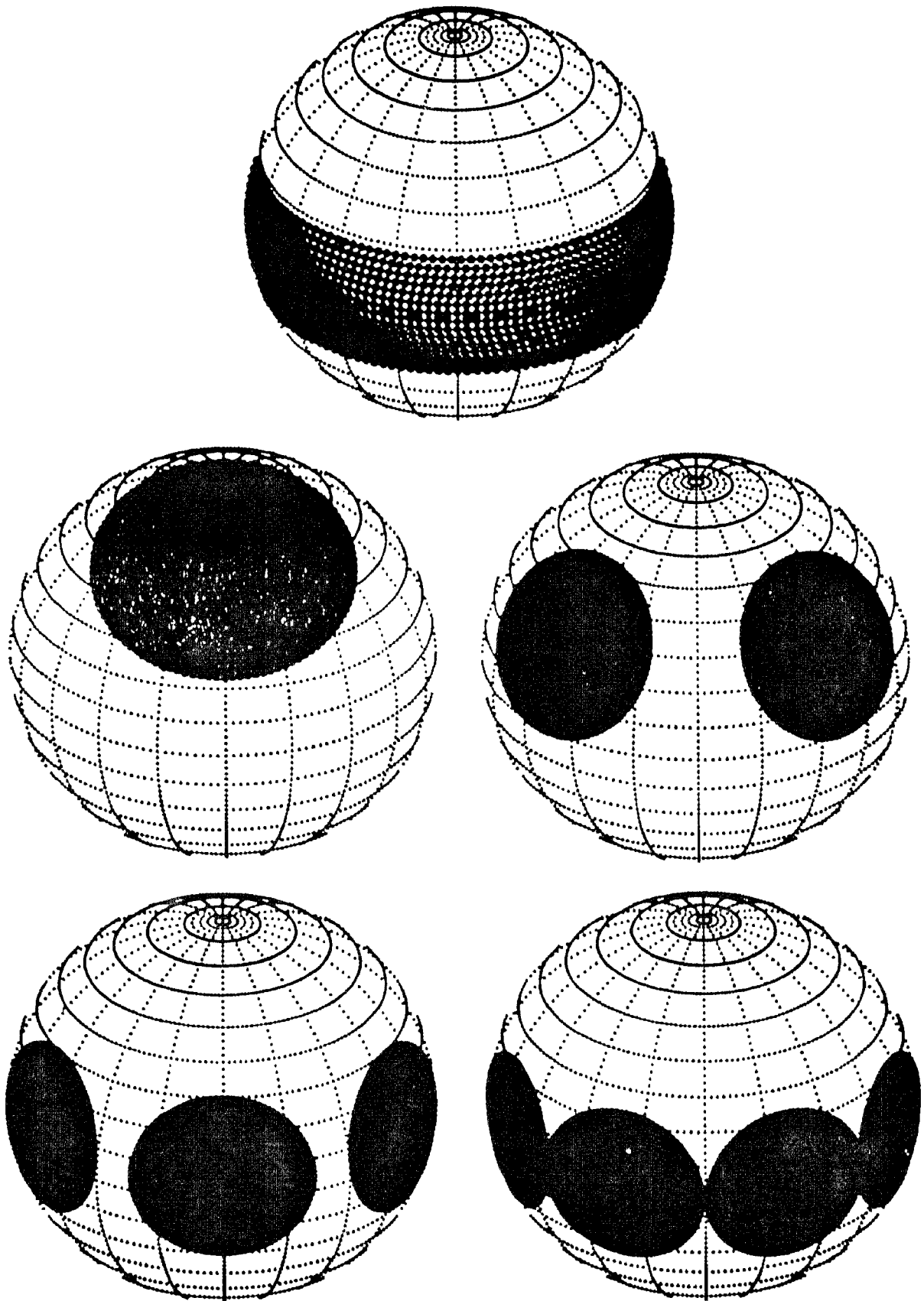


Fig. 9. Appearances of the spots at light minimum for the various configurations

than the photosphere by 1000 K. It is interesting to see from the Table 1 that the total range in the spot temperatures derived is only around 150 K; the four-spot assumption gives the assumed temperature exactly.

The light minimum of the synthetic curve occurs at 0.^p5, corresponding to a longitude of 180°. However, in the case of the two-spot assumption the spots are separated by 90° in longitude and therefore the light minimum occurs at their mean longitude. In the present case the spots are of equal size. In an actual case the spots could be of different sizes and the longitude estimated from the light curve would then correspond to a longitude weighted by the intensity distribution on the hemisphere visible at light minimum. Usually, the migration of the light minimum observed in RS CVn Systems is attributed to a migration of spot or spot group as a result of a difference between the actual period and the period used. If there are more than one prominent spot group, then the migration of the phase of the light minimum may not represent a true migration of a spot or spot group because the apparent shift in the phase of the light minimum may be arising from a change in the relative strengths of the various spot groups.

4

RS CANUM VENATICORUM OBJECTS

4.1. HD 81410

4.1.1. Introduction

The suspected light variability of HD 81410 (=IL Hya) by Cousins & Stoy (1963) was confirmed by Eggen (1973) whose observations of the star in 1971 and 1972 showed an amplitude of about 0.50 mag in the visual region. The light curves obtained during the two observing seasons differed appreciably, and he found that a period of 25.4 days satisfied the observations of each seasons separately. Bidelman & MacConnell (1973) lists HD 81410 as a star with K1III spectrum displaying strong *Ca II H & K* emissions and *filled Balmer lines*. The radial velocity observations by Wayman & Jones (Eggen 1973) showed HD 81410 to be a single-lined spectroscopic binary. Wayman also found that the strong *Ca II H & K* emission lines present in the spectrum of the star yielded the same velocity as the absorption lines. He assigned a spectral type K1IV to the star.

Raveendran et al. (1982), who observed HD 81410 almost a decade after Eggen (1973), found that the photometric period is in fact close to 12.87 days. They found that the amplitudes of light variation in both *B* and *V* had decreased and were only around 0.15 mag. From the observed (*U* - *B*)

and $(B - V)$ colors of HD 81410 at its light maximum, they suggested that the secondary component of HD 81410 is probably an F dwarf. Further, they concluded that HD 81410 belongs to the RS CVn type systems since it satisfied all the membership criteria proposed by Hall (1976), namely, the orbital period, strong *Ca II H & K* emissions, the spectral type of the primary component and the variable light curves. Fekkel et al. (1986) found HD 81410 to show very strong *Ca II H & K* emission features typical of a late type chromospheric active star, but no evidence for a *uv* continuum from an F type companion, as suggested by Raveendran et al. (1982). Recently, from the observed colours of HD 81410, Cutispoto (1993) assigned the spectral types K2-3IV and G4V to the components. He also derived a photometric period of 12.667 days from a Fourier analysis of the data obtained during January–March 1989.

The absorption line of *Li I* 6708 Å is very strong in the spectrum of HD 81410. The spectroscopic observations by Pallavicini et al. (1992, 1993) show that the equivalent width of this *Li I* line does not show any significant variation with the photospheric spot visibility. Pallavicini et al. (1992) have suggested that the observed high value of $\log n(\text{Li}) = 1.34$ in HD 81410 is most likely due to a real decrease of *Li* depletion.

Slee et al. (1987) detected HD 81410 as a highly variable radio source. They found that during the major flare of 1983 August 2, the flux density increased by a factor of 2 in 1.5 hours. Recently HD 81410 has also been detected as an X-ray source during the ROSAT-WFC all sky survey (Pounds et al. 1993).

4.1.2. Orbital elements

Raveendran et al. (1982) derived the orbital parameters of HD 81410 from the eight radial velocity measurements listed by Eggen (1973), which were supplied by Wayman and Jones. From the giant-subgiant nature of the visible primary component, they assumed that the HD 81410 system is sufficiently old and that the tidal coupling effects have brought about orbital circularization and near spin synchronization, and hence the orbital period is close to its photometric period. Their analysis of the photometric data obtained

by them in 1981 and those by Eggen in 1972 showed the period to be around 12.8 days. The radial velocity measurements showed that the maximum radial velocity occurred around JD 2441466.0, the systemic velocity was around 5.0 km s^{-1} and the amplitude of variation was around 40.0 km s^{-1} . These together with the photometric period obtained by them were taken as the preliminary values for T_0 , γ and K for the orbital solution which yielded an orbital period of 12.866 days.

Table 1. Spectroscopic orbital elements of HD 81410

Orbital elements	Solution (i)	Solution (ii)
P	$12.90514 \pm 0.00013 \text{ days}$	$12.90522 \pm 0.00013 \text{ days}$
e	0.0 (<i>assumed</i>)	0.043 ± 0.010
ω	—	$10.^{\circ}2 \pm 2.^{\circ}9$
κ	$41.2 \pm 0.4 \text{ km s}^{-1}$	$41.4 \pm 0.4 \text{ km s}^{-1}$
γ	$-7.9 \pm 0.3 \text{ km s}^{-1}$	$-7.9 \pm 0.3 \text{ km s}^{-1}$
T_0	JD 2444228.555 \pm 0.023	JD 2444228.560 \pm 0.023
T_{ω}	—	JD 2444228.926 \pm 0.072
$a \sin i$	$7.3086 \times 10^6 \text{ km}$	$7.3335 \times 10^6 \text{ km}$
$f(m)$	0.093	0.094
σ	3.6 km s^{-1}	3.4 km s^{-1}

The orbital period of 12.908 days, obtained by Balona (1987) by combining his own radial velocity measurements with those of Collier Cameron (1982), is slightly longer than that obtained by Raveendran et al. (1982). A fresh orbital solution was obtained making use of all the available radial velocity measurements. Jones & Fisher (1984) has since revised three of the measurements listed by Eggen (1973). Fekkel (1986) lists another five velocity measurements obtained by him. Sterne's (1941) method for orbits of small eccentricity was used for the least square solution. The solutions for both a circular and an elliptical orbits were obtained and these are given in Table 1. All observations were treated with equal weights.

The standard deviation reduces from 3.6 km s^{-1} to 3.4 km s^{-1} if the orbit is assumed to be elliptical instead of circular. Since the probable error in the eccentricity is significantly smaller than the eccentricity, following Lucy & Sweeney (1971), we assume that the orbit is elliptical. In Figure 1 the observed velocities are plotted along with the computed curve corresponding to the elliptical orbit.

The present analysis gives a 12.90522 day period which is slightly shorter than that derived by Balona (1987).

4.1.3. Photometry

HD 81410 was observed on a total of 221 nights during 13 observing seasons, in *UBVRI* during two seasons and in Stromgren *uvby* during the remaining eleven seasons. The comparison stars used were HD 81904 and HD 80991. All the observations were made differentially with respect to HD 81904. The probable errors in the differential *BVRI* magnitudes are typically

Table 2a. *UBVRI* magnitudes of comparison stars of HD 81410

Star	<i>U</i>	<i>B</i>	<i>V</i>	<i>R</i>	<i>I</i>
HD 81904	9.695 ±0.008	8.995 ±0.005	8.020 ±0.004	7.515 ±0.006	7.045 ±0.004
HD 80991	10.368 ±0.007	9.550 ±0.004	8.510 ±0.005	7.980 ±0.006	7.448 ±0.004

around 0.005 mag, while that in *U* and *uvby* are slightly higher. The average *UBVRI* and *uvby* magnitudes of the comparison stars obtained from the observations of several seasons are given in Table 2a and 2b. The differential measurements of HD 81410 are converted to *UBVRI* and *uvby* magnitudes using the values of HD 81904 given in Table 2a and 2b, and are tabulated in Tables 3 and 4.

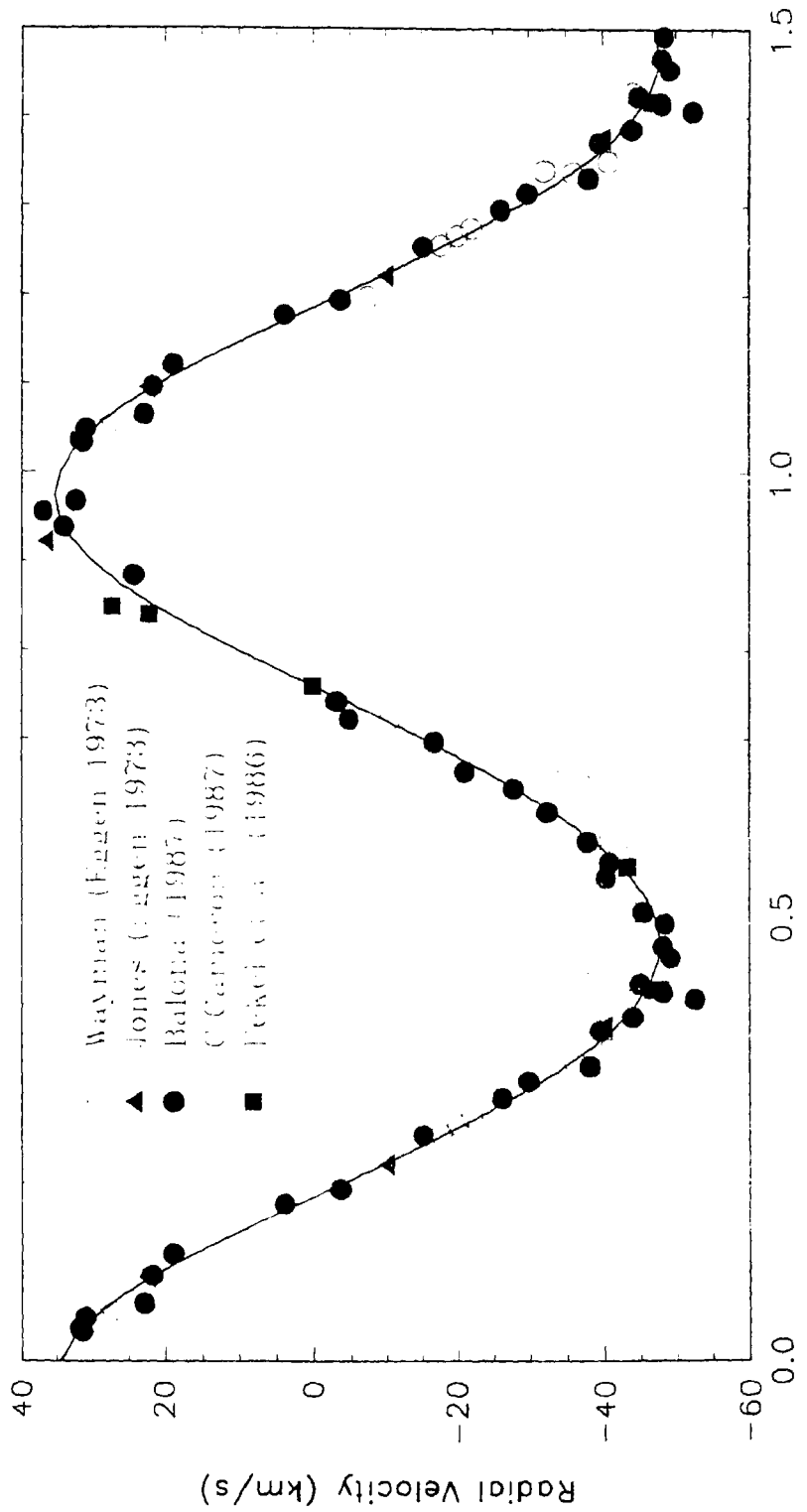


Fig. 1. Radial velocity curve of HD 81410.

Table 2b. *uvby* magnitudes of the comparison stars of HD 81410

Star	<i>u</i>	<i>v</i>	<i>b</i>	<i>y</i>
HD 81904	10.934 ±0.007	9.573 ±0.006	8.614 ±0.005	8.019 ±0.005
HD 80991	11.618 ±0.008	10.175 ±0.006	9.122 ±0.006	8.505 ±0.005

Table 3. *UBVRI* magnitudes of HD 81410

J.D. 2440000.+	<i>U</i>	<i>B</i>	<i>V</i>	<i>R</i>	<i>I</i>
6896.614	9.162	8.435	7.405	6.813	6.270
6897.513	9.118	8.400	7.363	6.792	6.263
6897.548	9.124	8.406	7.373	6.795	6.267
6898.509	9.090	8.363	7.332	6.767	6.237
6898.631	9.045	8.357	7.330	6.761	6.239
6899.504	9.032	8.326	7.308	6.735	6.214
6899.627	9.022	8.342	7.305	6.738	6.221
6900.524	9.017	8.327	7.300	6.743	6.212
6901.503	9.091	8.372	7.339	6.765	6.239
6902.505	9.112	8.381	7.357	6.782	6.253
6902.639	9.111	8.382	7.360	6.785	6.251
6903.505	9.087	8.382	7.345	6.777	6.245
6904.498	9.082	8.359	7.336	6.773	6.240
6905.494	9.083	8.368	7.339	6.767	6.237
7296.506	8.971	8.288	7.260	6.684	6.156
7298.542	8.998	8.275	7.263	6.707	6.187

Table 3. continued

J.D. 2440000.+	<i>U</i>	<i>B</i>	<i>V</i>	<i>R</i>	<i>I</i>
7299.478	9.012	8.296	7.281	6.714	6.196
7304.536	9.181	8.453	7.413	6.850	6.314
7305.492	9.174	8.440	7.406	6.842	6.305
7307.550		8.375	7.344	6.781	6.253
7308.499	9.030	8.342	7.323	6.760	6.236

Table 4. *uvby* magnitudes of HD 81410

J.D. 2440000.+	<i>u</i>	<i>v</i>	<i>b</i>	<i>y</i>
6068.748	10.391	9.069	8.050	7.413
6069.755	10.425	9.078	8.056	7.412
6070.750	10.418	9.096	8.062	7.415
6071.739	10.428	9.097	8.057	7.422
6072.771	10.413	9.095	8.067	7.423
6073.753	10.452	9.134	8.097	7.444
6076.778	10.560	9.256	8.214	7.560
6077.775	10.562	9.246	8.196	7.552
6078.808	10.510	9.192	8.165	7.510
6079.756	10.464	9.139	8.121	7.470
6080.754	10.422	9.097	8.062	7.422
6081.763	10.412	9.081	8.053	7.410
6082.751	10.427	9.094	8.045	7.403
6083.745	10.422	9.088	8.059	7.416
6083.799	10.414	9.094	8.061	7.420
6083.805	10.428	9.099	8.058	7.413
6087.749	10.524	9.194	8.156	7.502
6088.763	10.575	9.244	8.201	7.550

Table 4. continued

J.D. 2440000.+	<i>u</i>	<i>v</i>	<i>b</i>	<i>y</i>
6089.753	10.594	9.256	8.228	7.567
6091.763	10.514	9.200	8.167	7.521
6092.760	10.465	9.137	8.112	7.471
6093.715	10.432	9.098	8.073	7.435
6094.747	10.425	9.091	8.070	7.420
6095.732	10.419	9.101	8.064	7.422
6096.730	10.438	9.108	8.066	7.422
6097.742	10.438	9.109	8.073	7.427
6098.732	10.426	9.111	8.079	7.431
7148.818	10.413	9.080	8.040	7.404
7156.853	10.255	8.935	7.910	7.284
7159.838	10.341	9.020	7.985	7.355
7160.824	10.377	9.055	8.028	7.388
7164.817	10.345	9.018	7.992	7.358
7166.821	10.386	9.030	7.993	7.353
7167.857	10.350	9.008	7.974	7.333
7168.817	10.250	8.960	7.934	7.302
7169.856	10.257	8.928	7.906	7.278
7172.855	10.368	9.021	7.991	7.358
7173.811	10.407	9.064	8.027	7.383
7174.827	10.395	9.073	8.039	7.405
7175.788	10.404	9.067	8.036	7.411
7176.819	10.390	9.047	8.016	7.379
7177.802	10.363	9.023	7.995	7.361
7178.817	10.347	9.018	7.988	7.349
7179.807	10.358	9.017	7.978	7.345
7180.818	10.306	8.983	7.949	7.313
7228.660	10.405	9.046	8.028	7.383

Table 4. continued

J.D. 2440000.+	<i>u</i>	<i>v</i>	<i>b</i>	<i>y</i>
7233.720	10.317	8.946	7.920	7.292
7234.727	10.308	8.942	7.928	7.289
7235.669	10.336	8.976	7.954	7.310
7236.685	10.357	9.017	7.988	7.345
7238.651	10.404	9.072	8.038	7.395
7240.695	10.395	9.070	8.045	7.407
7242.679	10.341	9.016	7.992	7.360
7244.661	10.313	8.993	7.958	7.324
7246.647	10.278	8.947	7.928	7.295
7248.700	10.296	8.972	7.944	7.311
7250.642	10.358	9.031	8.000	7.364
7252.650	10.408	9.071	8.048	7.403
7253.650	10.402	9.058	8.033	7.399
7254.672	10.378	9.053	8.029	7.384
7258.679	10.284	8.949	7.933	7.302
7259.632	10.274	8.948	7.919	7.287
7316.485	10.397	9.061	8.017	7.409
7317.478	10.417	9.076	8.049	7.401
7319.473			8.066	7.421
7320.498	10.316	8.972	7.971	7.326
7321.492	10.271	8.956	7.932	7.290
7322.501	10.212	8.905	7.876	7.257
7324.529	10.302	8.950	7.902	7.267
7327.476	10.272	8.951	7.916	7.295
7328.466	10.368	9.012	7.990	7.355
7332.461	10.416	9.082	8.005	7.388
7333.496	10.310	8.979	7.946	7.322
7472.850	10.393	9.037	8.001	7.355

Table 4. continued

J.D. 2440000.+	<i>u</i>	<i>v</i>	<i>b</i>	<i>y</i>
7474.840	10.323	8.981	7.955	7.333
7475.796	10.322	8.972	7.960	7.323
7476.792	10.309	8.981	7.956	7.322
7477.799	10.315	8.980	7.949	7.313
7478.782	10.286	8.959	7.931	7.302
7479.774	10.276	8.939	7.914	7.283
7480.771	10.301	8.954	7.926	7.297
7481.769	10.310	8.981	7.958	7.324
7482.771	10.354	9.026	7.994	7.361
7483.829	10.346	9.039	8.000	7.368
7484.761	10.387	9.031	8.004	7.374
7487.764	10.315	8.983	7.956	7.320
7488.749	10.280	8.977	7.950	7.318
7489.747	10.337	8.985	7.964	7.324
7490.751	10.293	8.977	7.949	7.320
7491.742	10.310	8.960	7.931	7.304
7492.739	10.285	8.956	7.934	7.301
7493.737	10.314	8.966	7.940	7.306
7494.735	10.325	8.992	7.965	7.332
7495.732	10.364	9.022	7.994	7.354
7590.754	10.269	8.943	7.921	7.296
7591.702	10.268	8.950	7.926	7.309
7592.641	10.280	8.959	7.935	7.312
7593.596	10.296	8.950	7.938	7.303
7594.674	10.300	8.965	7.931	7.303
7596.620	10.319	8.991	7.972	7.332
7597.657	10.333	9.000	7.971	7.337
7598.692	10.332	8.997	7.967	7.333
7599.607	10.335	9.008	7.974	7.337

Table 4. continued

J.D. 2440000.+	<i>u</i>	<i>v</i>	<i>b</i>	<i>y</i>
7600.624	10.321	8.990	7.960	7.329
7601.645	10.287	8.967	7.943	7.309
7602.634	10.260	8.945	7.921	7.297
7603.606	10.258	8.932	7.916	7.292
7605.654	10.280	8.950	7.935	7.307
7606.627	10.296	8.960	7.947	7.319
7607.606	10.248	8.968	7.942	7.316
7608.615	10.296	8.979	7.956	7.324
7609.628	10.334	9.010	7.977	7.339
7610.613	10.316	9.003	7.974	7.342
7611.625	10.329	8.995	7.965	7.338
7612.630	10.302	8.984	7.952	7.329
7613.650	10.301	8.977	7.946	7.315
7614.558	10.295	8.953	7.929	7.297
7836.831	10.238	8.901	7.882	7.260
7839.850	10.423	9.076	8.033	7.393
7840.839	10.415	9.087	8.045	7.406
7841.844	10.407	9.074	8.039	7.398
7842.843	10.392	9.046	8.012	7.379
7843.851	10.340	9.010	7.981	7.345
7844.806	10.304	8.968	7.951	7.325
7845.847	10.291	8.961	7.938	7.307
7884.810	10.310	8.971	7.947	7.313
7887.691	10.202	8.875	7.862	7.234
7888.793	10.252	8.936	7.911	7.282
7889.671	10.362	9.012	7.980	7.348
7891.717	10.444	9.104	8.060	7.418
7893.732	10.386	9.065	8.027	7.391

Table 4. continued

J.D. 2440000.+	<i>u</i>	<i>v</i>	<i>b</i>	<i>y</i>
7910.720	10.309	8.991	7.943	7.313
7911.697	10.217	8.897	7.892	7.274
7912.250	10.185	8.869	7.851	7.237
7916.817	10.379	9.097	8.052	7.401
7917.731	10.412	9.095	8.070	7.424
7920.731	10.383	9.084	8.041	7.408
7921.715	10.379	9.057	8.016	7.390
7924.786	10.204	8.909	7.873	7.246
7925.716	10.188	8.860	7.855	7.229
7926.713	10.256	8.914	7.905	7.289
7929.708	10.482	9.119	8.058	7.431
7931.728	10.429	9.101	8.058	7.427
7935.732	10.251	8.967	7.967	7.327
7937.721	10.194	8.866	7.864	7.240
7938.722	10.209	8.874	7.876	7.235
7940.738	10.361	9.032	8.006	7.359
8063.502	10.400	9.061	8.029	7.392
8067.501	10.367	9.047	8.010	7.374
8068.494	10.451	9.102	8.053	7.416
8069.496		9.126	8.071	7.426
8075.481		9.082	8.062	7.427
8076.485	10.373	9.035	8.011	7.373
8077.473	10.347	8.996	7.982	7.348
8189.850	10.400	9.066	8.029	7.393
8190.851	10.358	9.016	7.992	7.354
8197.829	10.407	9.072	8.035	7.396
8200.808	10.482	9.144	8.100	7.458
8218.851	10.318	8.986	7.959	7.331

Table 4. continued

J.D. 2440000.+	<i>u</i>	<i>v</i>	<i>b</i>	<i>y</i>
8226.848	10.469	9.139	8.094	7.453
8228.792	10.362	9.037	7.996	7.359
8233.829	10.335	9.000	7.973	7.340
8235.806	10.347	9.011	7.981	7.344
8238.811	10.503	9.164	8.118	7.474
8245.836	10.326	9.000	7.970	7.337
8255.736	10.286	8.969	7.945	7.317
8259.839	10.339	8.998	7.968	7.335
8282.703	10.298	8.972	7.953	7.319
8283.712	10.335	8.997	7.965	7.332
8284.776	10.346	8.993	7.963	7.327
8285.752	10.310	8.984	7.951	7.317
8286.748	10.331	8.994	7.963	7.334
8287.700	10.376	9.041	8.004	7.366
8289.746	10.488	9.135	8.095	7.457
8290.709	10.465	9.134	8.095	7.451
8291.775	10.396	9.075	8.042	7.405
8292.784	10.348	9.015	7.986	7.356
8294.738	10.289	8.958	7.938	7.311
8646.734	10.362	9.031	8.000	7.366
8651.756	10.406	9.114	8.070	7.435
8654.733	10.277	8.949	7.934	7.306
8655.730	10.260	8.943	7.921	7.288
8656.772	10.244	8.922	7.914	7.287
8658.761	10.323	8.989	7.961	7.330
8957.781	10.418	9.090	8.041	7.400
8964.791	10.242		7.886	7.251
8966.746	10.296	8.976	7.936	7.310
8967.755	10.382	9.057	8.000	7.368

Table 4. continued

J.D. 2440000.+	<i>u</i>	<i>v</i>	<i>b</i>	<i>y</i>
8968.772	10.432	9.103	8.051	7.405
8973.718	10.415	9.088	8.035	7.401
8974.718	10.360	9.037	7.996	7.364
9019.807	10.409	9.073	8.024	7.378
9021.728	10.407	9.088	8.046	7.405
9025.759	10.422	9.074	8.033	7.386
9388.748	10.384	9.042	8.009	7.368
9390.736	10.423	9.083	8.043	7.403
9391.724	10.452	9.115	8.071	7.428
9392.723	10.431	9.099	8.060	7.418
9394.754	10.352	9.020	7.991	7.355
9395.724	10.315	8.975	7.950	7.318
9396.764	10.296	8.956	7.930	7.304
9397.777	10.306	8.971	7.945	7.312
9398.726	10.333	8.998	7.967	7.332
9399.769	10.349	9.022	7.988	7.354
9400.760	10.374	9.040	8.004	7.367
9401.694	10.387	9.060	8.021	7.381
9402.761	10.398	9.081	8.034	7.396

4.1.4. Light curves

The Julian days of observation given in Table 3 and 4 were converted into photometric phases using the following ephemeris:

$$JD(HeI.) = 2444225.508 + 12^d.90522E,$$

where the initial epoch corresponds to the conjunction with the primary in front calculated using the parameters given in Table 1 and the period is the orbital period given in the same table. Figures 2–14 show the plots of the

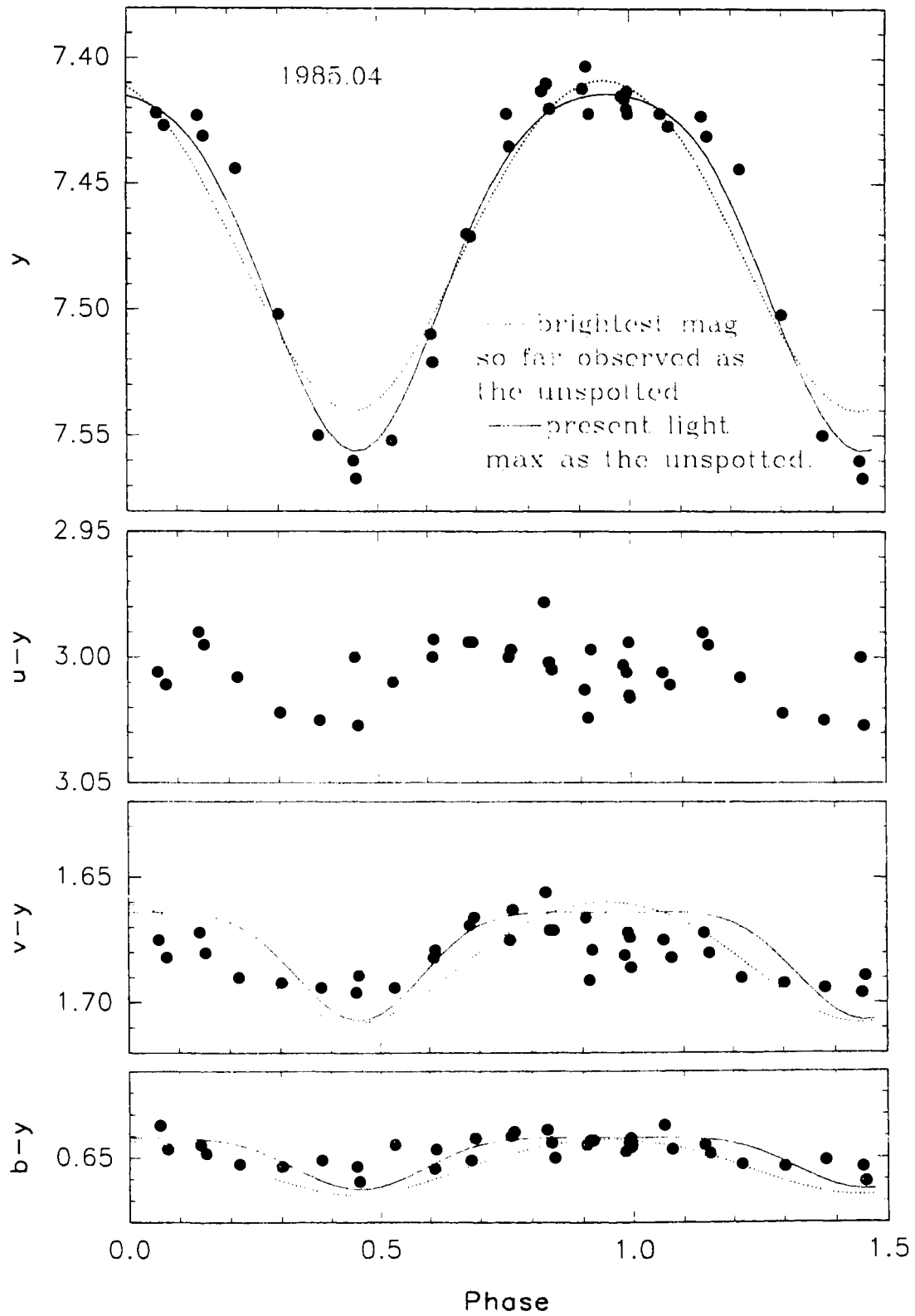


Fig. 2. Plots of y , $u-y$, $v-y$ and $b-y$ of HD 81410.

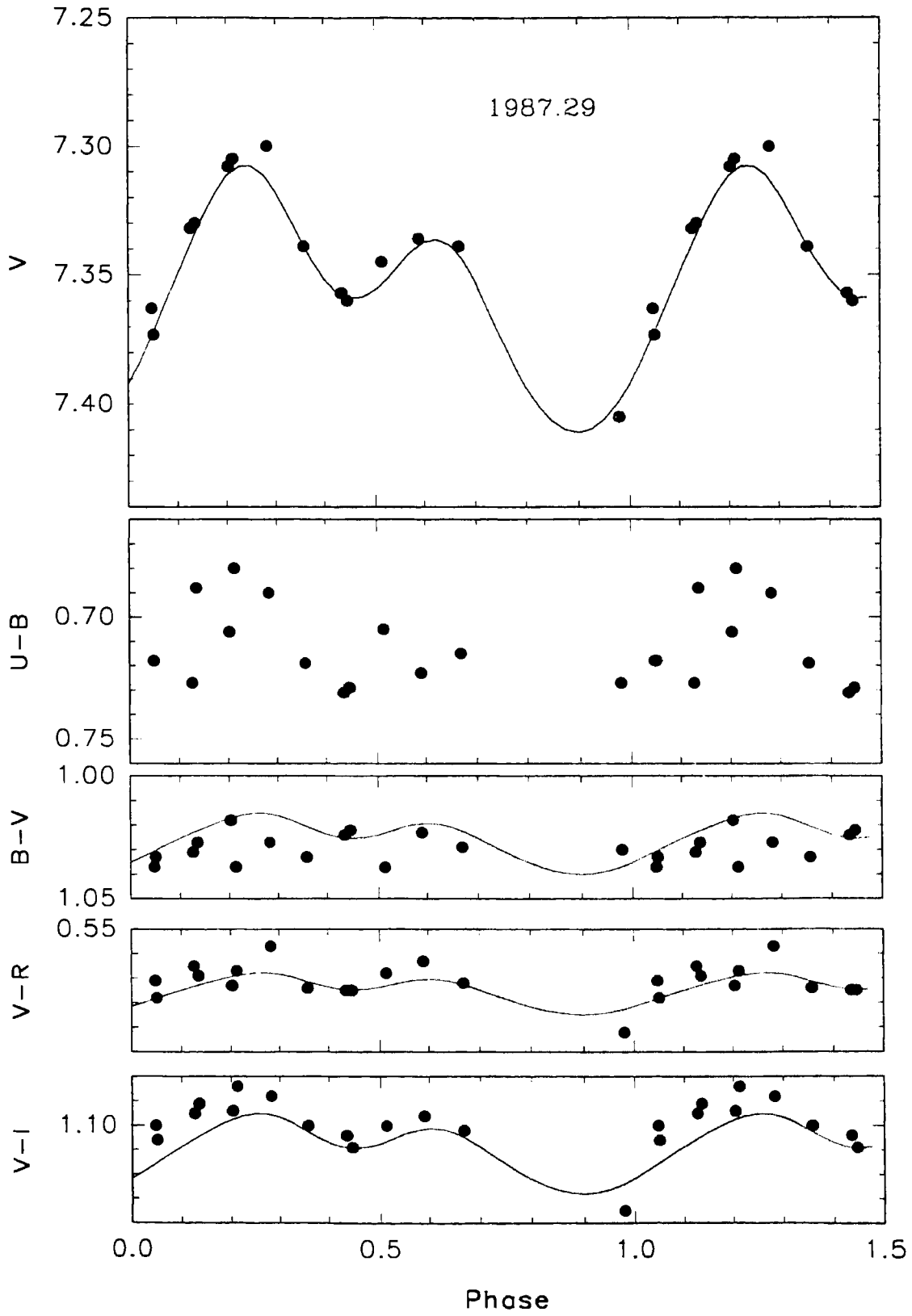


Fig. 3. Plots of V, U-B, B-V, V-R and V-I of HD 81410.

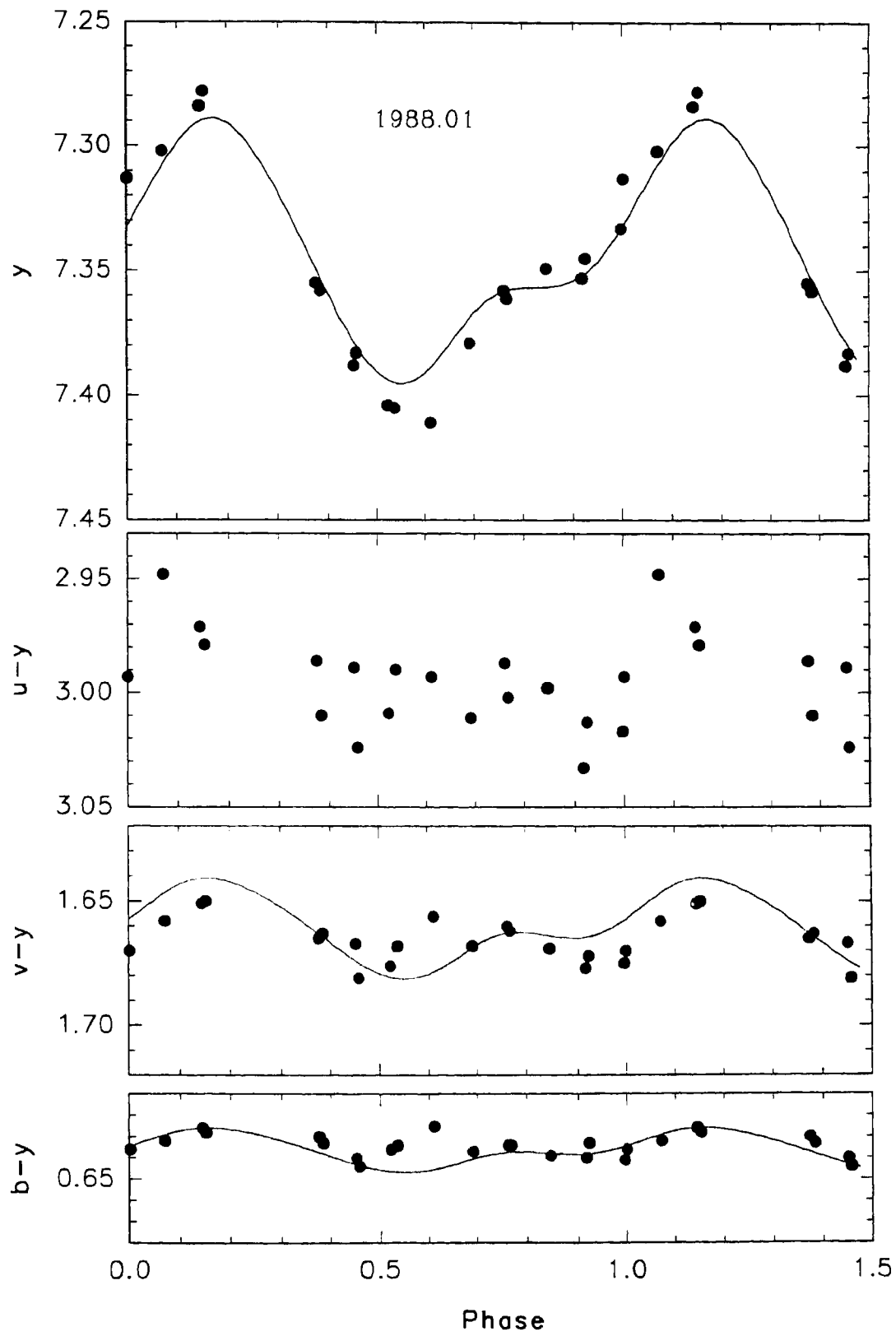


Fig. 4. Plots of y , $u-y$, $v-y$ and $b-y$ of HD 81410.

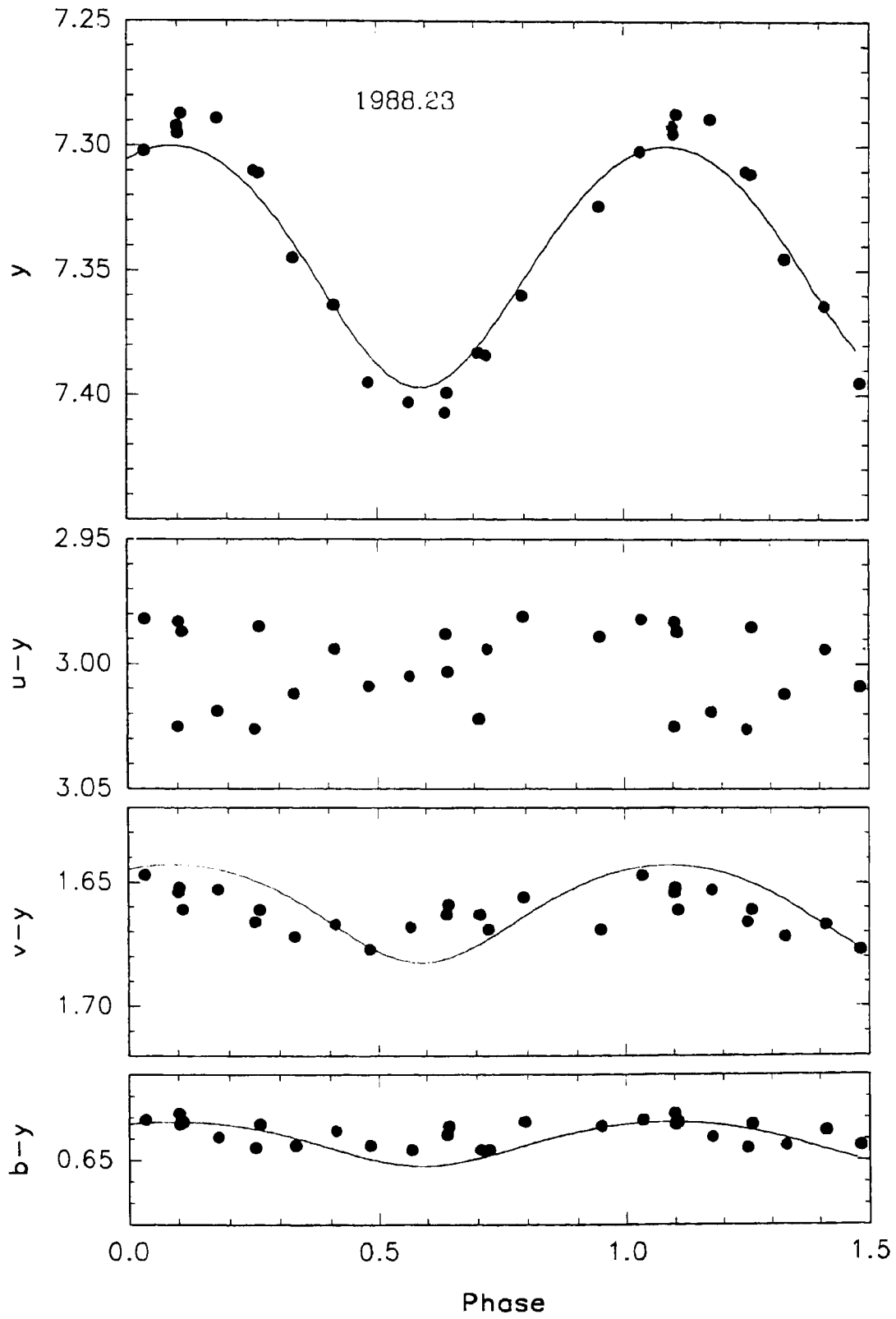


Fig. 5. Plots of y , $u-y$, $v-y$ and $b-y$ of HD 81410.

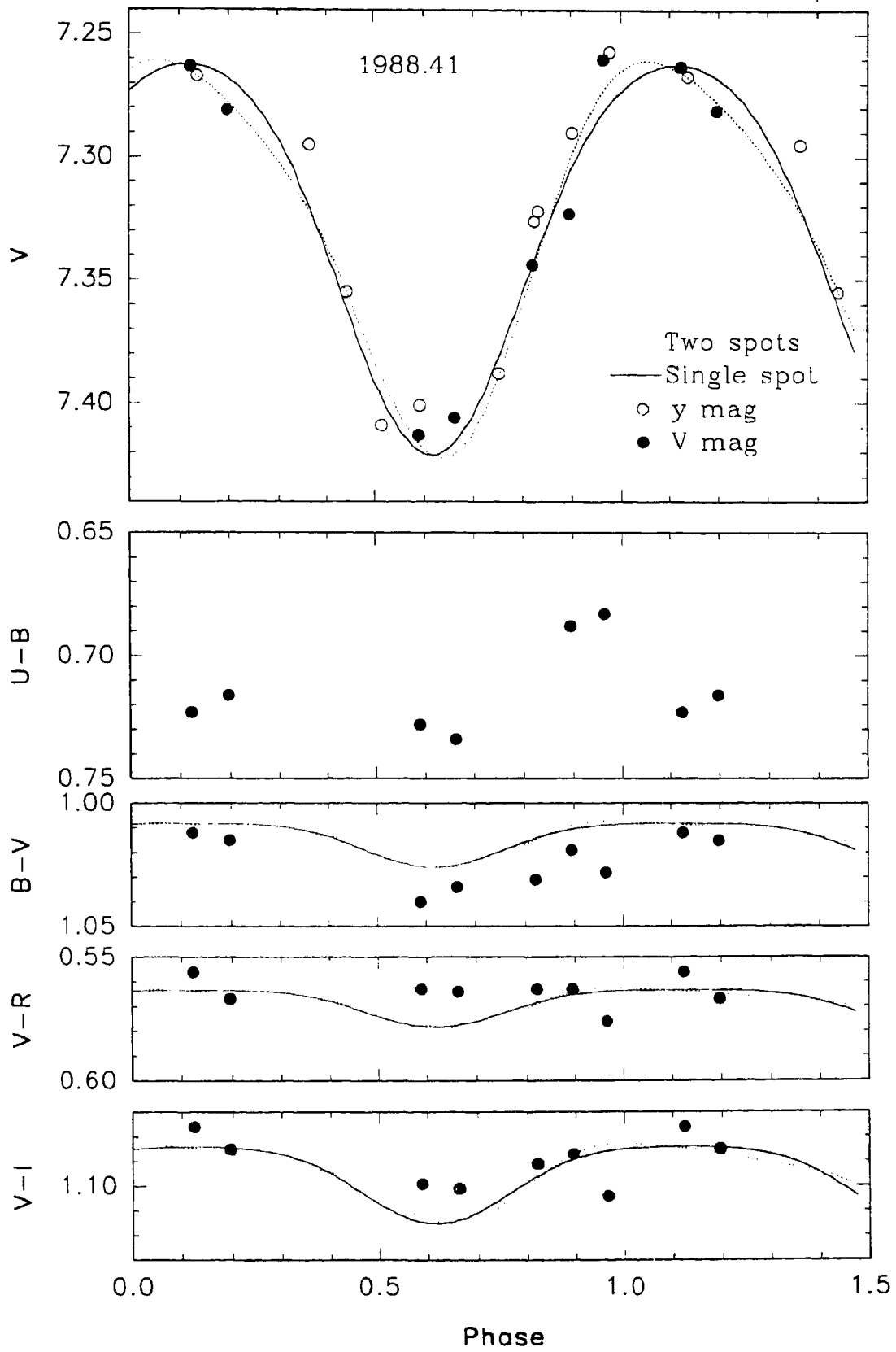


Fig. 6. Plots of V, U-B, B-V, V-R and V-I of HD 81410.

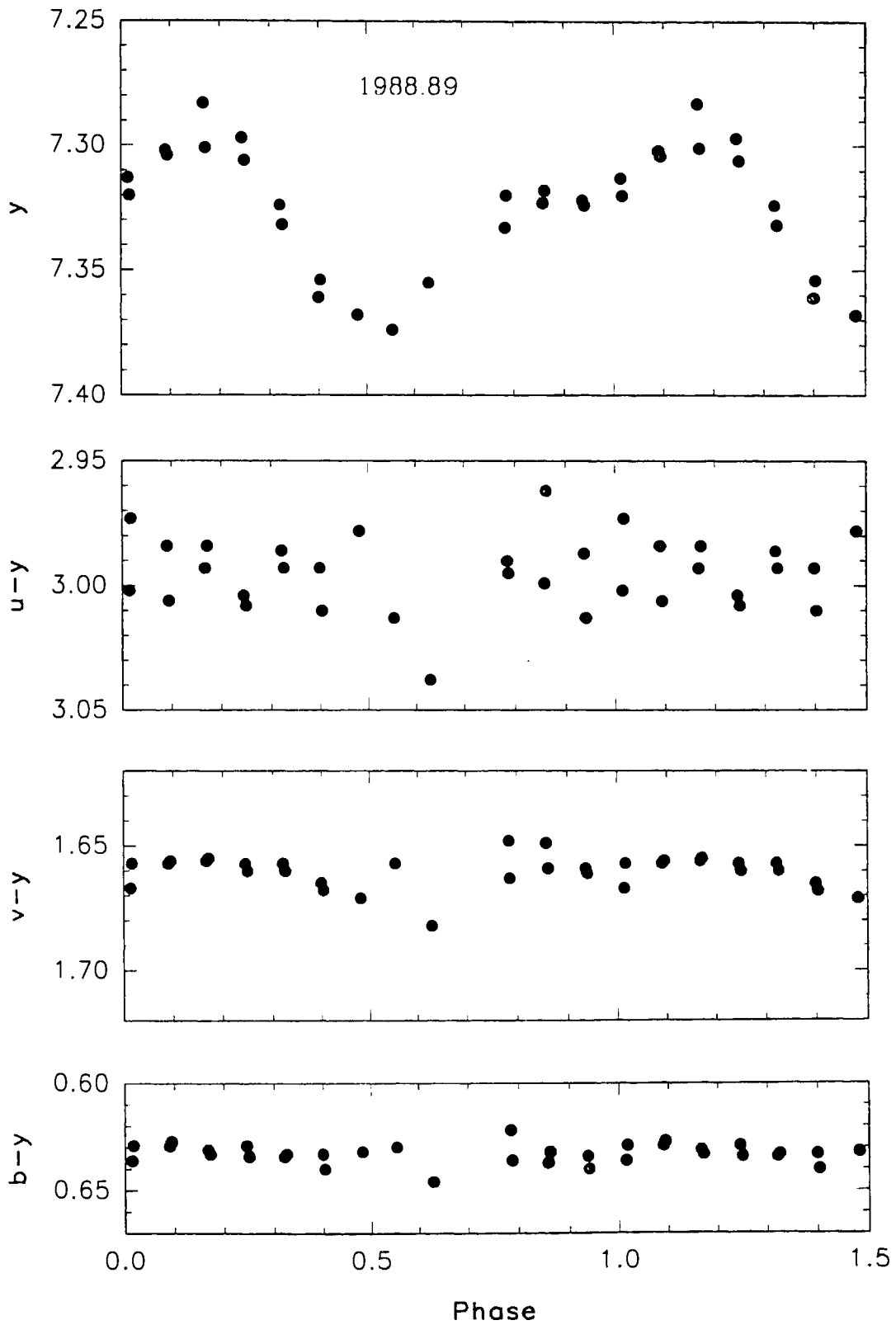


Fig. 7. Plots of y , $u-y$, $v-y$ and $b-y$ of HD 81410.

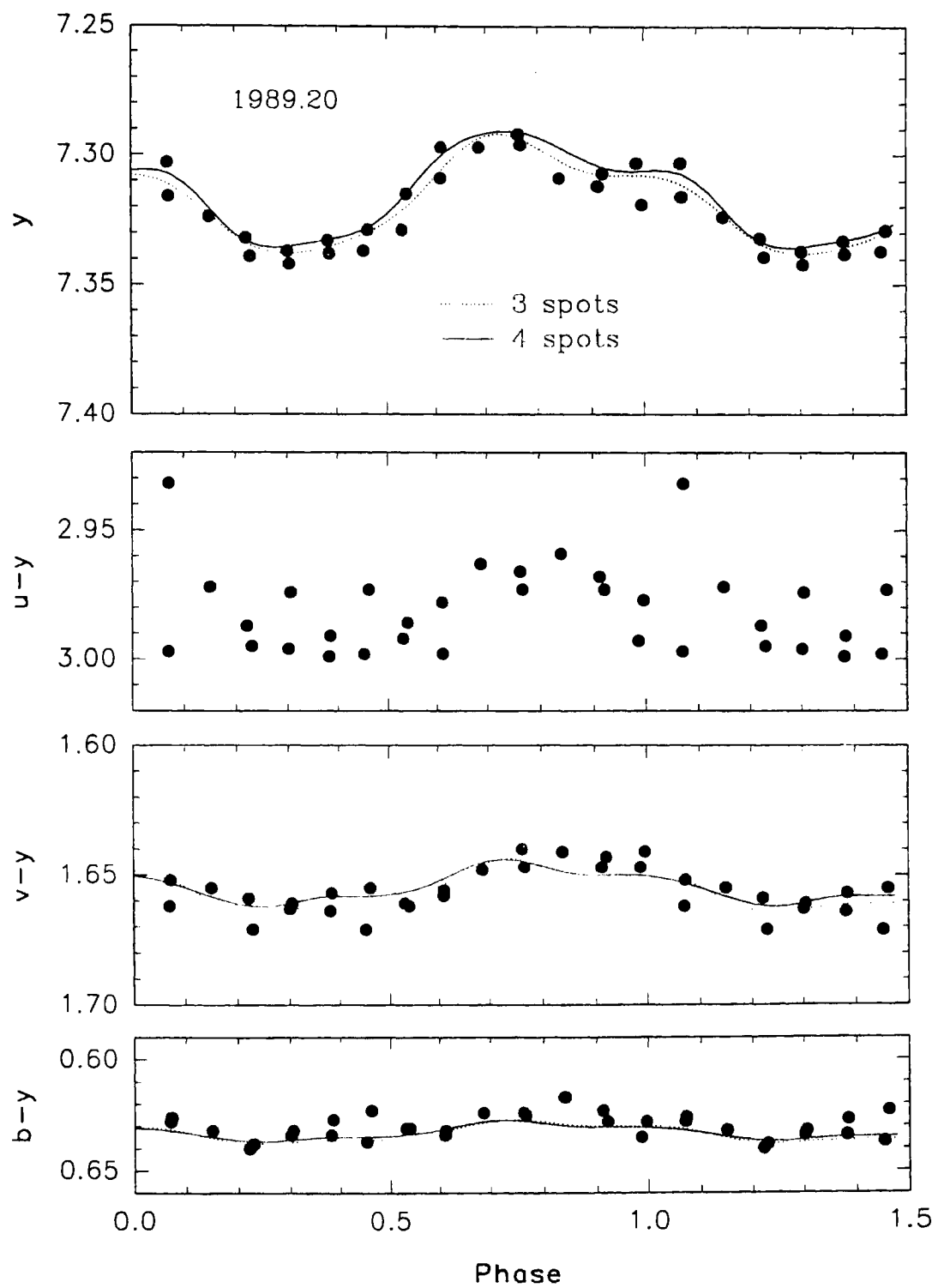


Fig. 8. Plots of y , $u-y$, $v-y$ and $b-y$ of HD 81410.

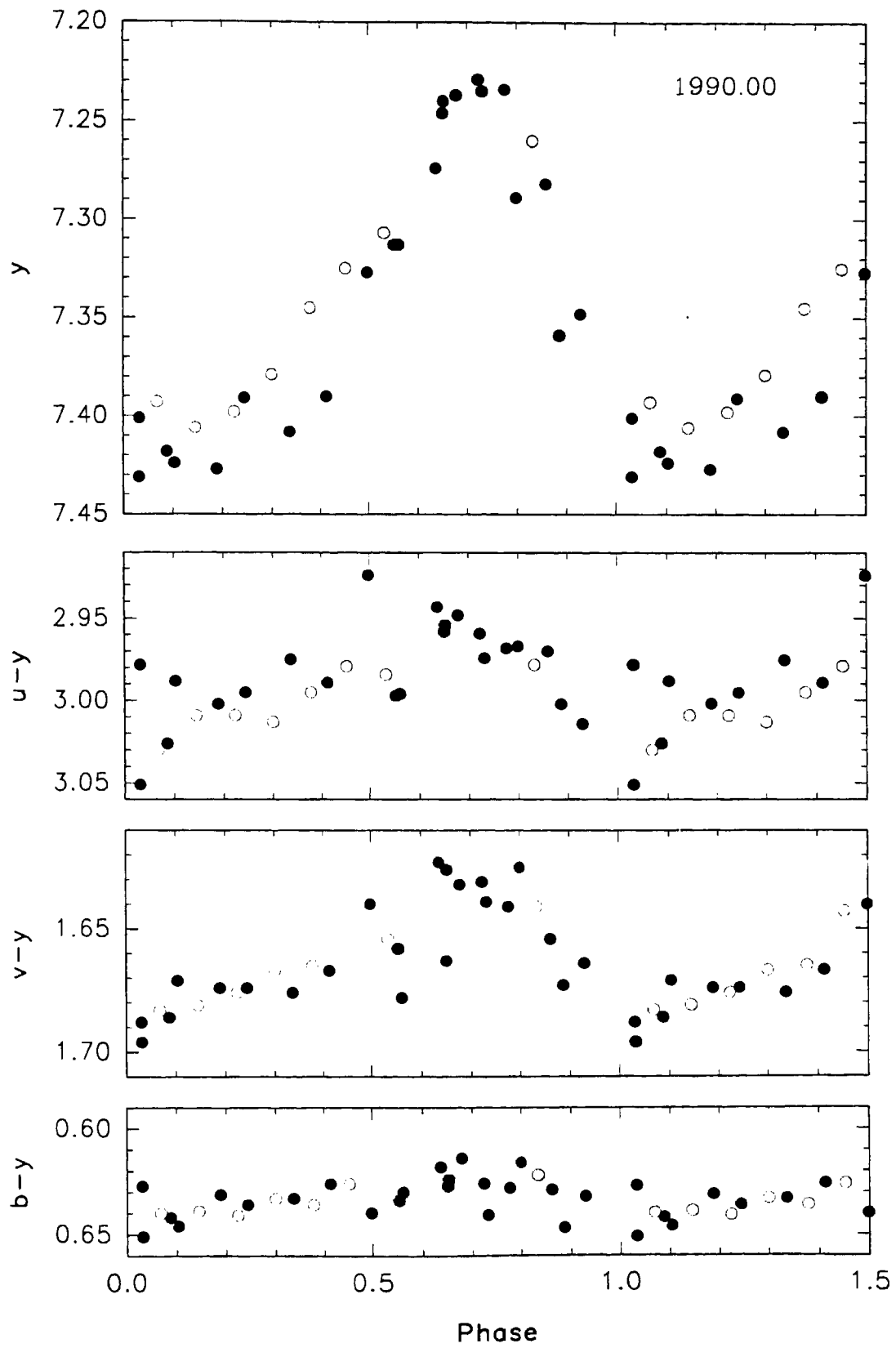


Fig. 9. Plots of y , $u-y$, $v-y$ and $b-y$ of HD 81410.

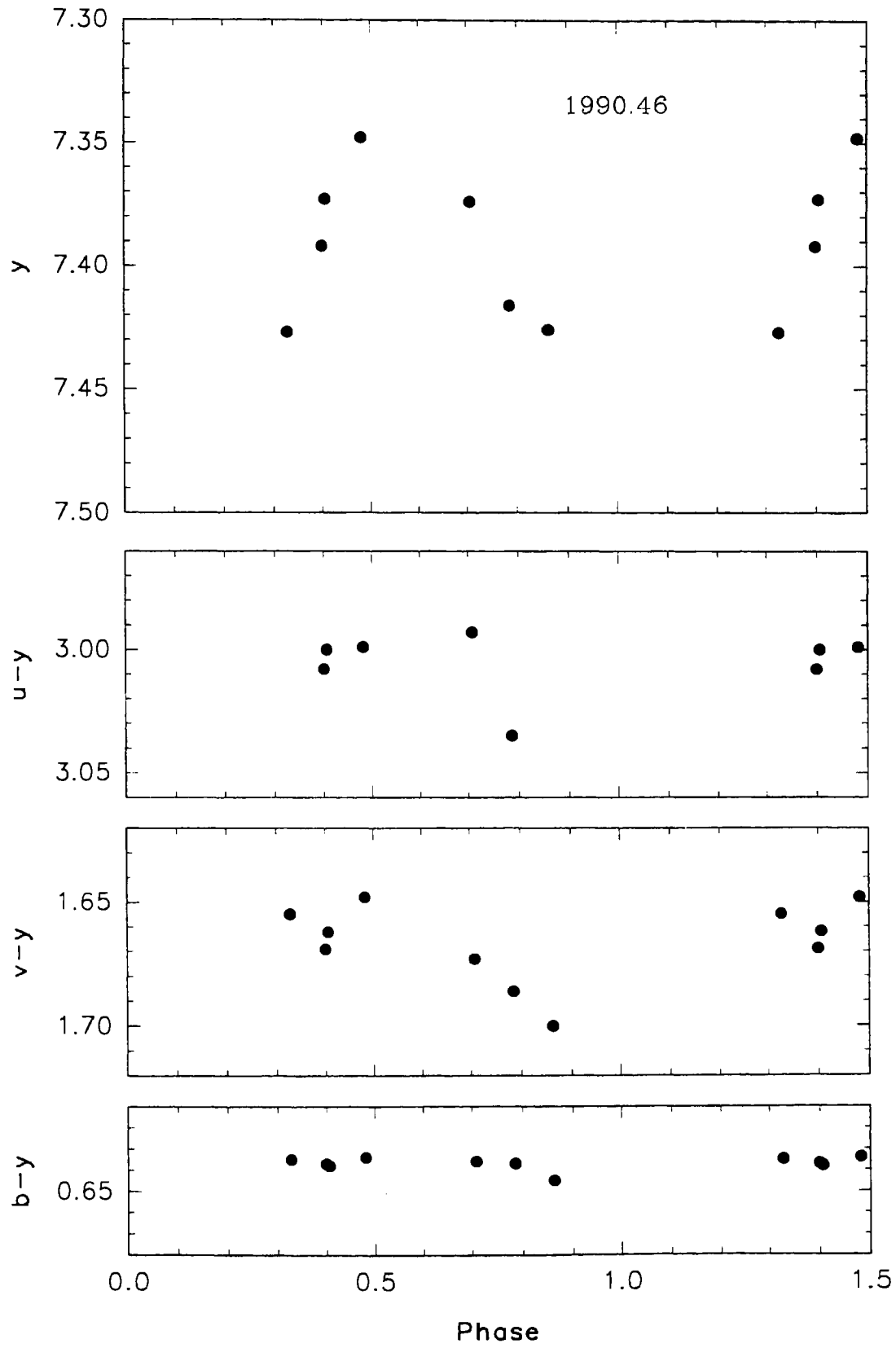


Fig. 10. Plots of y , $u-y$, $v-y$ and $b-y$ of HD 81410.

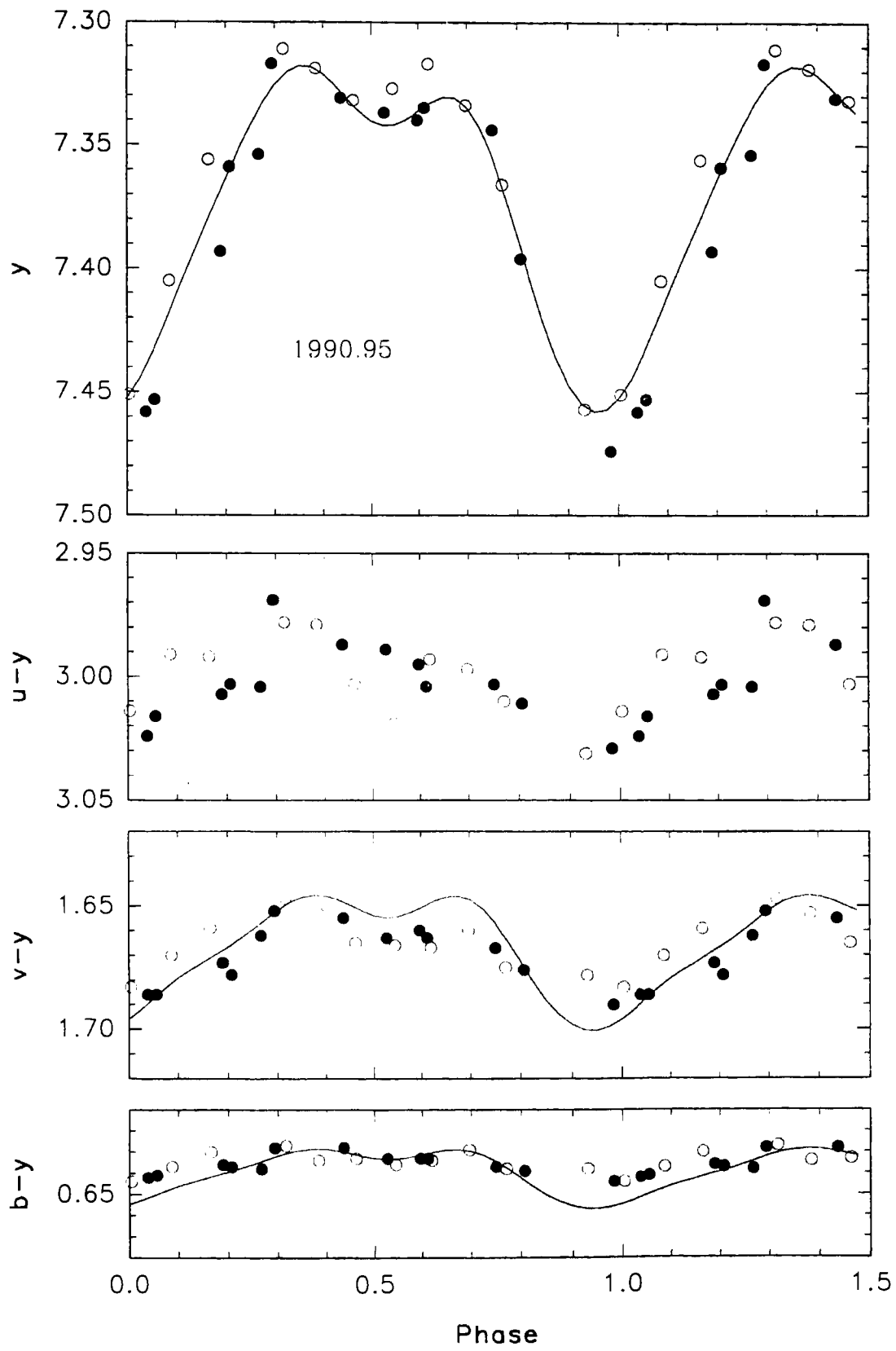


Fig. 11. Plots of y , $u-y$, $v-y$ and $b-y$ of HD 81410.

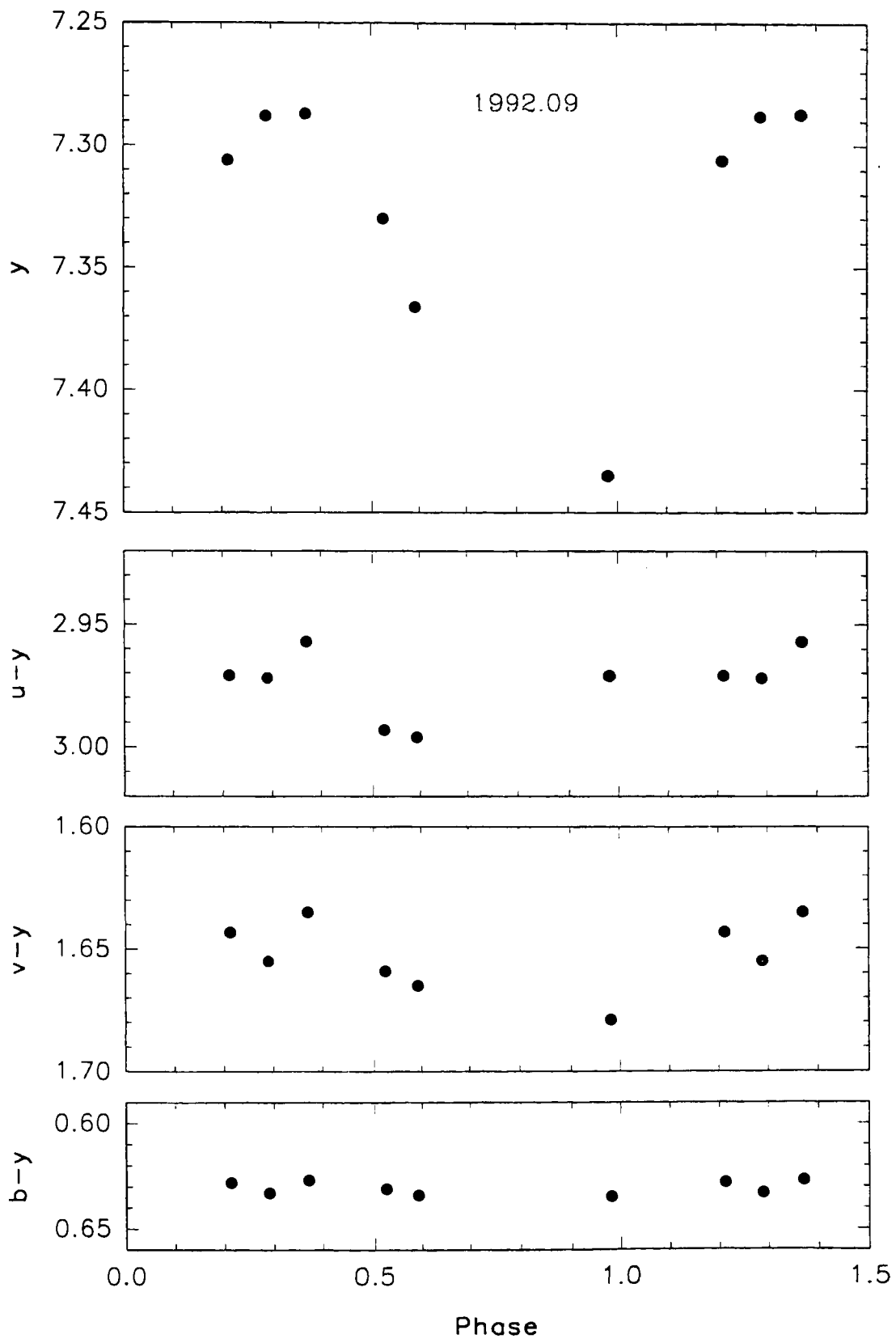


Fig. 12. Plots of y , $u-y$, $v-y$ and $b-y$ of HD 81410.

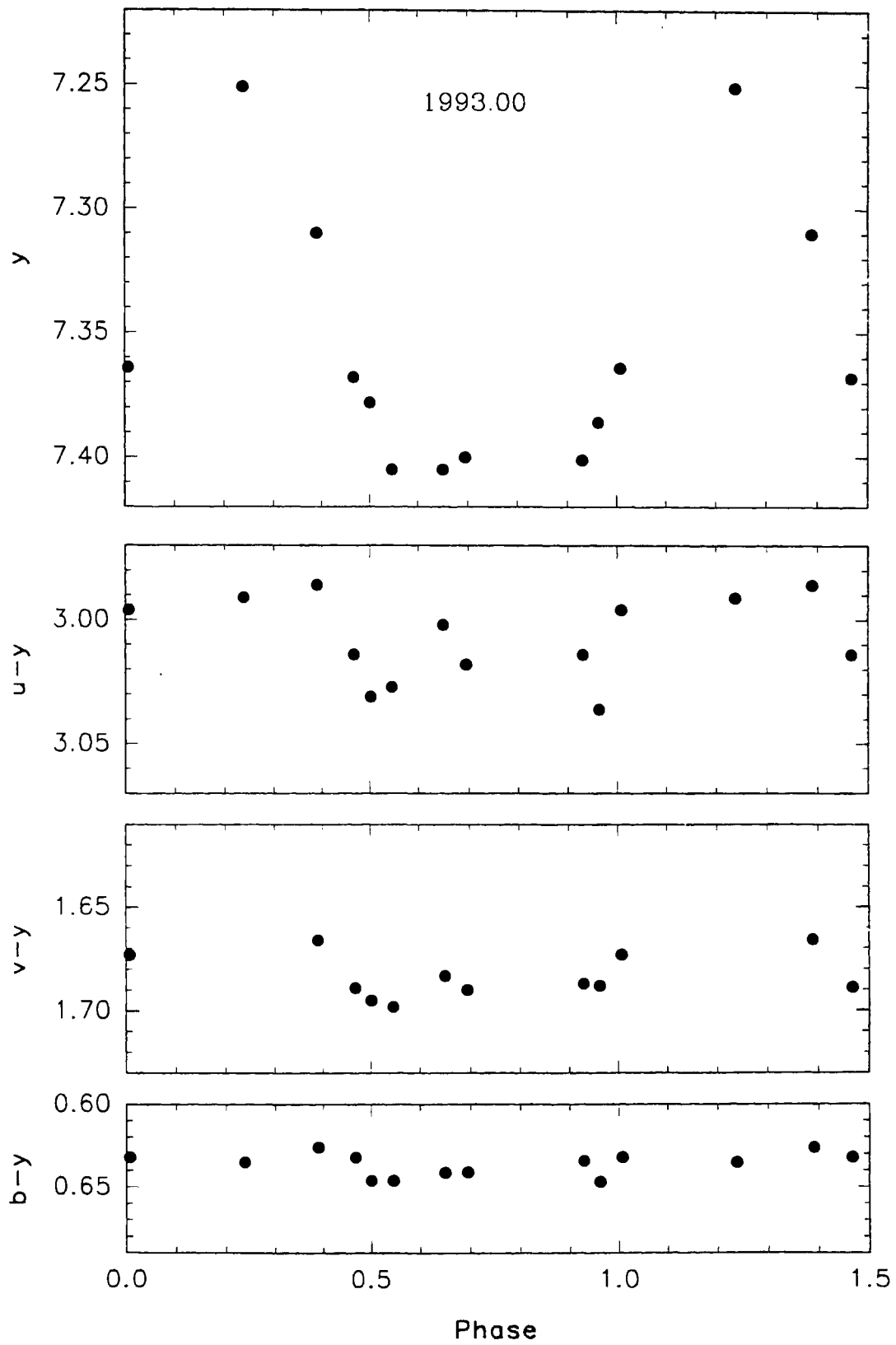


Fig. 13. Plots of y , $u-y$, $v-y$ and $b-y$ of HD 81410.

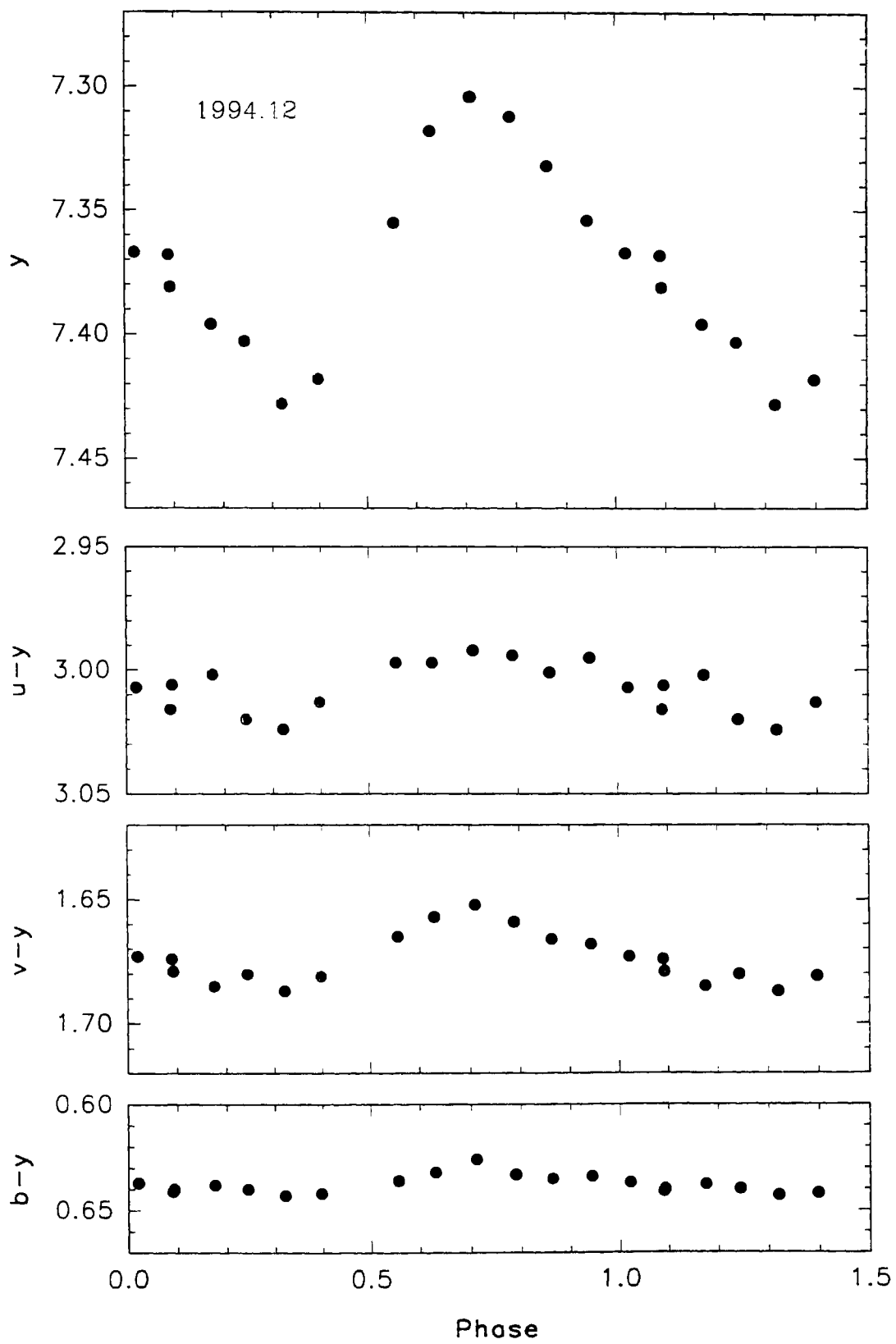


Fig. 14. Plots of y , $u-y$, $v-y$ and $b-y$ of HD 81410.

magnitudes V and y , and the colours $U - B$, $B - V$, $V - R$, $V - I$, $u - y$, $v - y$ and $b - y$ derived from the magnitudes, given in Tables 3 and 4. The mean epochs of observations are indicated in the corresponding figures.

All the photometry of HD 81410 available in the literature were also re-plotted using the above-mentioned ephemeris. The photometric parameters, the maximum and minimum magnitudes, V_{max} and V_{min} , the phase of the light minimum ϕ_{min} , and the amplitude of light variation were read directly from the all the graphical plots, including those presented in Figures 2–14, and are given in Table 5.

Table 5. Photometric characteristics of HD 81410

Epoch	Amplitude	V_{max}	V_{min}	ϕ_{min}	References
1971.17	0.430	7.520	7.950	0.00	Eggen (1973)
1972.20	0.440	7.450	7.890	0.90	Eggen (1973)
1978.98	0.270	7.430	7.700	0.85	Lloyd Evans & Koen (1987)
1980.05	0.145	7.460	7.630	0.60	Lloyd Evans & Koen (1987)
1981.10	0.145	7.470	7.615	0.45	Raveendran et al. (1982)
				0.84	
1982.00	0.090	7.510	7.600	0.80	Lloyd Evans & Koen (1987)
1985.04	0.153	7.410	7.563	0.45	Present study
1987.29	0.105	7.300	7.405	0.95	Present study
				0.45	
1988.01	0.130	7.280	7.410	0.61	Present study
				0.90	
1988.23	0.117	7.288	7.405	0.62	Present study
1988.41	0.145	7.260	7.405	0.60	Present study
1988.89	0.091	7.283	7.374	0.55	Present study
				0.95	
1989.12	0.060	7.300	7.360	0.45	Cutispoto (1993)
				0.85	

Table 5. continued

Epoch	Amplitude	V_{max}	V_{min}	ϕ_{min}	References
1989.20	0.046	7.294	7.340	0.30 0.85	Present study
1990.00	0.195	7.230	7.425	0.15	Present study
1990.46				0.10	Present study
1990.95	0.156	7.314	7.470	0.98 0.52	Present study
1992.09	0.148	7.287	7.435	0.85	Present study
1993.00	0.150	7.250	7.400	0.55	Present study
1994.12	0.120	7.305	7.425	0.32	Present study

The evolution of star spots in RS CVn systems is usually analyzed from the temporal behaviour of the phase of light minimum and amplitude of light curves. The ϕ_{min} gives an idea of the longitude of the spot group and the amplitude together with V_{max} and V_{min} indicate the extent of activity of the spot group.

Starting in 1971 with the observations of Eggen (1973), HD 81410 has been observed during a total of 20 seasons, including the present 15 seasons. The light curves of HD 81410 show two minima quite often, indicating the presence of two prominent and well-separated longitudes where starspots are formed. The shape of the light curve changes within a few orbital cycles. Cutispoto's (Pallavicini 1993) observations during November-December 1987 showed that the light curve had a single minimum and was almost sinusoidal. But the observations obtained after about a month, plotted in Figure 4, show a highly asymmetric light curve with two minima. The light curves obtained during the closely spaced epochs 1988.01, 1988.23, 1988.41, 1988.89, and 1989.20, which are plotted Figures 4–9, enable us to study the short-term variability of the active regions in HD 81410. The light curve changed from a double minima to a single minimum and again to double minima during 1988; all the while the deeper minimum remained more or less at the same

phase, between $0.^{\text{P}}5$ and $0.^{\text{P}}6$. The light curve of 1993.00, plotted in Figure 13, shows a flat minimum extending over almost half the photometric phase from $0.^{\text{P}}5$ to $1.^{\text{P}}0$.

The variations in $U - B$, $B - V$, $V - R$ and $V - I$ shown by HD 81410 are in phase with the V light curve in the sense that the colours tend to be redder at the light minimum. The amplitude of variation is maximum in $V - I$ colour. The colors $u - y$, $v - y$, and $b - y$ also show variation over the photometric phase in the same sense as the broadband colours with $v - y$ showing the largest amplitude.

Thus sudden changes in the location of spot groups happen within a short time. It is also noticed that the phase at which the minimum occurs also changes within a couple of orbital cycles (see Figure 9). From this behaviour we can infer that the deeper minimum that lasted almost an year at the same longitude is caused by a rather long-lived spot group and the short-term changes in ϕ_{min} are caused by short-lived spot groups. During this period both V_{max} and V_{min} also showed slight variations indicating minor changes in the activity of individual spots in the spot group.

4.1.5. The brightness at light maximum and minimum

Figure 15a is a plot of V_{max} and V_{min} , the brightness at light maximum and minimum, against the corresponding mean epoch of observations. The length of the vertical line corresponds to the amplitude of the light curve of that epoch. The largest amplitude of light variation so far observed occurred during 1971 and 1972 (0.45 mag) and the smallest during March 1989 (0.05 mag). Both V_{max} and V_{min} show a large range in magnitudes. The unspotted brightness is an important parameter in quantitative spot modeling. This can be determined if photometry spanning over a large time interval is available. As seen from Table 5, HD 81410 has been observed photometrically almost every year starting from 1978 till 1994. The maximum $V_{max} = 7.23$ mag observed during 1990 probably corresponds to the unspotted photospheric magnitude. A inspection of Figure 15a shows that during the period 1971–1985 the V_{max} remained more or less constant around 0.20 mag below the maximum, whereas the V_{min} monotonically became brighter from 1971

till 1987. The increase in V_{min} during this interval was more than 0.5 mag. After 1987 both V_{max} and V_{min} did not change appreciably, even though there were smaller fluctuations in their values.

The total range in brightness shown by HD 81410, in the sense V_{max} (brightest) minus V_{min} (faintest), is around 0.70 mag. This is comparable to that observed in active RS CVn systems like II Peg and DM UMa (Mohin & Raveendran 1993, 1994), and therefore, the V_{min} observed in 1971 by Eggen (1973) is probably close to the saturation value.

From 1971 to around 1985 the observed V_{max} of HD 81410 was about 0.20 mag below the probable unspotted magnitude quoted above. Hence there might have existed a region of activity that was always visible apart from that that was needed for the observed light modulation. Such a situation can happen if (a) a spot group is located near the polar region, or (b) if there is a component of the activity which is uniformly distributed across the entire longitudes. After 1985 V_{max} became brighter by almost 0.20 mag. A drastic change might have happened in the activity of the star around 1985 with a substantial reduction in the overall spot activity.

4.1.6. Phase of light minimum

Table 5 shows that seven light curves out of twenty obtained display two minima, implying a highly asymmetrical surface brightness distribution. The light curves of HD 81410, plotted in Figures 2–14 seldom shows a flat topped light curve with V_{max} close to its maximum observed value, indicating that the spot group responsible for the light modulation has a large longitudinal extent. Hence ϕ_{min} determined from the light curve gives the effective longitude of the spot or spot group. Similarly, it is reasonable to expect a large latitudinal extent also for the spots. Figure 15b is a plot of the phase of light minimum against the corresponding mean epoch of observations. The migration of ϕ_{min} , arising from a difference in the orbital and photometric periods, that are usually observed in RS CVn systems, is not at all seen in the case of HD 81410. This implies that the effective latitude of the spot or spot groups is in synchronous rotation with the orbit.

It is interesting to note from Figure 15b that irrespective of the shape

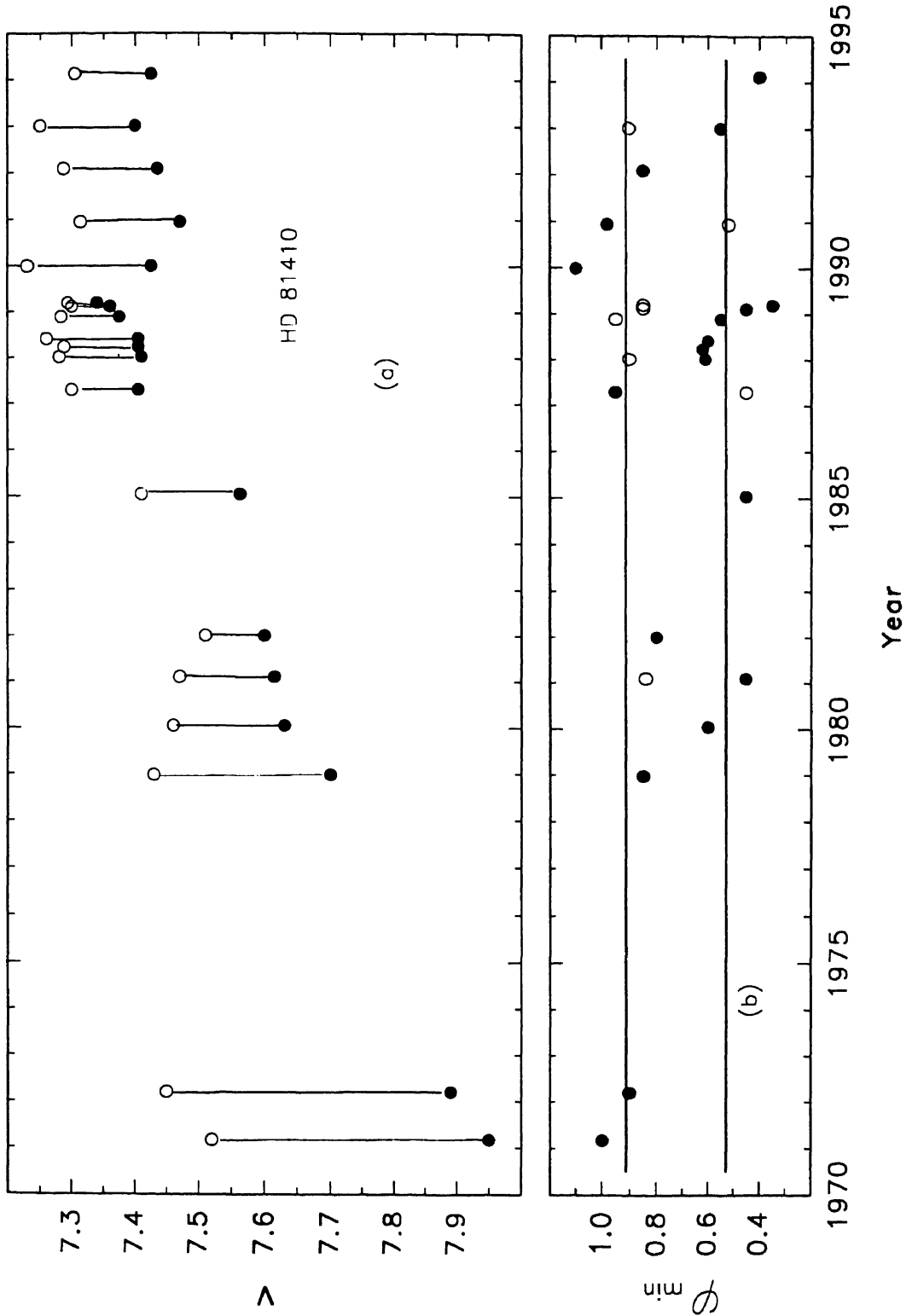


Fig. 15 (a). Plots of V_{max} (open circles) and V_{min} (filled circles) against the mean epoch. (b) Plot of phase minimum against the secondary minimum. Open circles denote the secondary minimum

or amplitude of the light curve there probably exists two preferred effective longitudes about which spots are generally formed, one around $0^{\text{p}}.50$ and the other around $0^{\text{p}}.90$. Whenever the light curves shows two minima, one minimum occurs $\sim 0^{\text{p}}.50$ the other occurs $\sim 0^{\text{p}}.90$. The scatter about these values seen in the figure partly arises from the errors in the determination of ϕ_{min} because of the observational uncertainty in magnitudes and the large longitudinal extent of the light minimum. Probably small variations take place in the effective longitudes. A prominent spot group may contain several individual spots. The small fluctuations about the preferred longitudes, probably, arises as a result of a finite life-time for the individual spots. A similar behaviour has been observed in the long period RS CVn binary σ Gem (Jetsu 1995).

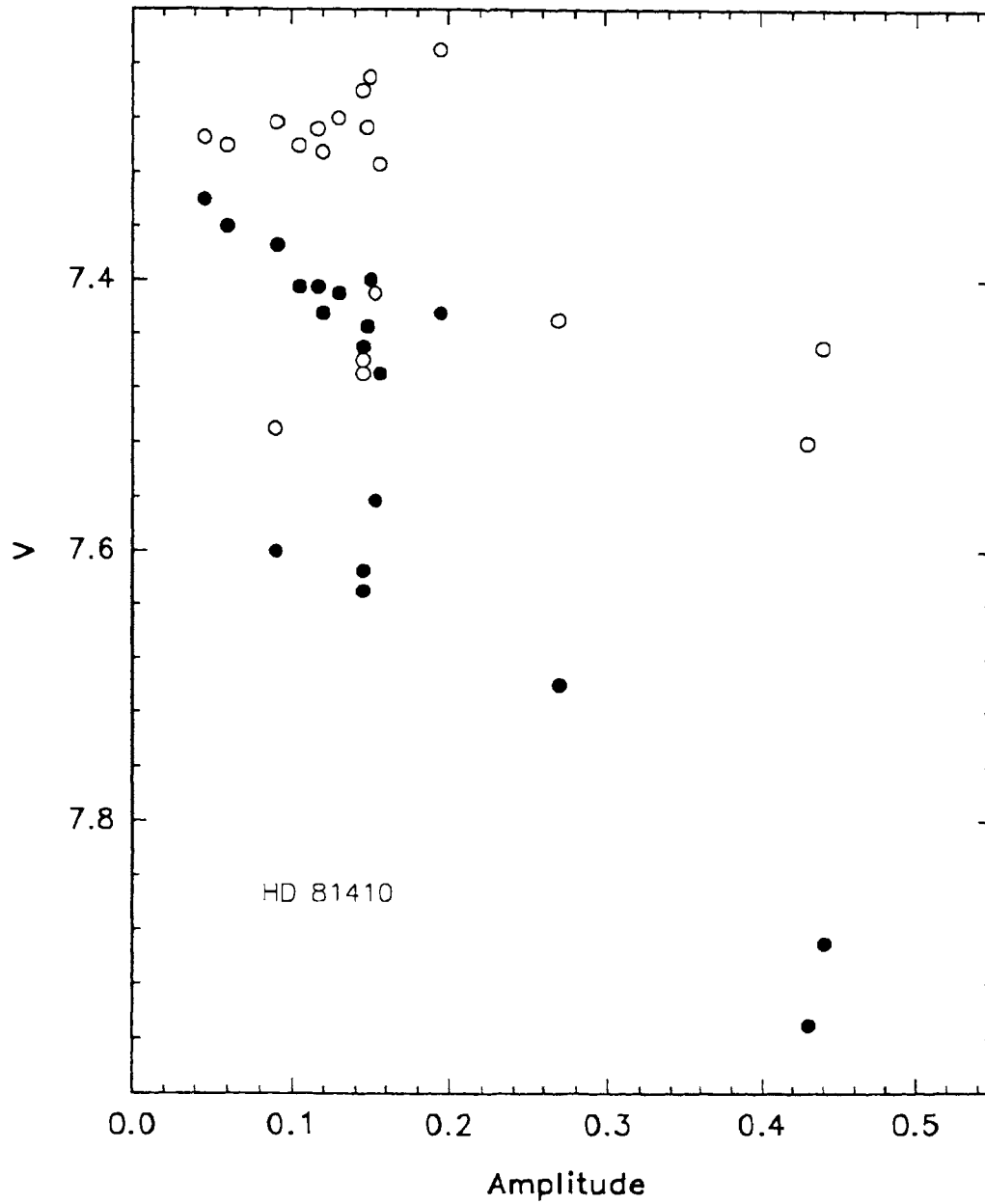
4.1.7. Amplitude of light variation

In Figure 16 we have plotted the brightness at maximum V_{max} and the brightness at minimum V_{min} given in Table 5 against the corresponding amplitudes. There is an indication that at amplitudes larger than 0.2 mag an increase in amplitude occurs as a result of a decrease in the brightness at light minimum; at amplitudes smaller than this apparently there is no such correlation. From the figure it is seen that at low amplitudes (< 0.1 mag) both the brightness at light maximum and minimum converge to the same value. Therefore a smaller amplitude, mostly likely, arises not from a reduction in the spot activity, but rather from a more uniform distribution of spots across the longitude.

4.1.8. Results of spot modeling

As mentioned in Chapter 3 modeling of a single light curve may not give definite results on the surface distribution and temperature of starspots. On the other hand, modeling of a series of light curves obtained over several consecutive seasons may provide meaningful information on the properties of spots.

HD 81410 is a non-eclipsing binary and hence its orbital inclination



is unknown. An uncertainty in the inclination will be directly reflected on the polar distance derived for the spots. Houk & Smith-Moore (1988) have assigned a spectral type of K2IV-V to HD 81410. The observed value of $V \sin i = 22 \text{ km s}^{-1}$ (Balona 1987) leads to a minimum value of $6R_{\odot}$ for the radius of the primary component, and hence indicates a high value for the inclination i . The large amplitude of light variation observed (~ 0.5 mag) also indicates a high value.

The unspotted brightness of the star in each wavelength band observed is an important parameter which has a direct effect on all the spot parameters, viz polar distance, radius and temperature. The problems associated with the assumption of the unspotted magnitudes have been discussed in detail by Poe & Eaton (1985). HD 81410 has been observed during a total of 20 seasons starting from 1971. The observations in U and u bands show a large scatter and therefore only those measurements in $BVRI$ and bvy bands were made use of in the derivation of spot parameters using the method described in § 3.4.. The following magnitudes, which are the brightest observed in the corresponding bands, are assumed to represent the unspotted values: $B = 8.240$, $V = 7.230$, $R = 6.650$, $I = 6.145$, $v = 8.860$, $b = 7.850$ and $y = 7.230$ mags.

The photospheric temperature was assumed to be 4900 K, consistent with the spectral type. Calculations were made with the same linear limb-darkening law for both the spots and unspotted photospheric regions. Mohin & Raveendran (1992) have shown that the spot parameters derived under such an assumption and the more general assumption that spotted and unspotted regions follow different quadratic limb-darkening laws differ only marginally and are well within the uncertainties involved in their determination. The linear limb-darkening coefficients in $BVRI$ bands were the same as those listed in § 3.3.. The coefficients in bvy bands, 0.91, 0.84 and 0.75, respectively, were derived by interpolation of the values given by Claret & Gimenez (1990).

The results of spot modeling are given in Table 6. The smooth curves in Figures 2-6, 8, 11 and 17 represent the computed light and colour curves. The observations plotted in Figure 17 were obtained by Cutispoto (1993) while

Table 6. Spot parameters derived from the light curves of HD 81410

Mean epoch	Polar distance (°)	Long. (°)	Radius (°)	Temp. (K)	Fract. area	σ (mag)
1985.04 ^a	9±1	161±1	54±2	4250±50	0.207	0.015
1985.04 ^b	32±	165±1	30±3	4357±130	0.067	0.010
1987.29	105±6	159±1	24±2	4209±45	0.042	0.005
	17±1	323±1	35±1	4209±45	0.092	
1988.01	22±2	199±2	46±4	4569±62	0.164	0.008
	84±15	337±2	24±2	4569±62	0.041	
1988.23	21±2	183±3	41±3	4508±50	0.130	0.009
	13±1	262±7	41±3	4508±50	0.041	
1988.41 ^c	20±1	222±2	28±1	3508±200	0.059	0.016
1988.41 ^d	37±4	244±5	20±1	3447±200	0.028	0.015
	14±4	160±9	20±1	3447±200	0.028	
1989.12	11±1	167±1	26±1	3594±44	0.050	0.006
	99±6	338±1	13±1	3594±44	0.012	
1989.20 ^e	38±5	73±3	33±4	4666±47	0.077	0.006
	33±4	188±3	33±4	4666±47	0.077	
	108±6	320±3	33±4	4666±47	0.077	
1989.20 ^f	51±10	47±13	23±4	4568±88	0.039	0.007
	83±16	123±10	23±4	4568±88	0.039	
	75±7	200±7	23±4	4568±88	0.039	
	90±8	308±7	23±4	4568±88	0.039	
1990.95	29±5	54±4	31±3	4460±89	0.069	0.015
	56±9	322±3	31±3	4460±89	0.069	
	105±4	194±3	31±3	4460±89	0.069	

^a: The brightest magnitudes so far observed as the unspotted, ^b: The current maximum as the unspotted, ^c: Single spot, ^d: Two spots, ^e: Three spots, ^f: Four spots

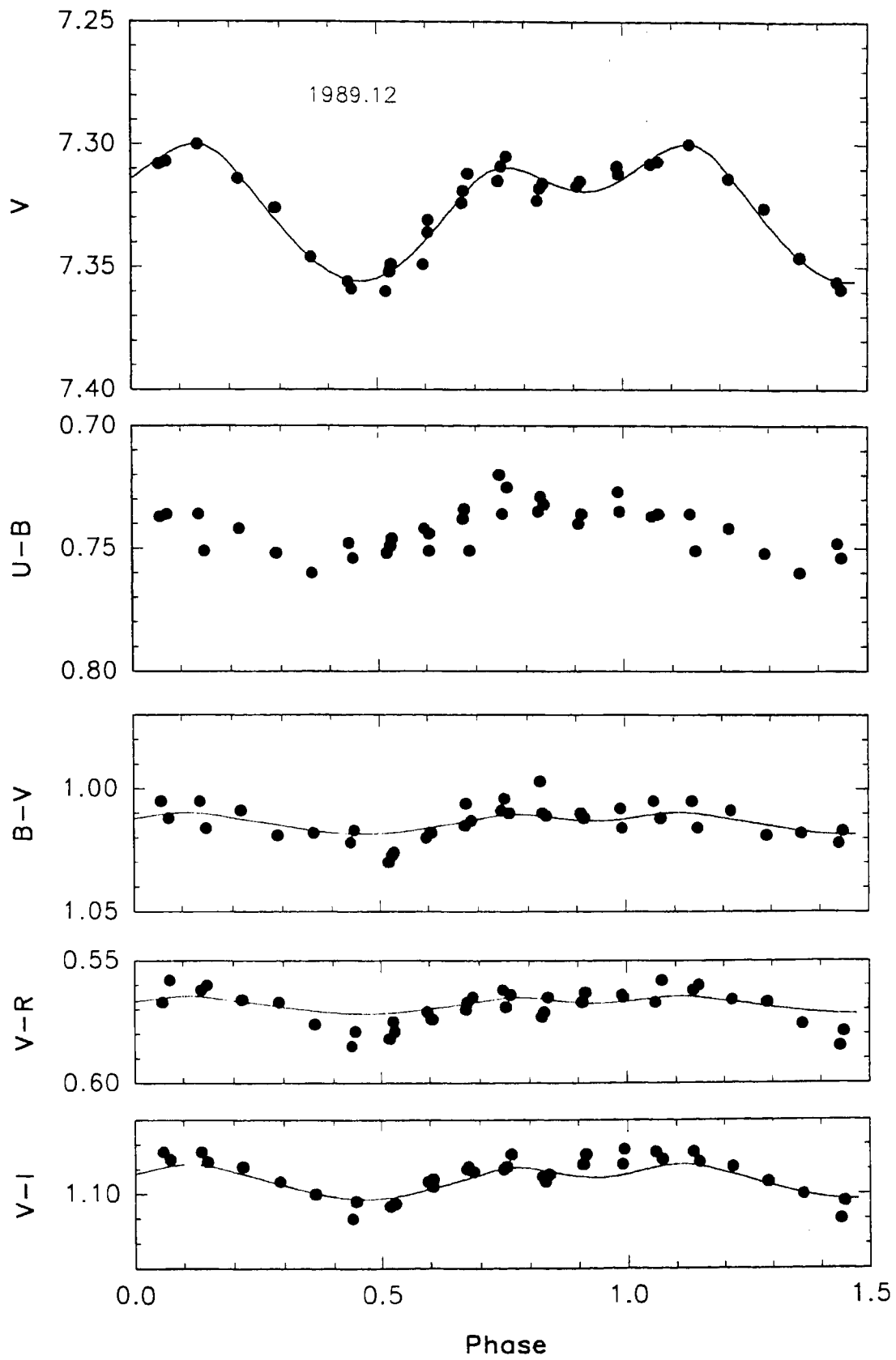


Fig. 17. Plots of V, U-B, B-V, V-R and V-I of HD 81410.

those in all the other figures are those listed in Tables 3 and 4. The computed curves in all cases closely approximates the observations. In general the standard deviations of fit σ are comparable to the observational errors.

The results presented in § 3.3. show that the spot parameters, polar distance and radius, and sometimes even longitudes derived from the observed light curves could completely misrepresent the actual situation, even when the computed light and colour curves computed from these parameters closely reproduce the observations; the only parameter less effected seems to be the spot temperature. This is amply demonstrated in Table 6.

For the observations obtained during 1985.04 (Figure 2) two solutions were obtained : (i) with the brightest magnitudes so far observed as the unspotted and (ii) the maximum brightness observed during this season as the unspotted. The latter solution gives a better fit close to light minimum while the former gives a better representation close to light maximum. The second solution is better if overall fit is considered. The temperatures corresponding to the two cases are within the uncertainties involved.

The single- and two-spot solutions give almost similar overall fit to the observations obtained during 1988.41 (Figure 6). In the latter solution both the spots were assumed to be of the same radius because the light curve shows a single well-defined minimum. Again the spot temperatures in the two cases agree mutually very closely.

The light curve obtained during 1989.20 (Figure 8) shows the smallest amplitude so far observed. It shows a broad and asymmetric light minimum. There is only a slight indication of a secondary minimum. In this case also two solutions were obtained, *viz* with three- and four-spot assumptions. The corresponding σ of fit are 0.006 mag and 0.007 mag. Both sets of computed curves closely match the observations. The temperature obtained in the two cases again agree mutually. In both cases the spots were assumed to be of the same radius.

The observations of Cutispoto (1993) plotted in Figure 17 were obtained about a month before the above mentioned observations. The corresponding light curve shows a slightly larger amplitude and a well-defined secondary minimum. The σ of fit is 0.006 mag similar to those for the solutions ob-

tained for the observations during 1989.20. It is interesting to see that the temperature in the two cases differ by ~ 1000 K; this is much larger than the error in their determination. In the light of the above results that the derived temperature of the equivalent circular spot(s) is less affected by the assumption on the number of spots it is tempting to conclude that the change in the spot temperature is real. The increase in the effective spot temperature from 1989.12 to 1989.20 could be due to either of the following reasons: (i) an intrinsic increase in the spot temperature occurred and (ii) the equivalent spot consists of several small spots whose the temperature did not change but in the latter case the individual spots in the group were more spread out than in the former case, *i.e.*, in the latter case the spots were less closely packed than in the former case. Here it may be noted that in the former case the observations were in *BVRI* bands while in the latter they were in *vby*. However, it is unlikely that the difference in the temperature resulted because of this. The temperature obtained from the observations of 1985.04 and 1987.29 are similar; the former observations were made in *vby* bands whereas the latter were made in *BVRI* bands.

4.2. HD 127535

4.2.1. Introduction

HD 127535 (= V841 Cen) is one of the most active RS CVn stars as evident from its strong and variable chromospheric $Ca II H$ & K and $H\alpha$ emissions (Weiler & Stencel 1979; Collier 1982). The visible component has been assigned a spectral type K2 IV-Ve by Houk & Cowley (1975). Weiler & Stencel (1979) classified HD 127535 as an RS CVn system on the basis of the presence of strong $Ca II H$ & K emissions in its spectrum. From a spectroscopic study, Collier (1982a) found that the star is a six day period single-lined spectroscopic binary, and derived its orbital parameters. HD 127535 is one of the few RS CVn systems which exhibit $H\alpha$ in emission. Additional radial velocity measurements were obtained by Innis et al. (1985) who refined the orbital period to 6.015 days. They observed HD 127535 also as part of a radio survey of southern active chromosphere stars at 5, 8.4 and 22 GHz. The star could not be detected at 5 GHz, possibly because of the confusion due to its angular proximity to the galactic plane. However, it was detected at 22 GHz and found to be a variable source (20-60 mJy). These observations together with the photometry obtained two orbital cycles before suggested a possible correlation between the radio emission and the spot visibility. Later, Vaghan & Large (1987) detected quiescent emission at 843 MHz in HD 127535. During the ROSAT All-Sky survey with the Position Sensitive Proportional Counter, Dempsey et al. (1993) detected the star as a strong X-ray source. In an extensive survey of the $Li I 6708 \text{ \AA}$ line in RS CVn binaries, Pallavicini et al. (1992) found that HD 127535 has a large Lithium abundance ($n(\text{Li}) = 1.15$) which, they suggested, could be due to a real decrease of Li depletion while the star was on the main sequence.

The photometric observations obtained during 1981 by Collier (1982b) showed that HD 127535 exhibits a six day period, quasi-sinusoidal light variation with an amplitude of 0.07 mag in V . Udalsky & Geyer (1984), who carried out photometric observations in April 1984, found that the amplitude had increased to 0.23 mag and the phase of light minimum had shifted by

more than 0.³. Photometry of HD 127535 obtained by Innis et al. (1985) during August 1984 and February-April 1985 showed that the light curve had changed remarkably within 20 or so orbital cycles from April 1984. The observations by Bopp et al. (1986) obtained during 1985 showed that the light variation had an amplitude of 0.20 mag and that the maximum observed brightness decreased by 0.15 mag compared to the 1984 values. Mekkaden & Geyer (1988), who made observations during 1987, found that the light variation was quasi-sinusoidal, and the amplitude and phase of light minimum differed drastically from those observed during the previous occasions. Such variations are typical of RS CVn systems and are caused by the changes in the location and formation of spots on the stellar surface.

4.2.2. Photometry

HD 127535 was observed on a total of 83 nights over five observing seasons 1987 (12 nights), 1988 (12 nights), March 1989 (27 nights), July-August 1989 (21 nights) and August 1990 (10 nights). During the first two runs the observations were done in *UBVRI* and during the next three seasons in *uvby*. HD 128227 and HD 128618 were used as the comparison stars, and all the observations were done differentially with respect to HD 128227 and transformed to the corresponding standard systems. The mean *UBVRI* magnitudes of HD 128227 and HD 128618 obtained from the present photometry are given in Table 7a, and the mean *uvby* magnitudes of the former are given in Table 7b. The differential magnitudes of HD 127535 were converted to *UBVRI* and *uvby* magnitudes using the values of HD 128227 given in Tables 7a and b, and are listed in Tables 8 and 9.

4.2.3. Photometric period

From an analysis of the radial velocity measurements of HD 127535 obtained by him, Collier (1982a) derived the orbital period as six days. Later, he found from the photometry that light variability also showed the same periodicity (Collier 1982b). However, Udalsky & Geyer (1984), and Cutispoto (1990) derived slightly shorter photometric periods, 5.97 days and 5.929 days,

respectively. In order to derive an accurate photometric period one requires

Table 7a. *UBVRI* magnitudes of the comparison stars

Star	<i>U</i>	<i>B</i>	<i>V</i>	<i>R</i>	<i>I</i>
HD 128227	10.195 ±0.009	9.388 ±0.005	8.319 ±0.005	7.754 ±0.005	7.222 ±0.004
HD 128616	11.110 ±0.015	9.493 ±0.006	8.028 ±0.007	7.254 ±0.005	6.554 ±0.005

Table 7b. *uvby* magnitudes of HD 128227

<i>u</i>	<i>v</i>	<i>b</i>	<i>y</i>
11.458 ±0.009	10.019 ±0.007	8.994 ±0.005	8.315 ±0.004

frequent observations spread over a sufficiently long time interval compared to the period involved. Of the five sets of data presented in Tables 8 and 9, two sets, namely those obtained during March 1989 (JD 2447590–616) and July–August 1989 (JD 2447709–71), are suitable for a period determination. The *V* observations of these two sets of data were subjected to the method of period determination as outlined in § 2.4. Figure 18 shows a plot of the quantity *Q*, taken as the measure of scatter in the phase–magnitude diagram, against the trial period for the first set of data. The period corresponding to the minimum value of *Q* is 5.98 days. A similar exercise with the second set of data mentioned above yielded a period of 6.00 days. Since the uncertainties in the above periods are of the order of 0.01 day as a result of the short time baseline covered by the data, and since these periods themselves are very close to the orbital period of 6.015 days derived by Innis et al. (1985) from the

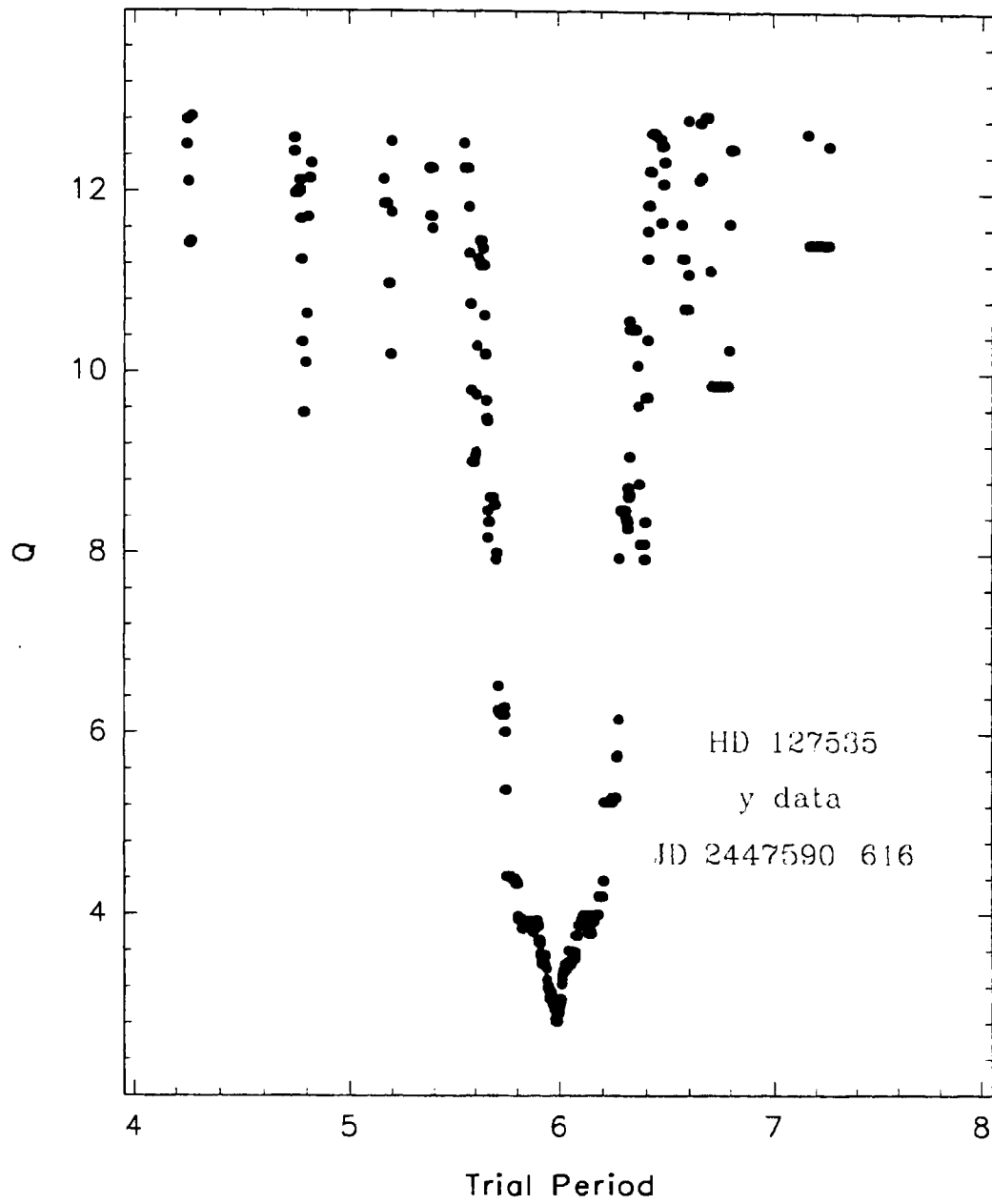


Fig. 18. Plot of Q, the measure of scatter in the magnitude-phase diagram, against trial period.

Table 8. *UBVRI* magnitudes of HD 127535

J.D. 2440000.+	<i>U</i>	<i>B</i>	<i>V</i>	<i>R</i>	<i>I</i>
6896.661	10.571	9.782	8.703	8.085	7.492
6896.813		9.768	8.695	8.075	7.483
6897.602	10.541	9.751	8.674	8.052	7.465
6897.679	10.541	9.746	8.663	8.056	7.459
6897.800	10.568	9.769	8.684	8.058	7.476
6898.599	10.590	9.786	8.699	8.076	7.482
6898.747	10.580	9.794	8.701	8.088	7.493
6898.864		9.801	8.714	8.093	7.504
6899.589	10.612	9.818	8.742		7.531
6899.726	10.629	9.818	8.744	8.133	7.532
6899.844		9.830	8.756	8.134	7.547
6900.601		9.870	8.774	8.152	7.556
6901.601			8.760		
6902.589	10.597	9.786	8.700	8.089	7.487
6902.735	10.576	9.781	8.704	8.086	7.491
6903.586	10.552	9.756	8.692	8.055	
6903.738	10.549	9.750	8.684	8.047	7.461
6903.854	10.516	9.746	8.673	8.041	7.459
6904.586	10.591	9.776	8.708	8.086	7.483
6904.731	10.601	9.789	8.720	8.087	7.497
6905.588	10.624	9.813	8.744	8.131	7.536
6906.771	10.683	9.865	8.766	8.132	7.533
6906.810	10.681	9.860	8.769	8.149	7.536
6907.821	10.649	9.838	8.751	8.119	7.532
7296.560	10.518	9.724	8.655	8.042	7.463
7296.727	10.493	9.683	8.638	8.042	7.464
7298.583	10.496	9.717	8.647	7.994	7.418

Table 8. continued

J.D. 2440000.+	<i>U</i>	<i>B</i>	<i>V</i>	<i>R</i>	<i>I</i>
7299.548	10.525	9.717	8.637	8.023	7.436
7300.655	10.578	9.706	8.588	7.954	7.343
7304.577	10.524	9.719	8.661	8.063	7.470
7304.700	10.508	9.727	8.663	8.050	7.470
7304.791	10.535	9.725	8.661	8.051	7.461
7305.511	10.492	9.697	8.636	8.021	7.447
7305.640	10.503	9.718	8.639	8.026	7.447
7305.760	10.498	9.705	8.635	8.022	7.435
7307.575	10.417	9.637	8.563	7.972	7.394
7307.807	10.421	9.601	8.548	7.922	7.388
7308.526	10.586	9.780	8.650	8.038	7.460
7309.574	10.596	9.801	8.698		
7309.615	10.604	9.801	8.714		
7311.625	10.514	9.751	8.641		
7313.602	10.431	9.632	8.559		
7315.601	10.600	9.808	8.707		

radial velocity measurements available over a much longer time base-line, for the present analysis the more accurate orbital period was used.

4.2.4. Light Curves

The Julian days of observation were converted to photometric phases using the ephemeris

$$JD(Hel) = 2444653.737 + 6.^d015 E,$$

where the initial epoch corresponds to the time of maximum radial velocity and period is the orbital period (Innis et al. 1985). The observations listed in Table 8 and 9 are plotted in Figures 19–23. The mean epochs of observation

Table 9. *uvby* magnitudes of HD 127535

J.D. 2440000.+	<i>u</i>	<i>v</i>	<i>b</i>	<i>y</i>
7590.866	11.686	10.319	9.253	8.576
7591.872	11.790	10.441	9.357	8.675
7592.778	11.825	10.427	9.344	8.661
7592.887	11.781	10.420	9.335	8.655
7593.715	11.740	10.380	9.298	8.618
7593.837	11.751	10.373	9.292	8.614
7594.741	11.651	10.292	9.224	8.553
7594.883	11.624	10.274	9.210	8.547
7595.741	11.587	10.224	9.165	8.501
7595.881	11.588	10.219	9.164	8.497
7596.738	11.683	10.313	9.240	8.565
7596.861	11.698	10.331	9.254	8.581
7597.726	11.832	10.442	9.355	8.677
7597.872	11.851	10.453	9.366	8.684
7598.765	11.806	10.427	9.340	8.689
7598.878	11.810	10.415	9.335	8.647
7599.749	11.737	10.375	9.296	8.618
7599.876	11.724	10.365	9.286	8.607
7600.773	11.646	10.289	9.223	8.550
7600.882	11.630	10.282	9.212	8.544
7601.724	11.581	10.235	9.170	8.503
7601.888	11.587	10.224	9.169	8.504
7602.753	11.653	10.306	9.243	8.568
7602.888	11.708	10.333	9.260	8.588
7603.698	11.793	10.433	9.341	8.660
7603.887	11.823	10.443	9.355	8.676
7604.799	11.763	10.402	9.327	8.647

Table 9. continued

J.D. 2440000.+	<i>u</i>	<i>v</i>	<i>b</i>	<i>y</i>
7605.759	11.722	10.371	9.296	8.615
7605.889	11.710	10.357	9.283	8.602
7606.758	11.640	10.298	9.229	8.560
7606.887	11.572	10.255	9.209	8.542
7607.736	11.569	10.196	9.153	8.499
7607.892	11.580	10.231	9.175	8.511
7608.690	11.662	10.301	9.233	8.557
7608.890	11.715	10.341	9.270	8.585
7609.691	11.799	10.424	9.350	8.669
7609.862	11.819	10.441	9.354	8.672
7610.709	11.774	10.402	9.332	8.650
7610.856	11.753	10.406	9.325	8.644
7611.711	11.754	10.386	9.299	8.617
7611.872	11.748	10.371	9.288	8.605
7612.688	11.698	10.317	9.240	8.563
7613.683	11.606	10.222	9.169	8.498
7613.845	11.585	10.222	9.168	8.504
7614.715	11.692	10.305	9.238	8.565
7614.872	11.695	10.327	9.255	8.584
7615.697	11.797	10.440	9.345	8.664
7615.852	11.797	10.433	9.351	8.669
7616.682	11.774	10.408	9.329	8.658
7709.676	11.629	10.265	9.192	8.510
7710.554	11.740	10.357	9.257	8.575
7711.538	11.799	10.437	9.337	8.651
7712.581	11.751	10.416	9.334	8.655
7714.561	11.688	10.321	9.235	8.554

Table 9. continued

J.D. 2440000.+	<i>u</i>	<i>v</i>	<i>b</i>	<i>y</i>
7719.607	11.781	10.390	9.308	8.619
7721.487	11.662	10.267	9.190	8.517
7722.474	11.710	10.338	9.265	8.584
7722.511	11.735	10.362	9.273	8.592
7723.468	11.762	10.391	9.311	8.634
7723.508	11.776	10.390	9.314	8.627
7724.627	11.767	10.414	9.323	8.640
7726.558	11.680	10.322	9.230	8.543
7731.556	11.772	10.400	9.297	8.612
7739.554	11.607	10.259	9.184	8.521
7743.572	11.752	10.381	9.292	8.612
7744.556	11.657	10.258	9.209	8.536
7749.513	11.767	10.379	9.292	8.609
7751.533	11.619	10.257	9.187	8.515
7752.512	11.726	10.356	9.271	8.594
7767.500	11.690	10.344	9.275	8.593
7770.500	11.710	10.332	9.252	8.571
7771.498	11.645	10.311	9.247	8.578
8088.817			9.229	8.553
8093.543			9.172	8.502
8094.553			9.238	8.561
8096.531			9.208	8.547
8096.557			9.214	8.542
8097.525			9.284	8.597
8099.507			9.177	8.503
8100.485			9.249	8.569

Table 9. continued

J.D. 2440000.+	u	v	b	y
8100.509			9.238	8.570
8101.488			9.227	8.551
8103.488			9.272	8.583
8111.501			9.196	8.520
8115.556			9.289	8.594

are indicated in the respective figures. An inspection of the light curves shows that significant changes in their shape and amplitude take place even within a few cycles. From the figures it is clear that phase modulations occur in all colours, with the star appearing redder at light minimum. The variation is more pronounced in the ($V - I$) colour.

Of all the light curves presented in Figures 19–23, only one (Figure 23) shows well-defined double minima; although highly asymmetric, all the remaining ones show only a single well-defined minimum. In order to investigate the evolution of starspots and their physical characteristics, systematic observations of the star over several seasons are needed. In the case of HD 127535 a total of eleven light curves are available, including the present five light curves, over a span of ten years. Amplitude and phase of light minimum are the two important parameters that can be deduced directly from the light curves which in turn are indicators of activity and the longitude of spot groups on the stellar surface. All the photometric data of HD 127535 available in the literature were replotted using the above-mentioned ephemeris. The light curve parameters, brightness at light maximum and minimum, V_{max} and V_{min} , phase of the light minimum ϕ_{min} and amplitude, were measured directly from the graphical plots. These quantities are listed in Table 10.

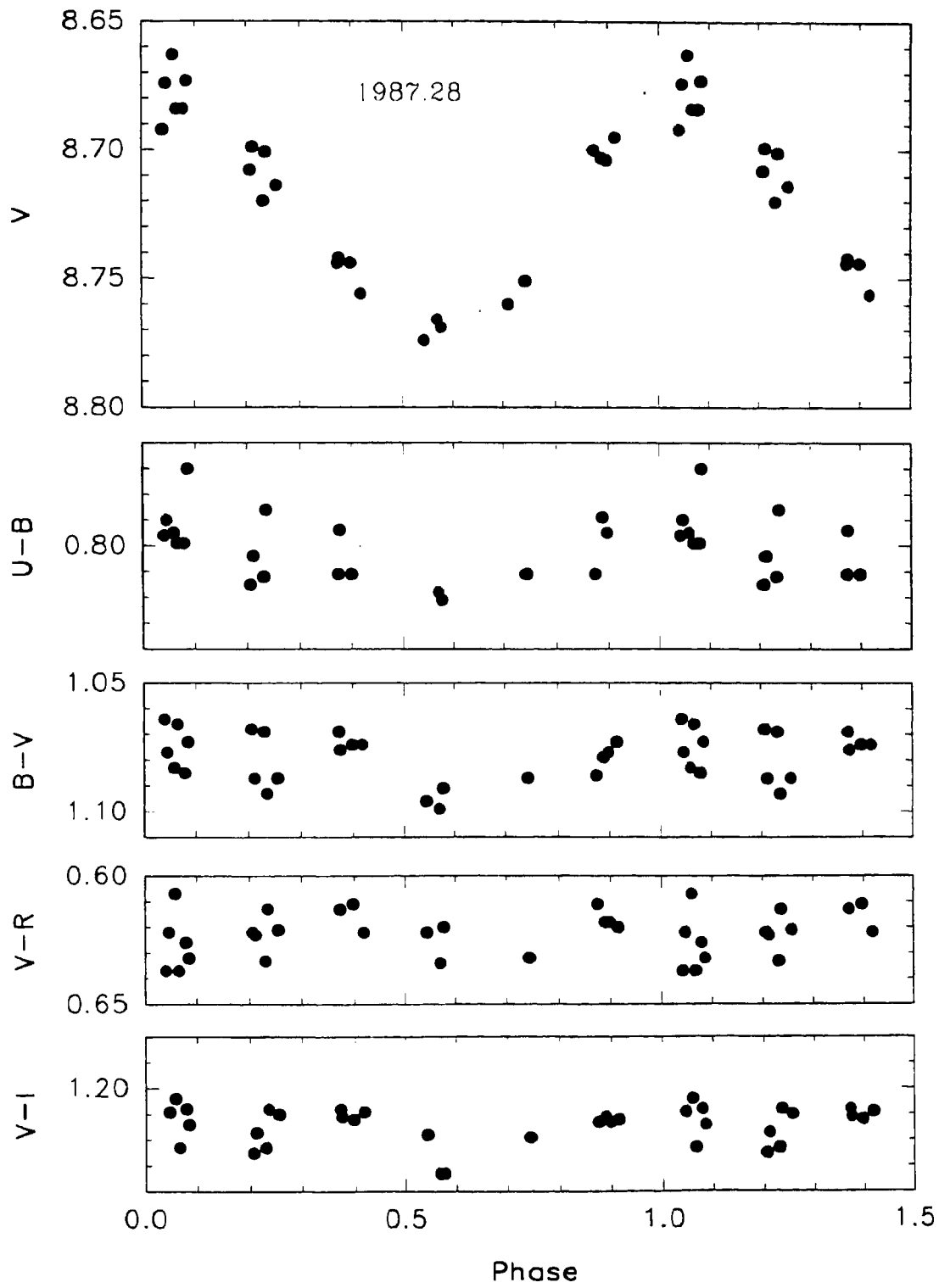


Fig. 19. Plots of V, U-B, B-V, V-R and V-I of IID 127535

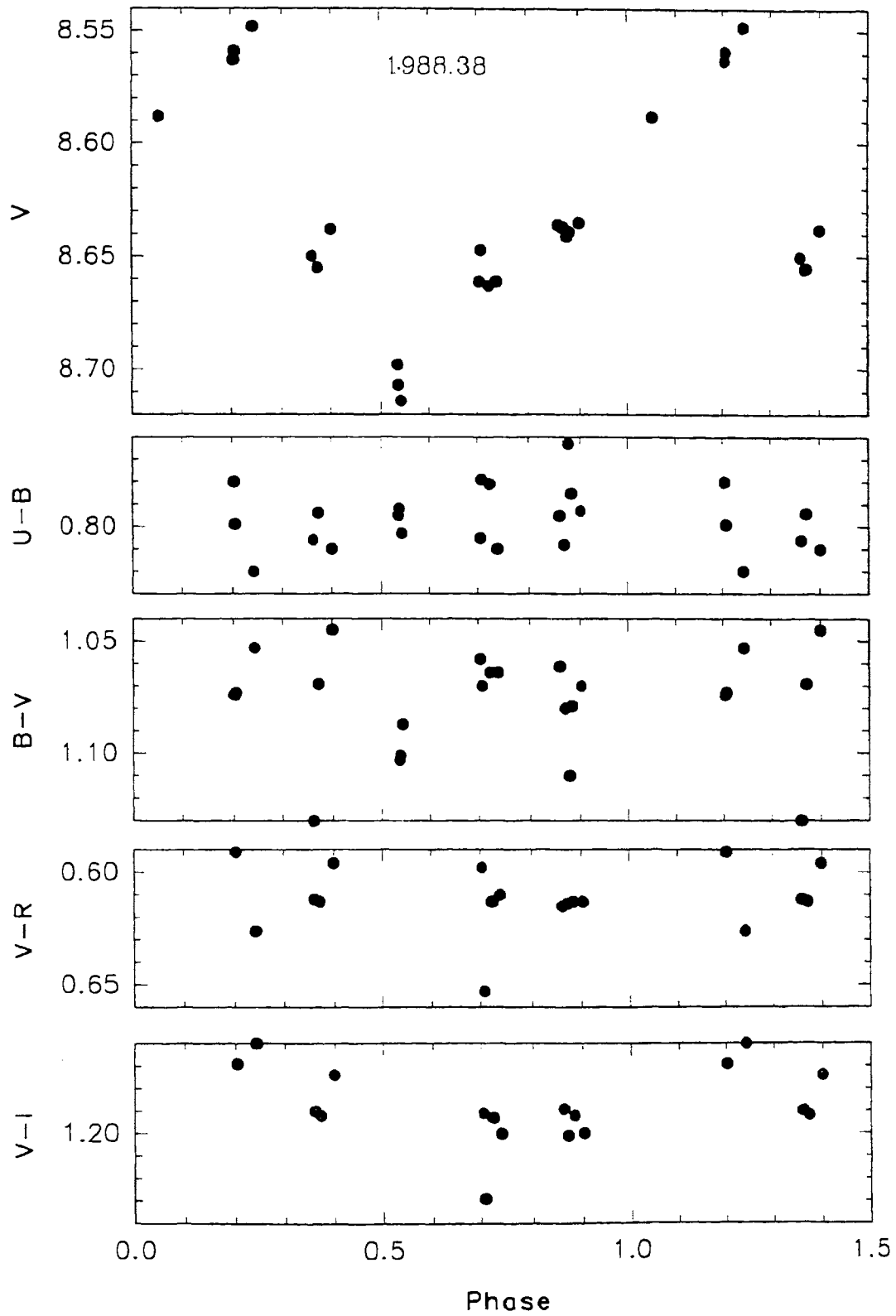


Fig. 20. Plots of V, U-B, B-V, V-R and V-I of HD 127535

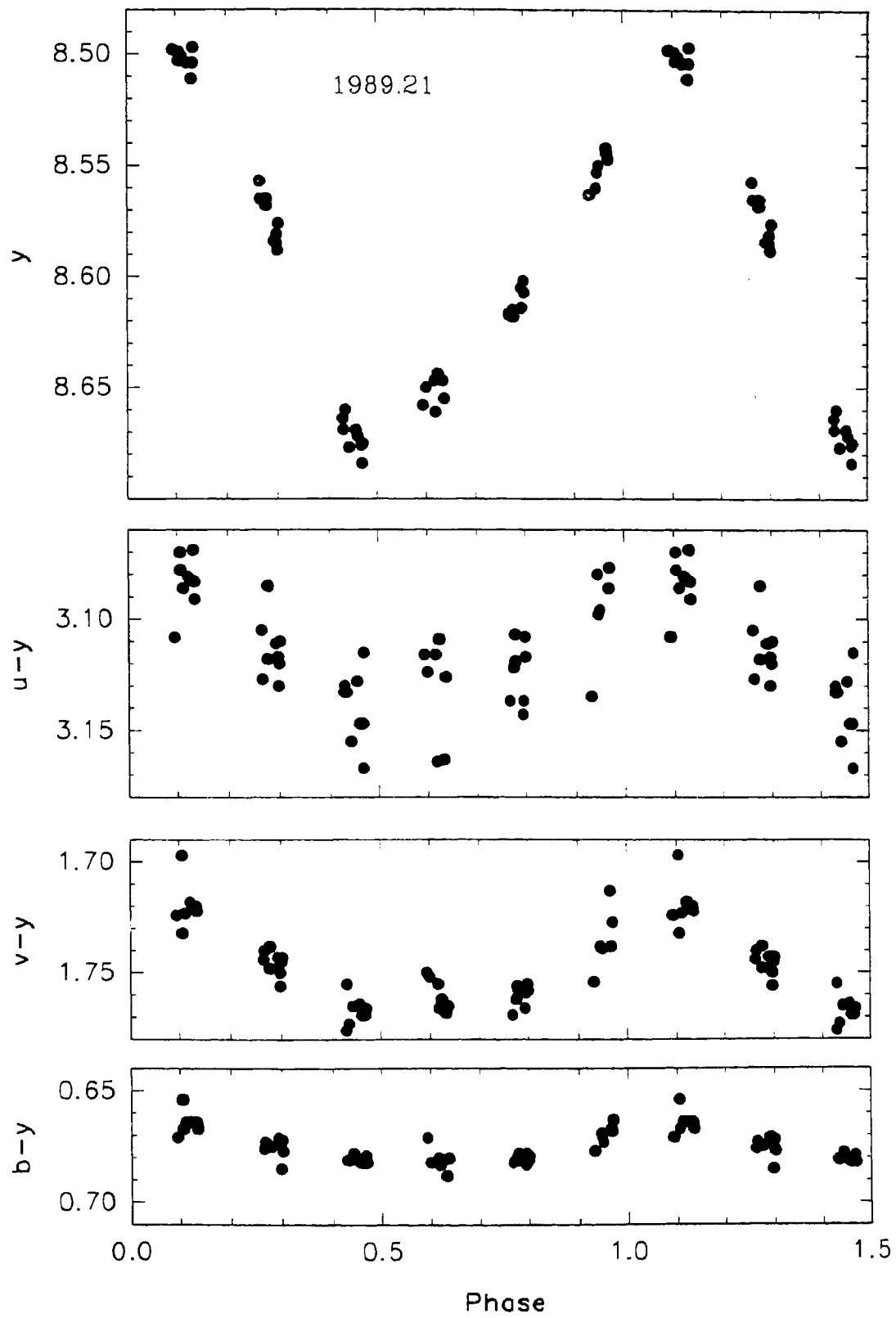


Fig. 21. Plots of y , $u-y$, $v-y$ and $b-y$ of HD 127535

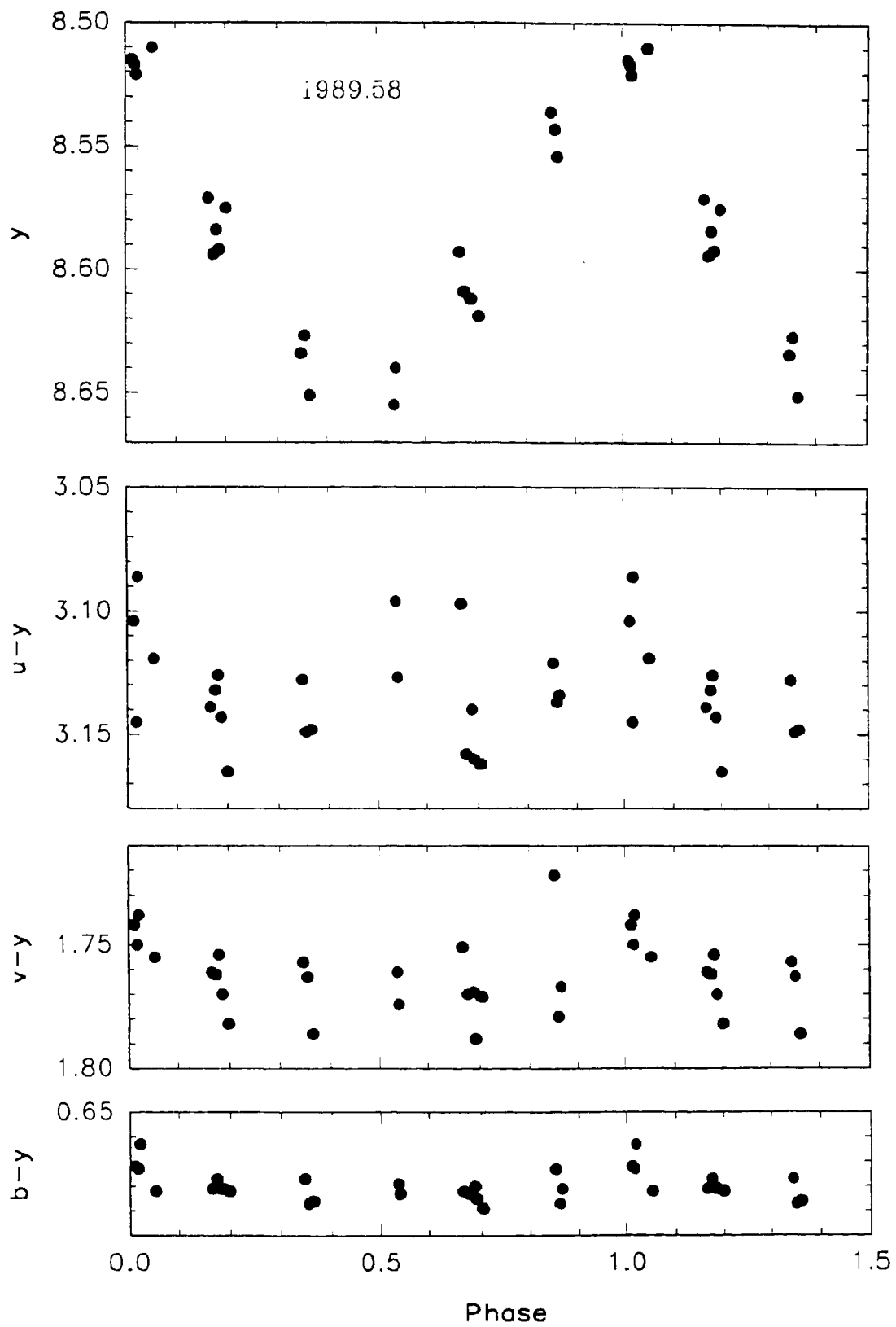


Fig. 22. Plots of y , $u-y$, $v-y$ and $b-y$ of HD 127535

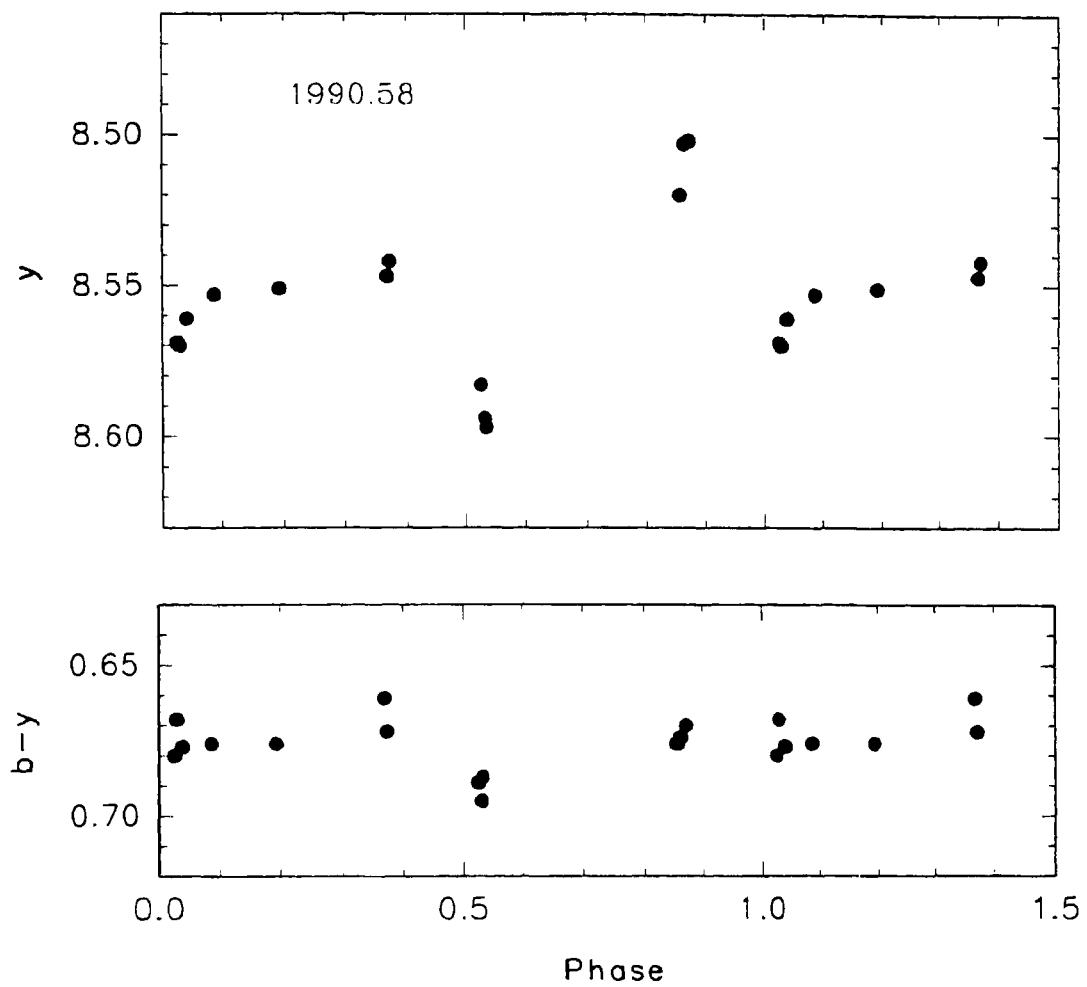


Fig. 23. Plots of y , $u-y$, $v-y$ and $b-y$ of HD 127535

4.2.5. Brightness at light maximum and minimum

The values of V_{max} and V_{min} given in Table 10 are plotted in Figure 24a against the corresponding mean epoch of observation. The length of the vertical bar in each case indicates the amplitude of light curve at that epoch. The unspotted magnitude of the star is an important parameter in light curve modeling using starspots. This parameter can be determined only if photometric data exist over a large time span, since the maximum observed brightness, most likely, will correspond to the unspotted brightness of the star. In the case of HD 127535 the maximum observed brightness over the ten year interval is 8.50 mag and probably represents the unspotted photospheric brightness. It is interesting to note that during the epochs 1981.33 and 1990.58 both V_{max} and V_{min} were at their brightest magnitudes. The corresponding amplitudes of light variation were also low. This implies that at these epochs both the hemispheres presented to the observer at light maximum and minimum had the least spot coverage when compared to the other epochs, and hence the star was at comparatively low spot activity levels.

Table 10. Photometric characteristics of HD 127535

Epoch	Amplitude	V_{max}	V_{min}	ϕ_{min}	References
1981.33	0.070	8.500	8.570	0.50	Collier (1982a)
1984.31	0.230	8.520	8.750	0.20	Udalsky & Geyer (1984)
1984.62	0.130	8.620	8.750	0.05	Innis et al. (1985)
1985.25	0.220	8.620	8.840	0.00	Innis et al. (1985)
1985.43	0.200	8.640	8.840	0.85	Bopp et al. (1986)
1987.28	0.105	8.670	8.775	0.55	Present study
1988.38	0.165	8.550	8.715	0.55	Present study
1989.16	0.180	8.700	8.520	0.45	Cutispoto (1993)
1989.21	0.190	8.495	8.685	0.45	Present study
1989.58	0.140	8.510	8.650	0.45	Present study
1990.58	0.095	8.500	8.595	0.50	Present study

It is also seen from the Figure 24a that during 1985–87 both V_{max} and V_{min} were at their faintest values observed. This means that starspots never disappeared from the line of sight through out the rotational period, and hence the area covered by the spots on the stellar surface were probably higher when compared to other epochs for which observations exist.

The amplitude of light variation observed was maximum during the epoch 1984.31. The observations obtained three months later (mean epoch 1984.62) show that V_{max} , which was close to the unspotted value mentioned above, became faint by around 0.15 mag whereas V_{min} remained nearly the same. The net result was a reduction in the corresponding amplitude by about 0.15 mag. This is possible only with the formation of new starspots close to longitudes opposite to those already present. The orbital inclination of HD 127535 is unknown. The largest amplitude of light variation in V so far observed is 0.23 mag, whereas in the case of HD 81410 it is around 0.50 mag. The formation of a spot in the circumpolar region will reduce both V_{max} and V_{min} . Since V_{min} remained unchanged while V_{max} decreased by 0.15 mag, it is more likely that formation of spots occurred at lower latitudes. The light curve obtained during the next occasion (mean epoch 1985.25) shows that V_{max} did not change from its value previously observed, but V_{min} became fainter by around 0.10 mag. Again, on the basis of the above argument, the formation of spots in the circumpolar region producing the observed change in V_{min} can be ruled out. It is possible that a further increase occurred in the spot area in the hemisphere visible at light minimum.

From Figure 24a it is seen that from about 1988.37 to about 1990.58 the brightness at light maximum remained approximately the same, and the amplitude of light variation increased mainly as a result of V_{min} getting brighter. Probably, during the period 1981.33–1984.31 also V_{max} remained approximately the same, and the increase in amplitude occurred as a result of V_{min} getting fainter. The amplitude does not give any information on the total spot area covered on the stellar surface; in fact it is only a measure of the asymmetry in the brightness distribution. Since the value of V_{max} was close to the unspotted magnitude on both the occasions the decrease in the amplitude observed actually coincided with an overall reduction in the spot

area, and an increase in the amplitude coincided with an increase in the spot area.

The amplitudes and the values of ϕ_{min} observed at the epochs 1989.21 and 1989.16 were nearly the same, but both V_{max} and V_{min} became brighter by similar amounts. This implies either a global reduction in the spot area, or a reduction in the spot area at higher latitudes occurred during that short period.

As seen in Figure 24a, during 1981–91 V_{min} showed a rather smooth variation when compared to V_{max} ; it became first fainter, attained a minimum value around 1985, and then became brighter. From the arguments given above, it follows that such a variation resulted from a corresponding variation in the spot area on the hemisphere visible at light minimum; it increased first, and then decreased after attaining a maximum sometime around 1985.

4.2.6. Phase of light minimum

In Figure 24b the values of ϕ_{min} given in Table 10 are plotted against the corresponding mean epoch of observation. From the figure it is clear that ϕ_{min} shows a migration towards decreasing orbital phase. A migration of ϕ_{min} will result if there is a difference in the assumed photometric period, which in the present case is the orbital period, and the actual period. A least square solution of the observed times of light minima gives the photometric period as 6.0016 ± 0.0006 days. The minimum observed during 1990.58 (Figure 23) was not included in the least square solution because the corresponding light curve is drastically different from all the other light curves, indicating a different brightness distribution on the stellar surface at that epoch.

Since the photometric period, indicated by a migration of light minimum is smaller than the orbital period, the starspots which produce the rotational modulation are located at latitudes which rotate slightly faster than the synchronous latitudes. If the equator is synchronously rotating with the orbit, then it implies that higher latitudes are rotating faster than the equator. This is contrary to what is observed in the sun. However, it is possible that

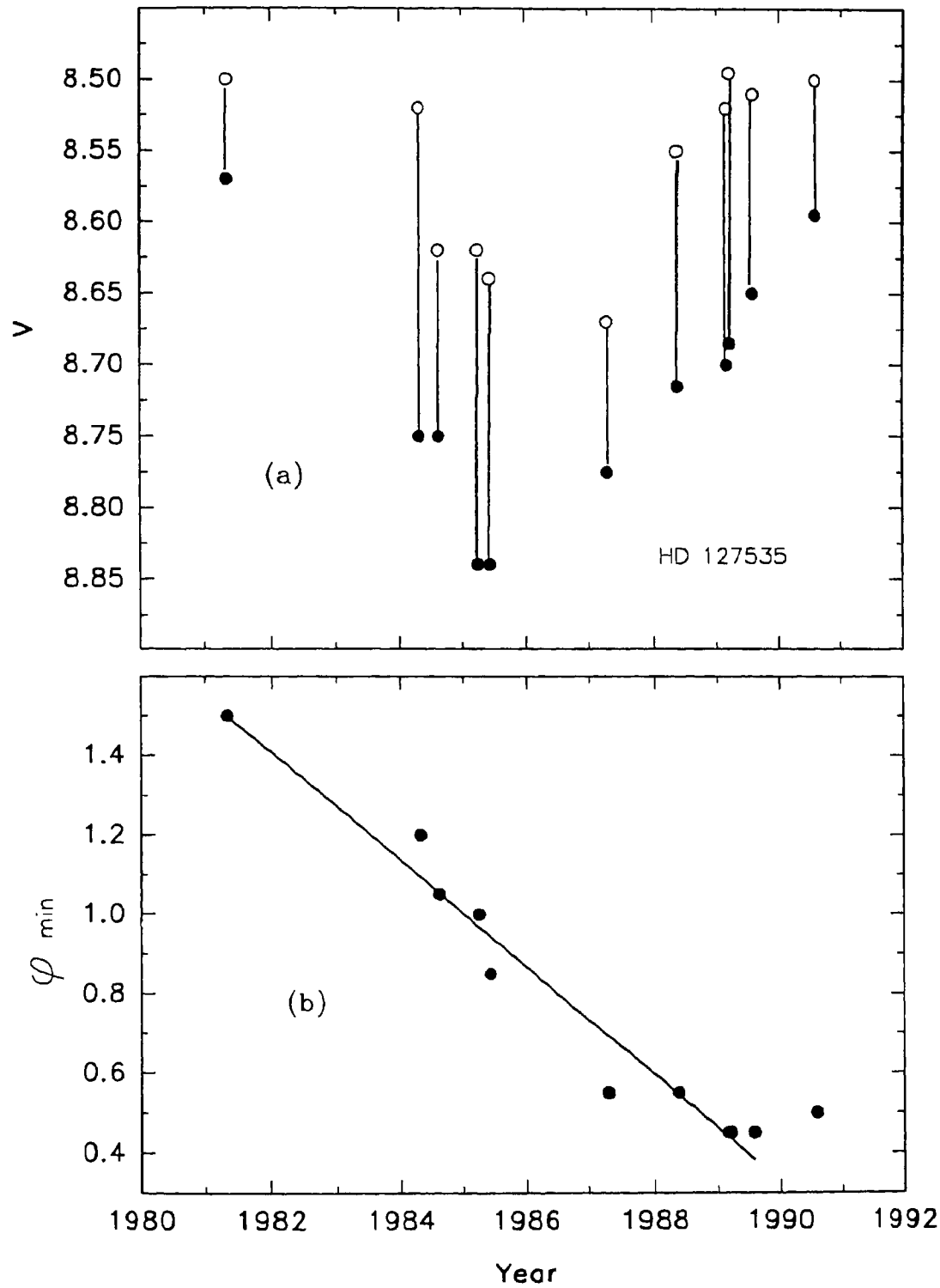


Fig. 24. (a) Plots of V_{max} and V_{min} against the mean epoch. (b) Plot of phase minimum against the mean epoch.

instead of the equator a higher latitude is in synchronous rotation with the orbit and the spots which cause the rotational modulation were confined to equatorial regions.

The ϕ_{min} that is observed is the weighted mean of the longitudes of the individual spots seen during the light minimum. As the short-lived spots appear and decay the weighted mean of the longitude of the starspots also will change causing slight changes in the observed ϕ_{min} . The spot group that was first observed during 1981.31 probably continued to exist till the epoch 1989.58 when probably major changes began to occur as indicated by the light curve obtained during 1990.58 (Figure 23). If the migration of the phase minimum that is seen in Figure 24b was due to the same spot group, which probably was the case, as evident from a rather smooth variation seen in the brightness at light minimum, then it indicates a time-scale of more than 10 years for a major spot group to form, evolve and decay.

4.2.7. Amplitude of light variation

Figure 25 is a plot of V_{max} and V_{min} against the corresponding amplitudes. It is clear that the amplitude of light variation does not show any correlation with the brightness at light maximum. However, there is an indication that the amplitude depends weakly on the brightness at light minimum, especially at larger amplitudes, with V_{min} showing fainter magnitudes. The V_{max} during 7 seasons were almost the same around 8.50 mag while the corresponding V_{min} shows a large scatter. During the other four seasons the values of V_{max} were about 0.15 mag fainter showing that the hemisphere seen at light maximum had a larger spot coverage during these seasons than the hemisphere seen at the light maximum during the earlier mentioned epochs.

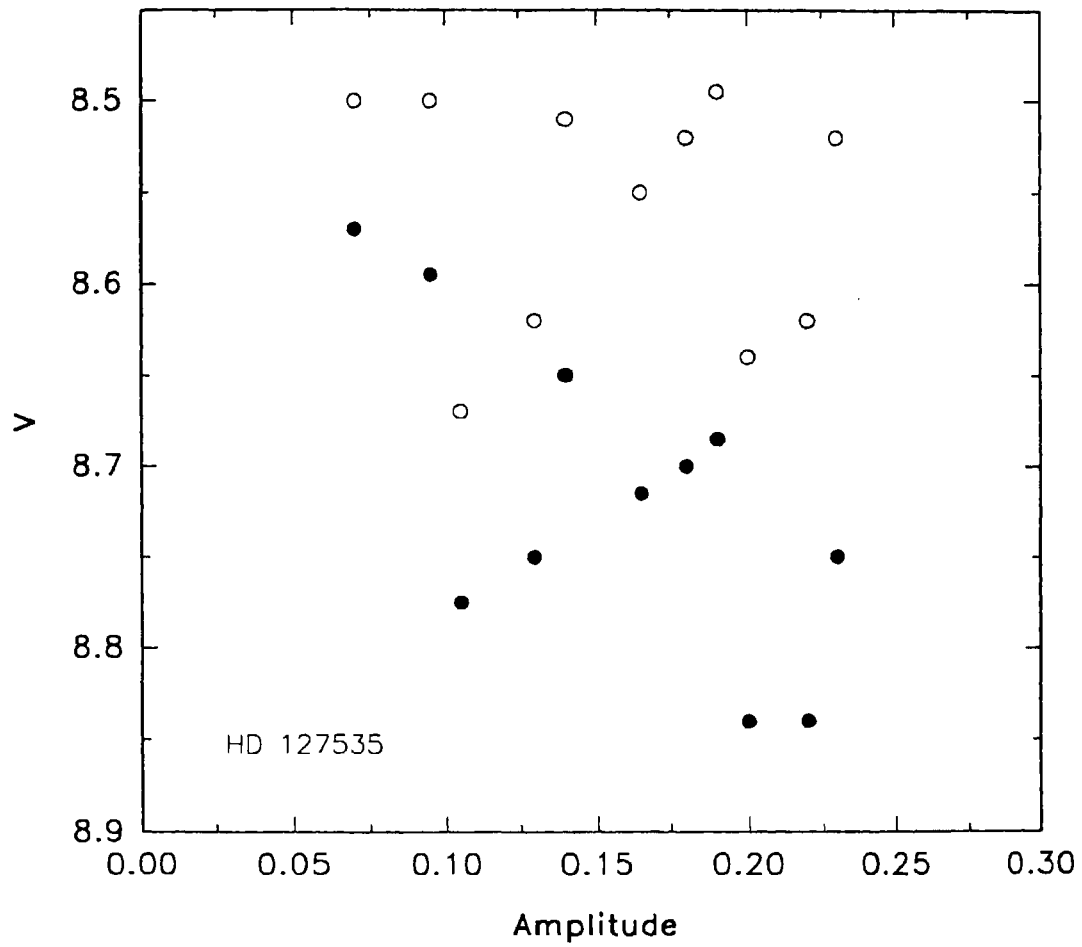


Fig. 25. Plots of V_{\max} (open circles) and V_{\min} (filled circles) against the corresponding amplitude.

5

YOUNG ACTIVE-CHROMOSPHERE OBJECTS

5.1. HD 139084

5.1.1. Introduction

HD 139084 (= V343 Nor) displays strong *Ca II H & K* and filled-in *H α* emissions (Bidelman & Maconnell 1973; Bopp & Hearnshaw 1983). The star has also been found to show emission at microwave frequencies (Slee et al. 1987). It was initially classified as a member of BY Draconis type stars on the basis of the nature of its light variation and strong chromospheric emission. Houk & Cowley (1975) had suggested earlier that the broadband colours are probably composite and had assigned spectral types K1 III and F for the components of HD 139084. However, the radial velocity measurements by Balona (1987) did not show any variations, confirming the star as single. Later, Pallavicini et al. (1992) reported that the *Li I* 6708 Å absorption line present in the spectrum of HD 139084 is much stronger than the nearby *Ca I* 6717 Å absorption line. Randich et al. (1993) proposed that the extremely high Lithium abundance ($n(\text{Li}) = 3.6$) in HD 139084 could be due to it being a young pre-main sequence object. Consolidating the data on the proper motions, rotational $V \sin i$ and radial velocities, Anders et al. (1991) concluded that HD 139084 belongs to the Pleiades super cluster, which

indicates an age of $7-10 \times 10^7$ years, consistent with the derived Lithium abundance. They also estimated a distance of 55 pc to the star, which they find implies an M_V ($= 4.3$ mag) much brighter than that expected from its K0 V spectral classification.

The light variability of HD 139084 was discovered by Udalsky & Geyer (1985) who derived a 4.2 day photometric period. The light curve which they obtained showed two minima and an amplitude of 0.15 mag. Bopp et al. (1985), who obtained additional photometry of HD 139084, found that their data also showed a similar photometric period, and based on the $U - B$ colour observed they suggested that the components are of spectral types K1 III and F. The nonvariability of radial velocity was attributed to a very low orbital inclination by them. But in such a case the light variability due to rotational modulation is expected to be negligible. The shape of the light curve which Bopp et al. (1985) obtained was similar to that obtained by Udalsky & Geyer (1985) one year earlier. The observations of Cutispoto (1990) during February 1987 showed that the maximum of the V light curve was about 0.06 mag brighter than its previously observed values. From an analysis of the observations during February–March 1989, Cutispoto (1993) found that a period of 4.56 days gives a better fit to his observations than the previously reported period of 4.2 days. Photometry of HD 139084 obtained by Anders et al. (1991) during 1990 showed an amplitude of 0.16 mag in V , which is the highest amplitude so far observed.

5.1.2. Photometry

HD 139084 was observed on a total of 45 nights over four seasons: 1987 (12 nights), 1988 (12 nights), 1989 (11 nights) and 1990 (10 nights). $UBVRI$ photometry was carried out during the first two seasons and *by* photometry during the remaining two seasons. The observations were restricted to *by* bands during 1989 and 1990 due to the low photon flux of the star at shorter wavelengths. The comparison stars were SAO 242701 and SAO 242788, and all the observations were made differentially with respect to SAO 242701. Several observations were made each night and averages were taken after grouping them into two or three. Table 1 gives the mean $UBVRI$ magni-

tudes of SAO 242701 and SAO 242788 and *by* magnitudes of the former. The differential quantities of HD 139084 were converted to *UBVRI* and *by* magnitudes using the corresponding values of SAO 242701 given in Table 1 and are tabulated in Tables 2 and 3.

Table 1. *UBVRI* and *by* magnitudes of the comparison stars of HD 139084

Star	<i>U</i>	<i>B</i>	<i>V</i>	<i>R</i>	<i>I</i>	<i>b</i>	<i>y</i>
SAO 242701	9.188 ±0.007	8.250 ±0.005	7.110 ±0.005	6.510 ±0.004	5.759 ±0.004	7.120 ±0.005	7.850 ±0.007
SAO 242788	10.570 ±0.010	9.795 ±0.005	8.682 ±0.005	8.090 ±0.005	7.521 ±0.004		

5.1.3. Photometric period

There is no consistency in the photometric period for HD 139084 quoted in the literature. Udalsky & Geyer (1985), for example, reported the photometric period as 4.2 days while Cutispoto (1993) reported the period to be 4.57 days. The discrepancy in the periods quoted could be partly due to the error involved in its determination. When the available observations are a few in number and the observations span over a short time interval, the period finding technique usually would not yield the correct value. The data obtained over a longer duration cannot be combined as in the case of the radial velocity measurements to yield a better period because the light curves in general show appreciable phase shifts and changes in shape as a result of short term fluctuations in the distribution of active regions on the stellar surface. A slight mismatch in the periods derived can also occur because of a difference in the approach adopted in their determination. To eliminate such a possibility, the *V* and *y* data given in Table 2 and 3, and the *V* data available in the literature were analyzed using the method described in § 2.4..

Table 2. *UBVRI* magnitudes of HD 139084

J.D. 2440000.+	<i>U</i>	<i>B</i>	<i>V</i>	<i>R</i>	<i>I</i>
6896.746	9.222	8.869	8.051	7.582	7.130
6896.840	9.200	8.851	8.043	7.578	7.124
6897.651	9.323	8.912	8.084	7.593	7.150
6897.770	9.318	8.929	8.093	7.606	7.150
6897.862	9.302	8.944	8.096	7.611	7.142
6898.649	9.320	8.927	8.103	7.619	7.150
6898.779	9.322	8.923	8.104	7.618	7.158
6898.875	9.306	8.922	8.104	7.620	7.167
6899.639	9.275	8.920	8.072	7.619	7.151
6899.779	9.269	8.902	8.077	7.597	7.141
6899.851	9.278	8.897	8.071	7.587	7.139
6900.616	9.205	8.854	8.031	7.552	7.107
6901.642	9.266	8.904	8.076	7.600	7.145
6902.627	9.331	8.923	8.088	7.609	7.147
6902.762	9.321	8.927	8.095	7.614	7.151
6902.845	9.321	8.922	8.096	7.622	7.151
6903.625	9.290	8.916	8.075	7.609	7.140
6903.785	9.282	8.918	8.071	7.609	7.148
6903.865	9.270	8.908	8.075	7.603	7.140
6904.629	9.245	8.863	8.043	7.574	7.115
6904.784	9.241	8.850	8.032	7.561	7.110
6904.871	9.235	8.850	8.033	7.565	7.112
6905.623	9.243	8.890	8.058	7.577	7.130
6906.781	9.329	8.935	8.089	7.620	7.177
6906.801	9.333	8.938	8.100	7.622	7.169

Table 2. continued

J.D. 2440000.+	<i>U</i>	<i>B</i>	<i>V</i>	<i>R</i>	<i>I</i>
6907.832	9.326	8.920	8.094	7.620	7.155
7296.582	9.278	8.889	8.063	7.587	7.136
7298.604	9.298	8.913	8.080	7.638	7.190
7299.560	9.279	8.905	8.063	7.590	7.126
7304.595	9.337	8.930	8.087	7.616	7.150
7304.708	9.321	8.923	8.089	7.606	7.144
7304.822	9.306	8.912	8.082	7.596	7.144
7305.518	9.282	8.898	8.069	7.592	7.129
7305.650	9.273	8.889	8.070	7.585	7.133
7305.789	9.287	8.900	8.069	7.597	7.138
7307.581	9.267	8.879	8.047	7.579	7.119
7307.818	9.278	8.902	8.060	7.590	7.120
7308.536	9.341	8.933	8.095	7.615	7.145
7308.666	9.286	8.919	8.086	7.605	7.145
7308.779	9.333	8.924	8.093	7.617	7.146
7309.626	9.252	8.901	8.070		
7309.669	9.246	8.899	8.066		
7311.629	9.246	8.896	8.068		
7311.695	9.260	8.897	8.073		
7313.607	9.266	8.901	8.070		
7314.684	9.267	8.898	8.063		
7315.607	9.257	8.905	8.065		

Totally there are 8 sets of data that are suitable for a period determination. They are listed in Table 4 along with their sources. The quantity *Q*, taken as the measure of scattering in the phase-magnitude plot, shows a flat minimum

in most cases because of the small number of photometric cycles covered in each case. The errors in the period listed in Table 4 refer to the half-width of the flat minimum. The comparatively large errors arise because of the low amplitudes of light variation and the short data lengths.

Table 3. *by* magnitudes of HD 139084

J.D. 2440000.+	<i>b</i>	<i>y</i>
7739.558	8.629	8.110
7742.581	8.600	8.076
7743.497	8.625	8.102
7743.588	8.610	8.108
7744.491	8.636	8.113
7744.595	8.656	8.126
7747.623	8.616	8.115
7748.476	8.634	8.106
7748.613	8.639	8.111
7749.481	8.693	8.144
7750.487	8.607	8.087
7750.589	8.610	8.094
7751.480	8.587	8.061
7751.571	8.593	8.081
7752.483	8.622	8.092
7752.569	8.612	8.101
7753.480	8.663	8.134
8088.830	8.722	8.231
8093.547	8.663	8.158
8093.681	8.657	8.135
8094.510	8.619	8.100

Table 3. continued

J.D. 2440000.+	b	y
8094.674	8.618	8.113
8096.488	8.799	8.279
8096.653	8.788	8.258
8097.495	8.699	8.182
8099.502	8.668	8.144
8099.656	8.684	8.156
8100.492	8.776	8.247
8100.665	8.785	8.253
8101.481	8.730	8.208
8101.700	8.726	8.195
8102.476	8.659	8.134
8102.668	8.645	8.130
8103.485	8.636	8.116

5.1.4. Light curves

The Julian days of observation given in Table 2 and 3 were converted to photometric phases using the following ephemeris:

$$JD(HeI.) = 2446898.8 + 4.^d294 E,$$

where the initial epoch corresponds to the light minimum observed in the present 1987 data and the period is the average of the periods given in Table 4. The V magnitudes and $U - B$, $B - V$, $V - R$, and $V - I$ colours are plotted in Figures 1 and 2, and y and $b - y$ in Figure 3. The corresponding mean epochs of observation are also indicated in the figures.

HD 139084 has been observed on nine occasions during the years 1981 to 1990. In order to study the long-term photometric behaviour all these observations were replotted with the above ephemeris, and the values of

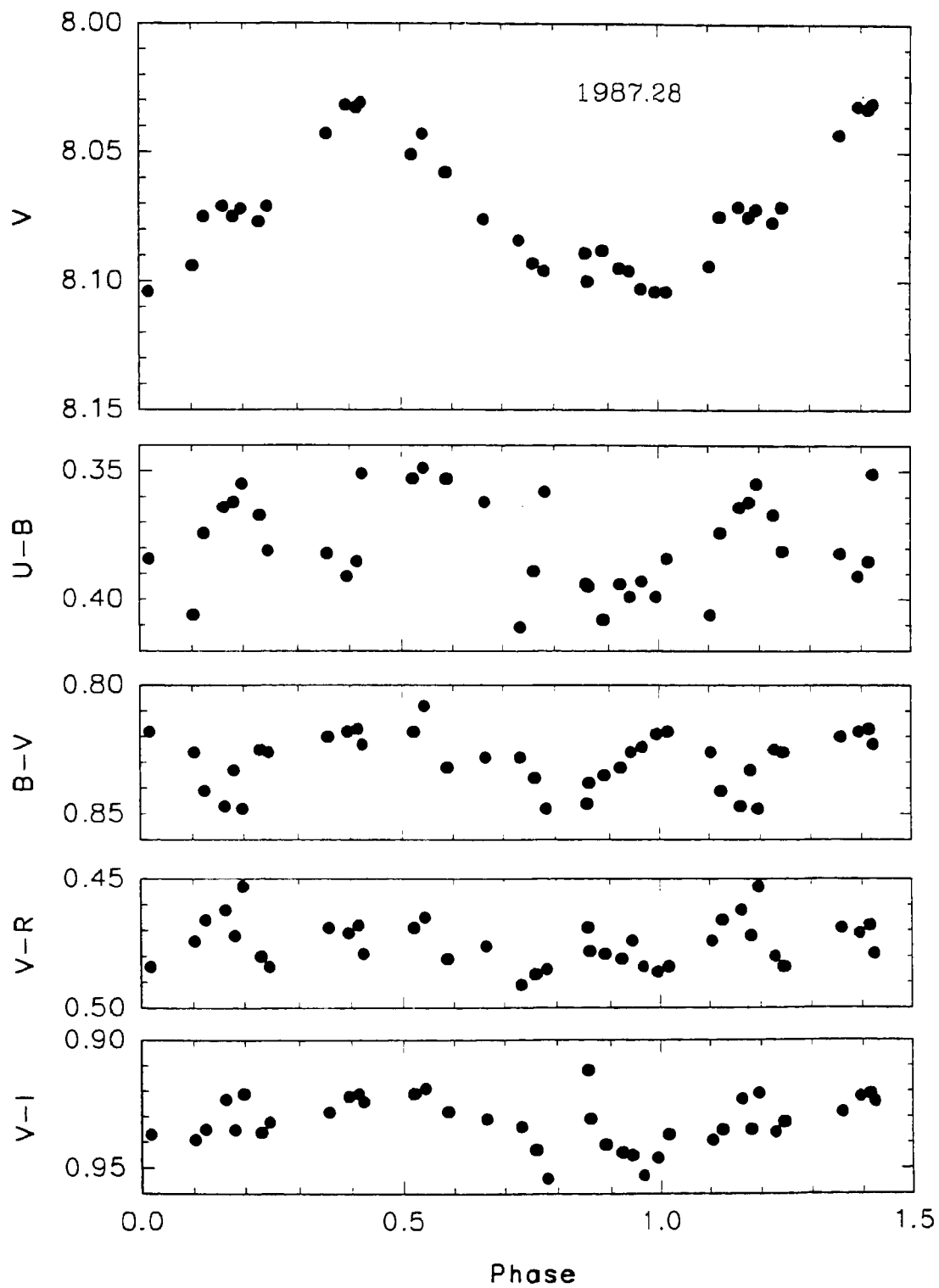


Fig. 1. Plots of V, U-B, B-V, V-R and V-I of HD 139084

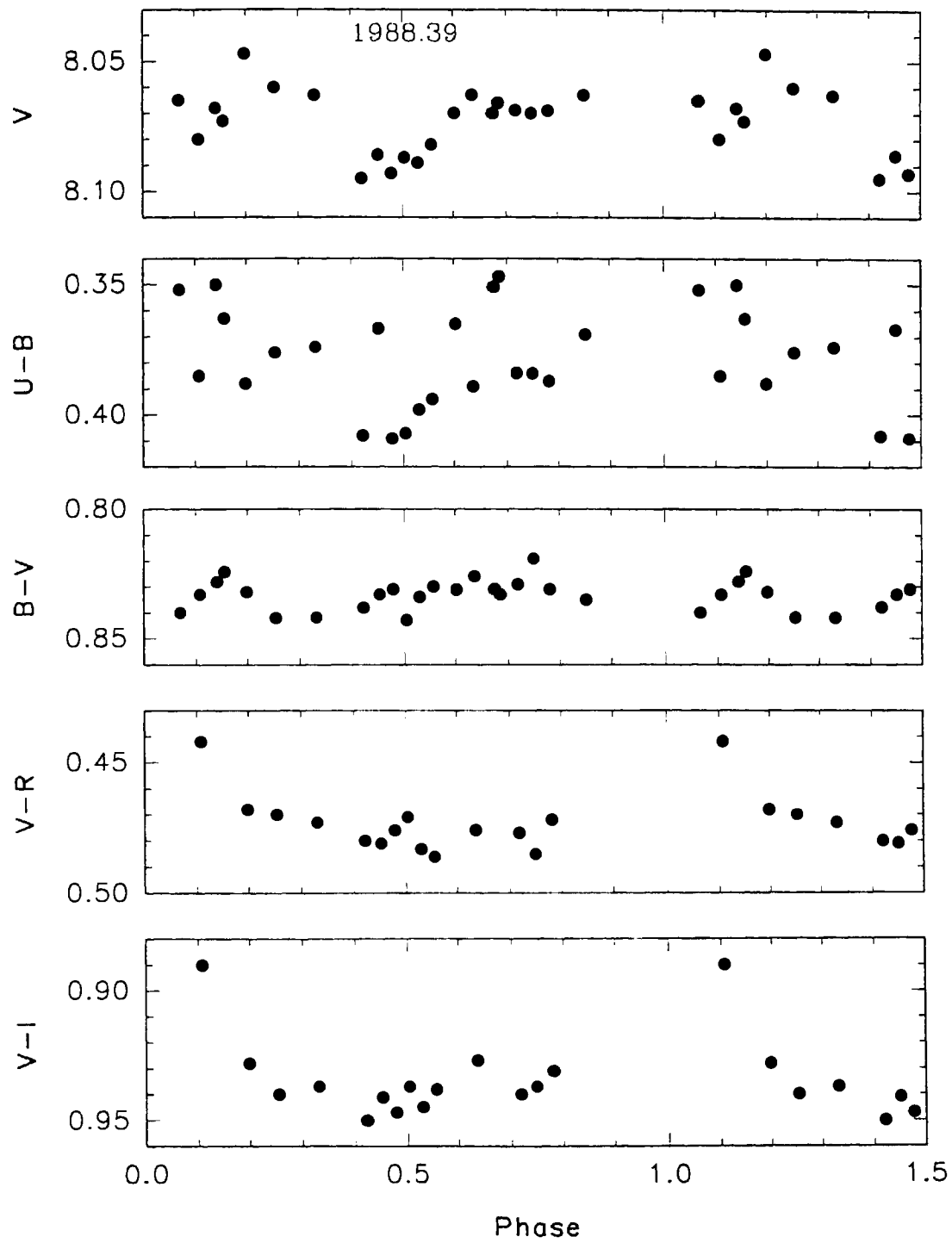


Fig. 2. Plots of V, U-B, B-V, V-R and V-I of HD 139084

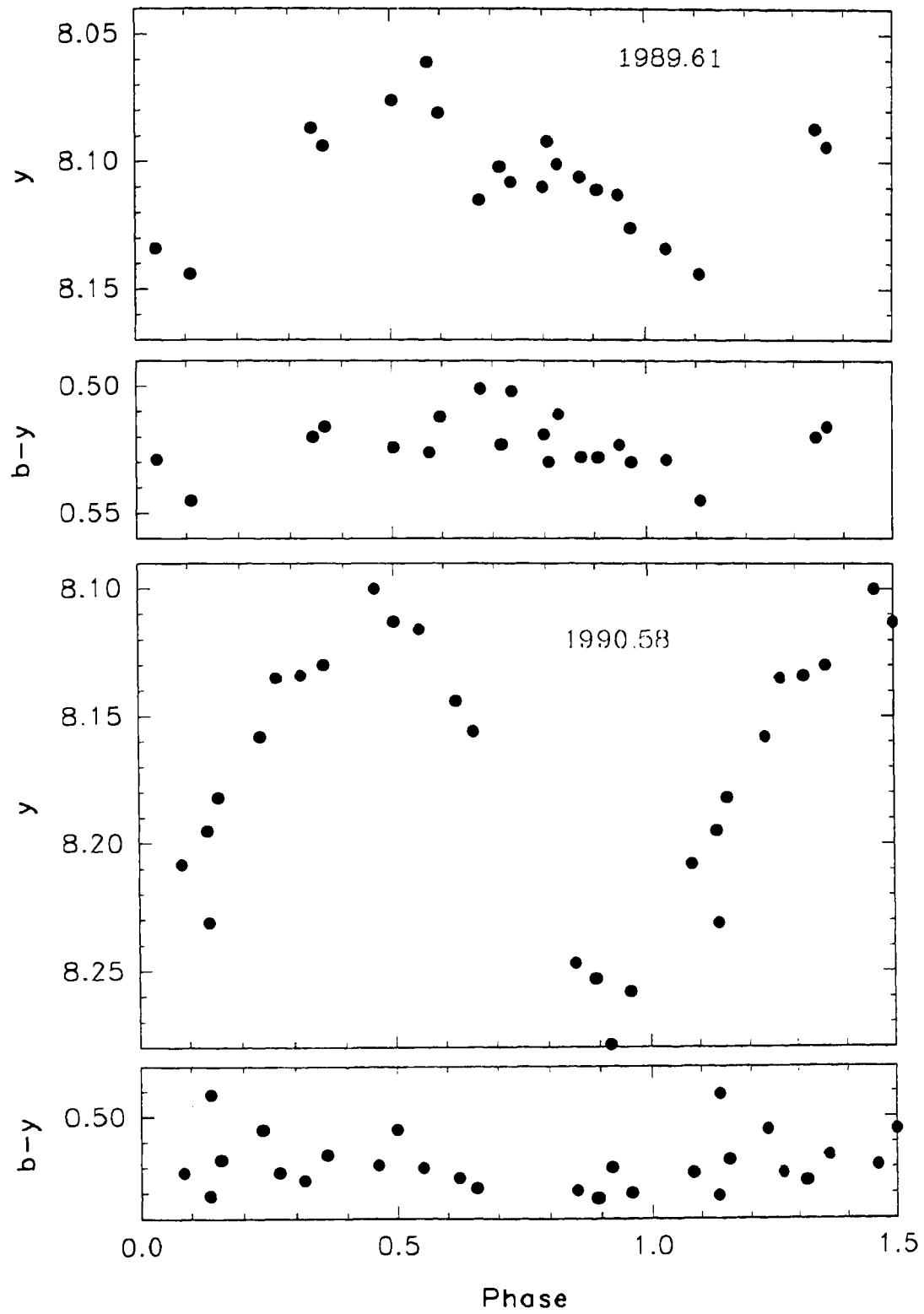


Fig. 3. Plots of y and $b-y$ of HD 139084

V_{max} , V_{min} , ϕ_{min} and the amplitudes were read out directly from the plots of the light curves and are given in Table 5. The amplitude observed is generally not large; usually it is less than 0.10 mag. The highest amplitude so far observed is ~ 0.16 mag (Anders et al. 1991). During three epochs the

Table 4. Photometric periods derived from various sets of data

Mean epoch	J D interval	Cycles covered	Period	Reference
	2440000+			
1981.50	4767-4806	9.1	4.38 ± 0.12	1
1984.30	5805-5815	2.3	4.26 ± 0.16	2
1985.43	6218-6226	1.9	4.10 ± 0.08	3
1987.28	6896-6907	2.6	4.30 ± 0.09	4
1988.39	7296-7315	4.4	4.39 ± 0.04	4
1989.16	7577-7595	4.2	4.48 ± 0.17	5
1989.61	7739-7753	3.3	4.26 ± 0.22	4
1990.58	8088-8103	3.5	4.18 ± 0.12	4

(1) Lloyd Evans 1987; (2) Udalasky & Geyer 1985; (3) Bopp et al. 1986; (4) Present study; (5) Cutispoto 1993

light curves showed double minima, if interpreted as due to spot activity suggests the presence of two prominent active regions well separated in longitudes at these epochs. The light curves obtained during 1988.39 (present study) and 1981.5 (Lloyd Evans 1987) are similar in amplitude and shape. Most probably, the spot groups at these epochs, though located at different longitudes, had similar spot coverage and spot temperature. As explained later in § 5.1.6. earlier the spots also had similar latitudes, below the equator as seen by the observer.

5.1.5. Brightness at light maximum and minimum

Figure 4a is a plot of V_{max} and V_{min} of HD 139084 given in Table 5 against

the corresponding epoch of observation. The extent of the vertical bar gives the amplitude corresponding to that epoch. An inspection of the figure shows that the brightest V_{max} so far observed is 7.995 mag. This probably corresponds to the unspotted magnitude. Neither the amplitude nor the brightness at light maximum and minimum does give directly any idea on

Table 5. Photometric characteristics of HD 139084

Epoch	Amplitude	V_{max}	V_{min}	ϕ_{min}	References
1981.50	0.035	8.055	8.090	0.55	Lloyd Evans (1987)
1984.30	0.110	8.075	8.185	0.70	Udalsky & Geyer (1985)
				0.05	
1985.43	0.075	8.090	8.165	0.50	Bopp et al. (1986)
				0.85	
1987.11	0.120	7.995	8.115	0.05	Cutispoto (1990)
1987.28	0.070	8.030	8.100	0.00	Present study
1988.39	0.035	8.060	8.095	0.50	Present study
1989.16	0.080	8.040	8.120	0.30	Cutispoto (1993)
1989.61	0.080	8.070	8.150	0.10	Present study
				0.75	
1990.58	0.155	8.255	8.100	0.95	Present study

spot coverage on the stellar surface. The amplitude is only a measure of the longitudinal asymmetry in the spot distribution. A comparison of the brightness at light maximum and minimum observed at two different epochs would give an indication of the relative spot coverage on the stellar surface. Since the star is viewed at a low inclination ($i \sim 40^\circ$, § 5.1.6.), spots that occur at high latitudes would appear as circumpolar and hence would not contribute to the light modulation appreciably, and hence the amplitude essentially gives the spot distribution about an equatorial belt whose width depends on the inclination. The V_{max} observed during 1984.30 was fainter than the V_{max} observed during 1981.50 by only ~ 0.02 while V_{min} observed

during the former occasion was about 0.10 mag fainter than that observed during the latter. This indicates that the spot coverage on the hemisphere visible at light minimum was higher on the former occasion than that on the latter, while the spot coverage on the hemisphere seen at light maximum during the two occasions remained nearly the same. The V_{min} observed during 1987.11 was close to the V_{max} observed during the previous occasion, *i.e.*, during 1985.43, which means that the hemisphere visible at light minimum during the former occasion had only a spot coverage similar to that of the hemisphere visible at light maximum at the latter epoch, indicating that the overall spot coverage during 1987.11 was significantly less than that during 1985.43. Therefore there was an overall increase in the spot coverage from 1981 till around 1985 which then decreased and became a minimum sometime around 1987. By a similar argument it follows that there was a near-continuous increase in the spot coverage on the stellar surface from 1987.11 onwards till 1990.58. During 1990 the star was at its maximum activity level, indicated by a low V_{max} and the extreme V_{min} observed till that epoch. The trend in Fig 4a suggests a period around 10 years for an activity cycle.

Figure 5 is a plot of V_{max} and V_{min} from Table 5 against the corresponding amplitudes. The V_{min} shows a larger range when compared to V_{max} . It is clear that on most occasions HD 139084 exhibits an amplitude less than 0.1 mag. The amplitude seems to be correlated with the brightness at light minimum, in the sense that at higher amplitudes the brightness at light minimum is fainter. There is no correlation between the amplitude and the brightness at light maximum.

5.1.6. Phase of light minimum

From Table 4 it is seen that the photometric period derived from the data obtained during different seasons varies from 4.10–4.50 days, with a mean period of 4.294 ± 0.043 days. It is tempting to conclude that the differences, at least partly, arises from the differential rotation that is expected in a late-type star. If the starspots have a large latitudinal extent, establishing the differential rotation from the photometric data would be rather difficult

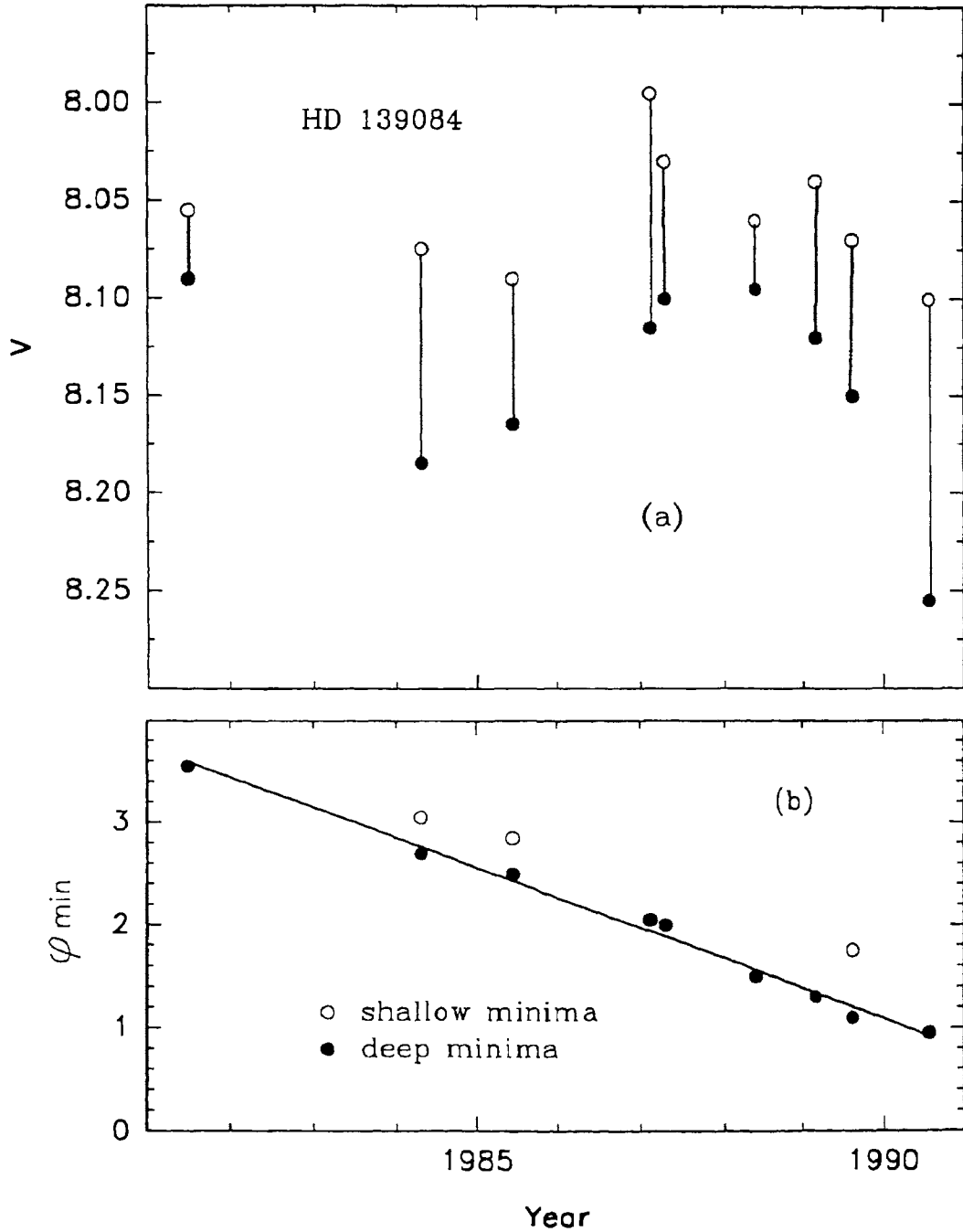


Fig. 4. Plots of (a) Vmax (open circles) and Vmin (filled circles) and (b) phase min. against the corresponding mean epoch.

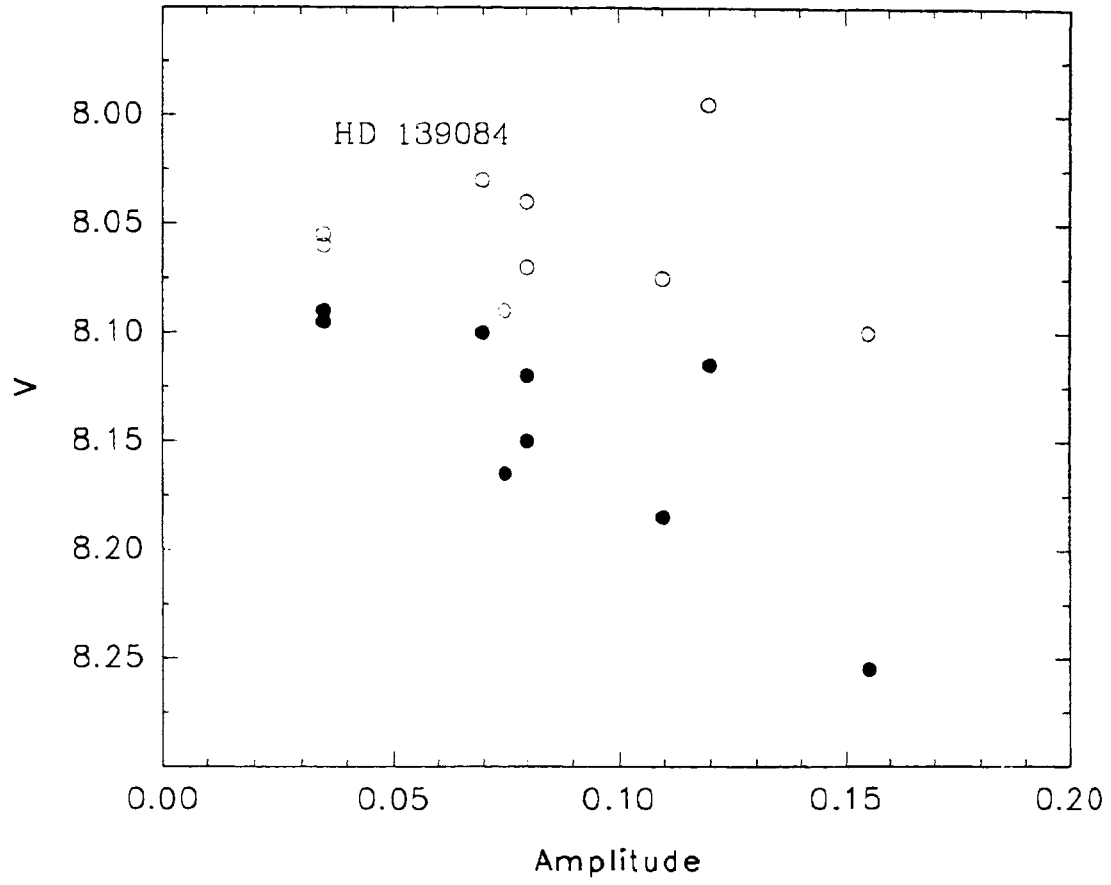


Fig. 5 Plots of Vmax (open circles) and Vmin (filled circles) against the corresponding amplitude.

because the photometric period would then correspond to the rotational period of the effective latitude of spot distribution. However, if spots that produce the rotational modulation are confined mostly to a narrow latitudinal belt at a particular epoch the photometric period derived would refer to the rotation period at that latitude. Hence, if the spots are predominantly present selectively at different latitudes at different epochs the photometric periods derived would show a range of values as a result of differential rotation.

The light curves obtained during 1981.50 and 1988.39 are similar in all respects; both light curves show flat maxima extending over more than $0.^m5$, and narrow light minima with depths around 0.03 mag. The above characteristics are possible for the light curves if the modulating spots disappear completely from the field of view for a substantial fraction of the rotational period, and this in turn is possible only if the corresponding spot groups had a large polar distance, measured from the pole above the sky plane. Anders et al. (1991) find that the $R\sin i$ and the space velocity (U, V, W) observed are consistent with an inclination $i = 40^\circ$ for the rotational axis, and hence the main contribution to the light modulation will come from spots within a $\pm 40^\circ$ latitudinal belt. Therefore it appears that the spots which produce the rotational modulation at the above two epochs were situated at the highest visible stellar latitudes below the equator as seen from the pole above the sky plane. Definitely spots were present at other locations on the stellar surface at these epochs because the light maximum was below its maximum value so far observed. Here it may be noted from Table 4 that the photometric periods derived for these two epochs are longer than all the other periods except one, corresponding to the epoch of 1989.16. This together with the above conclusion that the corresponding spot groups were predominantly located at the highest visible latitudes suggests that higher latitudes are rotating slower, as expected from the differential rotation that is characteristic of a late-type star. During 1989.16, when the photometry showed the largest period (4.48 days), the light curve showed a near-sinusoidal shape indicating that the spots never disappeared completely from the line of sight. This could happen if spots were situated near the circumpolar region above the

sky plane, and in that case a similar conclusion that highest latitudes that is involved in the light modulation has the slowest rotational period is again reached.

An investigation of the behaviour of the phase of light minimum can also provide some information on the differential rotation of the star. If there is only one prominent spot group on the star then the phase of the light minimum is an indicator of the location of spot group that cause the modulation of light. In Figure 4b the values of ϕ_{min} given in Table 5 are plotted against the corresponding epochs of observation. It is interesting to see that all the deep minima observed so far lie in a near-straight line, indicating that the effective longitude of the spot groups which produce the light modulation did not suffer any sudden change as a result of the formation of new spot groups, or the strengthening of the spot groups already existing at a different longitude. Since the migration is towards the decreasing photometric phase the actual period is slightly less than the mean photometric period of 4.294 days assumed in the folding of the observations. A least square fit to the times of minima gives the best fit photometric period as 4.2792 ± 0.0004 days. This corresponds to the rotational period of the equatorial belt which is involved in the light modulation.

If the differences in the photometric periods given in Table 4 is real, at least partly, then the phase of light minimum would not show the type of smooth migration as seen in Figure 4b. Further, The shapes of the light curves obtained during 1984.30 and 1985.43 are nearly identical suggesting that the major changes in the spot distribution did not occur even in about 90 intervening photometric cycles, and hence the modulating spot group did not get drawn out because of the differential rotation. This could happen if the spots were confined to a very narrow latitudinal belt, which is unlikely on account of the comparatively large amplitude of light variation observed, or if the spots in general do not take part in the differential rotation experienced by the star. Here it may be noted that the latitudinal belt that is actually involved in the light modulation is itself quite small since the star is seen at a low inclination, and therefore the range in photometric periods expected from a temporal distribution of spot latitudes may not be appreciable. It

is most likely that the differences in photometric periods seen in Table 4 reflects only the uncertainty involved in their determination and not the differential rotation experienced by the star, and the photometric period of 4.2792 ± 0.0004 day is the rotational period of the star.

From Figure 4b it is seen that during three epochs there were two prominent spot groups well separated in longitudes as indicated by two minima in the light curves. The two minima observed during the epoch 1984.30 were present in the light curve obtained a year later, indicating that the active regions might last longer than a year or so.

Further frequent photometry over several seasons are necessary to arrive at a clearer picture.

5.2. HD 155555

5.2.1. Introduction

HD 155555 (= V834 Ara, LDS 587A) is a 1.6817 day period double-lined spectroscopic binary with both components chromospherically active. Bennett et al. (1962) derived the orbital parameters and assigned the spectral types G5 IV and K0 to the components. The star was classified by Stacy et al. (1980) as an RS CVn system on the basis of the presence of strong *Ca II H & K* and *Mg II h & k* emissions. HD 155555 shows filled-in $H\alpha$ emission and strong X-ray emission (Bopp et al. 1986; Walter et al. 1980). From a spectroscopic analysis, Pasquini et al. (1991) found that both components of HD 155555, apart from strong *Ca II H & K* and $H\alpha$ emissions, also display strong *Li* 6708Å absorption in their spectra. By measuring the equivalent widths of the cross correlation dips for the two components they estimated a difference of around 0.90 mag between the hotter and the cooler components in the CORAVEL band. The M-dwarf visual companion (LDS 587B), which is at a separation of 33 arc sec, shows all the characteristics of an active young dMe star. On the basis of the presence of the strong emission lines and the unusually strong *Li I* line, Pasquini et al. (1991) suggested that the system HD 155555 consists of three coeval pre-main sequence stars of only a few tens of million years old. Further they found that its space velocities U, V and W are consistent with its membership of the young disk population if a distance of 39 ± 9 pc is assumed. Pallavicini et al. (1992) also reported the strong Lithium absorption lines; they derived an abundance of $\log N(\text{Li}) = 3.5$ for the cooler component and $\log N(\text{Li}) = 3.9$ for the hotter component. Lithium abundance of the order of ≈ 3.0 are usually found in pre-main sequence stars (Basri et al. 1991). Eggen (1995) re-analyzed the space motions and found that HD 155555 belongs to the Pleiades Super cluster. Since even a high spectral resolution study of the M-type companion did not reveal any *Li I* absorption line, Martin & Brandner (1995) suggested that the binary is in an evolutionary stage intermediate between the T Tauri stars and the Pleiades low mass stars. Slee et al. (1987) detected microwave

emission at 5.0 and 8.4 GHz in HD 155555. A quiescent emission at 843 MHz of the order of 5 mJy was also detected by Vaughan & Large (1987)

The light variability of HD 155555 was suspected because two independent observations performed a decade apart by Stoy (1963) and by Eggen (1978) differed by about 0.16 mag. The optical light variability was confirmed four years later by Collier (1982). Soon after Udalsky & Geyer (1984) reported that the light variation was sinusoidal with an amplitude of 0.08 mag and a period of 1.66 days, nearly the same as the orbital period. They also found that the colour variations, especially in $V-I$, are in phase with the light variation in the sense that the star is redder at the minimum light. Further photometric observations were carried out by Scaltriti & Busso (1984), Bopp et al. (1986), Lloyd Evans & Koen (1987), Collier Cameroon (1987), Rucinski (1988) and Cutispoto (1990, 1993).

5.2.2. Photometry

Photometric observations of HD 155555 were carried out on 35 nights during four observing seasons: 1987 (10 nights), 1988 (5 nights), 1989 (11 nights) and 1990 (9 nights). $UBVRI$ photometry was done during 1987 and 1988 seasons and by photometry during 1989 and 1990 seasons. SAO 253886 and

Table 6. $UBVRI$ and by magnitudes of the comparison stars of HD 155555

Star	U	B	V	R	I	b	y
SAO 253886	10.580 ± 0.013	8.908 ± 0.007	7.405 ± 0.006	6.605 ± 0.005	5.855 ± 0.005	8.322 ± 0.008	7.399 ± 0.008
SAO 253824	11.181 ± 0.010	9.195 ± 0.007	7.600 ± 0.006	6.737 ± 0.005	5.852 ± 0.005		

SAO 2538824 were used as comparison stars and all observations were done differentially with respect to SAO 253886. Sufficient care was taken to avoid

the light contamination from the visual companion LDS 587B which is 33 arc sec away. Several measurements were taken each night to obtain a good phase coverage of light variations. The observations were transformed to the respective standard systems. The mean magnitudes of comparison stars are given in Table 6. The differential magnitudes were converted to *UBVRI* and *by* magnitudes using the magnitudes of SAO 253886 given Table 6, and are listed in Tables 7 and 8, respectively.

Table 7. *UBVRI* magnitudes of HD 155555

J.D. 2440000.+	<i>U</i>	<i>B</i>	<i>V</i>	<i>R</i>	<i>I</i>
6896.760	7.898	7.591	6.797	6.322	5.894
6896.821	7.890	7.575	6.774	6.308	5.888
6896.874	7.860	7.567	6.764	6.293	5.871
6897.708	7.762	7.503	6.715	6.269	5.845
6897.757	7.787	7.506	6.722	6.268	5.853
6897.790	7.770	7.519	6.729	6.281	5.859
6897.831	7.807	7.542	6.739	6.284	5.864
6897.872	7.840	7.540	6.755	6.291	5.867
6898.707	7.791	7.511	6.727	6.267	5.840
6898.757		7.492	6.708	6.249	5.830
6898.811		7.475	6.693	6.240	5.820
6898.889	7.766	7.471	6.675	6.232	5.812
6899.699	7.920	7.592	6.786	6.318	5.889
6899.753	7.914	7.582	6.790	6.317	5.878
6899.795	7.944	7.610	6.806	6.335	5.896
6899.835	7.940	7.594	6.792	6.337	5.893
6899.885	7.960	7.612	6.810	6.348	5.896
6901.697	7.970	7.606	6.808	6.340	5.896
6902.689	7.773	7.496	6.700	6.262	5.839

Table 7. continued

J.D. 2440000.+	<i>U</i>	<i>B</i>	<i>V</i>	<i>R</i>	<i>I</i>
6902.741	7.820	7.502	6.718	6.263	5.848
6902.787	7.802	7.510	6.729	6.272	5.862
6902.836	7.830	7.523	6.730	6.275	5.864
6902.892	7.840	7.539	6.745	6.296	5.868
6903.748	7.786	7.498	6.701	6.252	5.832
6903.798	7.763	7.479	6.704	6.241	5.818
6903.836	7.764	7.477	6.685	6.238	5.814
6903.883	7.748	7.465	6.681	6.239	5.812
6904.693	7.920	7.580	6.780	6.319	5.890
6904.738	7.938	7.590	6.787	6.331	5.898
6904.796	7.971	7.602	6.794	6.335	5.904
6904.837	7.978	7.607	6.802	6.340	5.906
6904.880	7.997	7.611	6.808	6.348	5.904
6905.705	7.764	7.465	6.680	6.233	5.810
6907.881	7.860	7.560	6.741	6.300	5.871
7296.631	7.875	7.522	6.725	6.286	5.867
7296.900	7.854	7.502	6.717	6.269	5.837
7304.603	7.901	7.575	6.765	6.310	5.876
7304.749	7.892	7.550	6.758	6.303	5.874
7304.872	7.874	7.532	6.735	6.294	5.859
7305.596	7.864	7.539	6.745	6.296	5.860
7305.731	7.881	7.551	6.753	6.300	5.873
7305.855	7.905	7.564	6.761	6.309	5.876
7307.611	7.911	7.569	6.777	6.311	5.885
7307.798	7.914	7.578	6.782	6.319	5.885
7308.576	7.830	7.490	6.711	6.263	5.839
7308.723	7.835	7.498	6.719	6.268	5.850
7308.832	7.862	7.532	6.737	6.288	5.856

Table 8. *by* magnitudes of HD 155555

J.D. 2440000.+	<i>b</i>	<i>y</i>
7739.570	7.359	6.857
7742.593	7.346	6.838
7743.506	7.242	6.740
7743.627	7.255	6.771
7744.500	7.372	6.875
7744.618	7.374	6.860
7747.639	7.343	6.848
7748.485	7.248	6.764
7748.625	7.250	6.758
7749.508	7.383	6.871
7749.643	7.388	6.873
7750.513	7.258	6.782
7750.644	7.283	6.794
7751.490	7.354	6.824
7752.491	7.340	6.820
7752.618	7.348	6.857
7753.489	7.264	6.778
8088.542	7.399	6.868
8088.650	7.372	6.872
8088.729	7.370	6.866
8093.538	7.375	6.873
8093.580	7.376	6.872
8093.630	7.382	6.867
8093.678	7.376	6.870
8093.706	7.370	6.869
8093.737	7.369	6.875
8094.487	7.429	6.917
8094.523	7.425	6.918
8094.573	7.435	6.918
8094.615	7.414	6.908

Table 8. continued

J.D. 2440000.+	<i>b</i>	<i>y</i>
8094.669	7.420	6.914
8094.698	7.419	6.906
8094.739	7.416	6.910
8094.770	7.417	6.904
8096.483	7.402	6.896
8096.526	7.407	6.900
8096.575	7.407	6.898
8096.621	7.401	6.903
8096.669	7.407	6.904
8096.701	7.399	6.896
8096.740	7.391	6.880
8097.466	7.415	6.901
8097.565	7.421	6.913
8097.608	7.430	6.910
8097.640	7.436	6.905
8097.672	7.436	6.912
8097.708	7.426	6.910
8097.750	7.419	6.913
8097.779	7.425	6.907
8099.592	7.426	6.898
8099.633	7.405	6.902
8099.677	7.419	6.897
8099.712	7.415	6.904
8099.804	7.419	6.855
8100.479	7.381	6.879
8100.515	7.402	6.895
8100.575	7.425	6.898
8100.632	7.413	6.905
8100.683	7.424	6.905
8100.733	7.414	6.911

Table 8. continued

J.D. 2440000.+	b	y
8100.786	7.428	6.905
8101.528	7.411	6.889
8101.572	7.415	6.895
8101.632	7.405	6.888
8101.743	7.410	6.891
8102.580	7.417	6.915
8102.630	7.427	6.909
8102.687	7.412	6.910
8102.772	7.410	6.903

5.2.3. Light curves

The photometric period of 1.66 days reported by Udalsky & Geyer (1984) is very close to the orbital period determined by Pasquini et al. (1991), and hence for the conversion of Julian days of observation into photometric phases the following ephemeris provided by the latter authors for the radial velocity data were used:

$$JD(HeI.) = 2446998.410 + 1.661652E.$$

The initial epoch corresponds to the time of maximum radial velocity of the brighter component and the period is the orbital period. Figures 6 and 7 are the plots of V , $U - B$, $B - V$, $V - R$, and $V - I$ and Figure 8 is the plot of y and $b - y$ observations; the mean epochs of observations are indicated in the respective figures.

Starting in 1979 (Lloyd Evans & Koen 1987), HD 155555 has been observed during 11 seasons including the present 4 seasons. The light curve parameters are read directly from the respective graphical plots of the light curves and are listed in Table 9. None of the available light curves, though displays significant asymmetry, shows double minima, indicating a near continuous longitudinal distribution of spots over the stellar surface. The 1980

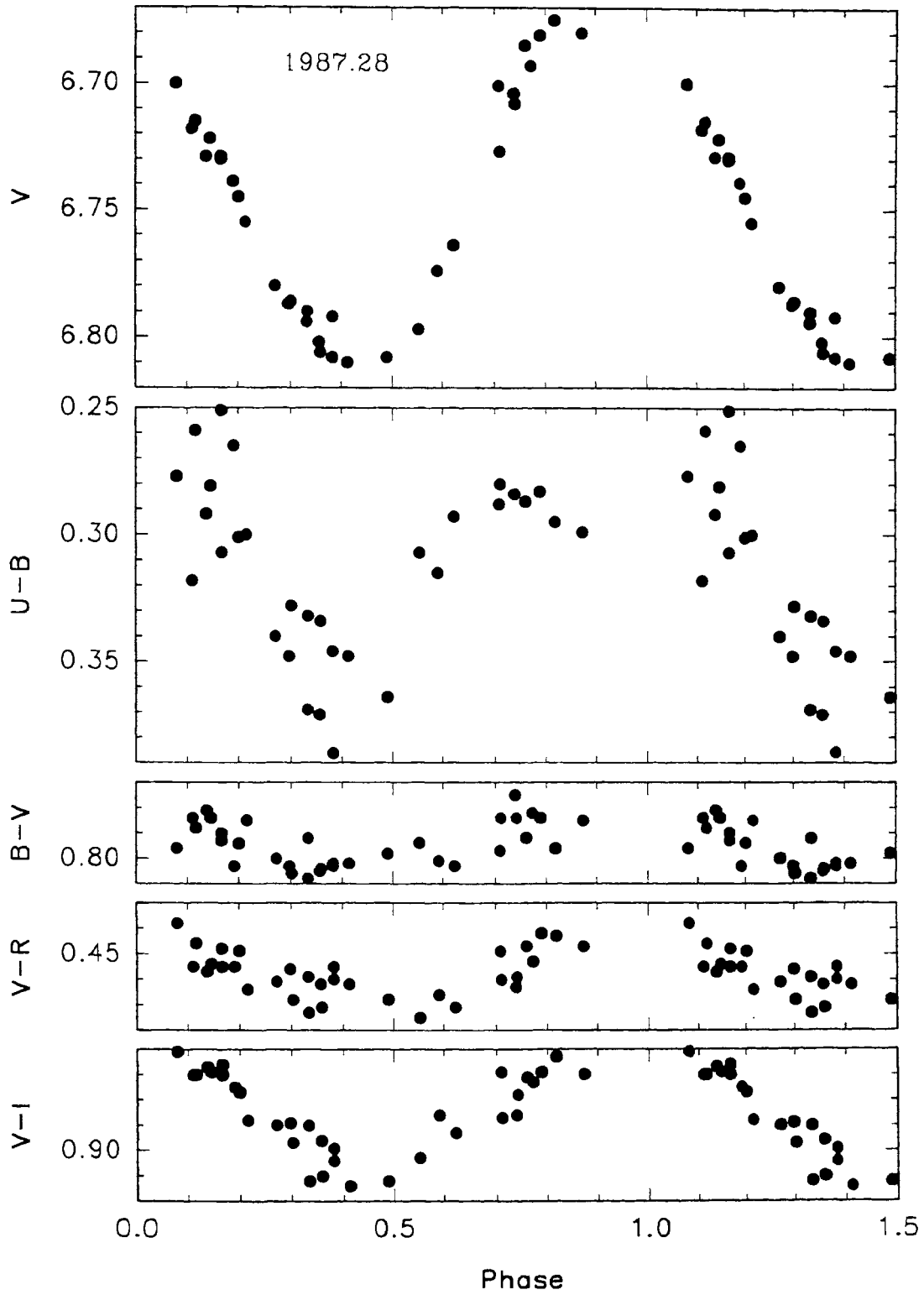


Fig. 6. Plots of V, U-B, B-V, V-R and V-I of HD 155555

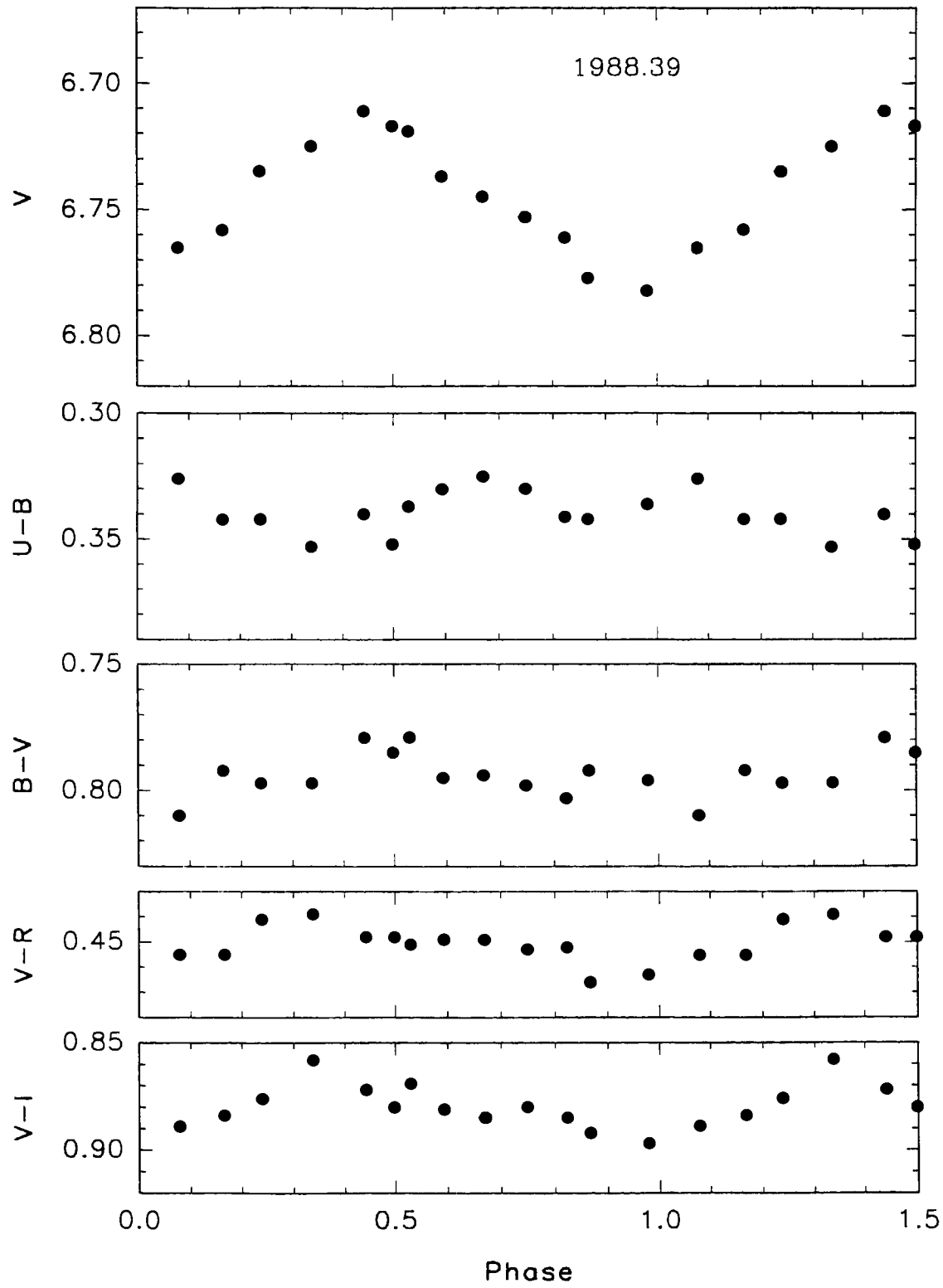


Fig. 7. Plots of V, U-B, B-V, V-R and V-I of HD 155555

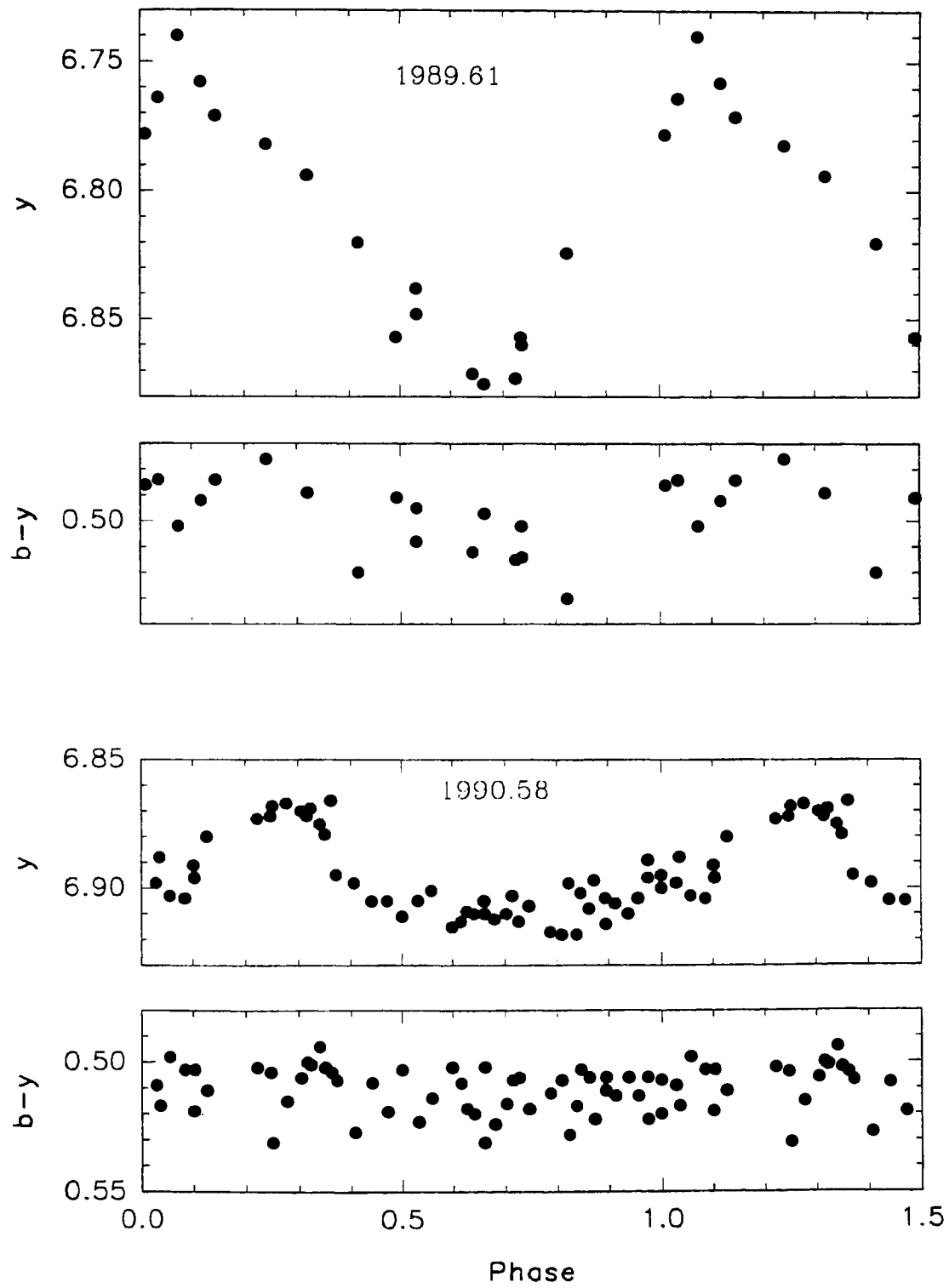


Fig. 8. Plots of y , $u-y$, $v-y$ and $b-y$ of HD HD 155555

observations of Lloyd Evans & Koen (1987) and 1983 observations of Scaltriti & Busso (1984) were not included in the present analysis because the corresponding light curves are not defined well as a result of poor phase coverage.

Table 9. Photometric characteristics of HD 155555

Epoch	Amplitude	V_{max}	V_{min}	ϕ_{min}	References
1979.70	0.095	6.730	6.825	0.20	Lloyd Evans & Koen (1987)
1981.47	0.070	6.730	6.800	0.20	Lloyd Evans & Koen (1987)
1984.30	0.080	6.630	6.710	0.15	Udalsky & Geyer (1984)
1985.43	0.080	6.685	6.765	0.25	Bopp et al. (1986)
1986.43	0.065	6.715	6.780	0.25	Rucinski (1988)
1987.15	0.100	6.700	6.800	0.35	Rucinski (1988), Cutispoto (1990)
1987.28	0.135	6.675	6.810	0.45	Present study
1988.39	0.070	6.710	6.780	0.95	Present study
1989.16	0.115	6.765	6.880	0.35	Cutispoto (1993)
1989.61	0.135	6.740	6.875	0.65	Present study
1990.58	0.050	6.865	6.915	0.50	Present study

5.2.4. $U - B$ variation

An inspection of Figures 6 and 7 shows that the variations in $B - V$, $V - R$ and $V - I$ colours are such that the star appears redder at light minimum, as expected when starspots cooler than the ambient photosphere are the causes of the light modulation. The modulation in $U - B$ colour is quite intriguing. It shows a rather large amplitude in Figure 6, almost the same amplitude as that of the V light curve. The photometry presented in earlier chapters shows that when cooler starspots are present the modulation in $U - B$ is much less than that in V . The $U - B$ colour also shows a large scatter in Figure 6, much larger than the observational uncertainty of ~ 0.01 mag, whereas the V light curve is rather smooth. Figure 7 shows a near-out-of-phase variation of $U - B$

with respect to the V light curve. The photometry obtained by Udalsky & Geyer (1984) during 1984.30 shows a phase lag between the $U - B$ colour and V light curves. These imply that in addition to the cooler starspots, there are other quasi-permanent surface features which contribute to the U band flux modulation. Bright photospheric plages is a likely candidate. Another possibility is the presence of bright chromospheric emission regions. The U band includes several Balmer lines which may exhibit emission or filled-in emission and $Ca H$ & K emissions. During light minimum the photospheric light is reduced and the chromospheric emission become prominent, affecting the measurements in U band significantly, and there by making $U - B$ bluer. The observations obtained by Cutispoto (1990) and Rucinski (1988), which are separated by twenty days, are re-plotted in Figure 9, as open circles and filled circles. The Julian day intervals are also indicated in the figure. The first set of observations lie systematically above the second set in all the plots shown. During the first spell the $U - B$ colour did not show any modulation with phase, whereas during the second it varied almost out-of-phase with the V light curve. It is clear from the figure that the hotter features that cause the additional modulation in U band are rather short-lived when compared to the cooler starspots; this probably accounts for the large scatter in the $U - B$ curve at certain epochs. The B band is also mostly affected, but to a lesser extent. The shorter life-time for these features is further evident when one compares the $U - B$ values plotted in Figure 9 with those plotted in Figure 6; the latter observations were obtained about 25 days after the former. The out of phase $U - B$ curve became nearly in phase with the V light curve within this short time span.

5.2.5. Broadband colours of the components

From a spectroscopic analysis Pasquini et al. (1991) found that the two components of HD 155555 have similar chromospheric activity. They also found that in the CORAVEL passband (3900-5200Å) the hotter component is brighter by about 0.9 mag. Therefore in the I band the contribution to the total light by the cooler component (K0) could be appreciable. In view of the similar chromospheric activity, as indicated by the $Ca II H$ & K ,

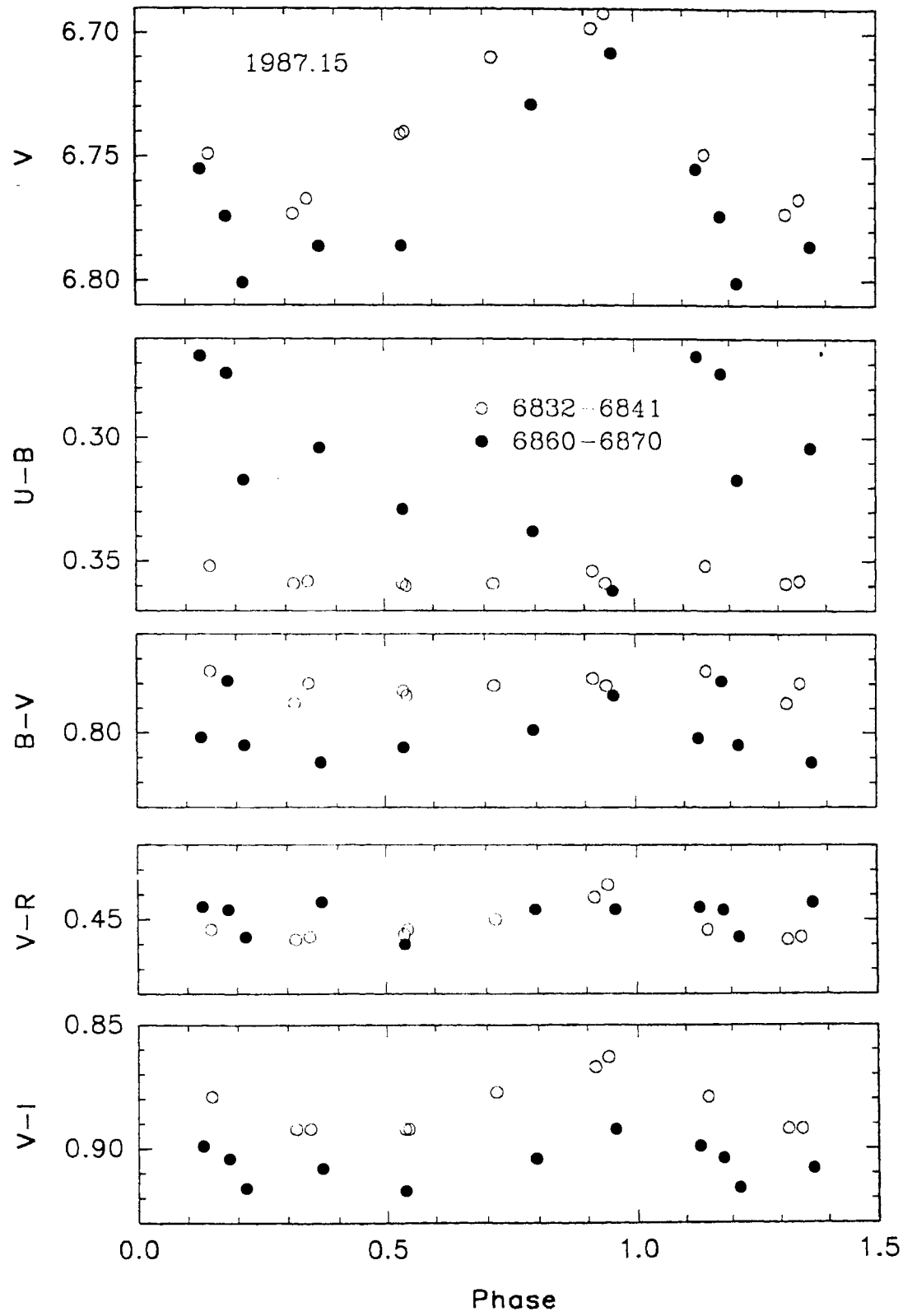


Fig. 9. Plots of V, U-B, B-V, V-R and V-I of HD 155555

it is reasonable to expect that both the components are light variables. Most of the light variation seen at shorter wavelengths would be due to hotter component, but at longer wavelengths the observed variation would be the combined effect of the two components. In this case one would expect to see a phase shift in the light curves obtained in B and I bands, at least at some epochs. As already seen the U band observations are complicated by the probable presence of photospheric plage-like regions and chromospheric emissions, otherwise U band observations would be better than B band observations. However, no such phase shift is seen between $B - V$ and $V - I$ colour curves in any of the 11 seasons' photometry that exists for HD 155555, implying that either the cooler component is not a light variable or the amplitude of light variation is significantly smaller than that shown by the hotter component. Udalsky & Geyer (1984) had already suggested that the hotter and the brighter component is probably causing the light variability.

The light and colour curves presented in the earlier sections show that an increase in the amplitude of V light curve is always followed by an increase in the amplitudes of colour curves. Assuming a linear relationship between the amplitudes in V and $X - V$ colour, with X representing any spectral band, the total flux observed in V and X bands at time t , F_t^V and F_t^X , can be written as

$$F_t^V = F_h^V A + F_c^V B$$

and

$$F_t^X = F_h^X A^\alpha + F_c^X B^\beta,$$

where F_h^V and F_c^V are the unspotted (or, alternatively any reference level) V band flux of hotter and cooler components, A and B are the reduction in V band flux of the components at time t , and α and β are coefficients which specify the relationship between the variation between the flux in X and V bands. As seen from the colour curves presented in earlier sections the values of α and β lie in the range 1.20 to 0.80 for the spectral band range U to I .

The quantities A and B can be evaluated if the difference in V magnitudes between the components and the $B - V$ colour of the hotter component at the reference level are known. If we assume the difference in V magnitudes between the components and the $B - V$ of the hotter component, from the

unspotted B and V magnitudes of the system, the values of F_h^V , F_c^V , F_h^B and F_c^B can be calculated. If suitable assumption of the values of α and β are made, the quantities A and B can be calculated from each set of B and V observations and the individual V and B light curves of the two components can be computed.

Assuming that both components are light variables an attempt was made to separate the individual V light curves of the components for possible ranges in their V mag difference and $B - V$ colour of the hotter component. The possible range in the values of α and β were also considered. It was found that for all the cases tried the resulting light curves of the two components show a large scatter (> 0.2 mag), indicating that the assumption that the cooler star also varies appreciably is not true. The large scatter results because neither A nor B thus derived represents the actual situation.

Table 10. Computed values of α in different spectral bands

Spectral band	$T_s = 4000$ K	$T_s = 3500$ K
U	1.133 ± 0.003	1.054 ± 0.003
B	1.078 ± 0.002	1.035 ± 0.002
R	0.961 ± 0.001	0.967 ± 0.001
I	0.851 ± 0.002	0.907 ± 0.002

The values of α in $UBRI$ bands computed for two spot temperatures $T_s = 3500$ K and $T_s = 4000$ K are given in Table 10. The photospheric temperature T_p was assumed to be 5500 K, corresponding to the spectral type G2IV. The limb-darkening coefficients were the same as those listed in § 3.3.. The light curves were generated in $UBVRI$ bands using the computer program described in § 3.3., assuming that the light variation is caused by a rectangular spot bounded by a latitudinal belt of $\pm 20^\circ$. The spots were also assumed to extend over the entire range in longitude on the hemisphere visible at light minimum. The angle of inclination of the rotational axis was taken as $i = 50^\circ$, same as that suggested for HD 155555 by Pasquini et al

(1991). The values of α listed in Table 10 were then derived assuming a linear relationship between the magnitudes in *UBRI* bands and that in *V* band.

If the cooler component is a non-variable then $B = 1.0$, and therefore

$$A = \frac{F_t^V - F_c^V}{F_h^V}$$

and the total flux observed in any other band *X* is given by

$$F_t^X = F_h^X A^\alpha + F_c^X.$$

Assuming the values of α , from the observed values X_t the values of F_h^X and F_c^X can be computed if *A* is known. The value of *A* depends on the relative brightness of the two components. The various broadband colours of the two components derived from the data are plotted against the corresponding assumed difference in *V* magnitudes of the two components in Figures 10 and 11. All the observations were treated with equal weights and the method of least square was used to derive the fluxes in the various spectral bands which in turn were converted to broadband colours.

Table 11. Computed colours of the hotter component for different spot temperatures

Spot Temp.	<i>U</i> - <i>B</i>	<i>B</i> - <i>V</i>	<i>V</i> - <i>R</i>	<i>V</i> - <i>I</i>
3500 K	0.12±0.02	0.68±0.01	0.38±0.01	0.60±0.01
4000 K	0.15±0.02	0.72±0.01	0.39±0.01	0.66±0.01

The colours derived for the hotter and the brighter component are nearly independent of the difference in brightness between the components at *V* band. Table 11 gives the results for the hotter component for the two cases of spot temperature. The two sets of values mutually agree. They are well within the errors of their determination, indicating that the dependence of the derived colours on the values of α is rather weak. For the same value of

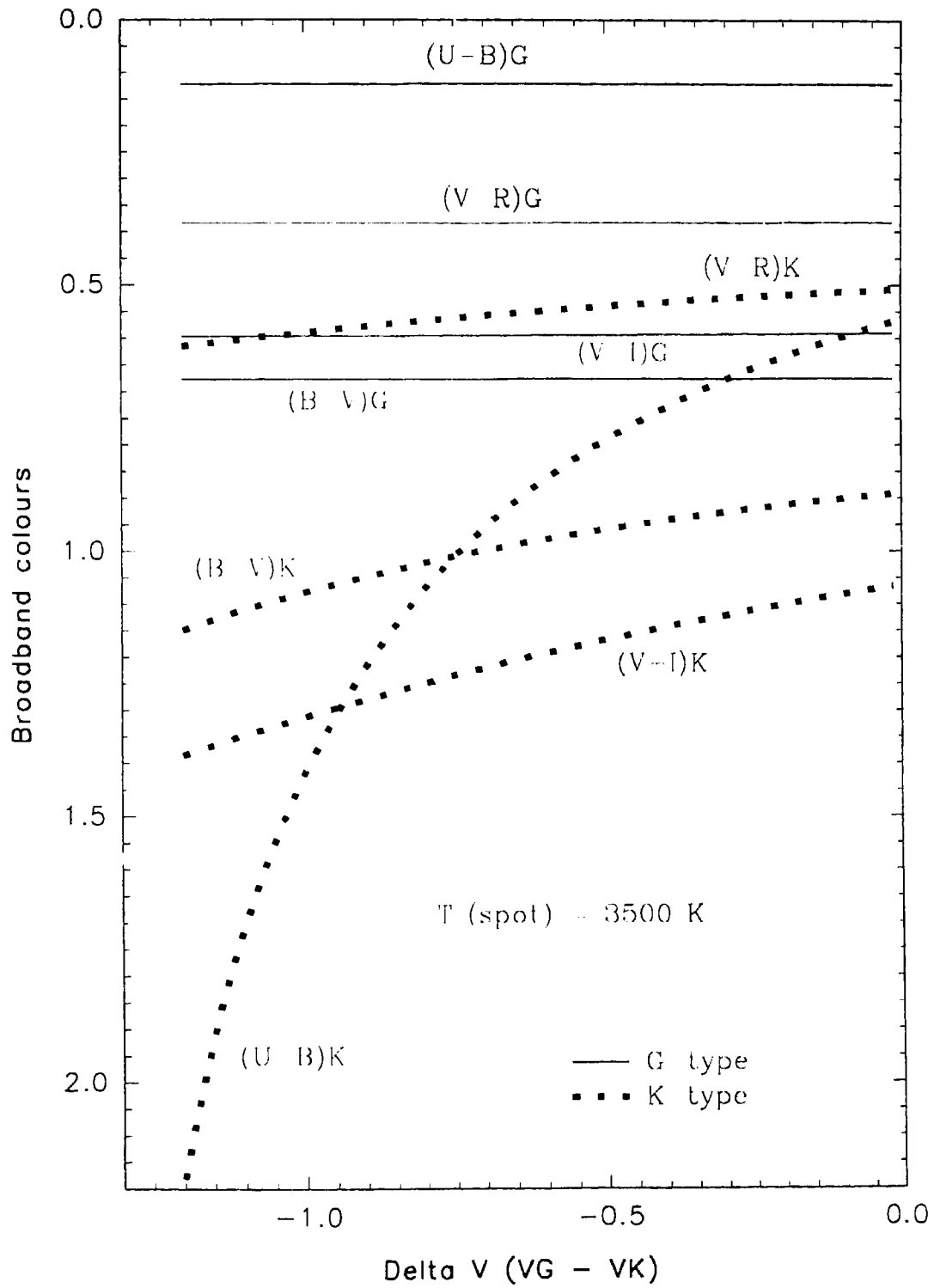


Fig. 10. Plots of broadband colours of the components against the assumed V mag difference between them

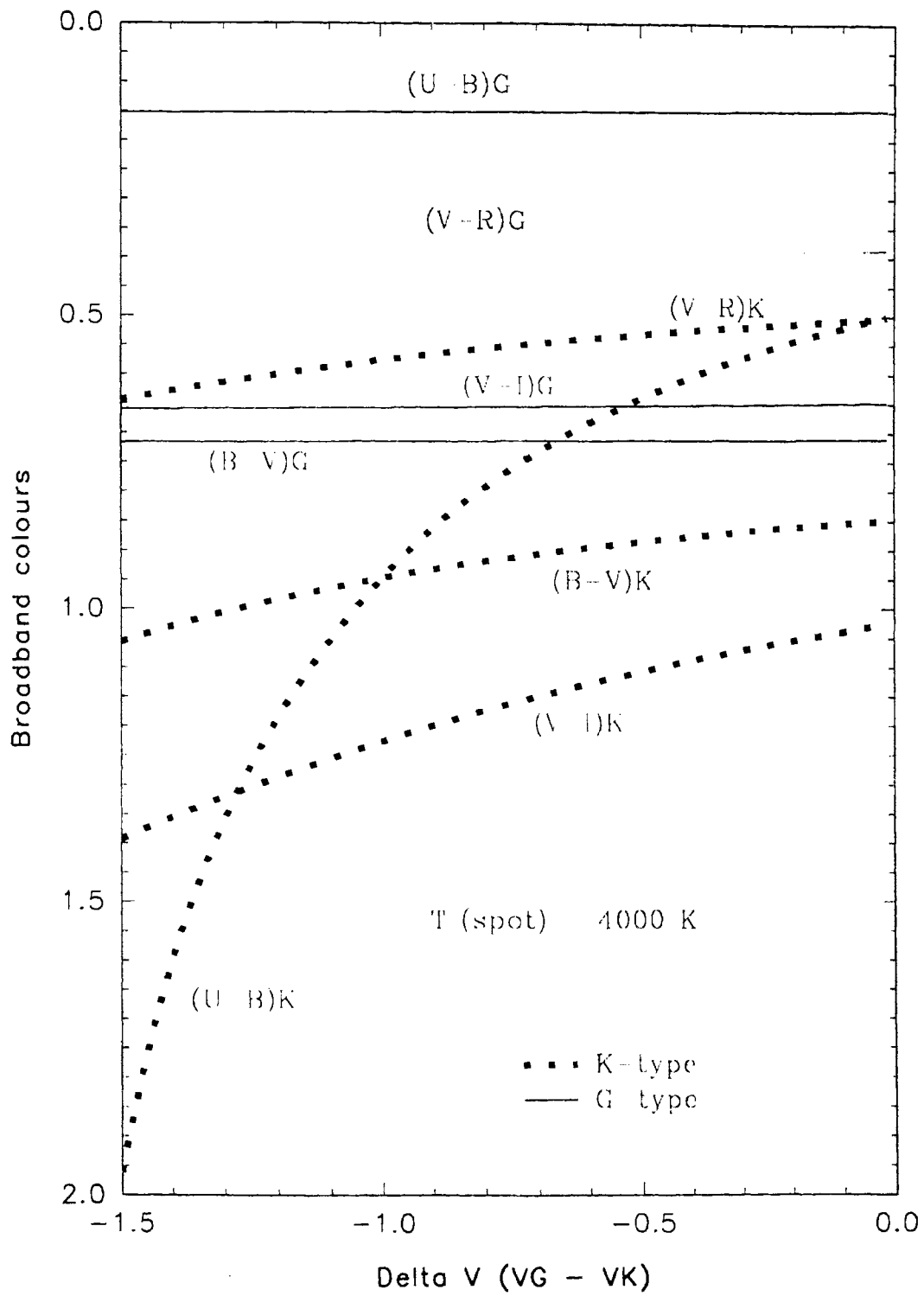


Fig. 11. Plots of broadband colours of the components against the assumed V mag difference between them

α the colours of the faint component derived depends appreciably on the V mag difference between the the two components that is assumed; they become redder as the cooler component becomes relatively fainter. The fraction A in the reduction of V band flux depends on the brightness difference between the components; the more the cooler star becomes fainter n V the larger the value of A since the observed variation directly gives variation in the hotter component. When the cooler star is relatively bright, the amplitude of light variation observed will be less than the actual amplitude.

The comparatively small errors in the derived colours given in Table 11 indicate that either the cooler star is a non-variable or the amplitude of light variation is insignificant; otherwise the assumption that $B = 1.0$ would have resulted in larger errors in the derived colours.

A limit on the brightness difference between the two components can be put if the cool component is a normal main sequence dwarf, *i.e.*, if it does not exhibit an excess either in the red or ultraviolet. The values of $U - B$, $V - R$ and $V - I$ colours derived for the two components are plotted against corresponding $B - V$ colours in Figure 12 and 13. The mean colours of main sequence stars taken from Johnson (1966) are also plotted in the figures. The $V - R$ and $V - I$ in the Johnson's system were converted to Cousin's system using the calibration given by Fernie (1983). The error in the $U - B$ colour of the hotter star is ~ 0.02 mag and for all the other colours it is ~ 0.01 mag. The errors in $B - V$, $V - R$ and $V - I$ of the cooler component are less than 0.03 mag in the entire brightness difference range considered while that in $U - B$ colour increases rapidly as the cooler component becomes relatively fainter and fainter. Therefore in Figures 12 and 13 the upper limits (bluer) on the colours of the cooler star are plotted.

The $V - R$ colour of the hotter star lies exactly on the curve defined by the mean colours of main-sequence stars in both Figures 12 and 13 while the $U - B$ and $V - I$ colours lie about 0.1 mag above the respective curves. In the case of the cooler star also the $V - R$ curve lie very close to the same defined by the main sequence stars while the $V - I$ curve lies on an average about 0.10-0.15 mag below that defined by the main-sequence stars. The near symmetric placing of the $V - I$ colours of the hotter and cooler

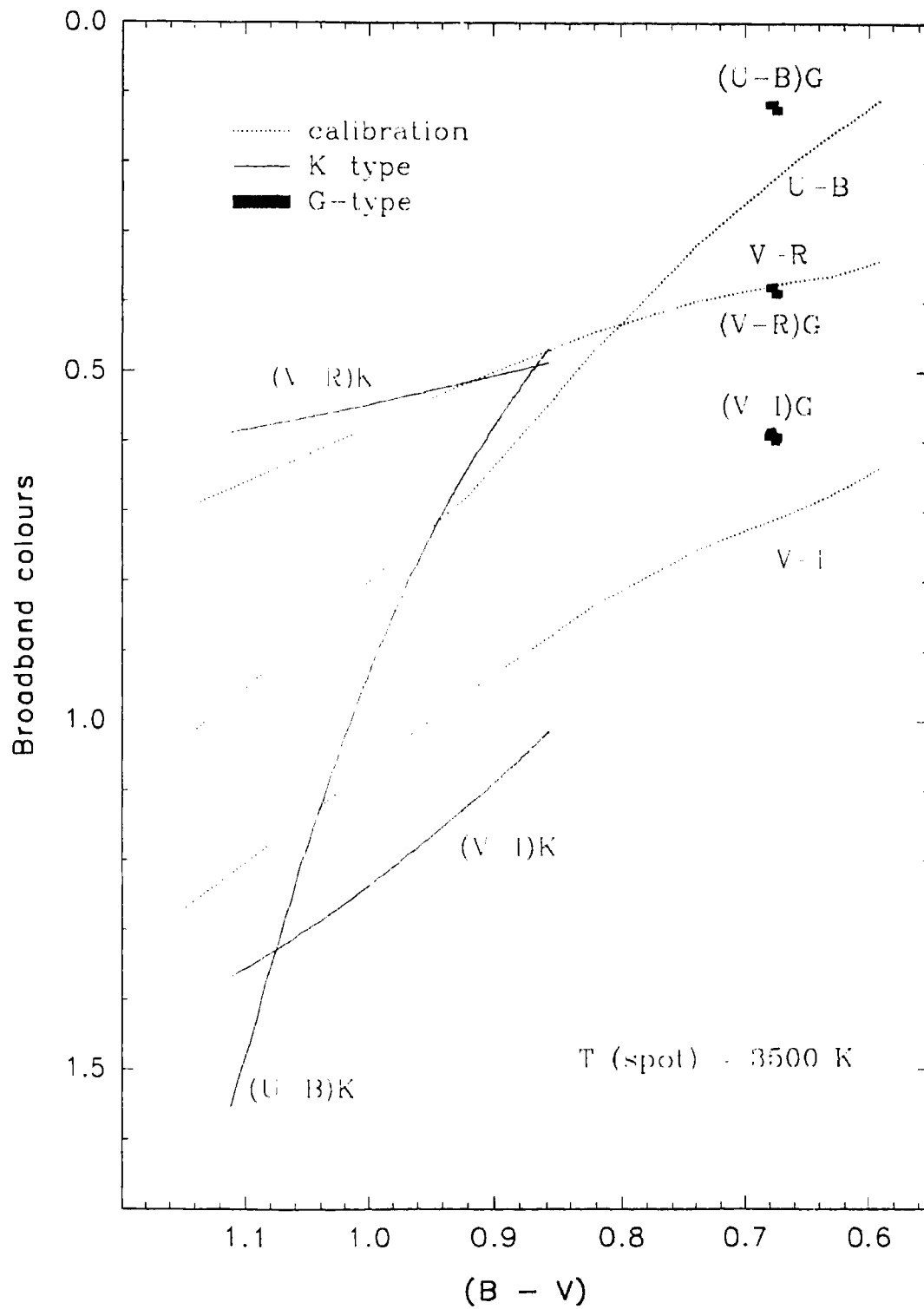


Fig. 12. Plots of $U - B$, $V - R$ and $V - I$ against the corresponding $B - V$ colour

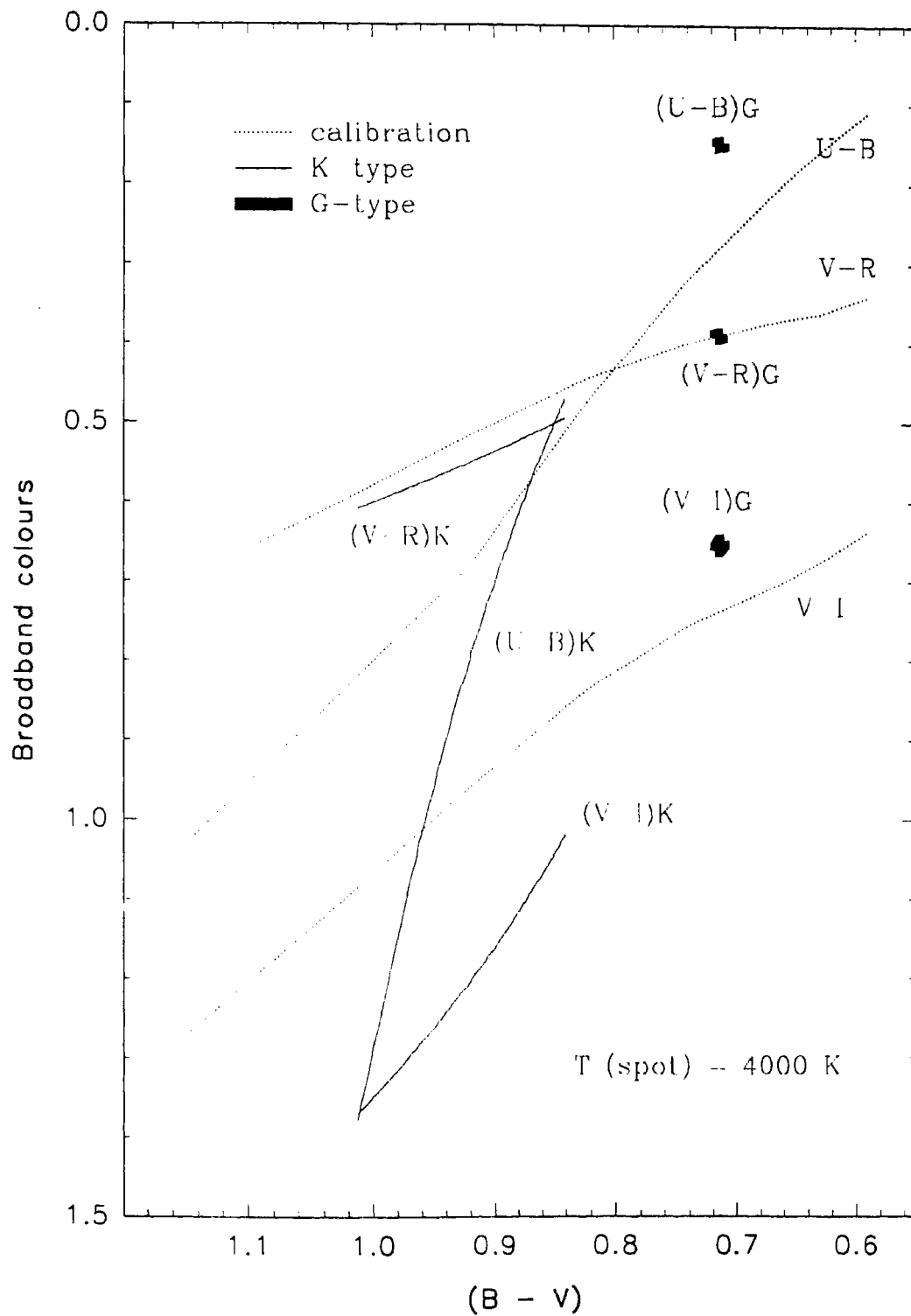


Fig. 13. Plots of U-B, V-R and V-I colours against the corresponding B-V colour

star about the mean colours of the main-sequence stars in Figures 12 and 13 probably results from the assumed linear relationship between the amplitudes in V band I bands. The corresponding effects in $B - V$ and $V - R$ colours will not be appreciable because the difference in the corresponding effective wavelengths are smaller.

If the above argument is true the $U - B$ of the cooler star should be only about 0.15-0.20 mag below the $U - B$ curve defined by the main-sequence stars since the $U - B$ of the hotter star is about 0.15 mag above it. This would be possible only if $B - V$ of the cooler star is about 0.92-0.98. From Figures 10 and 11 it is found that the the active star should be brighter than the other by 0.8 ± 0.2 mag when it is unspotted if its $B - V$ should lie in the above range. The colours of the cooler component corresponding to this brightness difference are given in Table 12.

Table 12. Expected colours of the cooler component if it is about 0.8 mag fainter than the hotter.

$U - B$	$B - V$	$V - R$	$V - I$
0.90 ± 0.10	0.95 ± 0.05	$0.56 \pm$	$1.20 \pm$

According to the spectral type — mean colour relation given by Johnson (1966) the colours given in Tables 11 and 12 correspond to a spectral type slightly later than G5 for the hotter component and slightly earlier than K5 for the cooler component.

5.2.6. Amplitude and phase of light minimum

The values of V_{max} and V_{min} of HD 155555 given Table 9 are plotted against the mean epochs of observation in Figure 14a. The vertical bar gives the amplitude of light variation at that epoch. Both V_{max} and V_{min} show similar pattern in their long-term behaviour; both increased from 1979.70 onwards and attained their maximum values during 1984.30 and afterwards

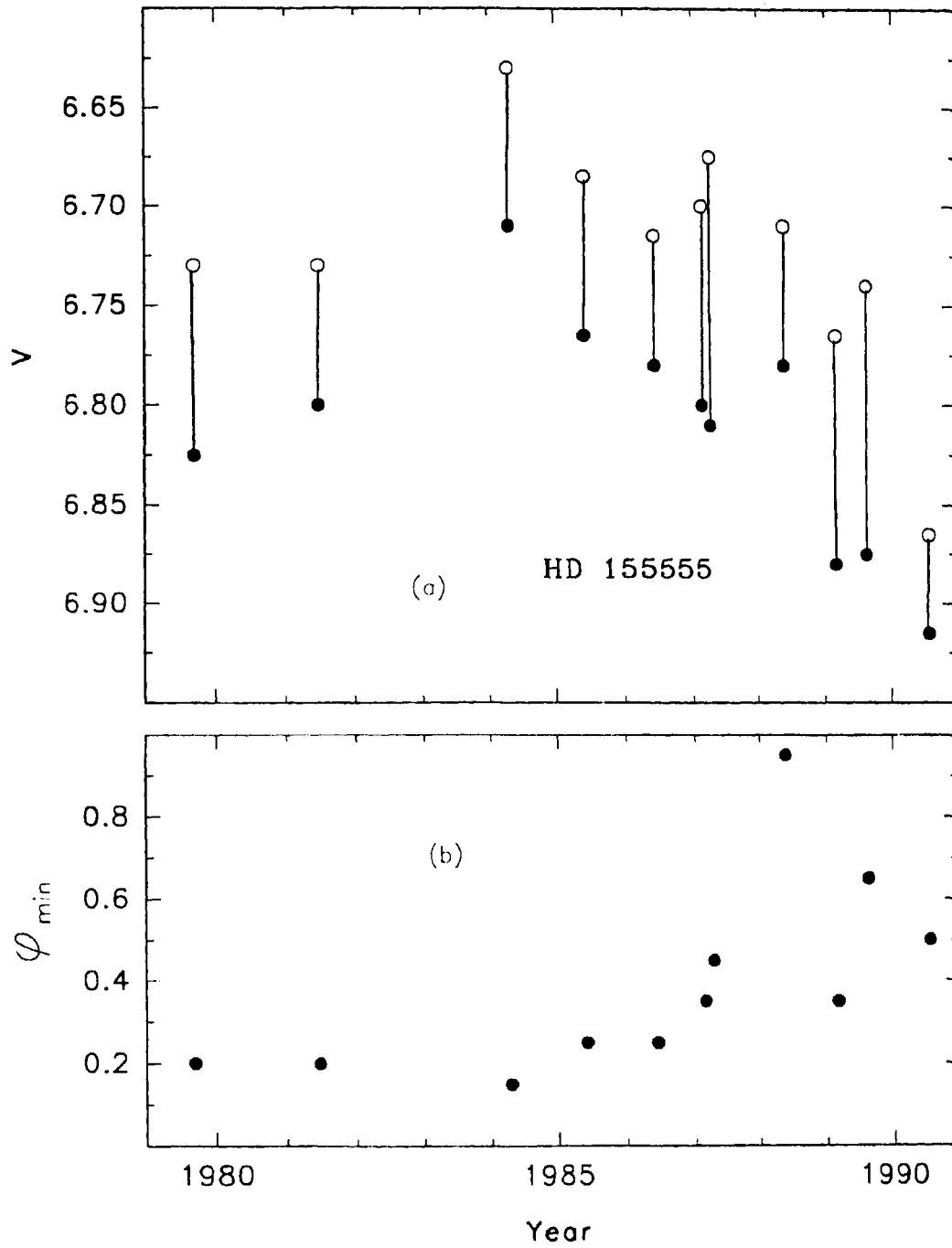


Fig. 14. (a) Plots of Vmax (open circles) and Vmin (filled circle) against the corresponding mean epoch. (b) plot of phase min. against the mean epoch

decreased. The trend continued till 1990.58 when the star was last observed. The maximum value of $V_{max} = 6.630$ mag that occurred during 1984.30 is probably close to the unspotted magnitude of the star. The maximum amplitude (0.135 mag) was observed during 1987.28 and 1989.61 and the minimum (0.05 mag) during 1990.58. Even though HD 155555 is observed at a fairly large inclination ($i > 50^\circ$, Pasquini et al. 1991) the amplitudes of light variation observed are relatively small (< 0.13 mag) when compared to that observed in RS CVn systems where amplitudes of the order of 0.20 to 0.30 mag are quite common. The smaller amplitudes most likely is due to the presence of active regions on both hemispheres because the amplitude depends only on the longitudinal asymmetry.

In Figure 14b we have plotted the observed ϕ_{min} listed in Table 9 against the corresponding mean epoch of observation. It appears from the figure that the phase of light minimum ϕ_{min} was within $0.^P2 - 0.^P4$ between 1979.70 and 1987.28 without any significant change. The light curve obtained during 1988.39 is nearly out of phase with that obtained one year earlier; the former curve is shown in Figure 7 and the latter in Figure 6. The sudden shift in the ϕ_{min} observed between 1987.28 and 1988.39 indicates that a new spot group had formed about an opposite longitude. The already existing spot group started decaying as indicated by the brightness at the corresponding photometric phase. The spots probably did not disappear completely since the V_{max} observed during 1987.28 was less than the brightest magnitude observed. During 1989.16 one more spot group appeared at a different longitude, shifting the effective longitude of active regions to $0.^P35$. The drop in V_{max} and the fact that the brightness around $0.^P8$ did not increase suggest that spot groups observed earlier were also present. The light curve obtained during 1990.58 shows that spots were nearly uniformly distributed over the entire longitude over the latitudinal belt that is involved in the rotational modulation because the amplitude of light modulation was only around 0.05 mag. The light minimum, as seen from Figure 8, is flat extending over more than $0.^P5$; the corresponding $b-y$ colour does not show any modulation, but appears redder than that seen during the earlier occasions.

6

WEAK EMISSION T TAURI STARS

6.1. FK Serpentis

6.1.1. Introduction

The flare-like variability of FK Ser (BD-10°4662) was discovered by Kirzenberg and reported by Steinon (1971) who suggested that the star might be a flare star with a spectral type earlier than dMe. Hidayat (1971) detected $H\delta$ and $H\epsilon$ emissions and absorption features in FK Ser which indicated a spectral type near K5. From objective prism studies MacConnel (1971) assigned a spectral type of dK5 and reported the presence of moderate $H\alpha$ emission. Herbig (1973) carried out a detailed study of FK Ser and found that the star is a close visual binary with an angular separation of 1.3 arc sec and the components which show similar spectra differ approximately by 1 mag. Both components show moderate $H\alpha$ emission and strong $Li\ I$ absorption. Herbig (1973) assigned a spectral type of dK5 to the brighter component and dK7 to the fainter component, and on the basis of the proper motion and radial velocity data found that FK Ser is associated with the early B type star HD 170740 which is at a angular distance of 2° and illuminates the reflection nebula IC 1287. If these two stars are associated, then both components of FK Ser lie 3-4 mag above the main sequence. Hence Herbig (1973) concluded

that both components of FK Ser are very young objects of mass about $2M_{\odot}$ that are in the Post T Tauri stage of evolution and are near the bottom of the Hyashi tracks. Herbig's criteria for identifying FK Ser with Post T Tauri stars are the presence of $Li\ I$ absorption line, irregular light variability and weaker hydrogen emissions and smaller near infrared excess when compared to the T Tauri stars.

Zappala (1974) made near infrared JHK observations of FK Ser and found that the near infrared colour excesses are similar to that of ordinary T Tauri stars; the colour-colour plots clearly indicate that the colour excess in FK ser is low when compared to CTTS. The V and $B - V$ magnitudes reported by Zappala (1974) are in good agreement with the earlier observations but the $U - B$ colour show significant differences. The radial velocity observations by Zappala and Herbig did not indicate any appreciable variations.

Hackwell et al. (1974) carried out infrared observations of FK Ser and confirmed the very small infrared excess discovered by Zappala. They suggested that the measurements at 3.5μ indicated that only 0.02 of the total luminosity of FK Ser is contained in the infrared excess. They also included FK Ser in the Post T Tauri category.

Herbig & Goodrich (1986) made near-simultaneous ultraviolet and optical spectrophotometric observations of FK Ser and found that the star has little extreme uv excess. Rucinski (1985) had identified FK Ser as an IRAS source; it is the only Post T Tauri star that has excess at IRAS wavelengths. Darius (1978) reported the detection of a uv flare in FK Ser from the data of the ultraviolet sky survey experiment aboard the TD-1 satellite.

Very few investigations exist in the literature regarding the nature of the light variability of FK Ser. Chugainov (1974) reported a BY Draconis type variability for FK Ser with an indication of periodicity. The limited available observations show that FK Ser has a large $U - B$ variation. The $U - B$ values obtained by N.K. Rao (Herbig 1973) on two different nights and those obtained by Brucato (Zappala 1974) show a large discrepancy while the corresponding $B - V$ observations show a good agreement. The $H\alpha$ and other moderate emission lines, and the low infrared and uv excess indicate

FK ser to be a typical Weak emission T Tauri Star (WTTS).

We have carried out a detailed photometric, spectroscopic and polarimetric investigation of FK Ser in order to study the nature of variability in light, $H\alpha$ emission strength and polarization.

6.1.2. Photometry

Photometric observations of FK Ser were made on 45 nights over five seasons; May 1988 (5 nights), June 1988 (12 nights), August 1989 (11 nights), July 1990 (11 nights) and March 1993 (6 nights). Observations were made in $UBVRI$ during May 1988, in V during March 1993, and in by during the remaining seasons. SAO 161307 and SAO 161342 were observed along with FK Ser as comparison stars during May 1988. SAO 161307 was found to be the more suitable comparison star and so during the remaining seasons all observations of FK Ser were done differentially with respect to this star. Table 1 gives the $UBVRI$ and by magnitudes of SAO 161307 and $UBVRI$ magnitudes SAO 161342. $UBVRI$, by and V magnitudes of FK Ser are presented in Tables 2, 3 and 4, respectively.

Table 1. $UBVRI$ and by magnitudes of the the comparison stars of FK Ser

Star	U	B	V	R	I	b	y
SAO 161307	12.065	11.015	9.495	8.668	7.787	10.525	9.500
	± 0.010	± 0.007	± 0.005	± 0.005	± 0.004	± 0.008	± 0.006
SAO 161342	11.212	9.583	7.954	7.100	6.263		
	± 0.008	± 0.005	± 0.004	± 0.005	± 0.004		

Though Chugainov (1974) reported a period of 5.2 days for the light variability of FK Ser, further observations confirming such a periodic variation does not exist in the literature. During June 1988, August 1989 and July 1990 the star was observed several times each night to build up a data base suitable for a period determination. The average of two or three indepen-

dent observations were taken as a single measurement in order to reduce the observational uncertainty. The data obtained during the above mentioned three seasons were analyzed by the period finding technique described in § 2.4. It was found that FK Ser has light variability with a period of the order of 5 days.

Table 2. *UBVRI* magnitudes of FK Ser

J.D. 2440000.+	<i>U</i>	<i>B</i>	<i>V</i>	<i>R</i>	<i>I</i>
7296.816	12.495	12.030	10.699	9.829	8.960
7304.794	12.821	11.932	10.577	9.713	8.839
7305.849	12.587	11.943	10.593	9.744	8.869
7307.835	12.577	12.000	10.663	9.819	8.927
7308.677	12.707	11.965	10.608	9.747	8.874

Table 3. *by* magnitudes of FK Ser

J.D. 2440000.+	<i>b</i>	<i>y</i>
7316.800	11.475	10.646
7317.800	11.510	10.671
7320.753	11.415	10.537
7322.724	11.575	10.720
7322.848	11.533	10.712
7323.703		10.528
7324.761	11.349	10.495
7326.752	11.418	10.590
7327.753	11.501	10.681
7328.722	11.363	10.548

Table 3. continued

J.D. 2440000.+	<i>b</i>	<i>y</i>
7330.750	11.314	10.479
7332.704	11.544	10.669
7333.751	11.415	10.603
7739.627	11.505	10.638
7743.558	11.461	10.590
7743.665	11.460	10.615
7744.561	11.520	10.626
7744.620	11.513	10.652
7747.676	11.355	10.511
7748.524	11.502	10.620
7748.680	11.488	10.611
7749.691	11.498	10.618
7750.580	11.503	10.626
7751.535	11.421	10.564
7752.542	11.346	10.512
7753.540	11.447	10.576
8088.723	11.396	10.543
8093.608	11.320	10.503
8093.804	11.414	10.552
8094.529	11.441	10.580
8094.799		10.620
8096.513	11.528	10.678
8096.772	11.575	10.718
8097.508	11.493	10.692
8097.774	11.448	10.611
8099.513	11.405	10.580
8099.762	11.422	10.558

Table 3. *b*y magnitudes of FK Ser

J.D. 2440000.+	<i>b</i>	<i>y</i>
8100.500	11.432	10.581
8100.764	11.469	10.630
8101.497	11.517	10.674
8102.492	11.510	10.665
8102.749	11.483	10.652
8103.503	11.311	10.504
8103.510	11.314	10.505
8104.763	11.420	10.590

Table 4. *V* magnitudes of FK Ser

J.D. 2440000.+	<i>V</i>
9064.456	10.603
9065.455	10.584
9066.450	10.624
9067.475	10.581
9068.478	10.561
9069.440	10.587

The Julian days of observations given in Tables 2, 3, and 4 were converted to photometric phases using the ephemeris,

$$JD(HeI.) = 2447316.7195 + 5^d.055E,$$

where the initial epoch corresponds to the first observation of June 1988 season and the period is the mean of the periods derived from the data obtained during the above mentioned three seasons. In general, WTTS rotate faster

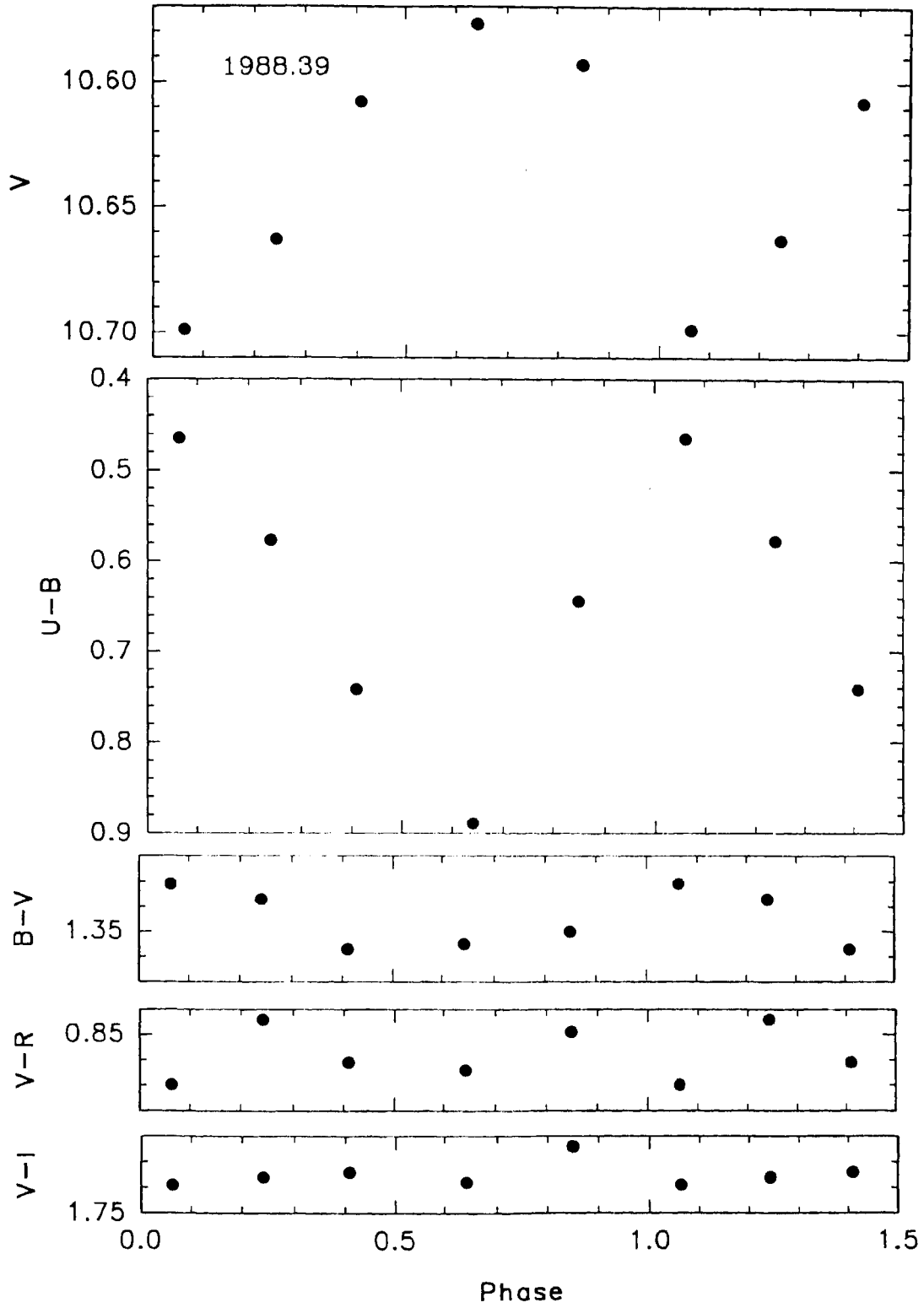


Fig. 1. Plots of V, U-B, B-V, V-R and V-I of HD FK Ser

than CTTS, and hence the former typically have rotation periods significantly less than 5 days. FK Ser appears to be an exception with a period of 5.055 days. The March 1993 observations were mainly done to obtain the V light curve close to the epochs of spectroscopic and polarimetric observations.

6.1.3. Light variations

The photometric observations listed in Tables 2, 3 and 4 are plotted in Figures 1, 2, 3, 4 and 5. The corresponding mean epoch of observation is given in each figure. Though the phase coverage is poor, Figure 1 still brings out the main characteristics of FK Ser. The V light curve has an amplitude of 0.12 mag. The $U - B$ colour shows an amplitude of 0.45 mag and varies almost out of phase with the V mag. The variations in $B - V$, $V - R$, and $V - I$ colours are small when compared to that in $U - B$, indicating that the amplitude in B , V , R and I are almost similar. A similar phenomenon was reported by Vrba et al. (1986) in the relatively weak CTT star DN Tau ($H\alpha$ EW = 12Å). The large amplitude U band light variations in DN Tau were found to be shifted in phase by 0.47 with respect to the variations at longer wavelengths. They interpreted this behaviour as due to the presence of a CTTS type hot spot existing almost co-spatially with a cool spot. Probably in FK Ser also a similar type of phenomenon might be causing the observed light variations.

The light curve obtained during June 1988 has a large amplitude (0.23 mag); the light maximum was also bright. The amplitude as well as the shape of the light curve changed considerably during August 1989. The amplitude was around 0.14 mag in y , and the $b - y$ colour variations were in phase with the y light curve. During July 1990, the ascending branch of the light curve had a steep increase and the amplitude was around 0.21 mag. The $b - y$ showed a redder colour at light minimum. The march 1993 light curve had the least amplitude observed so far (0.06 mag).

The periodic light variations observed during the five seasons show that the phenomenon that causes the light variation is more or less stable throughout the observing run and also the light curves show very less scatter, typical of WTTS. It is now established that the light modulation in WTTS is caused

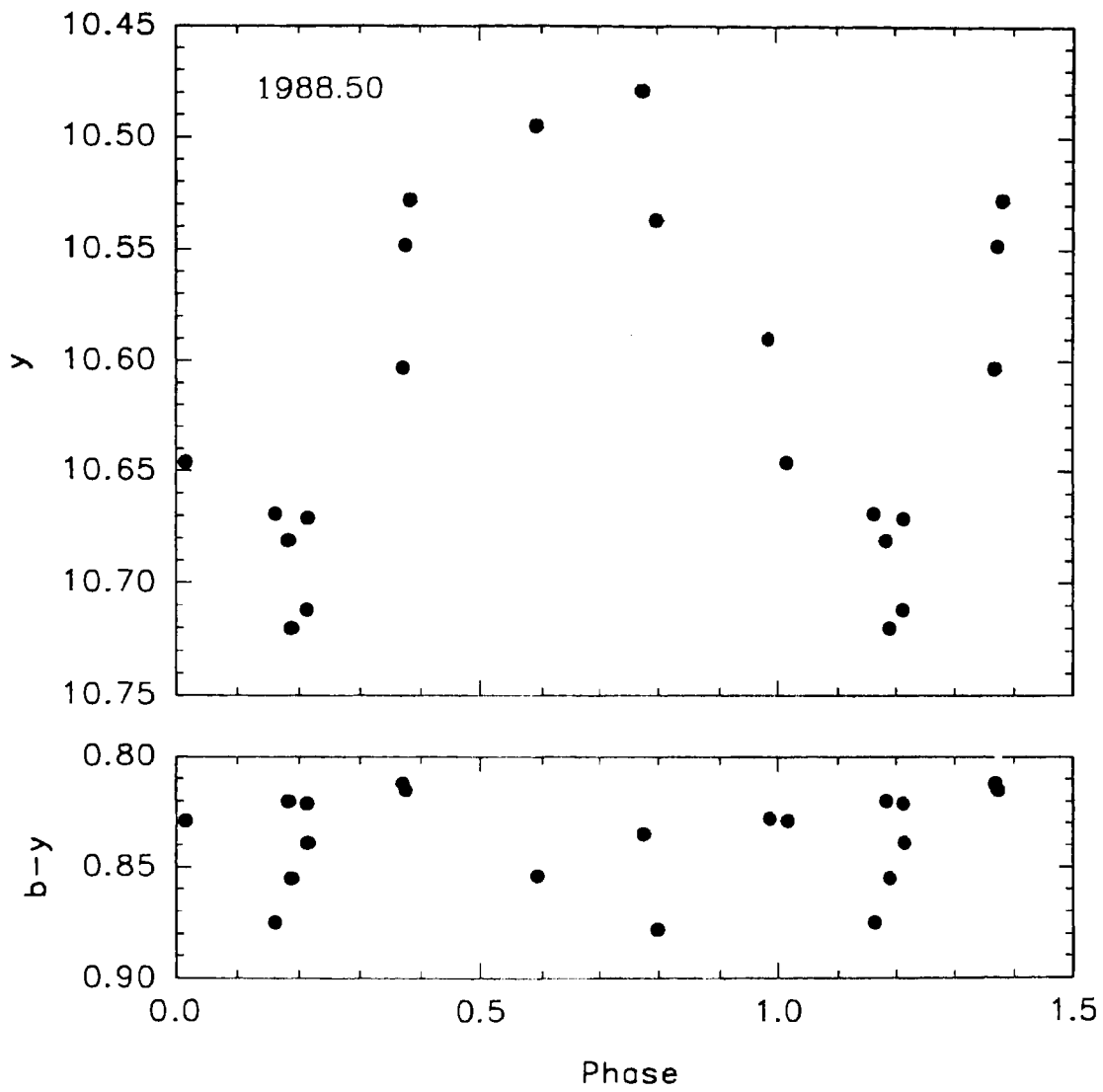


Fig. 2. Plots of y and $b-y$ of FK Ser

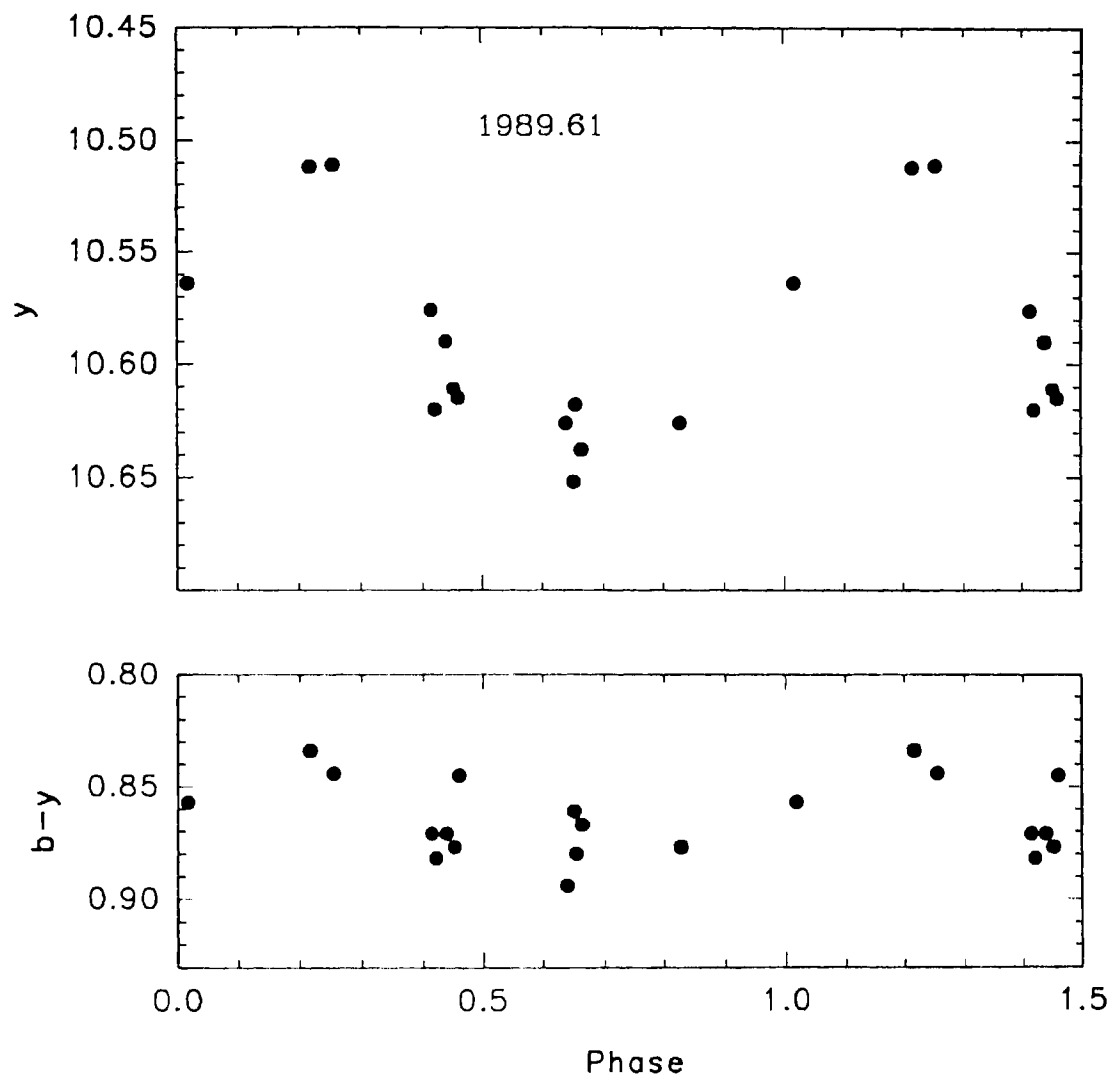


Fig. 3. Plots of y and $b-y$ of FK Ser

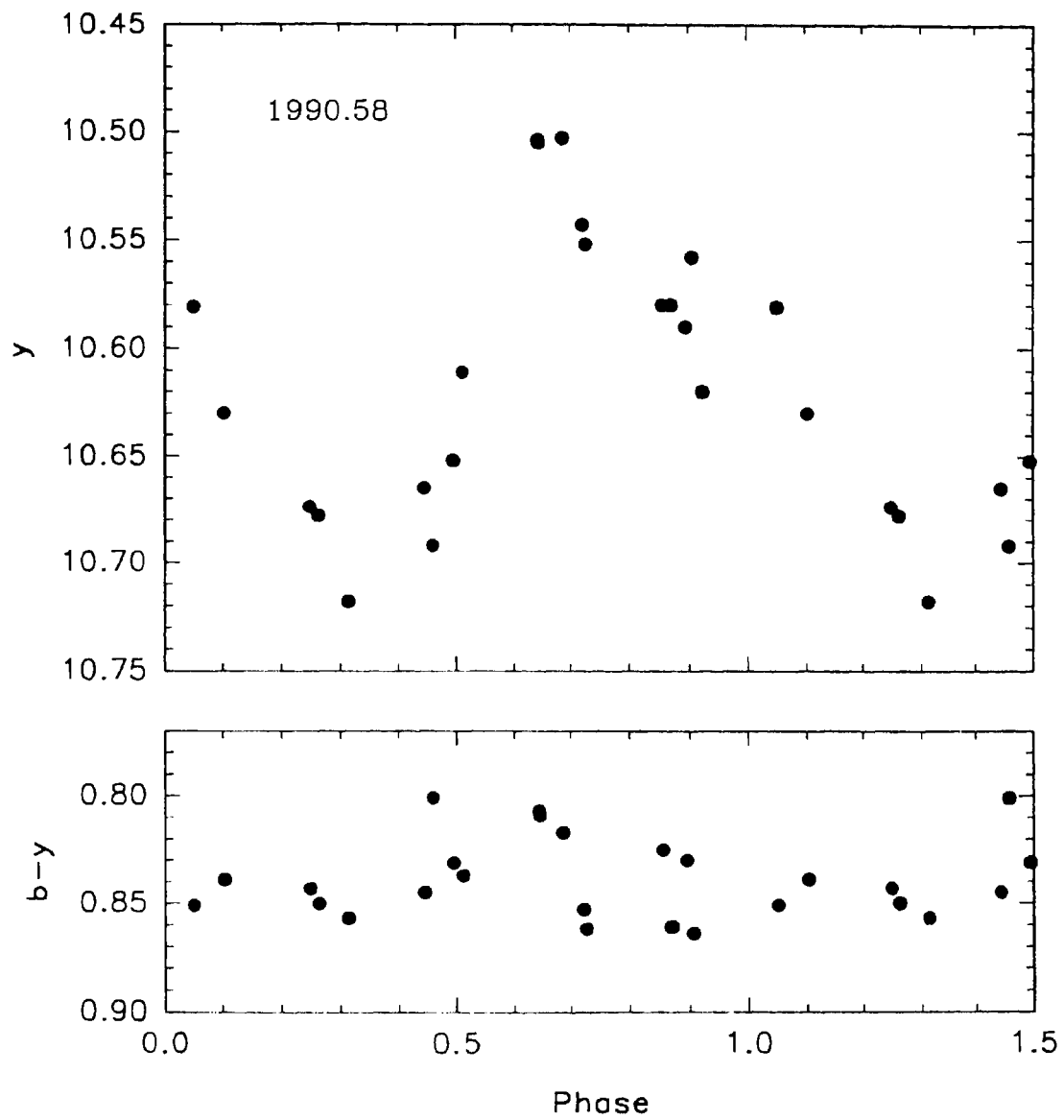


Fig. 4. Plots of y and $b-y$ of FK Ser

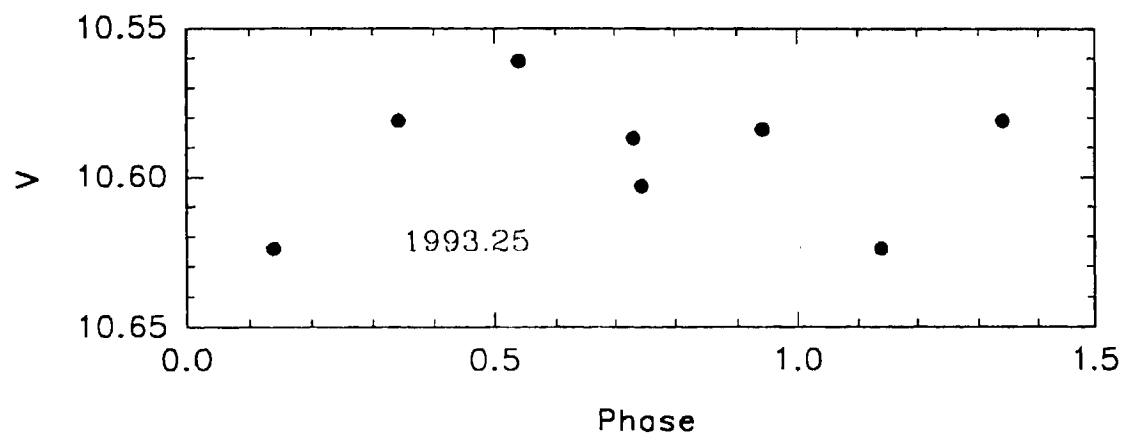


Fig. 5. Plot of V of FK Ser

by cool spots that cover up to 20% of the stellar surface (Vrba et al. 1988; Herbst 1989). In FK Ser the light curves indicate the presence of cool spots most of the time. But the light curve given Figure 1 does not point to a cool spot phenomenon alone. The co-existence of hot and cool spots seems to be a probable hypothesis but has to be considered with certain amount of caution. Another possibility is the occurrence of hot plages surrounding an active cool spot that could produce the observed properties in the different bands. The contribution to the total light variation by the fainter companion, which is of a later spectral type, is negligible because of the significantly fainter brightness and also slightly later in spectral type.

6.1.4. $H\alpha$ and $Li\ I$ lines

Near simultaneous spectroscopic and photometric observations of FK Ser were carried out during March-April 1993 to investigate the behaviour of the $H\alpha$ emission with respect to the light variations. Spectra in the region of $H\alpha$ and $Li\ I$ lines were obtained on six nights and the details are given in Table 5. It was not possible to resolve the components of FK Ser at the spectrograph slit, so the observed spectra are the composite of the two components. The spectra are plotted in Figure 6. Figure 7 shows the plots

Table 5. Equivalent widths of $H\alpha$ emission and $Li\ I$ absorption of FK Ser

Julian day 244000.+	Photometric phase	$H\alpha$ (EEW) $\pm 1\text{\AA}$	$Li\ I$ (EW) $\pm 0.04\text{\AA}$
9049.464	0.78	5.53	—
9079.458	0.71	4.44	0.535
9080.401	0.90	7.16	0.482
9081.401	0.09	8.03	0.550
9082.427	0.30	5.51	0.620
9107.462	0.25	6.38	0.554

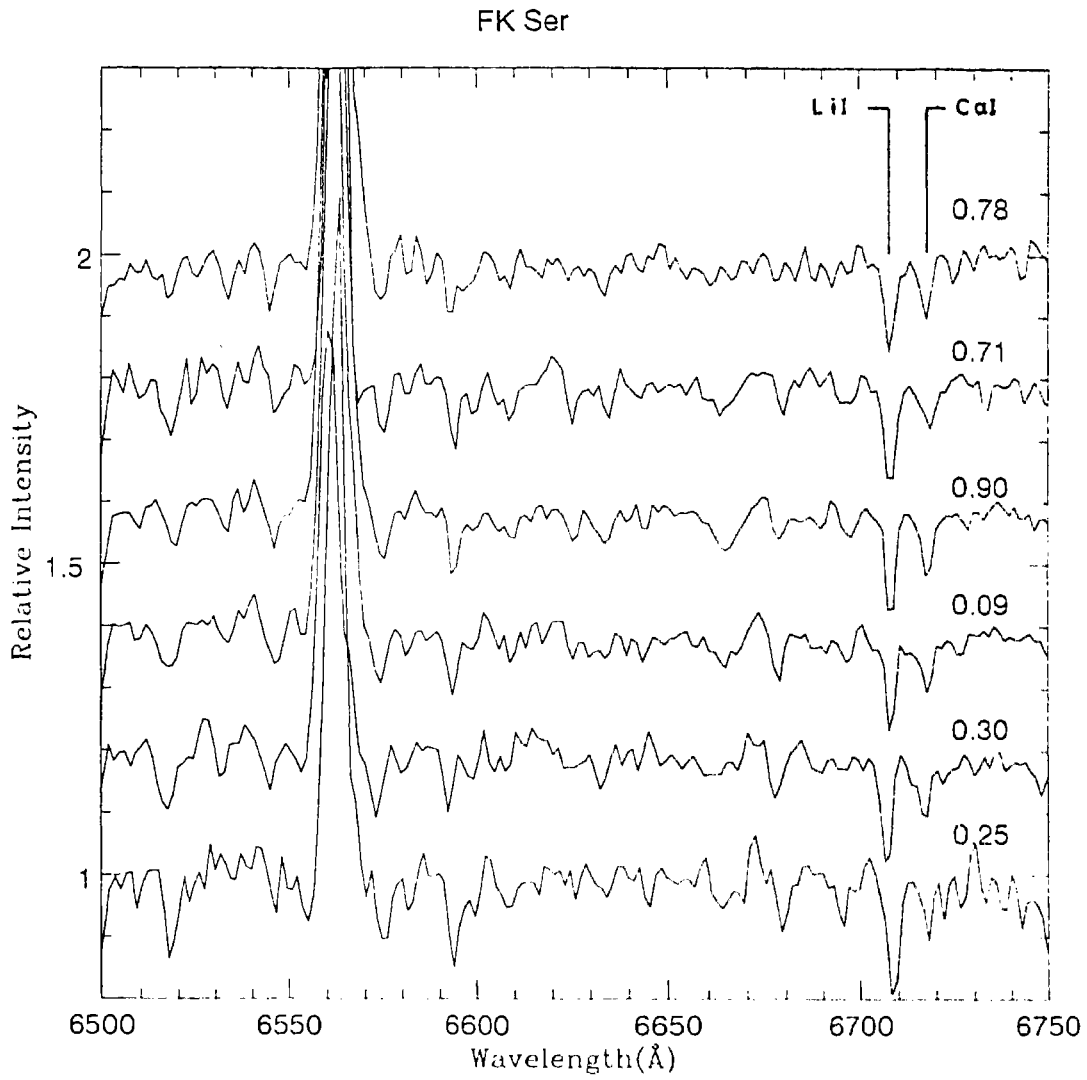


Fig. 6. $H\alpha$ and Li I spectra of FK Ser.

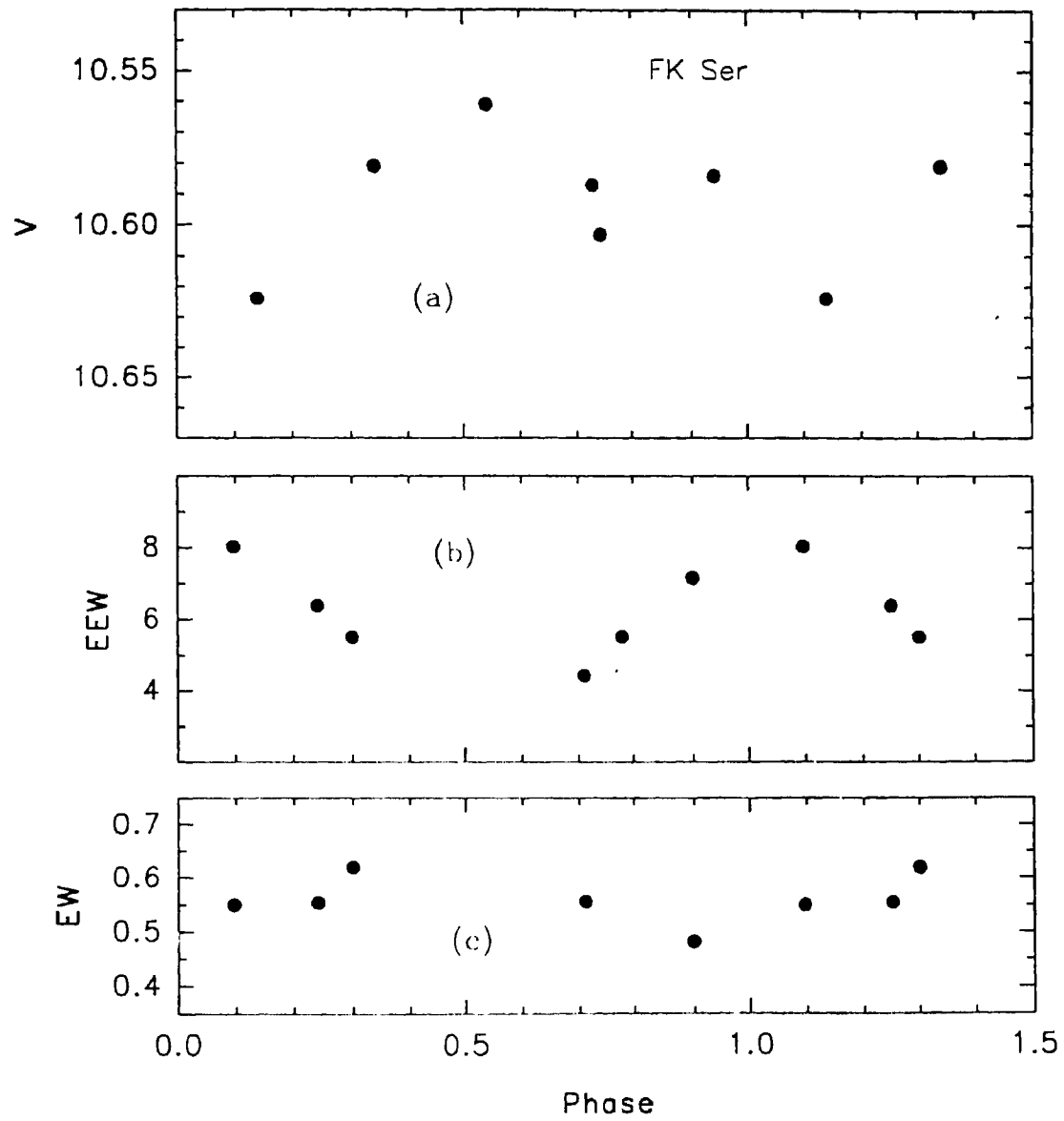


Fig. 7. Plots of (a) V mag, (b) H α emission equivalent width and (c) Li I absorption equivalent width.

of $H\alpha$ EEW, $Li\ I$ EW and the near simultaneous V observations against the photometric phase computed using the above mentioned ephemeris. The $H\alpha$ EEW varies from 4.4 to 8 Å (The corresponding variation in flux is 0.13 to $0.24 \times 10^{-11} \text{ erg cm}^{-2} \text{ s}^{-1}$) while the EW of $Li\ I$ line remains almost the same (~ 0.55), within the measurement error of 0.05Å. Though the spectroscopic observations did not have a good phase coverage, the trend in the variation of the $H\alpha$ emission strength is clearly seen. The maximum $H\alpha$ emission was observed when the star was at its light minimum. This phenomenon is usually observed in WTTS where the photospheric light variations are presumed to be caused by cool spots which usually have life-times of several rotation periods. FK Ser also has only Moderate $H\alpha$ emission, typical of a WTTS; the anticorrelation between the observed light variation and $H\alpha$ emission probably indicates the presence of cool spots.

Herbig (1973) had obtained the individual spectra of the components of FK Ser and found that the fainter component has slightly larger $H\alpha$ EEW. If both components exhibit variable emission and contributes nearly equally, then instead of the observed systematic variation of the $H\alpha$ emission with the light, where the contribution by the fainter component is negligible, one would have observed a more complex behaviour. Thus, though both components of FK Ser belong to the T Tauri stars the contribution of the fainter component to the net emission is not appreciable as in the case of the total light.

6.1.5. Linear polarization

Polarization measurements of FK Ser were made in BVR bands during the observing runs in 1991 and 1992. The observations showed that FK Ser has slightly larger and variable linear polarization compared to that observed in T Tauri stars. The star was again monitored on four nights during March 1993. Table 6 gives the journal of observations. The linear polarization $P\%$ and the position angle θ° in V band are plotted in Figure 8 against the corresponding Julian days of observation and the same are plotted in Figure 9 against the inverse of the effective wavelength. From Figure 8 it is seen that $P\%$ varied from 0.75 to 1.25 but θ° remained almost the same except on

Table 6. *BVR* polarimetry of FK Ser

Date	Julian day 244000.0+	Band	P%	θ°
18 May 91	8395.313	<i>B</i>	0.81 ± 0.07	90 ± 3
		<i>V</i>	0.86 ± 0.08	89 ± 2
		<i>R</i>	0.56 ± 0.13	86 ± 7
14 Mar 92	8696.472	<i>B</i>	1.00 ± 0.21	102 ± 6
		<i>V</i>	0.74 ± 0.09	90 ± 3
		<i>R</i>	1.10 ± 0.14	87 ± 4
15 Mar 92	8697.462	<i>B</i>	0.51 ± 0.19	116 ± 10
		<i>V</i>	0.88 ± 0.11	103 ± 4
		<i>R</i>	0.96 ± 0.14	87 ± 4
12 Mar 93	9059.450	<i>V</i>	1.25 ± 0.09	58 ± 3
		<i>R</i>	1.09 ± 0.12	100 ± 3
13 Mar 93	9061.483	<i>B</i>	1.59 ± 0.23	120 ± 2
		<i>V</i>	0.99 ± 0.12	85 ± 3
		<i>R</i>	0.92 ± 0.12	1011 ± 4
14 Mar 93	9061.448	<i>V</i>	0.87 ± 0.09	100 ± 3
		<i>R</i>	0.75 ± 0.13	98 ± 4
17 Mar 93	9064.464	<i>B</i>	0.97 ± 0.12	125 ± 2
		<i>V</i>	1.06 ± 0.05	91 ± 1
		<i>R</i>	0.74 ± 0.08	97 ± 3

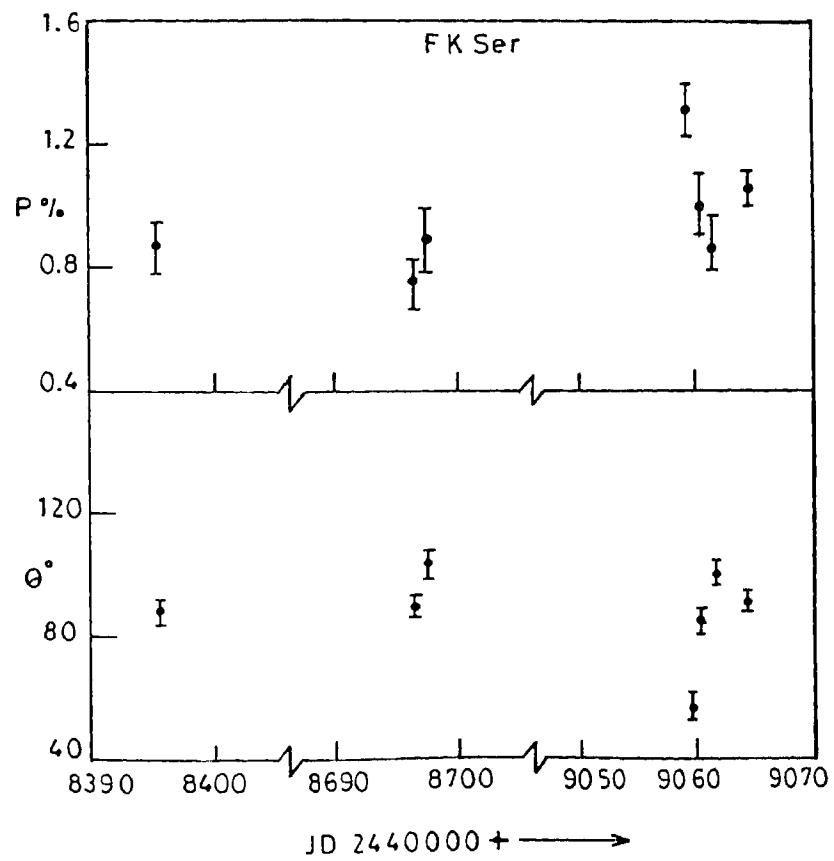


Fig. 8. Plot of the time dependence of linear polarization and position angle in V of FK Ser.

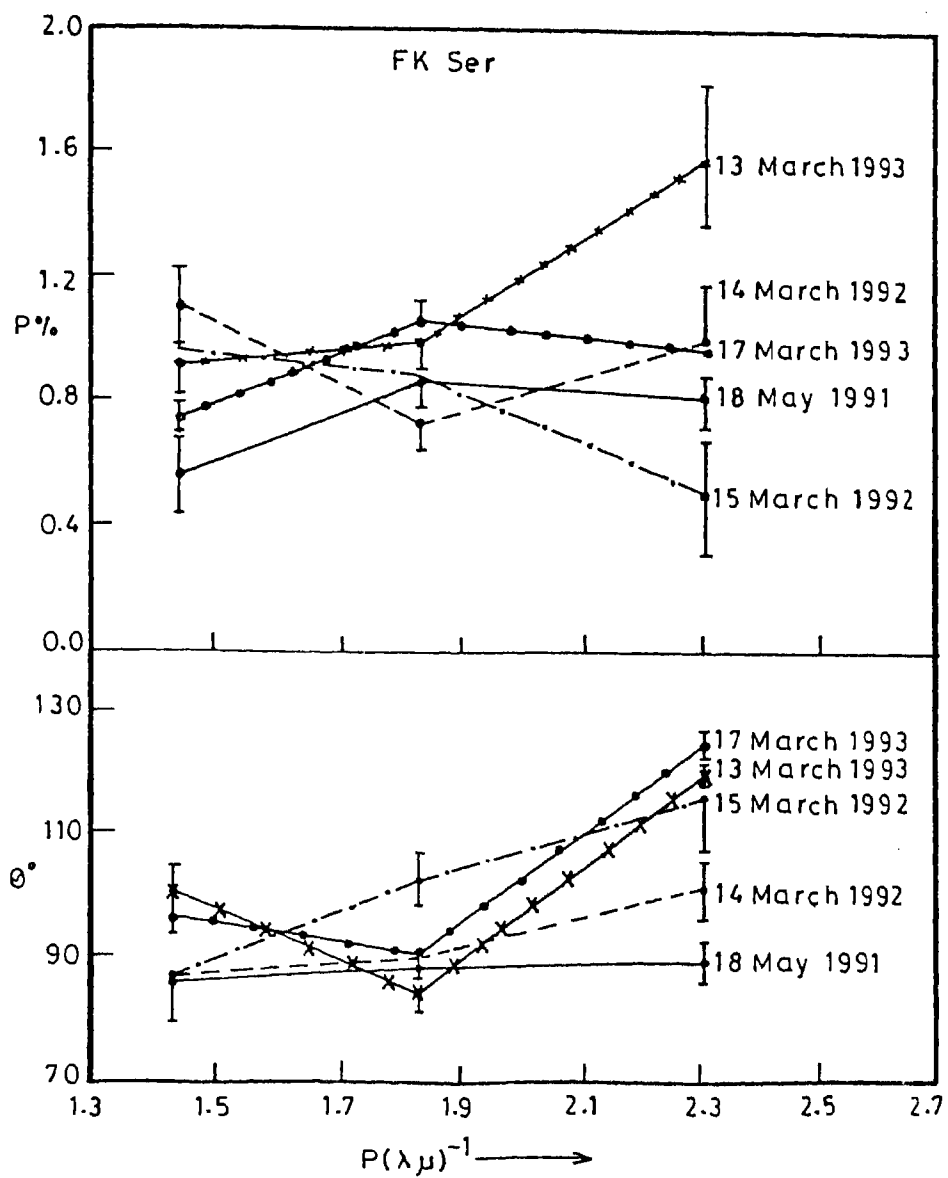


Fig. 9. Plot of linear polarization and position angle of FK Ser against the corresponding inverse of the effective wavelength of the filter band.

one occasion where it was below the usually observed values. Figure 9 shows that maximum variation in P% was observed in *B* band and the minimum in *V*. The value θ° shows a decreasing trend with wavelength. The observed variable nature of P% could be due to several reasons like, non-uniform distribution of the circumstellar material and/or variable illumination of the circumstellar material. The photometric and $H\alpha$ observations of FK Ser indicate the presence of cool spots and if the observed variation in P% is caused by the spots, that in turn illuminates the circumstellar dust variably due to the rotation of the star, then we would observe a periodic behaviour in P% as observed in the case of the WTT star V410 Tau. The fact that the polarization measurements of March 1993 did not show any periodic trend suggests the origin of variable P% as the nonuniform distribution of the circumstellar material.

6.2. V410 Tauri

6.2.1. Introduction

V410 Tau (HDE 283518, BD +28°637) is one of the most well studied T Tauri star. It has relatively weak $H\alpha$ emission and very little infrared excess (Cohen 1974; Rydgren et al. 1984; Rucinski 1985). This lack of strong emission, a property shared by some other T Tauri stars also, suggests that it is a member of the naked T Tauri stars (Walter 1987), which is now known as Weak emission T Tauri Stars (WTTS). The photospheric spectrum of V410 Tau was classified as K7 by Cohen & Kuhl (1979), K4 by Brown et al. (1980) and as K2 by Basri & Batalha (1990). V410 Tau exhibits large light variations, up to 1 mag in V (Rydgren & Vrba 1983), that are presumed to be caused by cool photospheric spots. The photometric observations by Vrba et al. (1988) showed that the cool spots responsible for the light modulation are long-lived. They have modeled the light curves and found that the spots have temperatures 1000-1400 K cooler than the photospheric temperature and cover up to 42% of the stellar surface.

Radio continuum observations of V410 Tau show the star to be highly variable. Bieging & Cohen (1989) measured the radio flux densities at monthly intervals over 1 year period with the VLA and found evidences for the modulation of the radio emission with a period of 0.933 days which is about half the optical period. This radio emission is probably non-thermal gyro-synchrotron emission induced by strong stellar magnetic fields (Stine et al. 1988). V410 Tau is also a variable X-ray source. Strom & Strom (1994) have found from their ROSAT PSPC observations that $L_X = 1.3 \times 10^{31} \text{ erg s}^{-1}$ and noted changes in L_X by a factor of about 2.

Ghez et al. (1993) detected the binary nature of V 410 Tau with a projected separation of 0.123 arc sec between the components. The companion contributes about 14% of the light at K band. Due to the large separation, the companion does not have any significant effect on the activity of the primary star.

Paterer et al. (1993) reported the $Li\ I\ 6708\ \text{\AA}$ line profile variations

in V410 Tau. The variation in $Li\ I$ line strength was suspected but is not confirmed in this star.

Welty & Ramsey (1995) found that the large amplitude quasi-sinusoidal radial velocity variations at the stellar rotation period in V410 Tau arises, probably, due to large scale photospheric temperature inhomogeneity caused by cool spots. They also found that the cooler regions of the photosphere were associated with greater $H\alpha$ emission.

A Doppler imaging of the spot distribution on V410 Tau was done by Hatzes (1995) who found that the spot distribution was dominated by a high latitude spot whose centre was offset from the rotational pole of the star. The observations also showed that rapid changes take place in $H\alpha$ emission; the maximum emission was observed when the spot visibility was highest, indicating that the emission probably arises from plages and flares that are associated with spots, in analogy with sunspots.

Petrov et al. (1994) made a detailed photometric and spectroscopic study of V410 Tau. They refined the photometric period as 1.872 days. They found a correlation between the TiO band strength and stellar brightness such that the band strength was maximum when the star was faintest. They also reported the presence of double peak in the $H\alpha$ emission strength versus photometric phase diagram, probably caused by two emitting regions.

Most of the observational properties of V410 Tau are similar to that of the evolved RS CVn binary systems, namely, the photospheric spot distribution, $H\alpha$ emission strength variation, etc. V410 Tau was included in our observational programme in order to compare the nature of activity in WTTS and RS CVn systems. We have carried out quasi-simultaneous photometric, spectroscopic, and polarimetric observations of V410 Tau during March-April 1993.

6.2.2. Photometry

Since extensive photometric observations of V410 Tau are available in the literature we have not done detailed photometry. The main aim of the present photometric observations was limited to obtain the shape and amplitude of the light curve close to the epochs of the $H\alpha$ and polarimetric observations.

Photometric observations in V band were carried out on seven nights during March 1993 with BD +27°651 as the comparison star. The photometric observations are given in Table 7. Each value given in the table is the average of two or three measurements. From the photometric observations of Petrov et al. (1994) it is found that the shape and the amplitude of the light curves of V410 Tau do not change rapidly and in fact the light curves are found to be stable over several hundred rotation periods indicating the long-lived nature of the spot group. In the lower panel of Figure 12 we have plotted the present observations along with that of Petrov et al. (1994) obtained during September 1992 using the ephemeris:

$$JD(HeI.) = 2446659.4389 + 1.^d872095E.$$

Table 7. V magnitudes of V410 Tau

Julian Day 2440000.0+	Phase	V
9064.144	0.500	10.630
9065.113	0.017	11.232
9066.087	0.537	10.665
9067.104	0.080	11.200
9068.097	0.611	10.680
9069.090	0.142	11.060
9070.107	0.685	10.803

The open circles indicate the present observations and the filled circles that of Petrov et al. (1994). From the figure it is seen that the shape of the light curve did not change from September 1992 to March 1993. The light minimum and maximum occurred at the same phases during both observing seasons. In March 1993 the light minimum was deeper by about 0.05 mag. An amplitude of 0.60 mag was observed in V band, which is comparable to the largest amplitudes observed in the RS CVn binary HD 81410. V410 Tau

has a large value of inclination ($i \sim 72^\circ$) which probably explains the large amplitude observed in the light variation.

6.2.3. $H\alpha$ and $Li\ I$ lines

Spectra in the region of $H\alpha$ and $Li\ I$ lines were obtained on 8 nights during March-April 1993. The resolution employed was not sufficient enough to study the line profile variations. Table 8 gives the details of the spectroscopic observations. The spectra are displayed in Figure 10 and the corresponding photometric phases indicated. Each spectra is shifted relatively along the

Table 8. Equivalent widths of $H\alpha$ emission and $Li\ I$ absorption of V410 Tau

Julian day 244000.+	Phase	$H\alpha$ (EEW) ± 0.05 \AA	$H\alpha$ Flux $\times 10^{-11}$ $erg\ cm^{-2}\ s^{-1}$	$Li\ I$ (EW) ± 0.04 \AA
9049.121	0.48	-0.16		0.55
9050.099	0.00	1.93	0.040	0.60
9051.100	0.53	0.19	0.006	0.53
9051.271	0.62	0.26	0.007	0.58
9052.128	0.08	2.37	0.049	0.52
9079.132	0.51	0.45	0.015	0.53
9081.097	0.56	0.53	0.017	0.52
9082.094	0.09	1.28	0.024	0.61

intensity scale so that the variations in $H\alpha$ strength can be clearly seen. The $H\alpha$ line shows variation from a shallow absorption to moderate emission. The maximum $H\alpha$ EEW observed was 2.37\AA . The $H\alpha$ EEWs and $Li\ I$ EWs are plotted against the photometric phase in Figure 11 where the filled circles denote the measurements obtained during March 1993 and open circles those obtained during April 1993. The figure shows that maximum in $H\alpha$

emission occurs when the star is at its light minimum and vice versa. This phenomenon indicates that the chromospheric active regions, like, plages that produce strong $H\alpha$ emission are associated with highly active photospheric cool spots, *i.e.*, the spots and the chromospheric active regions are co-spatial. As seen from Figure 11 the $H\alpha$ EEWs show variations at the maximum level within a period of one month. This implies that though the photospheric cool spots in V410 Tau have long life spans of the order of years, the changes in the chromospheric active regions take place at shorter time-scales. The chromospheric active regions need not be co-spatial with the spots all the time and so the maximum $H\alpha$ EEW might show phase shift with respect to the light minimum. The presence of two maxima in the $H\alpha$ emission observed by Petrov et al. (1994) might be due to the presence of two prominent chromospheric active regions.

From Figure 11 it is found that the $Li\ I$ EW does not show any appreciable variation with the photometric phase. The mean of the observed value is $0.56 \pm 0.04 \text{ \AA}$. Giampapa (1984) has postulated that the strong magnetic activity in spots should affect the $Li\ I$ EW as noticed in the Sun. But Patterer's (1993) high resolution study of $Li\ I$ line in V410 Tau did not indicate any notable variation in the line strength, though there is evidence for strong magnetic activity as manifested by cool spots that occupy up to 40% of the stellar surface. The $Li\ I$ EW in V410 Tau is similar to that usually observed in CTTS and hence the hypothesis that WTTS are more evolved than CTTS is questionable.

6.2.4. Linear polarization

Polarimetric observations of V410 Tau were obtained on eight consecutive nights during March 1993 mostly in V band and on two nights in BVR bands. Table 9 gives the journal of observations. Figure 12 shows the plots of $P\%$ and θ° and the quasi-simultaneous V band photometry against the phase computed using the ephemeris given before. From Figure 12 it is seen that the $P\%$ shows a periodic variation that is in anti-correlation with light variation, in the sense that, $P\%$ tends to be larger at the photometric minimum. The variation in θ° also exhibits a periodic trend. Figure 13 is a

V410 Tau

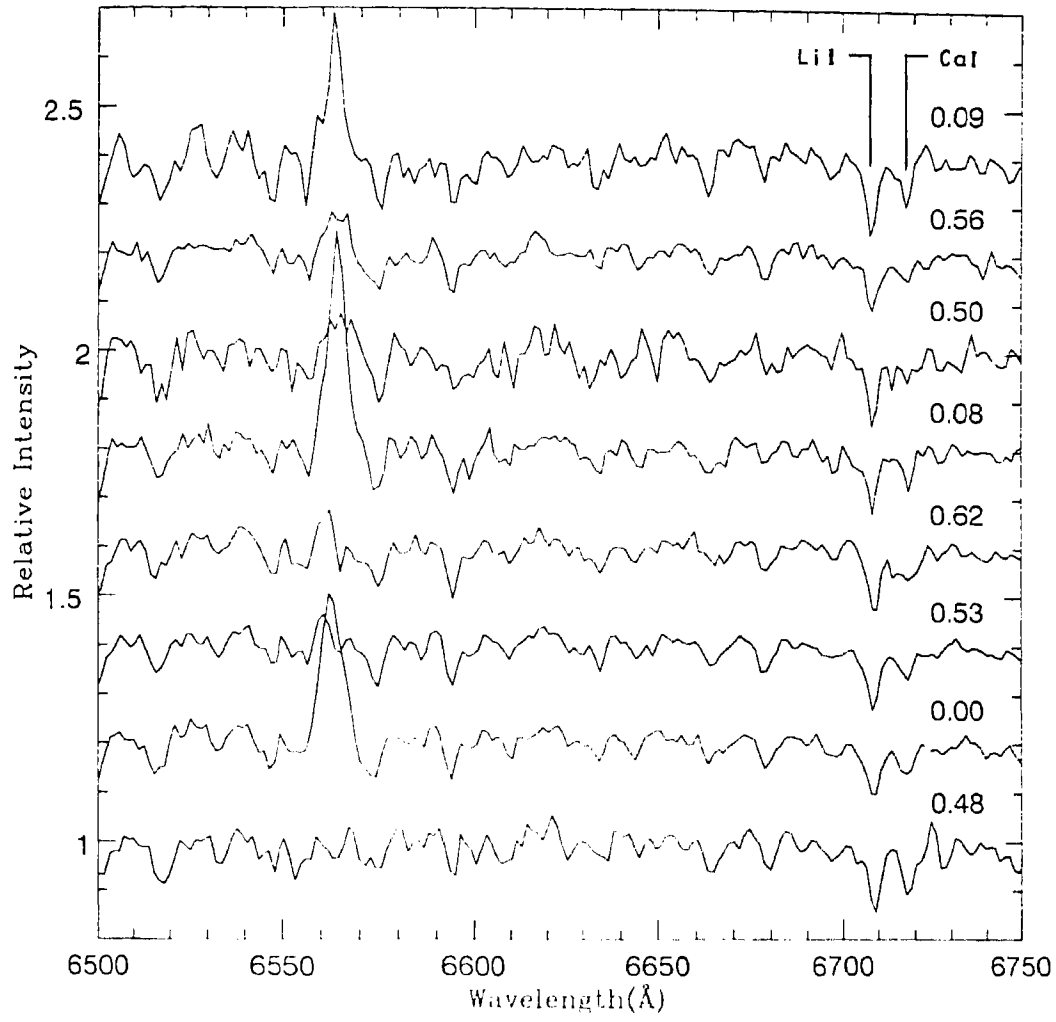


Fig. 10. H α and Li I spectra of V410 Tau.

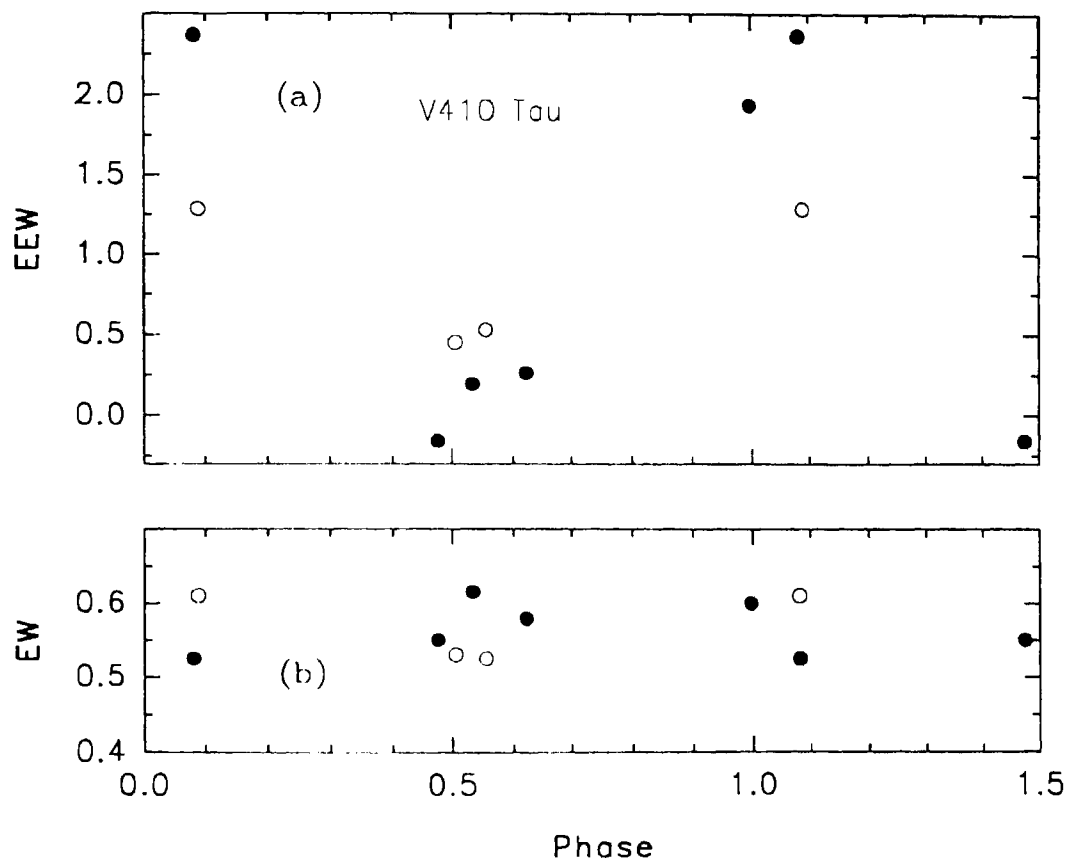


Fig. 11. Plots of (a) H α emission equivalent Width and (b) Li I absorption equivalent width

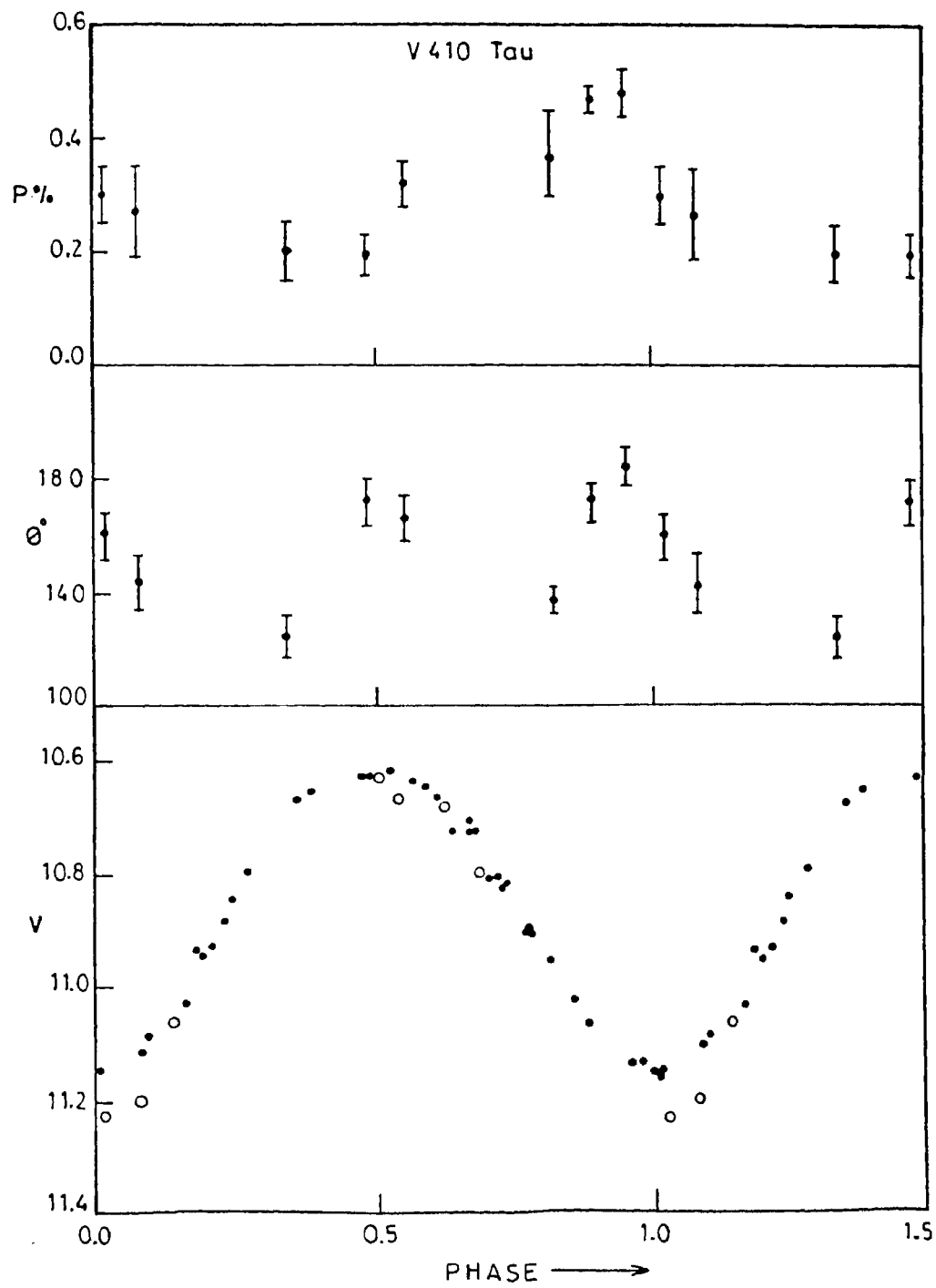


Fig. 12. Plot of linear polarization and position angle in V of V410 Tau phased with the period. The lower panel is the overlapping photometry.

plot of the Stokes parameters Q and U against the photometric phase and periodic trend is noticed in this figure too except on two occasions where large deviations noticed. In Figure 14 the P% and θ° are plotted against the inverse of the effective wavelength of observation. No drastic change in P% or any dependence of P% with wavelength is noticed. The maximum observed value of P% is around 0.45%. A slight dependence of θ° against wavelength is noticed in such away that θ tends to be large as the wavelength increases.

Table 9. *BVR* polarimetry of V410 Tau

Date	Julian day 244000.0+	Band	P%	θ°
12 Mar 93	9059.129	V	0.37±0.09	138±4
13 Mar 93	9060.108	V	0.20±0.05	124±7
14 Mar 93	9061.125	B	0.47±0.13	168±8
		V	0.47±0.02	172±
		R	0.21±0.11	10±10
16 Mar 93	9063.111	V	0.48±0.05	4±7
17 Mar 93	9064.109	V	0.20±0.02	172±9
18 Mar 93	9065.120	B	0.24±0.12	169±27
		V	0.30±0.05	160±8
		R	0.45±0.07	175±11
19 Mar 93	9066.108	V	0.33±0.04	166±8
20 Mar 93	9067.097	V	0.27±0.10	143±10

Menard & Bastien (1992) also reported the suspected polarization variability in V410 tau. The P% and θ° values reported by them are comparable to the presently obtained values. The infrared observations of V410 Tau show that the star has almost no infra-red excess and also very little far infra-red emission (Rucinski 1985). This indicates the absence of any considerable amount of circumstellar material; however, the presence of some distribution of circumstellar dust around V410 Tau cannot be ruled out. Hence the small

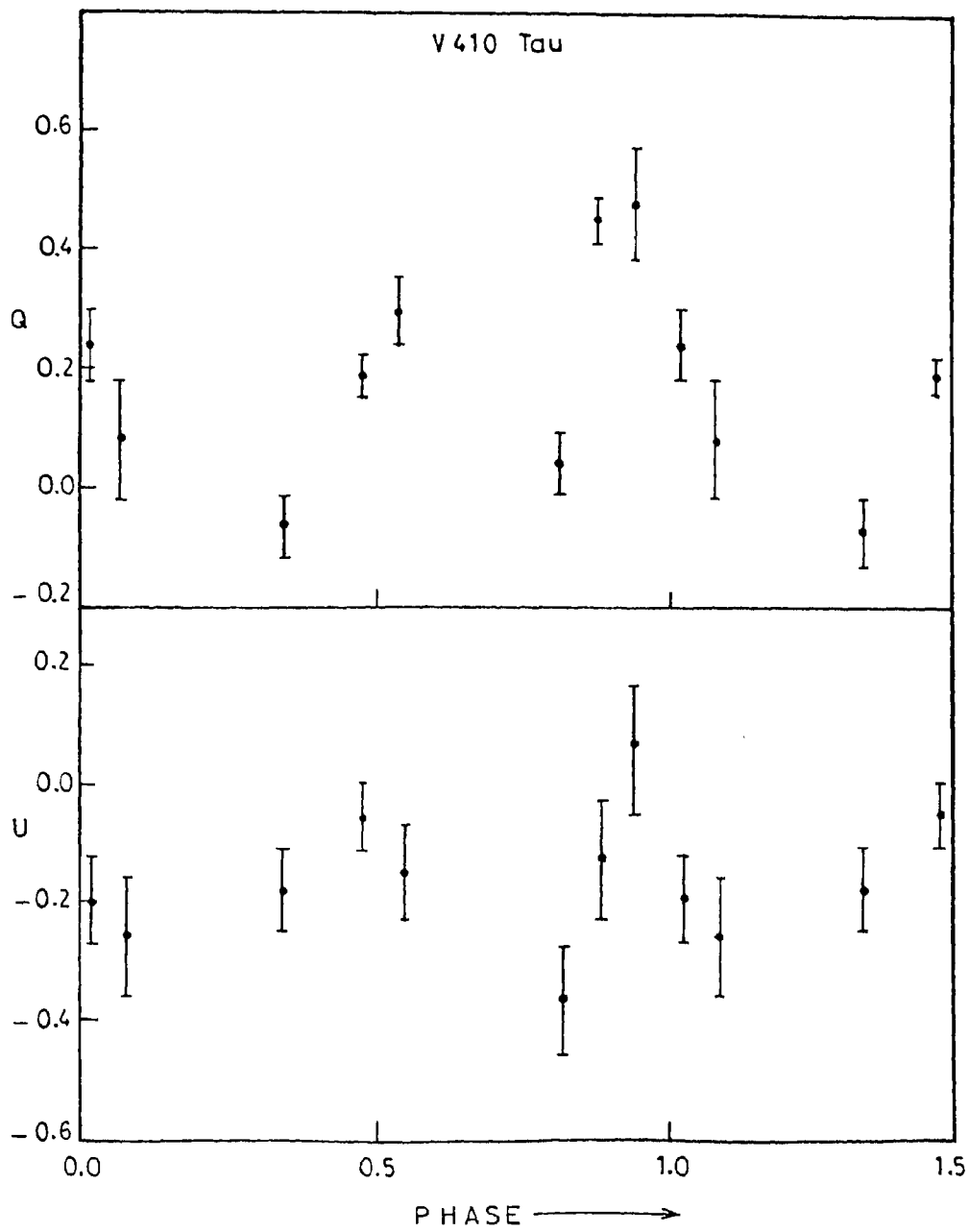


Fig. 13. Plot of the Stokes parameters Q and U of V410 Tau phased according to the period.

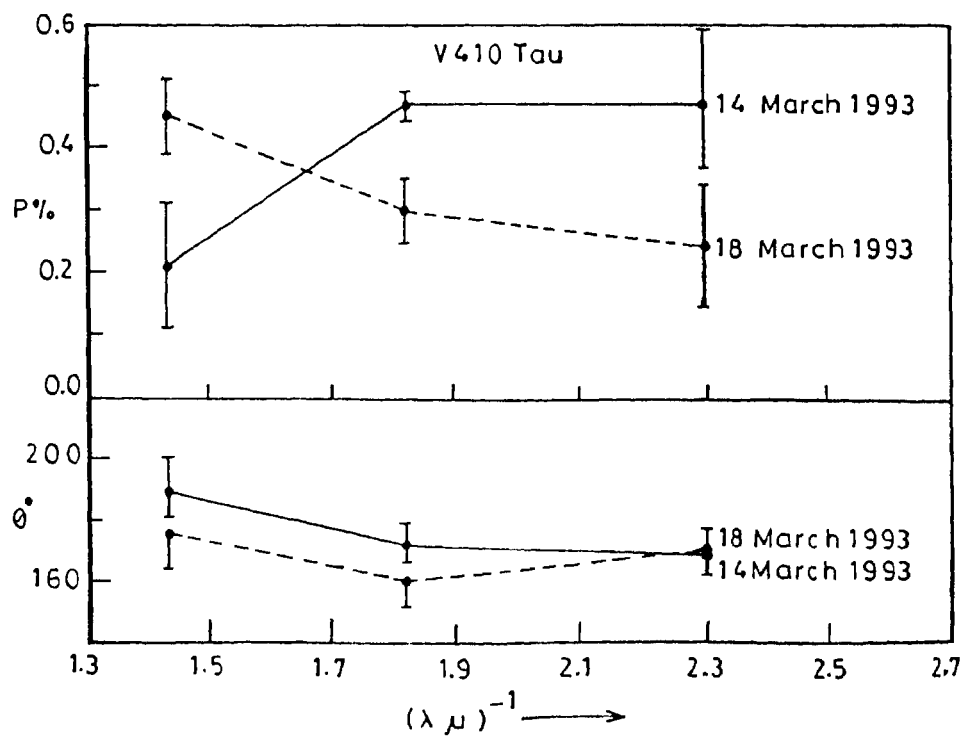


Fig. 14. Plot of linear polarization and position angle of V410 Tau against the corresponding inverse of the effective wavelength of the filter band.

amplitude periodic variation in P% observed in V410 Tau might be due to the presence of highly active cool spots.

6.3. Summary

The investigation of the two WTT stars FK Ser and V410 Tau gives significant results. The observed variations in light, $H\alpha$ emission strengths and polarization in V410 Tau give strong evidence for the presence of highly active cool spots whose life times are of the order of several rotation periods. Though very active, it is surprising to note that the starspots in V410 Tau do not show any rapid changes in their distribution on the stellar surface as usually observed in RS CVn objects and young active-chromosphere stars. However, the associated changes in the chromospheric active regions, as inferred from the changes in the $H\alpha$ emission strengths, are faster than the life times of spots in V410 Tau.

FK Ser has strong $H\alpha$ emission compared to other WTT stars. From photometric observations it is seen that, apart from cool spots, the star shows, sometimes, indications of photospheric bright regions which could be due to hot spots, short time-scale flares and chromospheric emissions. The near-simultaneous photometric and $H\alpha$ observations give evidence for the presence of cool spots and the associated chromospheric emission. The nature of spots in V410 Tau and FK Ser are quite different. While in V410 Tau cool spots that are present last for years, as inferred from the sudden changes in the shapes of the light curves, cool spots in FK Ser last for much shorter periods. FK Ser is the only WTT star that is identified as an IRAS source. The presence of hot as well as cool spots, higher $H\alpha$ emission strengths, the comparatively large variable polarization and the far infra-red excess make FK Ser to be better classified as a moderate CTT star.

7

CLASSICAL T TAURI STARS

7.1. TW Hydrae

7.1.1. Introduction

TW Hya (CoD -34°7151, He 3-549, HV4089) is one of the most peculiar T Tauri stars. Herbig (1978) suggested that this star is possibly a member of the Post T Tauri stars that are supposed to be more evolved than the classical T Tauri stars. Heinz (1976) detected the presence of strong $H\alpha$ emission in TW Hya. Hoffmeister (1943) reported a light variation between 10.5 and 12.2 mag in blue for TW Hya. From a spectroscopic study, Herbig (1978) found that TW Hya exhibits emissions in $O I 8446\text{\AA}$, $He I 5876\text{\AA}$ and $Ca II$ triplet lines and he assigned a spectral type of K7 Ve (Li I). Rucinski & Krautter (1983), who carried out optical and infrared photometry as well as low resolution spectroscopy of TW Hya, found that the star shows light variations in V between 10.9 and 11.3 mag, and the range in light variations decreased at longer wavelengths. They also detected uv and IR excesses. The emission equivalent width of $H\alpha$ was found to vary from 70 to 100 \AA . On the basis of strong $H\alpha$ and other emission lines, uv and IR excesses, Lithium abundance and irregular light variations, they classified the star as a member of the Classical T Tauri (CTTS) stars. However, TW Hya, whose

galactic latitude (b) is $+23^\circ$, stands apart from other CTTS in one respect which prompted the above authors to suggest that the star might have been formed in a tiny isolated dark cloud of low mass: it is quite far from any star forming region, dark cloud or concentration of young protostellar material.

Though Rucinski & Krautter (1983) detected short-term variability in TW Hya, they could not detect any periodic light variation. Rucinski (1988) also did not find any significant periodic light variation from the photometric observations obtained during 1986 and 1987. However, he reported the possible presence of a 2-day period in the 1982 observations obtained earlier by Rucinski & Krautter (1983). Herbst & Koret (1988) detected the presence of a 1.28 day period from their observations made in January 1988. They also found that the star showed significant light variations during each night. Their analysis of the photometric data obtained by Rucinski & Krautter (1983) gave a period of 1.83 days. They attributed the discrepancy in the derived period to a real change in the periodicity of TW Hya that occurred within six years and the light variations exhibited by the star to the presence of a hot spot.

From a survey of IRAS sources Rucinski (1985) identified TW Hya as a strong far-infrared source. He suggested that the far-infrared spectrum is due to the presence of a steady accretion disk. Weintraub et al. (1989) reported the detection of millimeter and submillimeter emissions in TW Hya, possibly arising from the circumstellar accretion disk. The search for interstellar matter, that could have remained in the field, through radio emission from TW Hya using Very Large Array by Rucinski (1992) gave a negative result.

Franchini et al. (1992) estimated the rotational velocity $V \sin i$ of TW Hya as around 15 km s^{-1} from a high resolution study. They detected strong $He I 5876\text{\AA}$ line emission with a radial velocity of 16.3 km s^{-1} ; this is about 10 km s^{-1} larger than the radial velocity of the star. Patten & Simon (1992), who analyzed the IUE spectra of TW Hya, detected substantial variability in both $Mg II$ lines and uv continuum on time-scales of a few hours to a few days.

But for a few peculiar characteristics, TW Hya is a typical CTTS. The near infrared excess is not so strong in TW Hya as in other CTTS and also

it is not associated with any star forming regions. So TW Hya is the prototype of another subgroup of T Tauri stars that are not associated with star forming regions and hence termed as *IsolatedTTauristars*. In order to obtain a better understanding of the photometric behaviour and circumstellar environment, it is necessary that the star is investigated at all possible wavelengths. Therefore photometric, spectroscopic and polarimetric observations of TW Hya were carried out simultaneously, whenever possible.

7.1.2. Photometry

Photometric observations of TW Hya were carried out on 34 nights over four seasons: 1987 (9 nights), 1988 (6 nights), 1990 (12 nights) and 1993 (7 nights). *UBVRI* observations were done during 1987 and 1988 seasons and *by* observations during 1990. Only *V* measurements were made during the 1993 season as the observations were mainly aimed at getting light curve information around the times of spectroscopic and polarimetric observations.

Table 1. *UBVRI* and *by* magnitudes of the HD 95740

<i>U</i>	<i>B</i>	<i>V</i>	<i>R</i>	<i>I</i>	<i>b</i>	<i>y</i>
11.419	10.004	8.704	8.033	7.431	9.493	8.705
±0.010	±0.007	±0.006	±0.004	±0.004	±0.005	±0.007

TW Hya was observed as frequently as possible each night to check for short-time scale light variations and hence only a single comparison star HD 95470, whose constancy had been well established earlier by several authors, was used. The differential magnitudes of TW Hya were transformed to the corresponding standard systems. The mean *UBVRI* and *by* magnitudes of HD 95470 are given in Table 1. The *UBVRI* magnitudes of TW Hya are given in Table 2, the *by* magnitudes in Table 3 and the *V* magnitudes in Table 4.

Table 2. *UBVRI* magnitudes of TW Hya

J.D. 2440000.+	<i>U</i>	<i>B</i>	<i>V</i>	<i>R</i>	<i>I</i>
6897.615	11.801	12.079	11.027	10.116	9.356
6898.527	12.041	12.034	10.986	10.146	9.374
6898.567	12.014	12.081	10.987	10.137	9.348
6898.615	11.824	12.001	10.958	10.134	9.366
6898.656	12.088	12.002	10.989	10.133	9.362
6898.720	11.984	12.040	11.006	10.152	9.361
6899.519	12.138	12.193	11.053	10.161	9.377
6899.552	12.012	12.166	11.065	10.183	9.392
6899.599	11.944	12.148	11.038	10.186	9.386
6899.644	12.111	12.191	11.103	10.186	9.401
6899.684	12.324	12.212	11.084	10.184	9.394
6900.578	11.811	11.987	10.958	10.099	9.337
6901.519	11.895	12.071	10.997	10.118	9.333
6901.565	12.012	12.101	11.020	10.141	9.341
6901.617	11.926	12.064	10.998	10.129	9.348
6901.660	12.007	12.135	11.003	10.122	9.336
6902.518	11.781	11.970	10.937	10.073	9.325
6902.561	11.621	11.941	10.943	10.067	9.316
6902.609	11.709	11.932	10.949	10.081	9.324
6092.660	11.653	11.937	10.938	10.089	9.335
6902.708	11.528	11.894	10.917	10.077	9.309
6903.519	12.081	12.149	11.053	10.145	9.362
6903.558	12.212	12.240	11.097	10.180	9.376
6903.601	12.329	12.239	11.074	10.174	9.384
6903.647	12.441	12.288	11.110	10.204	9.400
6903.709	12.312	12.265	11.102	10.186	9.379
6904.515	11.666	12.006	10.939	10.052	9.309

Table 2. continued

J.D. 2440000.+	<i>U</i>	<i>B</i>	<i>V</i>	<i>R</i>	<i>I</i>
6904.556	11.675	11.962	10.930	10.053	9.311
6904.601	11.549	11.885	10.893	10.028	9.309
6904.642	11.625	11.876	10.909	10.032	9.317
6904.707	11.859	11.985	10.957	10.070	9.324
6905.512	11.921	12.079	11.014	10.127	9.338
6905.550	12.080	12.126	11.021	10.156	9.351
6905.599	12.048	12.138	11.031	10.153	9.347
6905.642	11.968	12.098	11.020	10.146	9.350
7296.520	11.911	12.034	10.967	10.035	9.317
7296.603	11.798	12.002	10.948	10.042	9.327
7298.560	11.866	12.055	10.988	10.076	9.370
7304.550	11.948	12.081	10.990	10.095	9.327
7304.615	12.009	12.095	11.003	10.070	9.337
7305.480	11.733	11.964	10.929	10.015	9.301
7305.549	11.717	11.936	10.987	10.001	9.293
7305.630	11.651	11.864	10.882	9.973	9.297
7305.673	11.576	11.841	10.864	9.970	9.284
7307.563	11.510	11.864	10.895	10.036	9.313
7307.641	11.588	11.871	10.894	10.043	9.311
7308.494	11.480	11.735	10.847	10.028	9.299
7308.618	11.582	11.785	10.849	10.049	9.303

7.1.3. Light variations

A first look at the photometry obtained during April 1987 appeared to show a period around two days for the light variation superposed on which were the short time-scale fluctuations. The observations were subjected to the period finding technique as explained in §2.4 which yielded a period of 2.196

days for the light variation (Mekkaden 1990). The photometric observations of 1987, 1988, 1990 and 1993 seasons were phased using the ephemeris,

$$JD(HeI.) = 2446897.615 + 2^d.196E,$$

where the initial epoch corresponds to the first observation obtained during 1987. The observations listed in Tables 2, 3 and 4 are plotted in Figures 1, 2, 3 and 4e; the mean epoch of observations are indicated in the respective figures. From Figure 1 it is seen that the colours also vary in phase with the V light. The maximum changes occur in the U band which in turn is reflected in the $U - B$ colour plot. The $U - B$ colour shows a large scatter that is far more than the observational error. This may possibly be due to short-time scale flaring or short-lived plage-like bright areas on the stellar surface. A steep increase in the amplitude of light variation is observed as the wavelength decreases.

Table 3. by magnitudes of TW Hya

J.D. 2440000.+	b	y
7910.808	11.694	10.985
7910.856	11.640	10.976
7910.865	11.647	10.954
7911.701	11.413	10.788
7911.763	11.357	10.765
7911.840	11.330	10.742
7911.848	11.347	10.747
7912.689	11.496	10.865
7912.698	11.511	10.852
7912.755	11.439	10.769
7912.764	11.423	10.759
7912.838	11.309	10.718
7912.864	11.364	10.750

Table 3. continued

J.D. 2440000.+	<i>b</i>	<i>y</i>
7913.669	11.552	10.877
7913.719	11.593	10.931
7913.764	11.675	10.951
7913.812	11.728	10.993
7913.848	11.772	11.000
7916.775	11.536	10.860
7916.810	11.524	10.851
7916.870	11.483	10.834
7917.651	11.695	10.971
7917.699	11.702	10.989
7917.748	11.647	10.957
7917.808	11.696	10.994
7917.845	11.759	11.006
7920.611	11.376	10.799
7920.653	11.474	10.839
7920.735	11.393	10.770
7920.774	11.387	10.792
7920.819	11.431	10.824
7921.611	11.492	10.837
7921.649	11.490	10.851
7921.709	11.524	10.853
7921.750	11.510	10.857
7924.639	11.560	10.919
7924.680	11.551	10.888
7924.729	11.463	10.834
7924.781	11.426	10.821

Table 3. continued

J.D. 2440000.+	b	y
7924.842	11.393	10.813
7925.650	11.400	10.765
7925.686	11.470	10.837
7925.745	11.418	10.798
7925.788	11.383	10.801
7925.827	11.395	10.806
7925.869	11.380	10.784
7926.624	11.765	11.007
7926.667	11.766	11.003
7926.706	11.765	11.028
7926.750	11.762	11.014
7926.798	11.771	11.032
7926.835	11.747	11.014
7926.858	11.712	11.008
7929.642	11.247	10.696
7929.723	11.215	10.638
7929.762	11.234	10.655
7929.801	11.249	10.667
7929.831	11.213	10.638
7929.880	11.177	10.621

The 1987.3 light curve has been modeled using the spot modeling program explained in Chapter 3. It is found that a bright spot with $T_s = 8150$ K that occupies a fractional area of 0.007 could cause the observed light variations. The effect of hot spots is reflected maximum in U band and it is noticed that as the wavelength increases the amplitude decreases. Apart from the effect of the hot spot, the rapid changes in chromospheric emissions

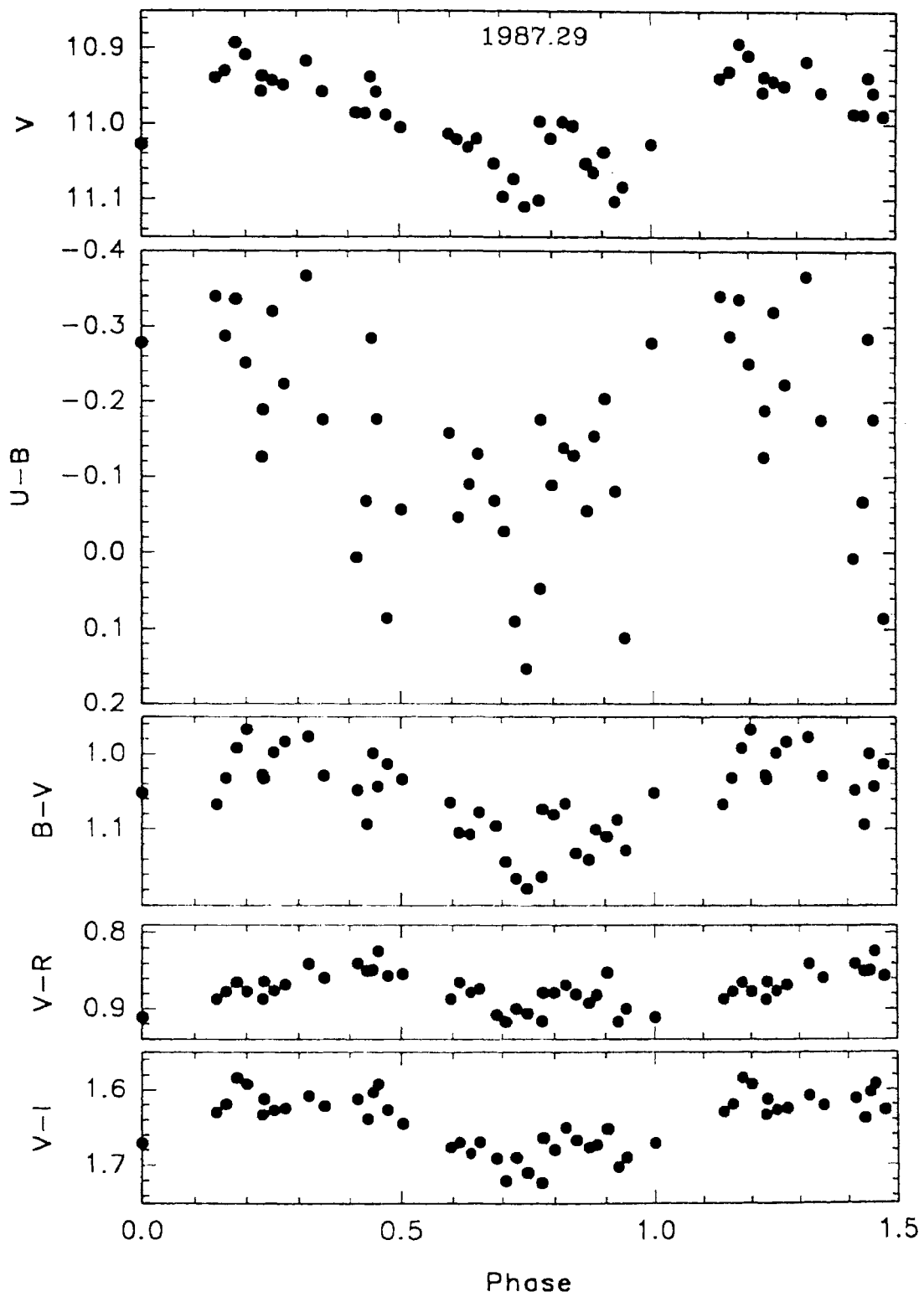


Fig. 1. Plots of V, U-B, B-V, V-R and V-I of TW Hya

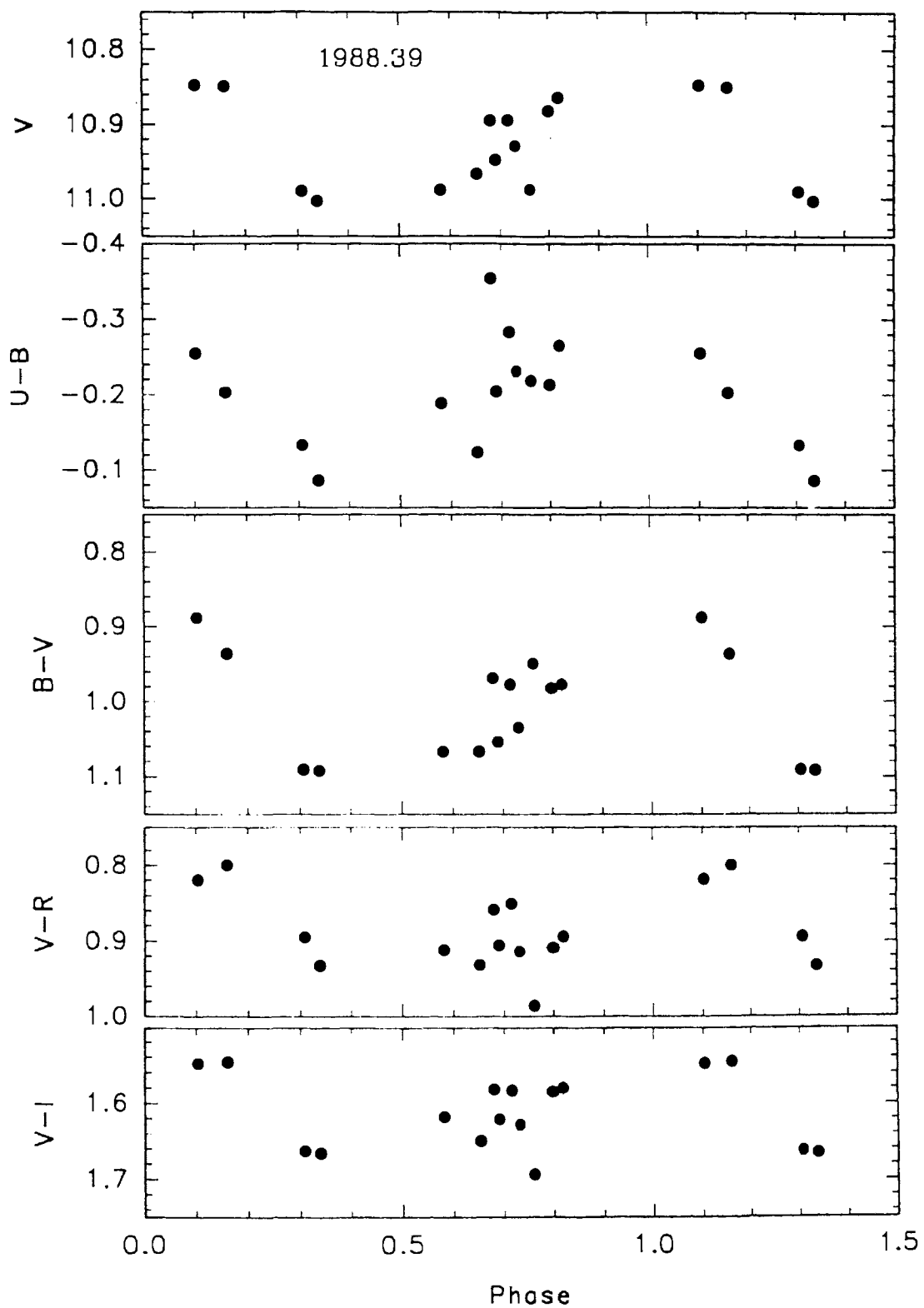


Fig. 2. Plots of V, U-B, B-V, V-R and V-I of TW Hya

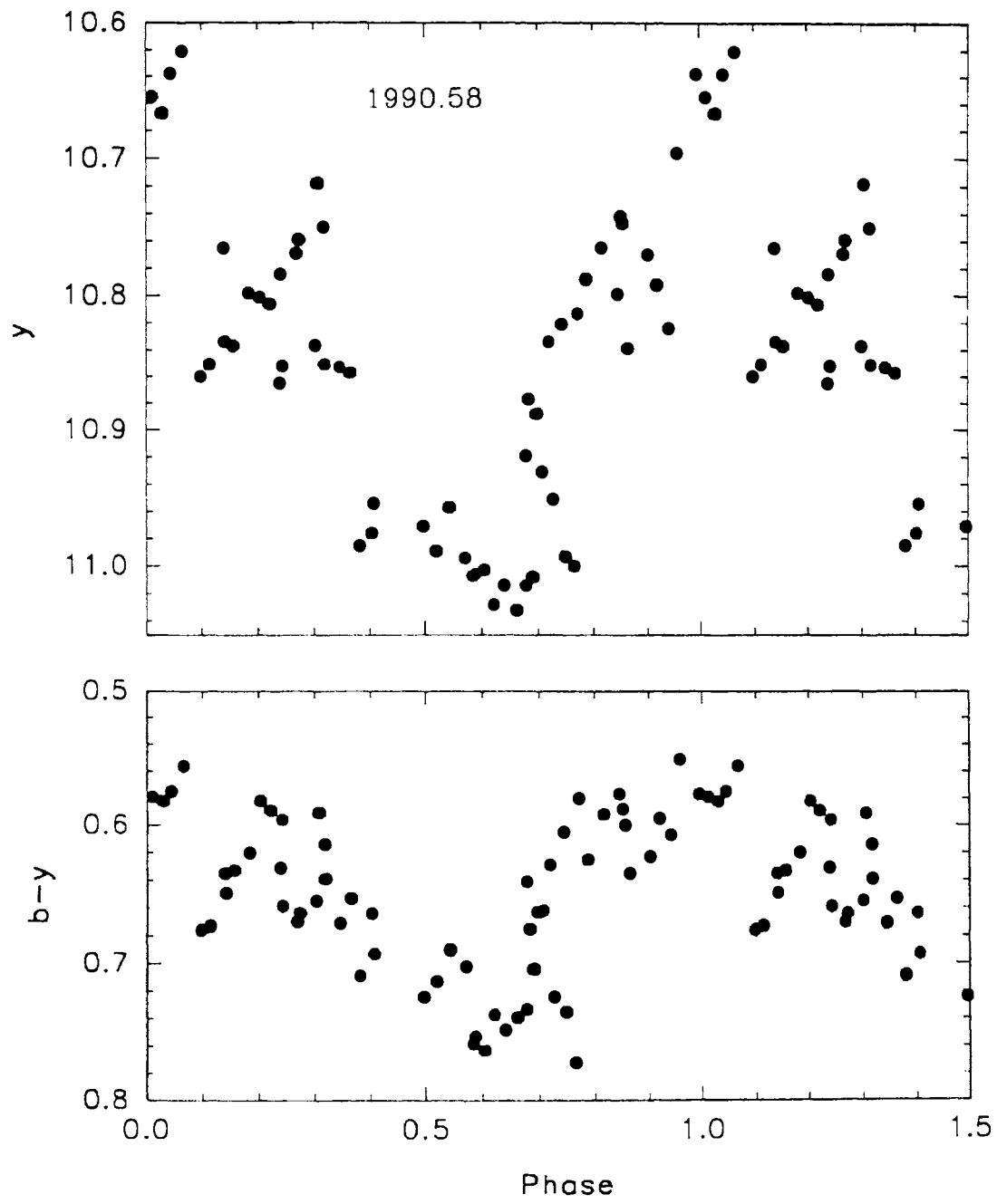


Fig. 3. Plots of y and $b-y$ of TW Hya

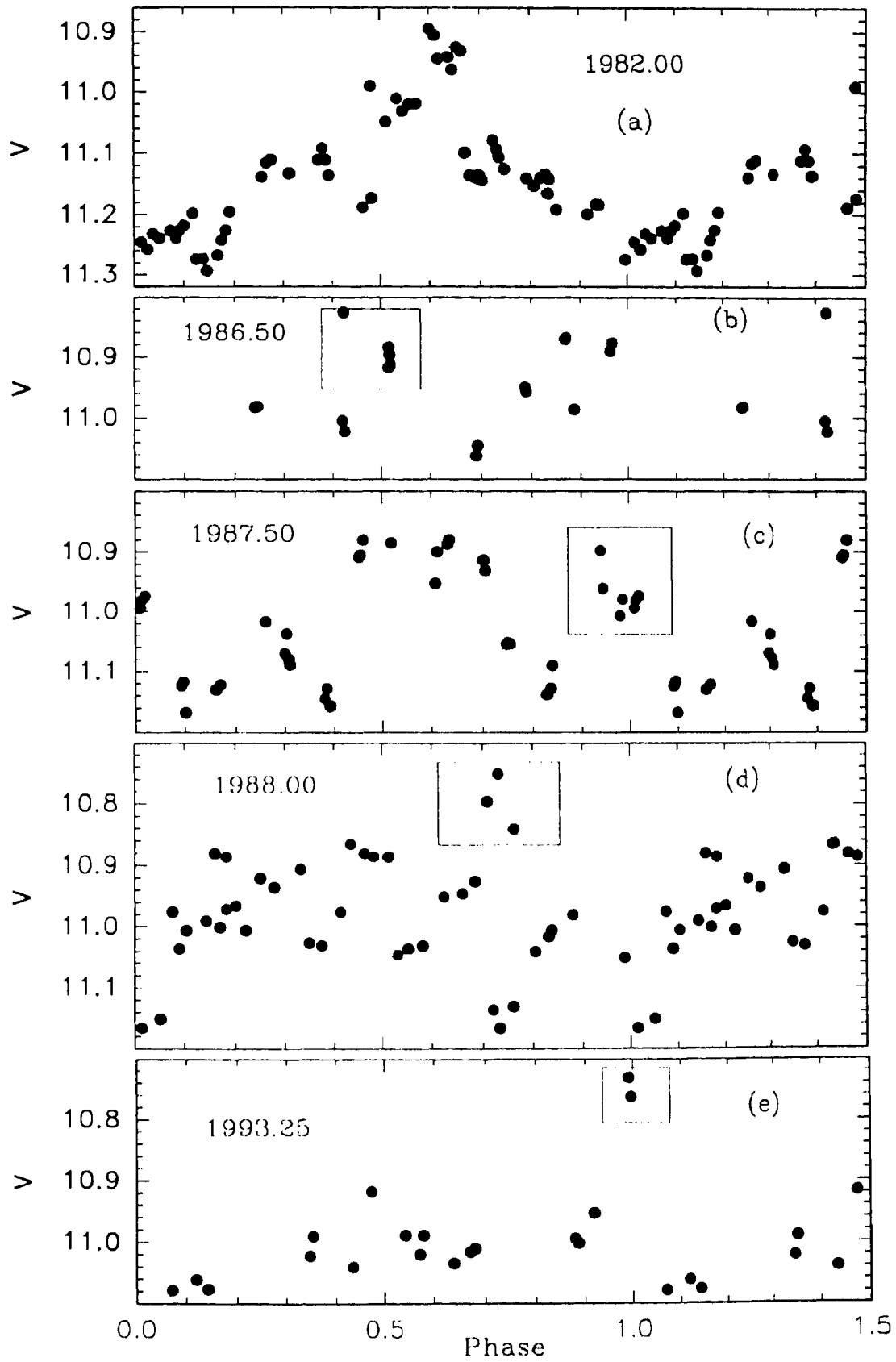


Fig. 4. Plots of V of TW Hya

Table 4. *V* magnitudes of TW Hya

J.D. 2440000.+	<i>V</i>
9064.274	11.034
9064.344	11.016
9064.365	11.010
9065.224	11.078
9065.330	11.061
9065.381	11.076
9066.258	10.988
9066.318	11.020
9066.337	10.988
9067.246	10.732
9067.257	10.763
9068.218	11.040
9068.304	10.917
9069.193	10.994
9069.208	11.002
9069.282	10.953
9070.221	11.022
9070.231	10.990

and plage-like bright areas if present on the stellar surface also affect the flux in the *U* band, resulting in large variations in *U* – *B* colour. The 1988, 1990 and 1993 data also satisfy the 2.196 day period, though the resulting light curves show a slightly larger scatter. Though the photometry obtained during 1988 shows an indication of periodic variation, it is not as well-defined as in the cases of other seasons; one reason for such a behaviour could be the poor phase coverage. The light curve of the mean epoch 1990.58 showed the highest amplitude of 0.4 mag. The scatter near the maximum brightness is large when compared to that at minimum brightness. The hot spot that

caused the light variation was present through out the observational period of 12 days. From the brightness at maximum (10.62 mag), which incidentally is the brightest magnitude of TW Hya observed so far, we can assume that the hot spot was very active and the large scatter observed at the maximum indicates that the hot spot was highly variable.

All the V band photometry of TW Hya available in the literature are plotted in Figures 4a-d. The observations were folded using the ephemeris given above. The observations obtained during 1982 (Rucinski & Krautter 1983), 1987.5 (Rucinski 1988) and 1988.00 (Herbst & Koret 1988) clearly show the light modulation with the 2.196 day period presently derived while those obtained during 1986.5 (Rucinski 1988) apparently does not show any indication of a periodicity. However, if the bright V measurements which lie in the interval $0.^{\text{p}}40 - 0.^{\text{p}}55$ are excluded from the latter set of observations the periodic light modulation becomes apparent. Sudden brightenings which last for a couple of days seems to be a regular feature of TW Hya. A sudden increase in brightness of the order of 0.2 mag that lasted for two days was noticed near $0.^{\text{p}}0$ in the light curve of 1987.5. Similarly the 1988 light curve also shows a brightening of 0.2 mag, which lasted for a single day around $0.^{\text{p}}7$. During the 1993.3 observations TW Hya brightened up to 10.75 mag in V for a day. All the above mentioned observations are enclosed in boxes in the respective figures.

The observations clearly indicate that the sudden brightening that lasts for one or two days occur quite frequently in TW Hya. This phenomenon can be either due to flaring activities or due to very short-lived hot spots produced by the interaction between the accretion disk and the star. The latter case seems to be more likely since the sudden increase in the brightness is around 0.2 mag whereas the brightness change expected due to a flare is more than 1 mag (Bertout 1989). Since the sudden brightness could occur at any photometric phase, frequent brightening could completely mask the periodic variation, and hence the period search would not give any positive result at certain epochs.

The light curves obtained by us during 1987.3 and by Rucinski (1988) one month earlier show entirely different shapes, amplitudes and phases of

the maximum light, indicating sudden changes in the location of the bright spot on the stellar surface. The sudden changes in the light variation and brightening observed in TW Hya is typical of CTTS. The hot spots that cause the light variability are the zones on the stellar surface heated by the infall of a column of matter from the active accretion disk surrounding the star (Herbst et al. 1994). Bertout (1989), Simon et al. (1991) and Bouvier et al. (1993) include stellar magnetosphere as an integral component in the evolution of the star/disk system in CTTS. They interpret the hot spots as the zones where material is channeled from the disk to the star in magnetospheric flows. The characteristics of the hot spots appear to change on time-scales of a few rotation periods or even less giving rise to rapid changes in the light variations that are noticed in CTTS.

The rotational velocity $V \sin i$ estimated from the line broadening by Franchini et al. (1992) of TW Hya is around 15 km s^{-1} . Assuming that the stellar radius is $2R_{\odot}$, then from

$$R \sin i = \frac{P v \sin i}{2\pi}$$

and the observed rotation period of 2.196 days, we get $i = 20^{\circ}$, which is too small to explain the large amplitude light variability. A better estimate of $V \sin i$ is required.

7.1.4. $H\alpha$ and $Li \ I$ lines

Spectroscopic observations of TW Hya in the $H\alpha$ and $Li \ I$ 6708Å region were obtained on eight nights during March-April 1993, overlapping with some of the photometric and polarimetric observations. Due to the low resolution employed it is not possible to study the variations in the line profiles. However, the dispersion employed is sufficient enough to study the variation in emission strengths with respect to light variability. The values of $H\alpha$ emission equivalent width (EEW) and $Li \ I$ 6708Å absorption equivalent (EW) are given in Table 5 along with Julian day of observation and the corresponding photometric phase computed using the above mentioned ephemeris. It is found that the $H\alpha$ EEW varied between 190 and 250 Å which is larger than that observed by Rucinski & Krautter (1983). The EW of $Li \ I$ 6708Å

absorption line is found to be of the order of 0.6 \AA , a value

Table 5. Equivalent widths of $H\alpha$ emission and $Li \ I$ absorption

Julian day 244000.+	Photometric phase	$H\alpha$ (EEW) $\pm 6 \text{ \AA}$	$Li \ I$ (EW) $\pm 0.05 \text{ \AA}$
9049.412	0.871	193	–
9050.300	0.276	243	0.659
9051.302	0.732	212	0.636
9052.288	0.181	188	0.675
9079.250	0.458	143	0.340
9080.234	0.907	188	0.566
9081.321	0.402	209	0.580
9082.274	0.835	245	0.619

typical of CTTS ($\sim 0.50 \text{ \AA}$). Figure 5 displays the spectra in the region of $H\alpha$ and $Li \ I$ lines. The S/N of the spectra were of the order of 80 to 100. The corresponding photometric phases computed using the ephemeris given above are indicated against each spectrum. The spectrum of 1 April 1993 (0.^p46) had the least $H\alpha$ EEW and also the least value of $Li \ I$ EW, comparable to the values reported by Rucinski & Krautter (1983). However, any possible correlation between the strengths of these two lines could be established only with high resolution spectroscopy. The spectrum also indicates moderate emission in $He \ I$ 6678 \AA line. The $Li \ I$ line did not show any significant day to day variations, except on 1 April 1993, indicating that no appreciable changes take place in the photospheric spectrum; however, the resolution employed in the present study is not sufficient enough to detect any small scale variations. Figure 6 is a plot of $H\alpha$ and $Li \ I$ line EWs against phase. The V light curve obtained in the intervening period is also plotted in the same figure. The $H\alpha$ EEW, though varies quite appreciably, does not show any correlation with photometric phase. Most of the known CTTS have $H\alpha$ EEW less than 100 \AA . So TW Hya shows unusually strong $H\alpha$ compared to

other CTTS. The mean observed R mag of TW Hya is 10.1 mag. Making use of the absolute flux calibration given by Bessel (1979) it is found that the mean flux in the $H\alpha$ line is around $4.1 \times 10^{-11} \text{ erg cm}^{-2} \text{ s}^{-1}$.

From a spectroscopic and photometric study of CTTS, Vrba et al. (1993) found that the $H\alpha$ emission strength does not show any correlation with photometric phase. They suggested that the variations in the $H\alpha$ EW do not support a single model of $H\alpha$ emitting regions associated with the hot spot indicated by the photometry. Johns & Basri (1995) found from their high resolution study of CTTS that most of the CTTS do not show any periodicity in the $H\alpha$ profile variations. They concluded that observed profile variations are stochastic in nature.

7.1.5. Linear polarization

Linear polarization measurements of TW Hya were carried out in $UBVR$ bands on 20 February 1990, 9 and 11 February 1991, and 24 March 1992 to search for the possible variability. These synoptic observations showed that TW Hya has variable linear polarization. In order to study in detail the behaviour of polarization the star was further observed on nine consecutive nights during March 1993. These observations were done mostly in V band due to the limited available telescope time. Table 6 gives the results of the polarization measurements. Figure 7 is a plot of linear polarization (P%) and position angle (θ°) obtained during 1990, 1991 and 1992 against the inverse of the effective wavelength of observation. The variations in both P% and θ° are quite evident from the figure. The linear polarization in B band observed on 24 March 1992 was around 3% while in V it was less than 0.5%. It is seen from the figure that the polarization observed on all other occasions were less than or close to 1% in all wavelength bands, and did not show any appreciable wavelength dependence.

Figure 8 shows the plots of the P% and θ° in V obtained during March 1993 and the V light curve obtained during the same period. On two consecutive nights P% was around 1%, significantly higher than that seen on other nights. TW Hya has a rotational period of 2.196 days, and hence the observations of these two nights are separated by around 0.45. If observations

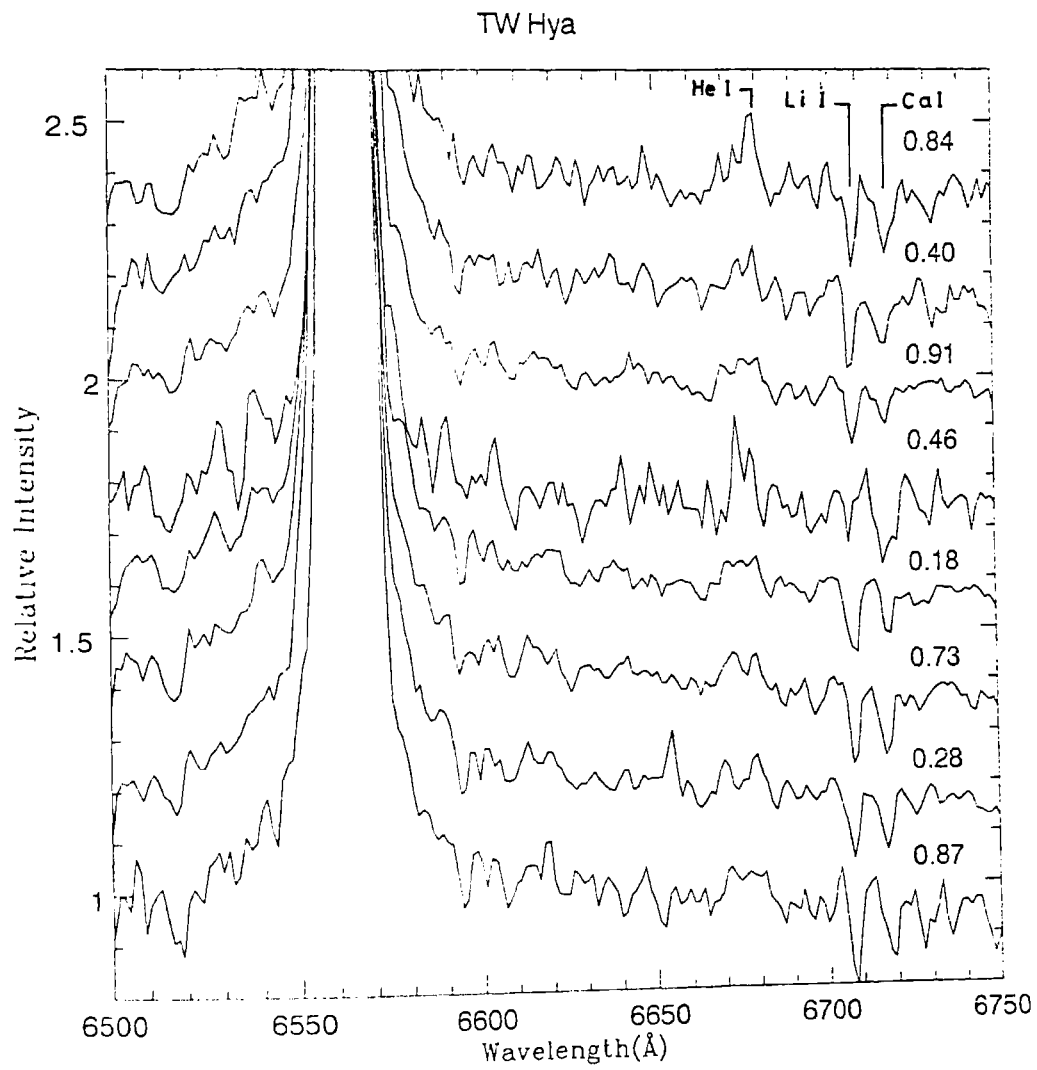


Fig. 5. $H\alpha$ and Li I spectra of TW Hya.

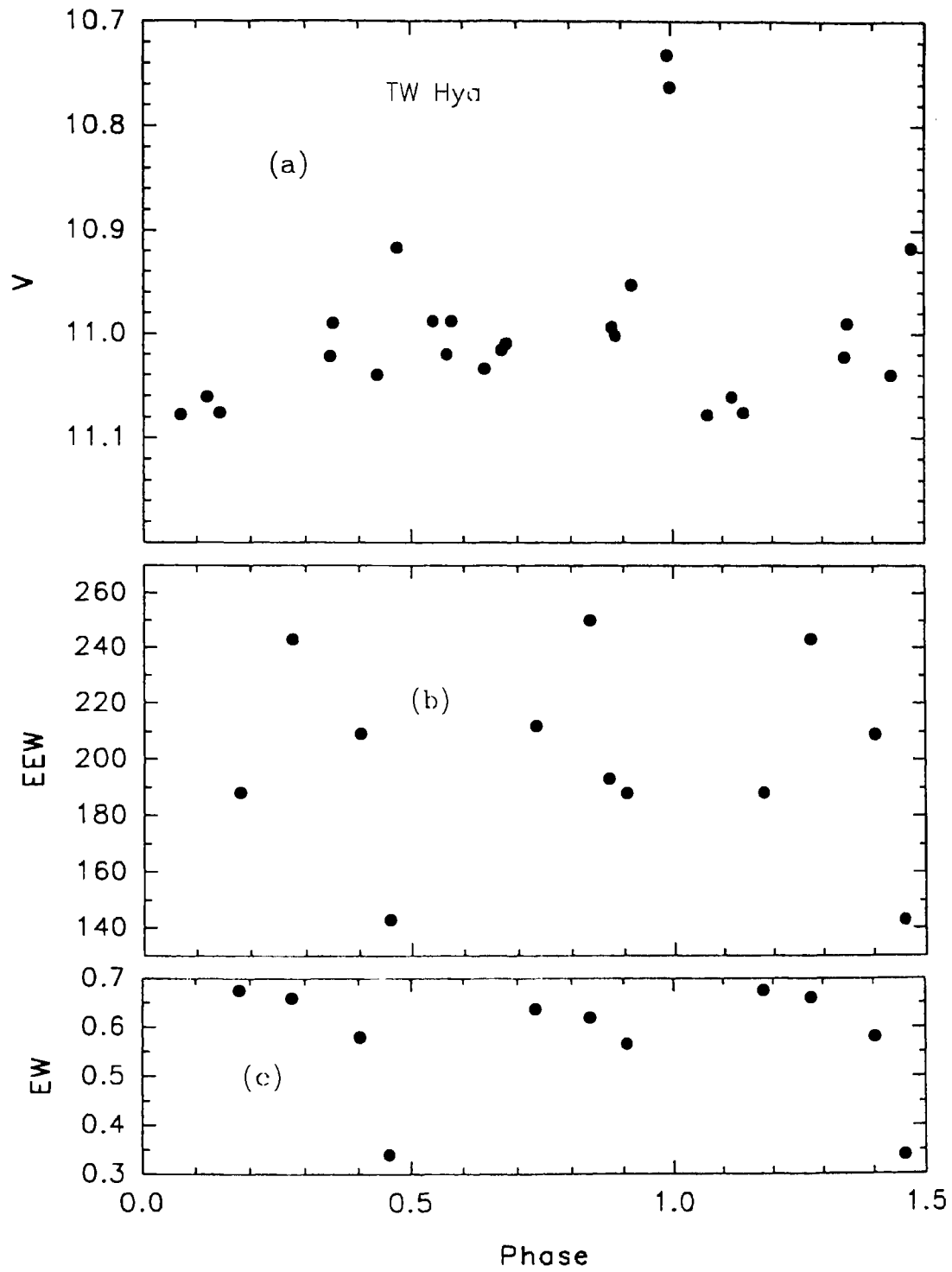


Fig. 6. Plots of (a) V mag, (b) H α emission equivalent Width and (c) Li I absorption equivalent width.

obtained on these two nights are excluded, then there is a slight indication of a modulation in the linear polarization with photometric phase. The values of P% are small ($< 0.2\%$) on most of the occasions. Apparently, there is a slight phase lag between the light curve and polarization curve, with the polarization maximum preceding the light maximum. In Figure 9 the values of P% and θ° are plotted against the Julian days of observation. It is clear from the figure that polarization usually is less than 0.2%, and superposed on this sudden changes with an amplitude around 0.8% occur at certain epochs, most likely, randomly distributed. From Figure 9 it is apparent that the linear polarization in TW Hya has two components: (1) a low amplitude component which exists through out and (2) a large amplitude, short-lived component which occurs suddenly at certain epochs.

Table 6. *UBVR* polarimetry of TW Hya

Date	Julian day 244000.0+	Band	P%	θ°
22 Jan 90	7914.472	<i>V</i>	0.27 ± 0.13	154 ± 15
20 Feb 90	7943.316	<i>B</i>	0.26 ± 0.13	46 ± 24
		<i>V</i>	0.67 ± 0.14	7 ± 5
		<i>R</i>	0.44 ± 0.24	167 ± 13
9 Feb 91	8297.324	<i>U</i>	1.03 ± 0.40	77 ± 11
		<i>B</i>	0.80 ± 0.20	72 ± 7
		<i>V</i>	0.92 ± 0.15	86 ± 5
		<i>R</i>	1.15 ± 0.24	84 ± 6
9 Feb 91	8297.412	<i>U</i>	0.78 ± 0.40	99 ± 14
		<i>B</i>	0.58 ± 0.18	63 ± 9
		<i>V</i>	0.31 ± 0.10	101 ± 9
		<i>R</i>	0.38 ± 0.13	90 ± 10
9 Feb 91	8297.474	<i>V</i>	0.16 ± 0.10	83 ± 18

Date	Julian day 244000.0+	Band	P%	θ°
11 Feb 91	8299.401	<i>B</i>	0.15 ±0.13	137±25
		<i>V</i>	0.26±0.11	165±12
		<i>R</i>	0.07±0.13	
15 Mar 92	8697.313	<i>V</i>	0.79±0.24	145±11
24 Mar 92	8706.274	<i>B</i>	3.14±0.54	176±5
		<i>V</i>	0.16±0.17	
		<i>R</i>	0.24±0.24	
26 Mar 92	8708.301	<i>V</i>	0.49±0.15	149±9
12 Mar 93	9059.312	<i>B</i>	1.350±0.28	144±6
		<i>V</i>	0.89±0.07	145±2
		<i>R</i>	0.61±0.03	45±6
13 Mar 93	9060.326	<i>V</i>	1.18±0.07	156±2
14 Mar 93	9061.306	<i>V</i>	0.30±0.08	19±7
15 Mar 93	9062.243	<i>V</i>	0.21±0.05	106±7
16 Mar 93	9063.292	<i>V</i>	0.25±0.07	76±9
17 Mar 93	9064.333	<i>V</i>	0.10±0.05	65±16
18 Mar 93	9065.363	<i>V</i>	0.26±0.02	172±6
19 mar 93	9066.339	<i>B</i>	0.34±0.09	156±10
		<i>V</i>	0.21±0.07	145±8
		<i>R</i>	0.14±0.07	132±12
20 Mar 93	9067.318	<i>V</i>	0.12±0.06	111±13

The $H\alpha$ emission strength and light variations observed in TW Hya is typical of a classical T Tauri star where the activity is presumed to be caused by the interaction between the accretion disc and the star. Sudden brightenings of TW Hya, that are supposed to be caused by the short-lived hot spots lasting for one or two days have been observed in TW Hya. Hence the large P% observed on two nights could be due to the illumination of the

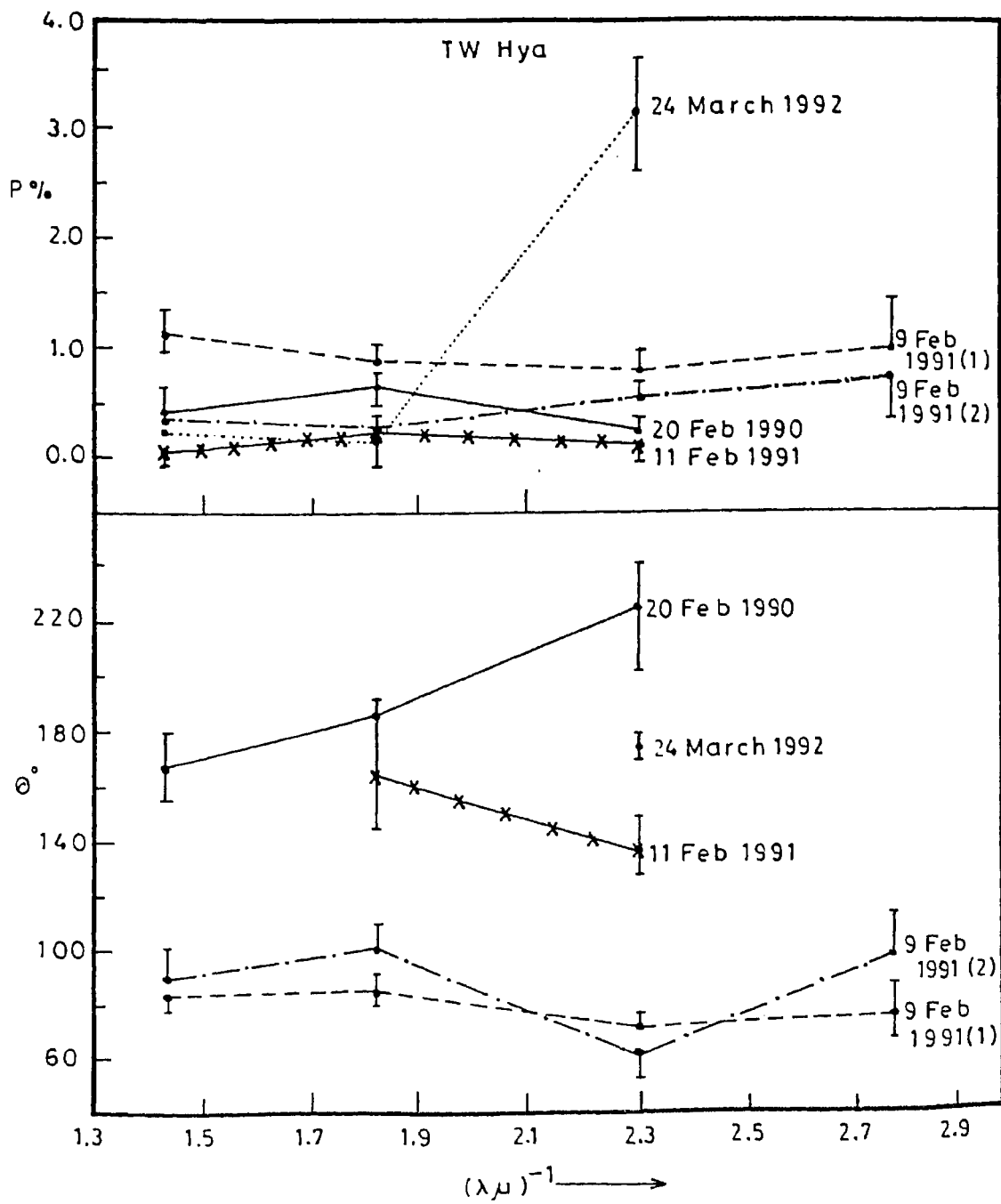


Fig. 7. Plot of linear polarization and position angle of TW Hya against the corresponding inverse of the effective wavelength of the filter band.

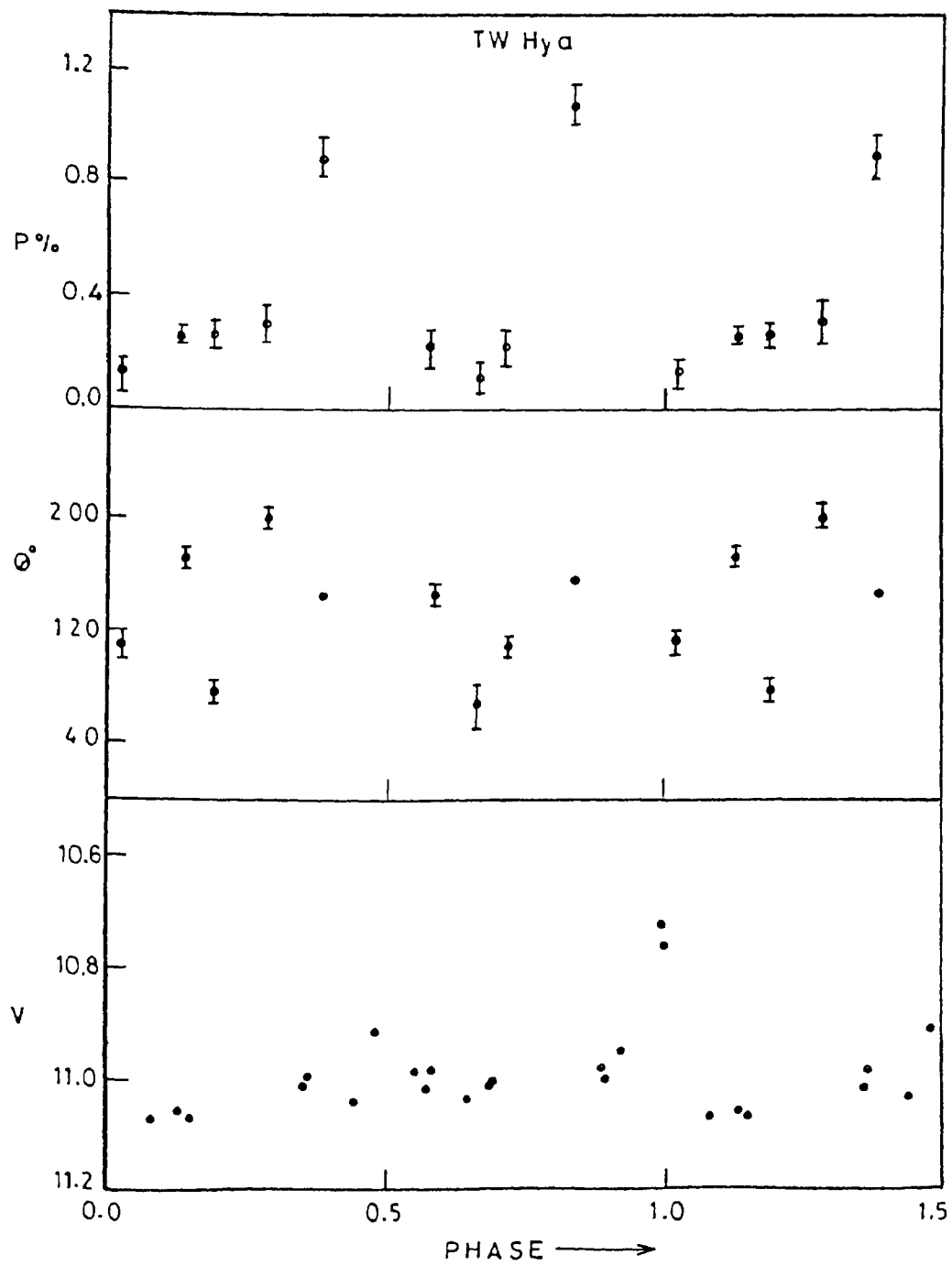


Fig. 8. Plot of linear polarization and position angle in V of TW Hya phased with the period. The lower panel is the overlapping photometry.

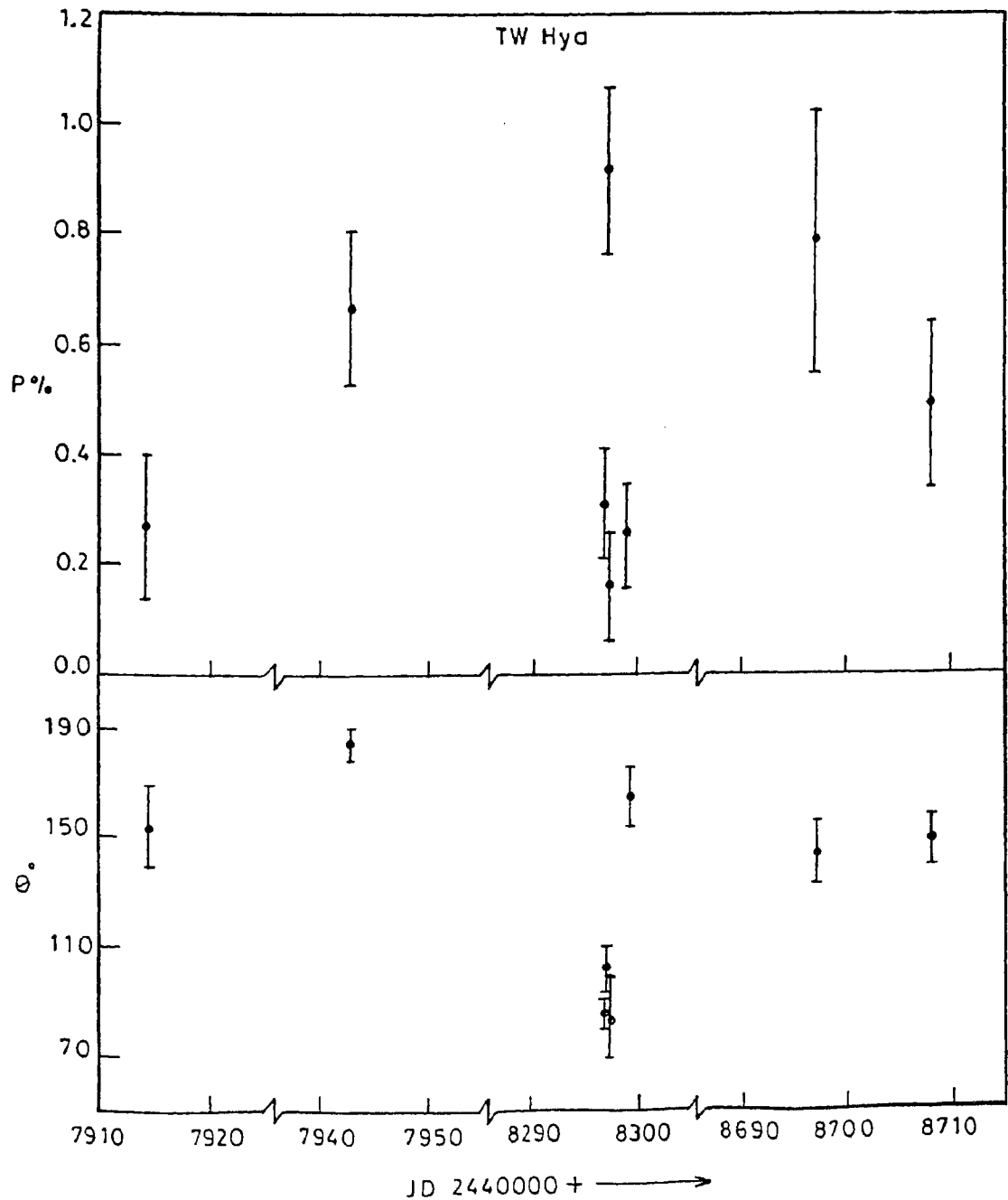


Fig. 9. Plot of the time dependence of linear polarization and position angle in V of TW Hya.

circumstellar dust grains by a hot spot which lasted for two days. Recently, Wood et al. (1996) made an investigation of the photopolarimetric variability of a magnetic accretion disk model for CTTS. Their model predicts a correlation between the brightness and linear polarization. The shape of the low amplitude periodic variation exhibited by TW Hya during March 1993 is similar to that derived by Wood et al. (1996).

7.2. V4046 Sagittarii

7.2.1. Introduction

The light variability of V4046 Sgr (HDE 319139) was discovered by Busko & Torres (1976, 1978) who found the star to show BY Draconis-type light variability with a period of 1.70 days. They also discovered U band flares and $U - B$ colour excess in the star. V4046 Sgr was found to display strong $H\alpha$ emission in its spectrum by Merrill & Burwell (1950), and was subsequently assigned the spectral type dK5e by Bidelman (1954).

The double-lined spectroscopic nature of V4046 Sgr was discovered by Byrne (1985). His photometry gave only a slight indication of periodic light variability with an amplitude of 0.02 mag in V . However the observations indicated a large scatter in $U - B$ colour. The radial velocity measurements obtained by him, though not of high accuracy, gave an orbital period of 2.45 days. He also found that the $H\alpha$ emission strength, which varied between 30 and 100 Å shows a modulation with a period nearly the same as the orbital period. From the overall behaviour of V4046 Sgr he concluded that it belongs to the Post T Tauri group.

de la Reza et al. (1986) carried out photometric, spectroscopic and CORAVEL radial velocity studies of V4046 Sgr. The spectroscopic observations showed that the star has strong $H\beta$ emission in addition to the $H\alpha$ emission already reported by several investigators, and that the strength of $Li I 6708 \text{ \AA}$ absorption line is typical of CTTS. The radial velocity measurements gave an orbital period of 2.4213 days and $V \sin i = 13 \text{ km s}^{-1}$ for the brighter component. Their CORAVEL observations showed that the ratio of cross correlation dips of the two components is nearly 0.5, and hence the secondary is fainter by about 0.7 mag. They classified the secondary to be of spectral type K7. The star was found to have a light variability of 2.25 days with an amplitude of 0.06 mag in V . They further identified V4046 Sgr as an IRAS source (IRAS, 1985) and found that the flux at IRAS bands are similar to those of other CTTS.

Hutchinson et al. (1990) made optical and infrared photometry of V4046

Sgr. Though the data did not indicate any substantial infrared excess, there was a clear evidence of silicate dust grain emission characteristic of a temperature of 200 K. They suggested that the far infrared flux could be due to the emission from dust at 100 K. Recently, Jenson has reported (Mathieu 1994) the detection of 800 and 1100 μ emissions from V4046 Sgr, possibly arising from the circumstellar disk.

The strong and variable $H\alpha$ emission and excess emissions in IR through mm wavelengths indicate the presence of material having a wide range of temperatures and extending over large distances from the component stars. The active accretion disk hypothesis, though developed in the context of single CTTS, is probably applicable to binary systems with components having similar properties (Mathieu 1994). Since the $H\alpha$ emission strength is comparatively easily observed, it is often used as a diagnostic tool to study the active accretion (Hartigan et al. 1991).

Like the CTTS TW Hya (§ 7.1.), V4046 Sgr is also not associated with any star forming regions or dark clouds. Since the the dark nearest cloud to V4046 Sgr is at a projected distance of 1° , de la Reza (1986) suggested that the star might have been formed in a tiny cloud that has since dispersed. However, Herbig (1978) had found, from the proper motion measurements, that the T Tauri star FK Ser had its origin from a cloud 2° away. So a similar explanation for V4046 Sgr cannot be ruled out which can be verified by proper motion measurements.

V4046 Sgr was included in the present study mainly to investigate the nature of variability in light, $H\alpha$ emission, and $Li\ I$ absorption strengths, and linear polarization.

7.2.2. Photometry

V4046 Sgr was observed on a total of 40 nights over four seasons: May 1988 (5 nights), June 1988 (14 nights), August 1989 (10 nights) and July 1990 (11 nights). Out of the four seasons, *UBVRI* observations were done during May 1988 and *by* observations during the remaining seasons. During the observing run of May 1988 several stars of similar spectral types were observed in the field of V4046 Sgr for a few nights and it was found that the

the most suitable comparison star is SAO 209861. So all the observations were done differentially with respect to SAO 209861 and the magnitudes in various bands thus obtained were converted to the corresponding standard systems. The mean *UBVRI* and *by* magnitudes of SAO 209861 are given in Table 7.

Table 7. *UBVRI* and *by* magnitudes of the SAO 209861

<i>U</i>	<i>B</i>	<i>V</i>	<i>R</i>	<i>I</i>	<i>b</i>	<i>y</i>
10.795	9.880	8.778	8.213	7.689	9.472	8.780
±0.010	±0.007	±0.006	±0.005	±0.004	±0.008	±0.006

The *UBVRI* and *by* magnitudes of V4046 Sgr are given in Tables 8 and 9, respectively. The photometric observations were aimed mainly at determining the broadband colours and their variations and an accurate rotational period for the star. The observations of August 1990 were carried out mainly to determine the periodicity of light variation, and hence as many observations as possible were made each night. No averaging was done, and each of the observations was treated as an independent measurement.

7.2.3. Light variations

No systematic investigation of the light variability of V4046 Sgr exists in the literature; the reported periods of light variability range from 1.8 to 2.45 days (Busko & Torres 1976, 1978; Byrne 1985). The data obtained during August 1990 was analyzed using the period finding technique described in § 2.4., resulting in a period of 2.445 days which satisfied the data. Since this period is very close to the orbital period, the active component is rotating nearly synchronously with the orbital motion. Using this period the Julian days of observation given in Tables 2 and 3 were converted to photometric

phases with the following ephemeris:

$$JD(Hel.) = 2447296.805 + 2.^d4457E,$$

where the initial epoch corresponds to the first observation during the season May 1988.

Table 8. *UBVRI* magnitudes of 4046 Sgr

J.D. 2440000.+	<i>U</i>	<i>B</i>	<i>V</i>	<i>R</i>	<i>I</i>
7296.805		11.577	10.430	9.672	9.009
7304.677	12.264	11.604	10.449	9.685	9.010
7304.804	12.262	11.613	10.445	9.687	9.004
7304.887	12.280	11.623	10.455	9.695	9.011
7305.627	12.300	11.570	10.411	9.669	8.991
7305.788			10.406	9.652	8.989
7305.883	12.192	11.542	10.395	9.643	8.979
7307.638	12.354	11.634	10.467	9.697	9.015
7308.600	12.211	11.556	10.460	9.645	8.982
7308.775	12.291	11.553	10.412	9.647	8.987

Table 9. *by* magnitudes of 4046 Sgr

J.D. 2440000.+	<i>b</i>	<i>y</i>
7316.688	11.137	10.410
7316.857	11.159	10.441
7317.688	11.109	10.407
7320.652	11.071	10.358
7320.790	11.077	10.363
7321.617	11.131	10.429

Table 9. continued

J.D. 2440000.+	<i>b</i>	<i>y</i>
7321.747	11.138	10.420
7322.693		10.420
7322.824	11.108	10.397
7323.665		10.402
7324.797	11.120	10.412
7326.741	11.131	10.427
7327.708	11.087	10.381
7327.866	11.077	10.371
7328.833		10.421
7329.677	11.107	10.415
7331.826		10.427
7332.669	11.086	10.391
7332.847	11.084	10.361
7333.730		10.400
7739.599	11.146	10.418
7739.696	11.124	10.412
7739.701	11.128	10.414
7743.527		10.396
7743.532		10.404
7743.641	11.128	10.418
7744.536		10.395
7744.684	11.151	10.439
7747.653	11.171	10.435
7748.510	11.119	10.415
7748.667	11.144	10.417
7749.544	11.132	10.414
7750.567	11.152	10.428

Table 9. continued

J.D. 2440000.+	<i>b</i>	<i>y</i>
7751.521	11.145	10.423
7752.528	11.151	10.468
7752.671	11.143	10.438
7753.529	11.156	10.437
8088.549		10.412
8088.791		10.387
8093.571	11.152	10.419
8093.619	11.119	10.401
8093.650	11.102	10.399
8093.704	11.099	10.396
8093.747	11.118	10.384
8093.784	11.108	10.396
8094.506	11.101	10.407
8094.550	11.124	10.401
8094.597	11.112	10.412
8094.641	11.134	10.429
8094.688	11.143	10.426
8094.714	11.123	10.411
8094.748	11.130	10.435
8094.795	11.138	10.424
8094.835	11.155	10.425
8096.506	11.085	10.376
8096.556	11.085	10.381
8096.650	11.096	10.382
8096.690	11.090	10.394
8096.725	11.093	10.392

Table 9. continued

J.D. 2440000.+	<i>b</i>	<i>y</i>
8096.767	11.106	10.385
8097.503	11.179	10.465
8097.548	11.189	10.480
8097.628	11.189	10.463
8097.695	11.192	10.475
8097.734	11.190	10.465
8097.770	11.201	10.461
8097.804	11.195	10.455
8099.536	11.141	10.433
8099.577	11.134	10.431
8099.615	11.168	10.432
8099.664	11.151	10.434
8099.741	11.149	10.439
8099.784	11.178	10.437
8100.489	11.188	10.472
8100.549	11.197	10.469
8100.610	11.166	10.429
8100.660	11.158	10.443
8100.716	11.155	10.439
8100.760	11.154	10.430
8101.549	11.094	10.391
8101.668	11.103	10.398
8101.731	11.093	10.391
8101.763	11.110	10.391
8101.805	11.113	10.389
8102.507	11.183	10.464

Table 9. continued

J.D. 2440000.+	b	y
8102.554	11.209	10.467
8102.605	11.184	10.460
8102.732	11.205	10.473
8102.790	11.186	10.449
8103.479	11.089	10.389
8104.756	11.182	10.446

The V mag and $U - B$, $B - V$, $V - R$ and $V - I$ colours are plotted in Figure 10 and y mag and $b - y$ colour in Figures 11 and 12; the corresponding mean epochs are indicated in the figures. From Figure 10 it is seen that the amplitude of light variation is very low, of the order of 0.06 mag. The $B - V$, $V - R$ and $V - I$ colours tend to be redder as the star becomes fainter. The $U - B$ colour shows a large scatter, far exceeding the observational error. The quasi-regular variations observed in CTTS are supposed to be caused by bright spots that are caused by accretion from circumstellar disks (Herbst et al. 1994; Kenyon et al. 1994; Safer 1995, etc.). The effect of bright spots would be seen more in the U band. Vrba et al. (1993) have found that CTTS generally show stochastic flaring and the effect of flaring would be again felt to a large extent in U band. In U band the combined effect of frequent flares and short-lived bright spots, sometimes, can completely mask the modulation seen at longer wavelengths. This could be the reason for the large scatter observed in $U - B$ colour. The light curve obtained after one month (June 1988) had a slightly different shape and amplitude. The maximum brightness also increased from 10.40 mag to 10.36 mag. Sudden change in the shape and amplitude of light curve is a common phenomenon in CTTS since the bright spots that cause these changes are highly unstable and at certain epochs completely distort the light curve and thereby display no periodicity. The data obtained during August 1989 showed a large scatter and only a slight indication of rotational modulation. During 1990.58,

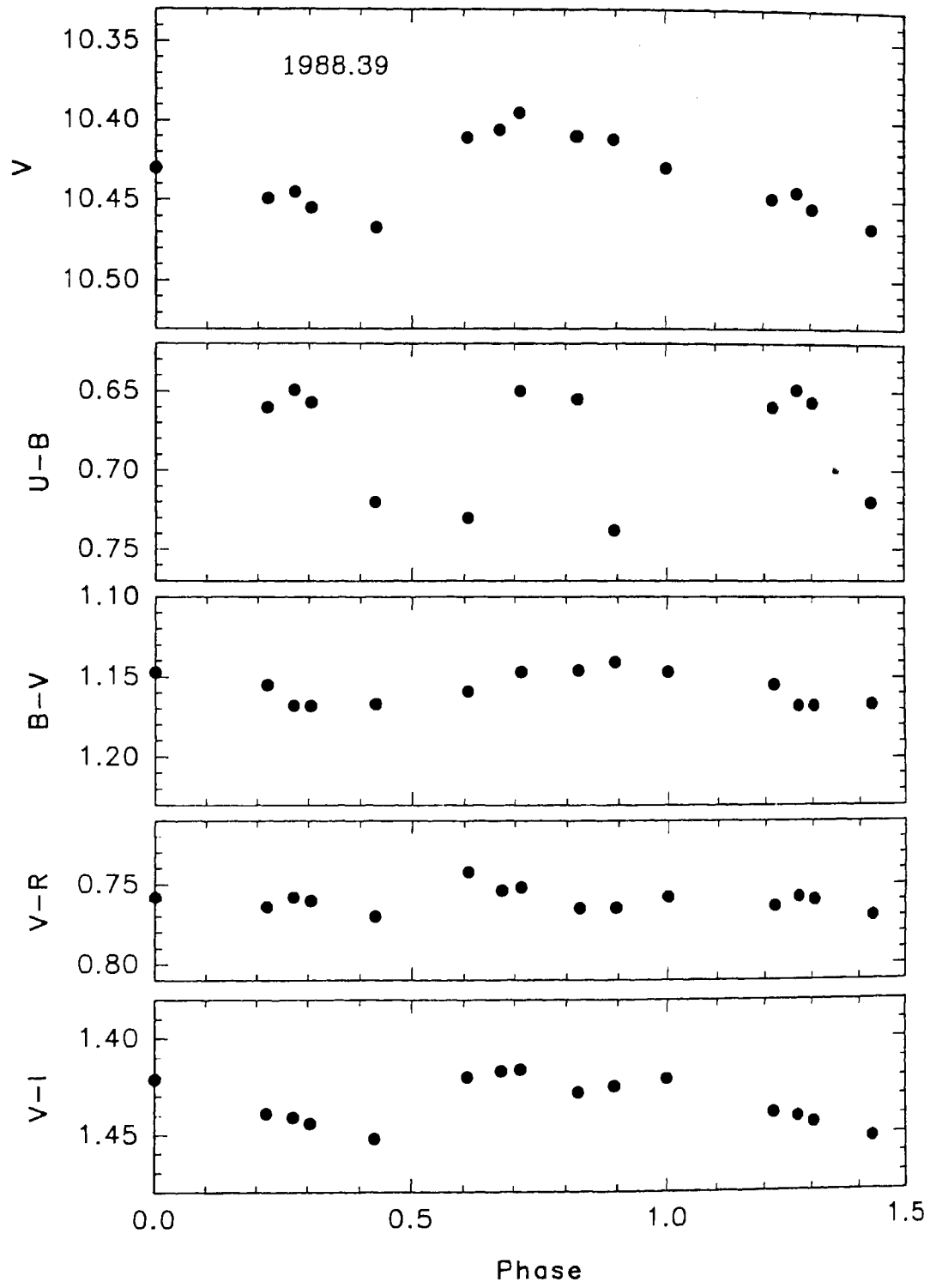


Fig. 10. Plots of V, U-B, B-V, V-R and V-I of 4046Sgr

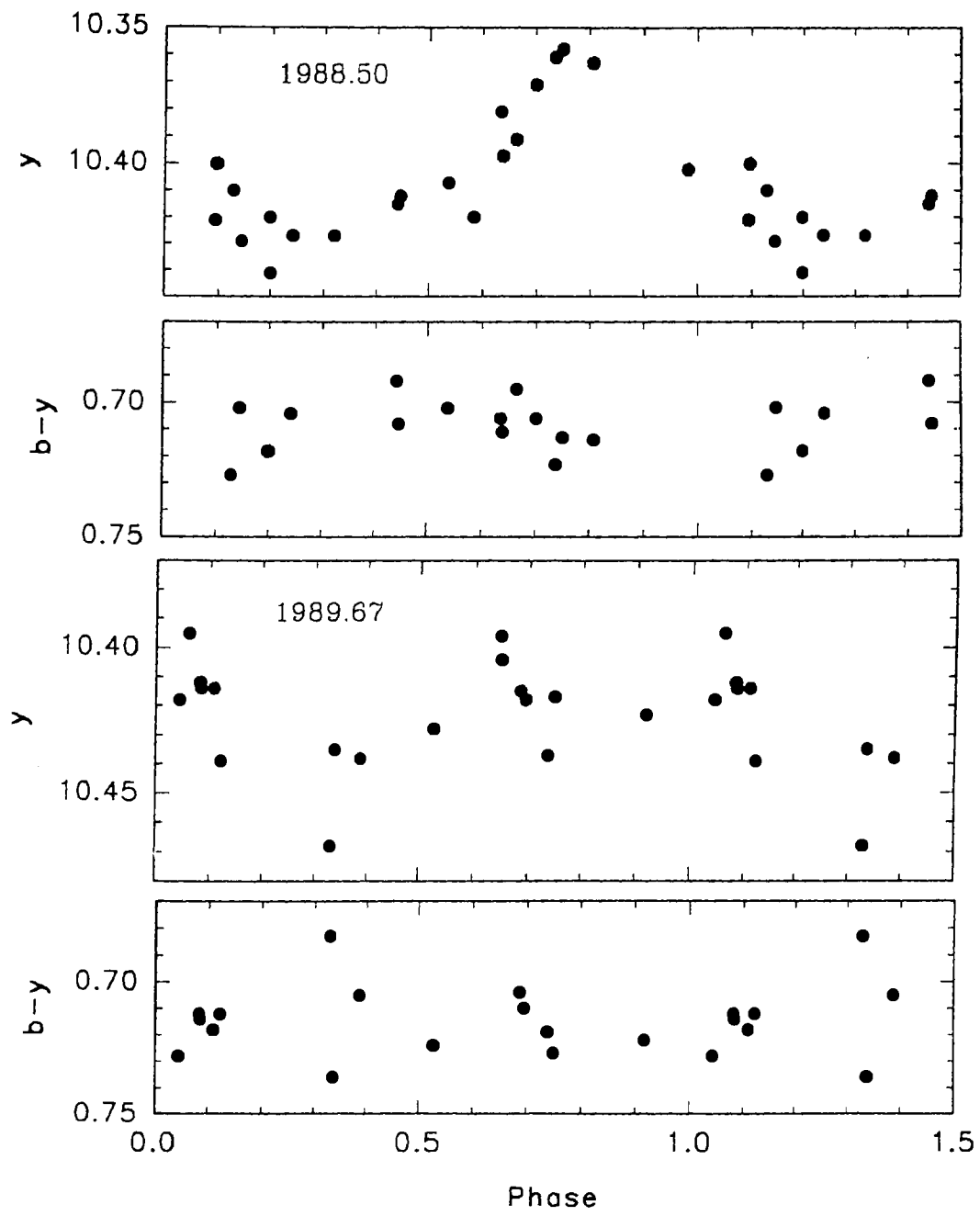


Fig. 11. Plots of y and $b-y$ of 4046Sgr

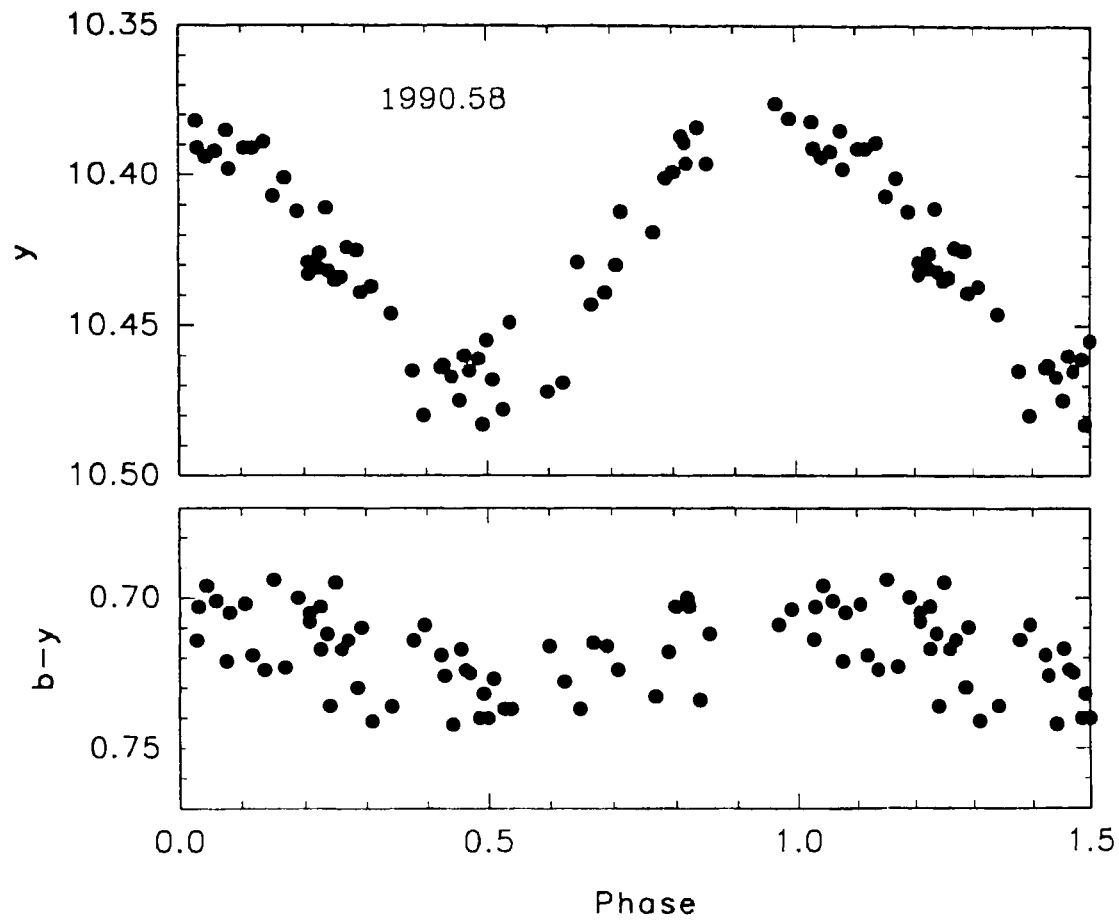


Fig. 12. Plots of y and $b - y$ of 4046Sgr

the light curve showed a quasi-sinusoidal shape with little scatter; the variation in $b - y$ colour was in phase with the light curve. The amplitude of the light curve was around 0.10 mag, which is the largest amplitude observed so far in V4046 Sgr. The minimum scatter indicates that the surface brightness inhomogeneity that caused the light variation remained in the same location with out much change through out the observing run of approximately 4.5 rotation periods duration.

No attempt was made to model the light curves in order to determine the spot parameters. The light curve modeling is complicated by the binary nature of V4046 Sgr. The secondary component is fainter than the primary by 0.7 mag and its spectral type is K7. So the light contribution to the total light variation by the secondary may be negligible. Usually, the CTTS show large amplitude (> 0.2 mag) variations. V4046 Sgr is probably viewed at a low inclination ($i < 40^\circ$) and this could be the reason why only very low amplitude light variations are observed.

7.2.4. $H\alpha$ and $Li I$ lines

$H\alpha$ and $Li I$ 6708 Å spectra of V4046 Sgr were obtained on five nights during March-April 1993 overlapping with the polarimetric observations described

Table 10. Equivalent widths of $H\alpha$ emission and $Li I$ absorption of V4046 Sgr

Julian day 244000.+	Phase	$H\alpha$ (EEW) $\pm 1\text{Å}$	LiI (EW) $\pm 0.04\text{Å}$
9049.493	0.610	38.6	-
9050.496	0.020	64.0	0.530
9080.440	0.264	37.7	0.620
9081.437	0.672	79.7	0.550
9082.467	0.093	39.8	0.470

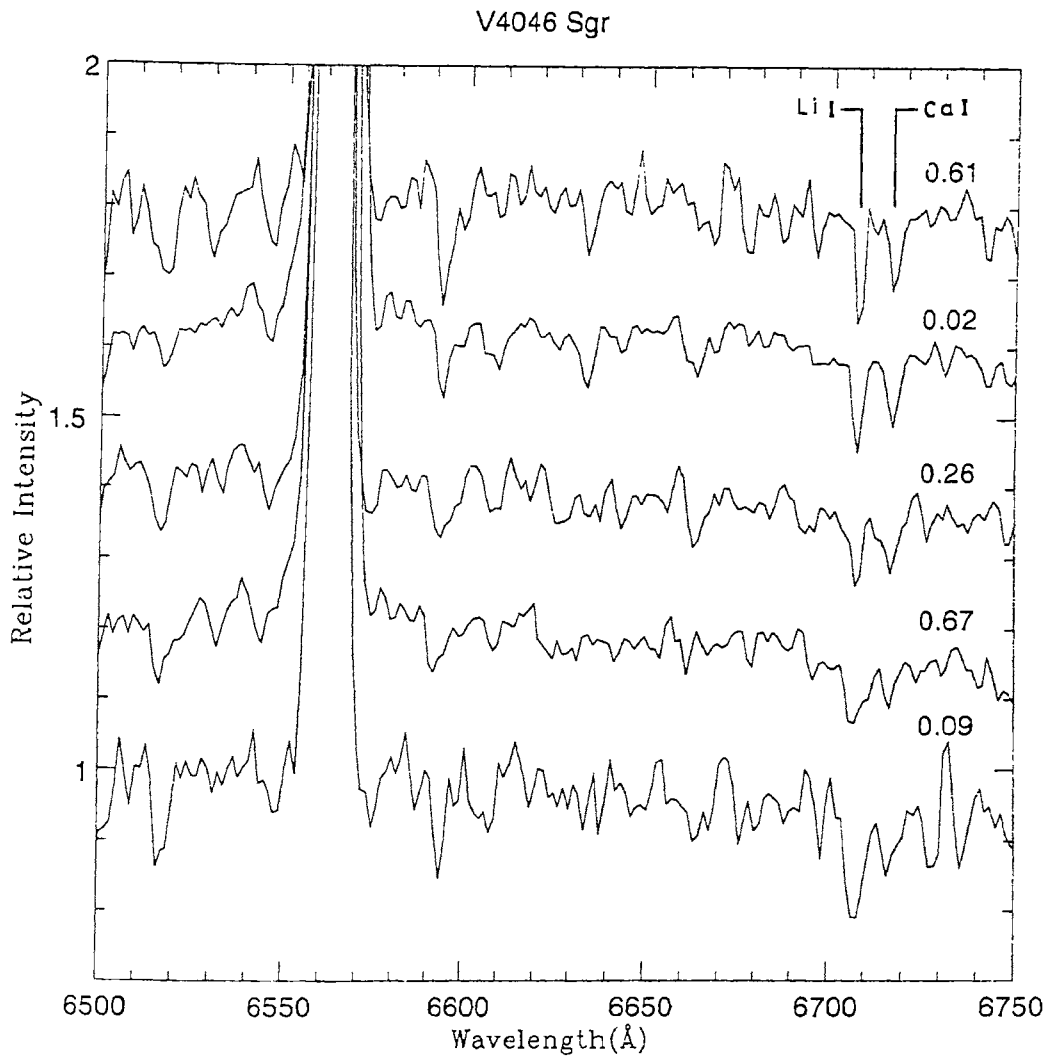


Fig. 13. $H\alpha$ and Li I spectra of V4046 Sgr.

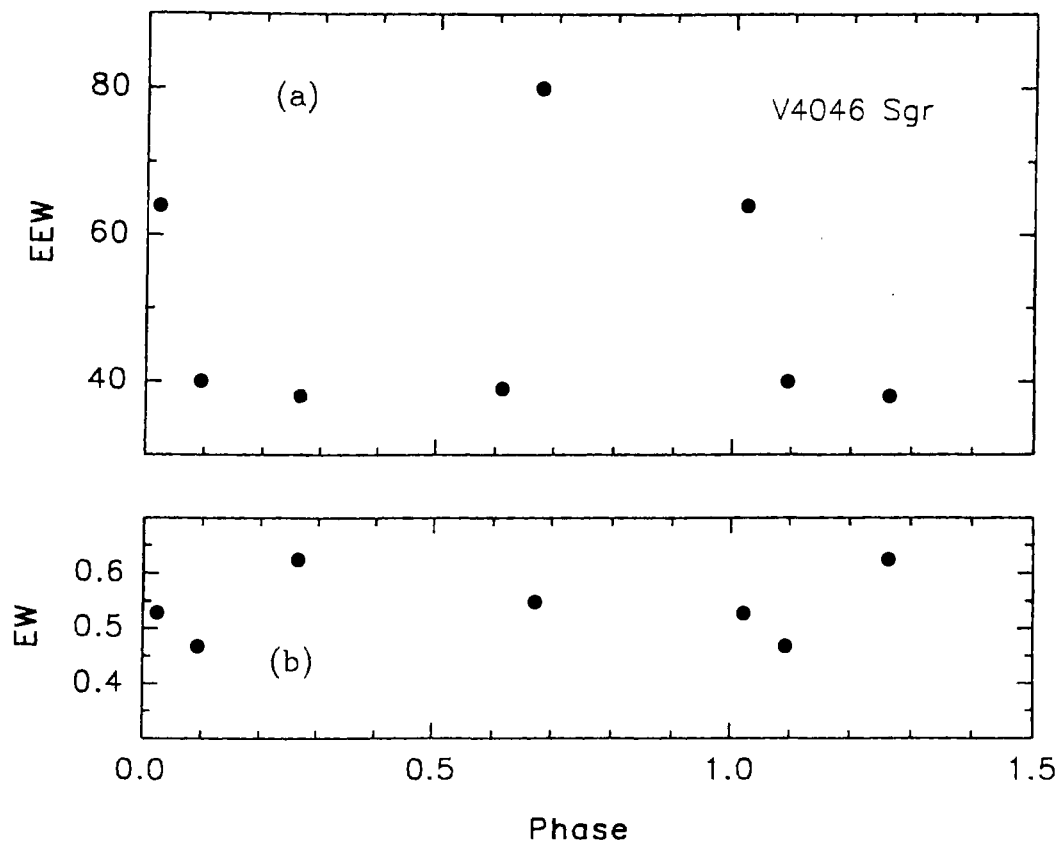


Fig. 14. Plots of (a) H α emission equivalent Width and (b) Li I absorption equivalent width

in the next section. The journal of observations are given in Table 10. Figure 13 displays the spectra; the photometric phases are indicated against each spectrum. Figure 14 shows the plots of $H\alpha$ emission equivalent widths (EEW) and $Li\ I$ absorption EWs against the photometric phase. The $H\alpha$ EEW was found to vary from 39 to 80 Å and showed a trend of periodicity. Byrne (1985) and de la Reza (1986) also reported the periodic variations of $H\alpha$ EEW. Byrne (1985) suggested that the modulation of $H\alpha$ emission is caused either due to the orbital motion, or due to an inhomogeneously distributed $H\alpha$ emitting region. However, from the far infrared and sub mm and mm observations there is convincing evidence that V4046 Sgr has an active accretion disk which could be circumbinary as suggested by Mathieu (1994).

The $H\alpha$ emission is supposed to be formed in the boundary layer, the interface between the relatively slowly rotating star and the inner disk rotating at Keplerian velocities. It is probable that the orbital motion produces the periodicity in $H\alpha$ emission. The nature of the accretion disk and hence also the $H\alpha$ emitting region is quite complex in V4046 Sgr. A conclusive inference can be made only by a high resolution $H\alpha$ study over a few rotation periods. From the mean value of $H\alpha$ EEW and the mean magnitude in R band (9.65 mag), the mean $H\alpha$ flux estimated is around $2.43 \times 10^{-11} \text{ erg cm}^2 \text{ s}^{-1}$. The EW of $Li\ I$ absorption line does not show any appreciable variation with the photometric phase; its value is found to be $0.54 \pm 0.05 \text{ Å}$, similar to that usually found in CTTS.

7.2.5. Linear polarization

V4046 Sgr was observed in BVR bands on 18 May 1991 and 15 March 1992 for the detection of possible variation in linear polarization. Since these observations indicated polarization variation, polarimetry was done on three nights during March 1993 to look for the short time-scale variations. The details of the observations are given in Table 11. Figure 15 shows the plots of $P\%$ and θ° observed during 18 May 1991, 15 March 1992 and 13 March 1993 against the corresponding inverse of the effective wavelength of observation. From Figure 15 it is seen that V4046 Sgr shows large variations in $P\%$ and θ° .

During 15 March 1992 and 13 March 1993 P% was quite large and showed a steeper wavelength dependence when compared to that on 18 May 1991. The range in P% is the highest in *B* band. The values of θ° observed during 18 May 1991 and 15 March 1992 are almost the same while those observed on 13 March 1993 show a change of about 90° .

Table 11. *BVR* polarimetry of V4046 Sgr

Date	Julian day 244000.0+	Band	P%	θ°
18 May 91	8395.333	<i>B</i>	0.34 ± 0.17	176 ± 15
		<i>V</i>	0.10 ± 0.10	
		<i>R</i>	0.12 ± 0.15	
14 Mar 92	8696.497	<i>V</i>	0.50 ± 0.09	154 ± 5
15 Mar 92	8697.490	<i>B</i>	1.41 ± 0.24	156 ± 5
		<i>V</i>	0.46 ± 0.10	159 ± 6
		<i>R</i>	0.36 ± 0.13	161 ± 10
13 Mar 93	9060.481	<i>B</i>	1.74 ± 0.30	57 ± 7
		<i>V</i>	0.47 ± 0.07	58 ± 5
		<i>R</i>	0.19 ± 0.12	89 ± 18
14 Mar 93	9061.483	<i>V</i>	0.92 ± 0.21	77 ± 3
17 Mar 93	9064.492	<i>V</i>	0.44 ± 0.07	135 ± 3

Figure 16 is a plot of P% in *V* band and the corresponding θ° against the Julian day of observation. The figure shows the highly variable nature of the P% and θ° in V4046 Sgr. Sudden variations in P% and θ° were also observed within a few days. Hence from this behaviour we can conclude that the geometry of the circumstellar material as well as the illuminating source changes in V4046 Sgr. The observations at several wavelengths indicate that V4046 Sgr has active accretion disk and so hot spots formed by accretion on to the stellar surface might cause variable illumination of the circumstellar material and also the observed highly variable P%. Menard & Bastien (1992)

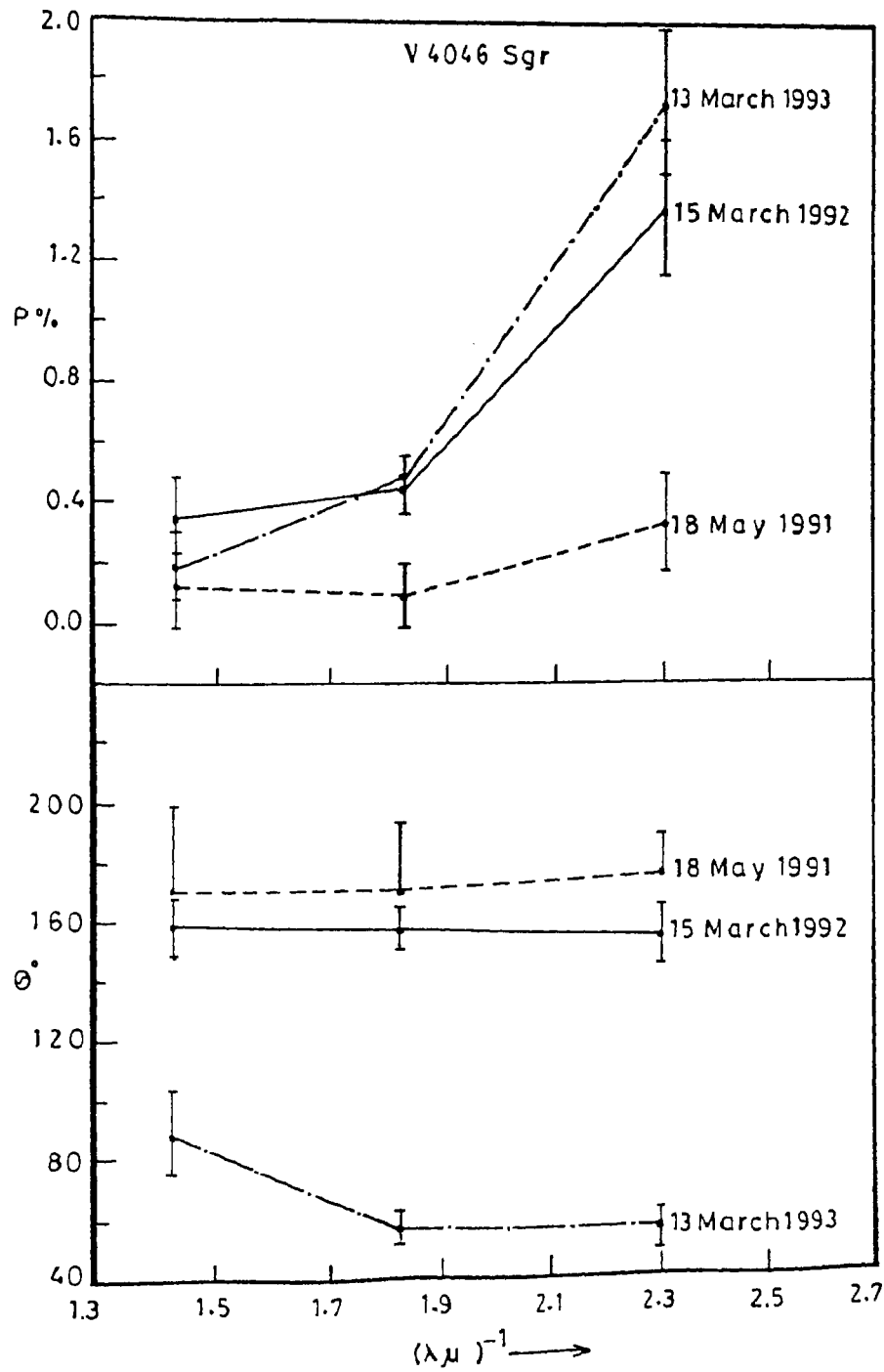


Fig. 15. Plot of linear polarization and position angle of V4046 Sgr against the corresponding inverse of the effective wavelength of the filter band.

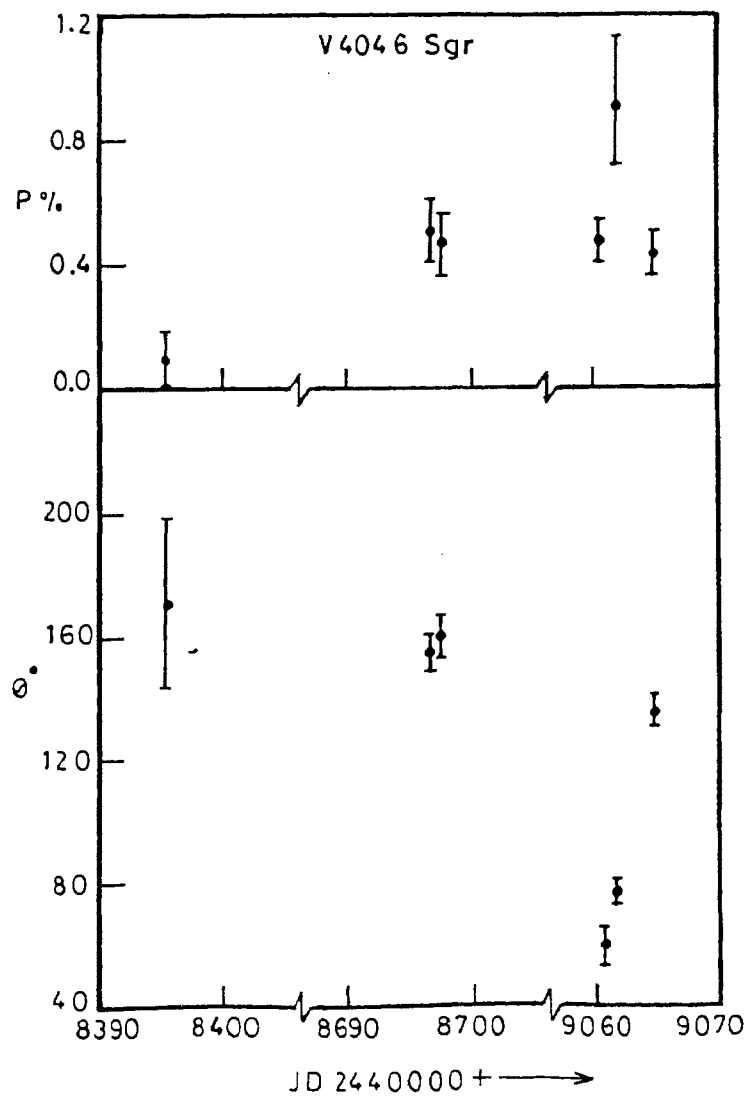


Fig. 16. Plot of the time dependence of linear polarization and position angle in V of V4046 Sgr.

found that 85% of the known T Tauri stars are polarization variables. They suggested that the variable polarization seen in CTTS could be due to the inhomogeneities in the accreting disk. However, continuous polarimetric observations over a few rotation periods of V4046 Sgr are essential to interpret the circumstellar environment.

7.3. Summary

The observations and analysis of the CTT stars TW Hya and V4046 Sgr have gives important information regarding the activity in these stars. The analysis of the photometric observations of TW Hya and V4046 Sgr obtained over several seasons shows periodic light variations enabling us to derive their rotation periods. In addition to the periodic light variation, TW Hya also exhibits sudden brightenings that last for one or two days These phenomena are attributed to hot spots which are highly unstable and are caused by accretion flow on to the star from the circumstellar disc. In CTT stars the strong $H\alpha$ emissions are supposed to be originating from the boundary layer between the accretion disc and the star. TW Hya has exceptionally strong $H\alpha$ emission and does not show any periodicity. The polarization study also points to the presence of bright photospheric spots.

The interpretation of the light variation observed in V4046 Sgr is rather complicated due to its binary nature. Though the $H\alpha$ emission strength is comparable to other CTT stars the star has comparatively less near and far infra-red excesses. We could say that V4046 Sgr is a peculiar CTT star in the sense that it shows more regular, small amplitude light variations like the WTT stars, but with strong $H\alpha$ emission. The light variations could be due to cool spots since the light curves show less scatter and no sudden brightening has been noticed as in the case of TW Hya. The $H\alpha$ emission may be arising from the circumbinary environment and so we observe some sort of a of periodicity. However, it is too early to speculate the nature of spots in this star. Extensive, simultaneous multi-band photometric and high resolution spectroscopic studies are essential to arrive at definite conclusions on the nature of activity in V4046 Sgr.

8

CONCLUSIONS

8.1. Results of the present work

8.1.1. Photometric study

We have carried out extensive photometry of two RS CVn systems (HD 81410 and HD 127535), two young active-chromosphere stars (HD 139084 and HD 155555), two CTT stars (TW Hya and V4046 Sgr) and one WTT star FK Ser. Photometry of another WTT star V410 Tau was also done during one observing season.

Analysis of the light curves of HD 81410 obtained during 20 seasons which includes 13 seasons of the present study gave very interesting results. The light curves of HD 81410 showed two prominent spot groups, well separated in longitudes, quite often, indicated by the presence of two minima. The largest amplitude observed was 0.45 mag and the smallest 0.05 mag. The total range of brightness observed is around 0.70 mag which is similar to other active RS CVn systems like II Peg and DM UMa. Another important finding from the photometric study is that there exists two preferred longitudes at $0.^{\circ}40$ and $0.^{\circ}90$ about which the spots are generally formed. Spot modeling could be done for 8 light curves and it is found that the maximum temperature difference between spots and the photosphere was around 1500

K in HD 81410. Spots are formed at higher as well as lower latitudes. It is found from the spot modeling that when the light curve shows a shallow minimum then the spot temperature is comparatively higher (around 4500 K) and during such a situation spots are more widely spread and so the spot modeling gives only the weighted mean of the longitudes and latitudes of spots. We have re-analyzed the radial velocity measurements of HD 81410 and refined its spectroscopic orbital parameters. The refined orbital period is 12.90522 days.

HD 127535 is another active RS CVn system that has been investigated. The photometric derived period from our observations is almost the same as its orbital period of 6.015 days. The light curves showed double-minima only during one season indicating that in HD 127535 only one predominant spot group is present most of the time. From a plot of V_{max} and V_{min} against the epochs of observation it is found that the V_{max} and V_{min} were the brightest during the epochs 1981.33 and 1990.58 and the faintest during the epoch 1984.62. From the behaviour of V_{max} and V_{min} it appears that the star has an activity cycle of about 10 years. From a plot of ϕ_{min} against the corresponding mean epochs of observation, it was found that ϕ_{min} showed a migration towards the decreasing orbital phase. The photometric period derived from the migration of light minima is found to be smaller than the orbital period and hence the starspots that produce the rotational modulation are located at latitudes which rotate slightly faster than the synchronous latitude.

We have done a period analysis of the photometric data on HD 139084 and derived a period of 4.294 days for the light variation which gives good fit to all available observations. The analysis of the light curves has shown that the observed amplitude of light variation is not as large as seen in RS CVn systems. Usually the amplitudes are around 0.10 mag. One of the reasons for the low amplitude of light variability is the low value of i (around 40°). HD 139084 probably has a large longitudinal spread of spot groups and so we observe only low amplitude light variation since the amplitude reflects only the contrast in distribution of spots in both hemispheres. The plot of V_{max} and V_{min} against the mean epoch suggests that HD 139084 has an activity

cycle of around 10 years.

An investigation of the photometric light variability of HD 155555 has shown that none of the light curves have double minima. Also the amplitudes of light variation are small compared to that observed in RS CVn systems. The smaller observed amplitudes is most probably due to a large longitudinal spread of spots. The $U - B$ colour observed during different seasons showed a rather complex behaviour; it changes from a near-out-of phase to a phase lag and sometimes no modulation with respect to the V light variation. We interpret this behaviour as due to the presence of short-lived photospheric plages. We have also investigated the possibility that both components are variable, but the analysis showed that the variability is mainly due to the brighter component and if at all the fainter component is variable it is not at an appreciable scale. We have assigned a spectral type G5 for the brighter component and K5 for the fainter component based on the observed colours.

The photometric observations of TW Hya were subjected to period analysis and we derived a photometric period of 2.196 days. The observed amplitude in V varies from 0.20 to 0.40 mag. The maximum range of amplitude was observed in U band. The U band measurements showed a large scatter compared to the observational error. The dependence of amplitude with wavelength showed that the modulation of the light was caused by hot spots. We have modeled the light curve of epoch 1987.3 and found that a hot spot with $T_s = 8150$ K with a fractional coverage of 0.007 could cause the observed light variation. The shape and the amplitude of the light curve showed rapid changes even within a few rotation periods. This is due to the highly unstable nature of the hot spot. We have re-analyzed all the available photometry of TW Hya in the literature using the derived period and found that, apart from periodic variations, the star also shows sudden brightenings that last for one or two days. We interpret this sudden brightening as due to short lived hot spots. The reason why other investigators have not been able to detect periodicity is probably due to the sudden brightening in TW Hya which occur randomly. A period analysis in such a case would naturally give negative result.

Analysis of the light variations of V4046 Sgr observed August 1990 gave

a period of 2.445 days. The amplitude of light variation was quite low, of the order of 0.06 mag. Only during one season the amplitude was 0.10 mag. The light curves obtained during the four seasons did not indicate any sudden brightening as noticed in TW Hya. The light variations were very low in the sense that the maximum observed amplitude was only around 0.10 mag. Our spectroscopic and polarimetric observations show that the star has strong $H\alpha$ and variable polarization. The low amplitude light variations in V4046 Sgr could be explained as follows. V4046 Sgr has a low value of inclination, around 40° (de la Reza 1986). If the accretion of matter is magnetically channeled then the impact zone where the hot spot is formed would be at higher latitudes (Kenyon et al. 1994). Any hot spot at higher latitudes would be either visible through out the rotation if it is formed near the polar region facing the observer or would not be visible at all if it is formed near the other polar region. In this scenario, the light variability is observed if there is a tilt in the magnetic axis relative to the rotational axis. However, the interpretation of the light curve is also complicated by the fact that V4046 Sgr is a binary and both components being T Tauri stars the effect of the activity of both components would be manifested in the overall behaviour of the light curve.

We have carried out photometric observations of FK Ser over 5 seasons and the analysis of the data showed that there exists a 5.055 day periodicity in the light variations. The amplitude of light variation varied between 0.06 and 0.23 mag in V . The shape and the amplitude of the light curves indicate the presence of cool spots. Also a confirmative evidence for the presence of cool spots is obtained from our near-simultaneous photometric and $H\alpha$ emission study. However, during one season (May 1988), the light curve showed a peculiar nature. The U band light variation showed an anti-correlation with the V light curve and also the amplitude observed in U band was the maximum. This behaviour of FK Ser is almost similar to that observed in another relatively weak CTT star DN Tau (Vrba et al. 1986). They interpreted this phenomenon as due to the presence of a hot spot almost co-spatial with a cool spot. However, from the weak $H\alpha$ emission and also the slightly evolved stage of FK Ser compared to CTTS, it is unlikely that the star has

hot spots due to accretion. An alternative interpretation of the light curve is the occurrence of hot plages co-spatially with the cool spot. If the plages are co-spatial then we would observe this phenomenon.

V410 Tau is the other WTTS in our observational programme. Extensive photometry of this star is available in the literature and so we have not done a long-term photometry. The observations by Vrba et al. (1988) and Petrov et al. (1994) have shown that V410 Tau has large scale spot activity and the cool spots have life-times of the order of years and hence the shape and amplitude of light curves remain unchanged for months together. We have done photometry of V410 Tau during March 1993 along with near-simultaneous observations in $H\alpha$ and polarimetry. Our photometric observations showed the same trend as that obtained during September 1992 by Petrov et al. (1994); but the minimum light level has decreased by around 0.05mag. The observed amplitude was 0.060 mag.

Table 1 gives the photometric properties of the programme stars obtained by us. A comparative study of the photometric results of these stars that are at different stages of stellar evolution provide important clues regarding the nature of activity. Most of the late type stars show enhanced solar type magnetic dynamo activity at different scales. The large scale activity exhibited by RS CVn systems, young active-chromosphere stars and WTT stars are due to the enhanced solar type activity. They all show clear evidences of cool spots that cover an appreciable area of the stellar surface. The RS CVn systems and young active-chromosphere stars show double minima usually in their light curves indicating the presence of two predominant spot groups. Long term activity cycles of the order of 10 years have been detected in HD 127535 and HD 139084. The range of amplitude between the maximum and minimum brightness observed in RS CVn systems is larger compared to that of young active-chromosphere stars. This could be due to the large longitudinal spread of spot groups in young active stars. The light curves of CTTS could be explained on the basis of the presence of hot spots. WTT stars behave in a similar way as the RS CVn systems in their light variability. A major difference between the light curves of these two groups is that the cool spots in WTTS have life-times far more than that of

its counterpart in RS CVns.

Table 1. Photometric parameters

Type	Star	Period (d)	Maximum amplitude (V)	Maximum range (V)
RS CV _n	HD 81410	12.905 _a	0.44	0.70
RS CV _n	HD 127535	6.015	0.23	0.35
YACS*	HD 139084	4.294 _a	0.16	0.19
YACS*	HD 155555	1.682	0.14	0.29
CTTS	TW Hya	2.196 _a	0.40	0.70
CTTS	V4046 Sgr	2.446 _a	0.10	0.12
WTTS	FK Ser	5.055 _a	0.21	0.25
WTTS	V410 Tau	1.872	0.60	

* Young Active-Chromosphere Stars

a. Present study

8.1.2. Spot modeling

The existing spot models derive spot parameters by trial and error until the desired accuracy of the fit is achieved. The model developed by us employs the method of least squares using differential correction to the parameters to arrive at the best fit values for the different parameters, including the temperature, assuming that the light variation is caused by a limited number of large, circular spots. The advantage of the present model is that all spot parameters are optimized simultaneously. This method allows the simultaneous determination of the spot temperature when observations are available in multi-wavelength bands.

We have also investigated synthetic light curves which provide information on the influence of various parameters like, latitude, area and spot temperature and hence the effect of these parameters on the general characteristics of a light curve that would in turn help in interpreting the observed

light curve.

We have applied our spot model to HD 81410 for which a large data base is available. The results indicate the presence of high as well as low latitude spots. The derived spot temperatures range from 3500 to 4600 K. We have also derived the spot parameters of TW Hya for one season.

8.1.3. Spectroscopic observations

Spectroscopic observations of TW Hya, V4046 Sgr, FK Ser and V410 Tau were obtained in the region of $H\alpha$ and $Li I$ lines at a resolution of 1.38 Å per pixel during March 1993 along with quasi simultaneous photometric and polarimetric observations.

The $H\alpha$ emission equivalent width (EEW) in TW Hya showed variations from 140 to 250 Å. The emission strength do not show any correlation with the photometric light variability indicating that different mechanisms are responsible for the photometric variation and $H\alpha$ emission. The large scale variations in $H\alpha$ shows that the boundary layer, where the emission is supposed to be formed in CTTS, has also random luminosity variations that are not related to rotation period. The $Li I$ EW also did not show any appreciable change. The mean of the observed values is 0.60 Å. However, on one occasion the $H\alpha$ EEW and $Li I$ EW were found to be the lowest, 140 Å and 0.34 Å, respectively, and also there was moderate emission at $He I$ 6678 line too. The $H\alpha$ EEW and $Li I$ EW obtained during that night were similar to the values obtained by Rucinski & Krautter (1983) during their 1982 observations. The low value of $Li I$ EW was not due to the larger veiling of photospheric spectrum since $H\alpha$ EEW was at the minimum value observed. The $He I$ 6678 Å line is an indicator of strong chromospheric activity. This shows that the strong emission in TW Hya have chromospheric contribution also.

The $H\alpha$ EEW in V4046 Sgr is found to vary from 39 to 80 Å which is less than the strength and variation observed by Byrne (1995). The fact that V4046 Sgr is a binary and both components are T Tauri stars and hence active complicates the interpretation. As suggested by Mathieu (1994) the system may have circumstellar and or circumbinary discs. But surprisingly

the $H\alpha$ EEW showed periodic trend as reported by Byrne (1985) and de la Reza (1986). It seems that the emissions are originating in the circumbinary environment and hence we observe the periodic variation. However, a periodic variation might also be possible if only one of the components is very active and the $H\alpha$ emission is originating from it. But an $H\alpha$ EEW of around 100\AA cannot be explained as of chromospheric origin. The $Li\ I$ did not show any appreciable change and the mean of the observed value is 0.50\AA .

FK Ser is a visual binary with moderate emissions. The $H\alpha$ EEW showed variations between 4.4 and 8.0\AA . From our near-simultaneous photometry it is found that the $H\alpha$ EEW shows anti-correlation with respect to light variation in the sense that the EEW was maximum at the photometric minimum. The near-simultaneous photometry had an amplitude of only 0.06 mag, the lowest observed in FK Ser. So we would naturally expect larger variation in $H\alpha$ EEW when the light curve amplitude is larger. This phenomenon, usually observed in WTTS, strongly indicates the presence of magnetically active cool spots and the corresponding $H\alpha$ emissions found in the stellar chromosphere. Though Herbig (1973) have shown that both components have strong $H\alpha$, the nature of light and $H\alpha$ EEW variations clearly indicate the variability of one component with the observed period. But, we cannot rule out the possible variability of the other component with an entirely different period. Since both components are well separated they may have different rotational periods. The $Li\ I$ EW observed in FK Ser is 0.55\AA which is the mean of our observations. The strength is similar to that reported by Herbig (1973).

V410 Tau is an extensively observed WTT star. Our spectroscopic observations showed that $H\alpha$ line had variation from shallow absorption to moderate emission. The near simultaneous photometry showed that the maximum $H\alpha$ strength was observed when the star was at its light minimum. This behaviour clearly shows the existence of cool spots on V410 Tau. The strong anticorrelation between $H\alpha$ EEW and light variability is due to the occurrence of $H\alpha$ emitting regions co-spatially in the chromosphere with respect to the photospheric cool spots. The $H\alpha$ EEW is found to vary within

a period of one month indicating that the restructuring of $H\alpha$ emitting regions happen faster than the life-times of the cool spots in V410 Tau. The $Li I$ did not show any correlation with respect to the light variation.

Table 2 gives the results of spectroscopic observations of CTT and WTT stars. The CTT stars TW Hya and V4046 Sgr have very strong and variable $H\alpha$ emission. While TW Hya does not show any periodic changes in its $H\alpha$ EEW, V4046 Sgr has a periodic trend. On the other hand, the $H\alpha$ emissions in WTT stars FK Ser and V410 Tau have moderate strengths and both objects show periodic variations which are in anticorrelation with respect to the photospheric light in such a way that the emission strength were maximum when the photospheric cool spots were visible.

Table 2. $H\alpha$ and $Li I$ line strengths

Type	Star	$H\alpha$ EEW range (Å)	$H\alpha$ flux $\times 10^{-11} \text{ erg cm}^{-2} \text{ s}^{-1}$	$Li I$ EW Å
CTTS	TW Hya	190 - 250	4.14	0.60
CTTS	V4046 Sgr	39 - 80	2.43	0.54
WTTS	FK Ser	4.4 - 8.0	0.22	0.55
WTTS	V410 Tau	0.16 _a - 2.37	0.05	0.56

^a absorption

8.1.4. Polarimetric Study

We have carried out polarimetric study of TW Hya, V4046 Sgr, FK Ser and V410 Tau. The polarimetric observations of TW Hya were aimed at studying the long as well as the short term variability. P% showed a range of 0.2% to 1.0% in V band while θ° remained almost the same except during a few occasions when θ° showed a shift of 90° . The sudden change in θ° usually occurs due to the change in the geometry of the scattering medium. A large value of P% (around 3%) was observed in B band on one night. From the

polarimetric observations of March 1993 it was found that P% was most of the time less than 0.2%. The overlapping photometry has shown that as the star becomes fainter the P% also shows a tendency to be smaller. A variation of the order of 60° was also noticed in θ° . Sudden increase in P% (around 1%) was noticed on two consecutive nights. From our long-term photometric observations it is seen that TW Hya shows sudden brightening caused by short lived spots. Hence the sudden increase in polarization might be due to a short lived hot spot. Recently Wood et al. (1996) proposed a model for the polarization variability in CTT stars where they assumed two hot spots on the stellar surface produced by the magnetically channeled accretion flow from the disk. The low amplitude variations in P% observed in TW Hya during March 1993 has a similar shape that predicted by Wood et al. (1996).

Table 3. Polarimetric properties

Type	Star	P % range (<i>V</i>)	θ° Range (<i>V</i>)	Type of variability
CTTS	TW Hya	0.16 - 0.92	86 - 187	Periodic
CTTS	V4046 Sgr	0.10 - 0.92	58 - 171	Irregular
WTTS	FK Ser	0.74 - 1.25	58 - 103	Irregular
WTTS	V410 Tau	0.20 - 0.48	124 - 184	Periodic

Polarization observations of V4046 Sgr has shown that there exists a strong dependence of P% on wavelength. Also P% and θ show variations from epoch to epoch. P% shows long time variation from 0.1% to 1.0%. Unfortunately we could not carry out simultaneous photometry during our polarimetric observations and hence we are unable to examine the type of variability.

The polarimetry of FK Ser has shown that the star has slightly larger P% compared to the other T Tauri stars. The P% showed variability between 0.75% and 1.25% in *V*. The variable nature of P% could be due to

several reasons like non-uniform distribution of circumstellar material and/or variable illumination of the circumstellar material. The photometric and $H\alpha$ observations of FK Ser indicate the presence of cool spots. If the observed variation in P% is caused by the cool spots then we would observe a periodic behaviour in P% as observed in V410 Tau. The fact that the polarization measurements of March 1993 did not show any periodic trend suggests that the origin of variability is most probably the non-uniform distribution of circumstellar material.

The polarimetric observations of V410 Tau gave very important results regarding the origin of variable polarization in this star. It is now an established fact that the photometric and spectroscopic variabilities in V410 Tau are due to the presence of long lived cool spots. From the quasi-simultaneous photometric and polarimetric observations it is found that the P% variability also shows the same periodicity as the light variation with P% tending to be larger at the light minimum. The variation in θ also has the same periodicity. The periodic variability of P% that is in anti-correlation with respect to the photometric light variation clearly shows that the mechanism that causes the variable P% is the nonuniform illumination of the circumstellar material by the cool spot. Probably this is the first time that quasi-simultaneous photometry and polarimetry of V410 Tau were carried out.

Table 3 gives the polarization properties of TW Hya, V4046 Sgr, FK Ser and V410 Tau. All four stars show variable polarization and TW Hya and V410 Tau exhibit periodic polarization variability due to different types of mechanism. In V410 Tau we have convincing evidence for the variable polarization mechanism as cool spots where as in TW Hya the trend of variability in P% points to hot spots. FK Ser has a larger mean value of P% and also its $K - L$ colour is larger than the other stars. Probably the non uniformity of the circumstellar material causes the variability in FK Ser as well as in V4046 Sgr. Our observations points to the importance of carrying out simultaneous observations for arriving at definite conclusions.

8.2. Future prospects

The present study of a group of late type stars that are at different stages

of stellar evolution has shown that the RS CVn systems, young active-chromosphere stars, and WTT stars display various forms of activity caused by dynamo processes and the most important manifestation of magnetic activity is the formation of dark spots on the stellar surface. In CTT stars the predominant factor that causes activity is the interaction between the star and the accretion disk. Though the study, which is based on photometric observations to a large extent, gives a general picture of the nature of activity, more detailed observations simultaneously in multiwavelengths are necessary to probe the causes of activity in detail.

Photometry of RS CVn systems and young-active chromosphere stars should be continued so that we would be able to determine the period of activity cycles and also obtain more information regarding the differential rotation in these objects. We have found that in young active-chromosphere stars the spots have large longitudinal extension and so the amplitudes of light variation are small. In the case of HD 155555 there is evidence for the presence of active plages. So simultaneous photometry and high resolution $H\alpha$ spectroscopy would give definite clues about the spots and the associated plages.

The photometric and polarimetric observations of several CTTS and WTTS, with known periods, have to be done to examine whether they exhibit the periodic variations similar to that we have observed which in turn would enable us to study the nature of cool spots in WTTS and the circumstellar environment in CTTS.

High resolution spectroscopy in $H\alpha$ and in $O I$ 6300 Å forbidden lines would provide indirect evidence for the presence of accretion disk and the study of profile variations would greatly help to investigate the connection between winds and accretion disks in CTTs.

Most of the variations observed are probably caused by the brighter component in FK Ser; it is necessary to determine the exact contribution by the fainter component. So it is highly desirable to carry out a spectroscopic study of the individual components, preferably in $H\alpha$, over at least a few rotation periods along with photometric observations. The separation being

1.3 arc sec, this work could be done only at excellent sites.

It is worth investigating the tidal effects of the companion on the accretion disk in V4046 Sgr as postulated recently by Terquem & Bertout (1996). In this model the disk gets twisted due to the tidal effects of the companion and hence accordingly the part of the disk visible to the observer also gets affected. V4046 Sgr and TW Hya show comparatively less $K - L$ excess than the other CTT stars indicating that the warm dust contribution is less. On the other hand, if the model by Terquem & Bertout (1996) is correct, then due to the tidal distortion of the disk the warm dust region of the accretion disk may not be visible to the observer at all. On the basis of the same argument probably TW Hya also has a companion that could distort the disk. So a search for the companion of TW Hya is highly desirable.

References

- Anders, G.J., et al. 1991, MNRAS **252**, 408
- Appenzellar, I., Mundt, R. 1989, A&A Review **1**, 291
- Balona, L.A. 1987, S. Afr. Astr. Obs. Circ. **11**, 1
- Basri, G., Batalha, C. 1990, ApJ **363**, 654
- Basri, G., Martin, E.L., Bertout, C. 1991, A&A **252**, 625
- Basri, G., Bertout, C. 1993, in *Protostars and Planets, III* (eds: E.H. Levy & M.S. Matthews) Univ. Arizona, p. 543
- Bastien, P. 1982, A&AS **48**, 153
- Bastien, P. 1982, A&AS **48**, 513
- Bastien, P. 1985, ApJS **59**, 277
- Beekwith, S.V.W., et al. 1989, ApJ **343**, 393
- Beiging, J. H., Cohen, M. 1989, AJ **98**, 1686
- Bennett, N.W.W., Evans, D.S., Laing, F.D. 1962, R. Obs. Bull. No. 61
- Bertout, C. 1989, ARA&A **27**, 351
- Bessel, M.S. 1979, PASP **91**, 589
- Bidelman, W.P. 1954, ApJS **1**, 175
- Bidelman, W.P., MacConnell, D.J. 1973, AJ **78**, 687
- Bookbinder, J.A. 1988 in *Activity in Cool Star Envelopes* (eds: O.H. Havens, B.R. Petterson, J.H.M.M. Schmitt & J.E. Solheim) Kluwer, p. 257
- Bopp, B.W., et al. 1970, MNRAS **147**, 355
- Bopp, B.W. 1983, in *IAU Coll. 71 Activity in Red-Dwarf Stars* (eds: P.B. Byrne & M. Rodono) Reidel, p. 363
- Bopp, B.W., Hearnshaw, J.B. 1983, ApJ **267**, 653
- Bopp, B.W., Africano, J., Quigley, R. 1986, AJ **92**, 1409

- Bopp, B.W., et al. 1989, ApJ **339**, 1059
- Bopp, B.W. 1990, Mem. S. A. It. **61**, 723
- Bouvier, J., Bertout, C. 1989, A&A **211**, 99
- Bouvier, J., et al. 1993, A&A **272**, 176
- Budding, E. 1977, Ap & SS **48**, 20
- Budding, E., Zeilik, M. 1990 in *Active Close Binaries* (ed: C. Ibanoglu) Kluwer, p. 831
- Busko, I.C., Torres, C.A.O. 1976, IBVS No. 1186
- Busko, I.C., Torres, C.A.O. 1978, A&A **64**, 153
- Buzasi, D.L., Ramsey, L.W., Huenemoerder, D.P. 1987, ApJ **322**, 353
- Byrne, P.B. 1985, Irish Astron. J. **17**, 3
- Chini, R. 1989, in *Proc. ESO Workshop on Low Mass Star formation and Pre-main Sequence Objects* (ed: B. Reipurth) ESO, p. 173
- Chugainov, P.F. 1974, Izv. Krymsk. Astrofiz. Obs **52**, 3
- Claret, A., Gimenez, A. 1990, A&A **230**, 412
- Cohen, M. 1974, MNRAS **169**, 257
- Cohen, M., Kuhl, L.V. 1979, ApJS **41**, 709
- Collier, A.C. 1982a, Ph. D. Thesis
- Collier, A.C. 1982b, South. Stars **30**, 177
- Collier, A.C. 1987, South Afr. Astron. Obs. Circ. **11**, 57
- Cousins, A.W.J., Stoy, R.H. 1963, R.OBs. Bull. No. 64
- Cox, R.E., Sinnott, R.W. 1977, Sky and Telescope **54**, 60
- Crampton, D., Dobias, J., Margon, B. 1979, ApJ **234**, 993
- Cutispoto, G. 1990, A&AS **84**, 397
- Cutispoto, G. 1993, A&AS **102**, 655
- Danks, A.C. 1982, ESO Users Manual
- de la Reza, R., et al. 1986, in *New Insights in Astrophysics* ESA Sp-263, p 107
- Darius, J. 1978, IBVS No.1429
- Dempsey, C.R., et al. 1993, ApJ **413**, 333
- Deshpande, M.R., et al. 1985, Bull. Astron. Soc. India **13**, 157
- Dorren, J.D., Guinan, E.F. 1982, ApJ **252**, 296
- Dorren, J.D. 1987, ApJ **320**, 756

- Drissen, L., Bastien, P., St. Louis, N. 1989, AJ **97**, 814
- Eaton, J.A., Hall, D.S. 1979, ApJ **227**, 907
- Eggen, O.J. 1973, PASP **85**, 42
- Eggen, O.J. 1978, IBVS No. 1426
- Eggen, O.J. 1995, AJ **110**, 1749
- Eker, Z. 1994, ApJ **420**, 373
- Fekel, E.C., Moffett, T.J., Henry, G.W. 1986, ApJS **60**, 551
- Fernie, J.D. 1983, PASP **92**, 782
- Florentin Nielson, R. 1983, Report Inst. Theor. Astrophys. Oslo **59**, 141
- Franchini, M., et al. 1992, A&A **256**, 525
- Frecker, J.E., Serkowski, K. 1976, Appl. Optics **15**, 605
- Friedman, G., Gurtler, J. 1975, Astr. Nachr. **296**, 125
- Ghez, A.M., Neugebauer, G., Matthews, K. 1993, AJ **106**, 2005
- Giampapa, M.S. 1984, ApJ **277**, 235
- Gray, R.O, Olsen, E.H. 1991, A&AS **87**, 54
- Hackwell, J.A., Bopp, B.W., Gehrz, R.D. 1974, ApJ **192**, L79
- Hall, D.S. 1972, PASP **84**, 323
- Hall, D.S. 1976 in *IAU Coll. No.29: Multiple Periodic Variable Stars* (ed. : W. S. Fitch) Reidel, p. 287
- Hardie, R.H., 1962, in *Astronomical Techniques* (ed: W.A. Hiltner) The Univ. Chicago Press, London, p. 178
- Hartigan et al. 1991, ApJ **382**, 617
- Hatzes, A.P. 1993, ApJ **410**, 777
- Hatzes, A.P. 1995, ApJ **451**, 784
- Heinze, K.G. 1976, ApJS **30**, 491
- Herbig, G.H. 1962, Adv. Astr. Astrophysics **1**, 47
- Herbig, G.H., Rao, N.K. 1972, ApJ **174**, 401
- Herbig, G.H. 1973, ApJ **182**, 129
- Herbig, G.H. 1978, in *Problems of Physics and Evolution of the Universe* (Yeravan Ac. of Sciences of the Armenian SSR) p. 171
- Herbig, G.H., Goodrich, R.W. 1986, ApJ **309**, 294
- Herbig, G.H., Bell, K.R. 1988, Lick Obs. Bull. No. 1111
- Herbst, W., Koret, D.L. 1988, AJ **96**, 1949

- Herbst, W. 1989, AJ **98**, 2268
- Herbst, W., et al. 1994, AJ **108**, 1906
- Hidayat, B. 1971, IBVS No. 559
- Hiltner, W.A. 1962, in *Astronomical Techniques* (ed: W.A. Hiltner) The Univ. Chicago Press, London, p. 229
- Hoffmeister, C. 1943, Kleinere Veroff. Berlin-Babelsberg No. 27
- Houk, N., Cowley, A. 1975, Michigan Catalogue of two dimensional Spectral types for the HD Stars Vol. 1
- Houk, N., Smith-Moore, M. 1988, Michigan Catalogue of two dimensional Spectral types for the HD Stars Vol. 4
- Hutchinson, M.G., et al. 1990, A&A **234**, 230
- Innis, J.L., et al. 1985, Proc. Astron. Soc. Australia **6**, 160
- Innis, J.L., Thompson, K., Coates, D. 1986, MNRAS **223**, 183
- IRAS, 1985, IRAS Point Source Catalogue, eds. C.Beichman et al. JPL
- Johnson, H.L. 1966, ARA&A **4**, 196
- Johns, M.C., Basri, G. 1995, AJ **109**, 2800
- Jones, D.H.P., Fischer, J.L. 1984, A&AS **56**, 449
- Joy, A.H. 1945, ApJ **102**, 168
- Joy, A.H. 1949, ApJ **110**, 424
- Jetsu, L. 1996, A&A (Submitted)
- Kenyön, S.J. et al. 1994, AJ **107**, 2153
- Kimble, R.A., Kahn, S.M., Bowyer, S. 1981, ApJ **251**, 585
- Kopal, Z. 1959, in *Close Binary Systems*, Chapman & Hall, London, p. 450
- Kron, G.E. 1947, PASP **59**, 261
- Kron, G.E. 1952, ApJ **115**, 301
- Linsky, J.L. 1980, ARA&A **18**, 439
- Linsky, J.L. 1988, in *Multi-wavelength Astrophysics* (ed: F.A. Cordova) Cambridge University Press, p. 49
- Lloyd Evans, T., Koen, M.C.J. 1987, S. Afr. Astron. Obs. Cir. **11**, 21
- Lucy, L.B., Sweeny, M.A. 1971, AJ **76**, 544
- MacConnell, D.J. 1971, IBVS No. bf570.
- Manfroid, J., Sterken, C. 1987, A&AS **71**, 539
- Manfroid, J., et al. 1991, ESO Scientific Report No. 8

- Marstad, N., et al. 1982, in *Advances in Ultraviolet Astronomy: Four Years of IUE Research*, NASA Conf. Pub. No. 2238, p. 554
- Martin, E.L., Brandner, W. 1995, *A&A* 294, 744
- Mathieu, D.R. 1994, *ARA&A* 32,
- Mekkaden, M.V., Raveendran, A.V., Mohin, S.M. 1982, *J. Astr. Ap.* 3, 27
- Mekkaden, M.V., Geyer, E.H. 1988, *A&A* 195, 214
- Mekkaden, M.V. 1990, *Bull. Ast. Soc. India* 18, 351
- Menard, F. 1986, M.Sc. Thesis, Uni. of Montreal
- Menard, F., Bastien, P. 1992, *AJ* 103, 564
- Merril, P.W., Burwell, C.G. 1950, *ApJ* 112, 72
- Mohin, S., Raveendran, A.V. 1992, *A&A* 256, 487
- Mohin, S., Raveendran, A.V. 1993, *A&A* 277, 155
- Mohin, S., Raveendran, A.V. 1994, *A&A* 286, 824
- Morgan, J.E., Eggleton, P.P. 1979, *MNRAS* 187, 661
- Mutel, R.L., et al. 1987, *AJ* 93, 1220
- Neff, E.J., O'Neal, D., Saar, S.H. 1995, *ApJ* 452, 879
- Nolthenius, R. 1991, *IBVS* No. 3589
- Olsen, E.H. 1983, *A&AS* 54, 55
- Pallavicini, R., Randich, S., Giampapa, M. 1992, *A&A* 253, 185
- Pallavicini, et al. 1993, *A&A* 267, 145
- Pancharatnam, S. 1955, *Proc. Indian Acad. Sci.*, A41, 137
- Pasquini, L., et al. 1991, *A&A* 248, 72
- Patten, M.B., Simon, T. 1992, in *Seventh Cambridge Workshop on Cool Stars, Stellar Systems and the Sun* p. 58
- Patterer R. J., et al. 1993, *AJ* 105, 1519
- Perry, C.L., Olsen, E.H., Crawford, D.L. 1987, *PASP* 99, 1184
- Petrov, P.P., et al. 1994, *A&AS* 107, 9
- Poe, C.H., Eaton, J.A. 1985, *ApJ* 289, 644
- Pounds, K.A., et al. 1993, *MNRAS* 260, 77
- Radick, R.R., et al. 1982, *PASP* 94, 934
- Radick, R.R., et al. 1983, *PASP* 95, 621
- Randich, S., Gratton, R., Pallavicini, R. 1993, *A&A* 273, 194

- Ramsey, L.W. 1987, in *Fifth Cambridge Workshop on Cool Stars, Stellar Systems and the Sun* p. 195
- Raveendran, A.V., Mekkadon, M.V., Mohin, S. 1982, MNRAS **199**, 707
- Robinson, R.D., Kraft, R.P. 1974, AJ **79**, 698
- Rodono, M., et al. 1986, A&A **165**, 135
- Rodono, M., et al. 1987, A&A **176**, 267
- Rucinski, S.M., Krautter, J. 1983, A&A **121**, 217
- Rucinski, S.M. 1985, AJ **90**, 2321
- Rucinski, S.M. 1988, IBVS No. 3139
- Rucinski, S.M. 1992, PASP **104**, 311
- Rydgren, A.E., Vrba, F.K. 1983, ApJ **267**, 191
- Rydgren, A.E. et al. 1984, Pub. US Naval Obs. Ser. 2, 25
- Safier, P.N. 1995, ApJ **408**, 115
- Scaltriti, F., Busso, M. 1984, A&A **135**, 23
- Serkowski, K. 1974, in *Planets, Stars, and Nebulae Studied with Photopolarimetry* (ed: T. Gehrels) The University of Arizona Press, p. 135
- Serkowski, K., Mathewson, D.S., Ford, V.L. 1975, ApJ **196**, 261
- Shulte-Ladbeck, R.E. 1983, A&A **120**, 203
- Simon, T., Sonneborn, G. 1987, AJ **94**, 1657
- Simon, T., Vrba, F.J., Herbst, W. 1991, AJ **100**, 1957
- Slee, O.B., et al. 1987, MNRAS **229**, 659
- Spangler, S.R., Owen, F.N., Hulse, R.A. 1976, AJ **82**, 169
- Stacy, J.G., Stencel, R.E., Weiler, E.J. 1980, AJ **85**, 858
- Stauffer, J., et al. 1987, PASP **99**, 471
- Sterken, C., Manfroid, J. 1992, *Astronomical Photometry a Guide*, Kluwer Ac. Publ. Dordrecht
- Sterken, C., et al. 1993, ESO Scientific Report No. 12
- Sterne, T. 1941, Proc. Nat. Acad. Sci. **27**, 175
- Stienon, F.M. 1971, IBVS No. 545
- Stine, P.C., et al. 1988, AJ **96**, 1394
- Stoy, R.H. 1963, Mon. Not. Ast. Soc. S. Africa **22**, 157
- Strassmeier, K.G., et al. 1988, A&AS **72**, 291
- Strassmeier, K.G. 1988, AP&SS **140**, 223

- Strassmeier, K.G., Bopp, B.W. 1992, A&A **259**, 183
- Strassmeier, K.G., Olah, K. 1992, A&A **259**, 595
- Strom, K.M., Strom, S.E. 1994, ApJ **424**, 237
- Terquem, C., Bertout, C. 1996, MNRAS **279**, 415
- Torres, C.A.O., Ferraz Mello, S. 1973, A&A **27**, 231
- Treanor, P.J. 1962, in *Astronomical Techniques* (ed: W.A. Hiltner) The Univ. Chicago Press, London, p. 247
- Udalski, A., Geyer, E.H. 1984, IBVS No. 2593
- Udalski, A., Geyer, E.H. 1984, IBVS No. 2594
- Udalski, A., Geyer, E.H. 1985, IBVS No. 2692
- Valenti, J.A., Basri, G., Johns, C.M. 1993, AJ **106**, 2024
- van Leeuwen, F., Alphenaar, P. 1982, ESO Messenger **28**, 15
- Vaughan, A.E., Large, M.I. 1987, Proc. Astron. Soc. Australia **7**, 42
- Vogt, N., Geisse, H.S., Rojas, S. 1981, A&AS **46**, 7
- Vogt, S.S. 1981, ApJ **247**, 975
- Vogt, S.S., Penrod, G.D. 1983, PASP **95**, 565
- Vogt, S.S., Penrod, G.D., Hatzes, A.P. 1987, ApJ **321**, 496
- Vogt, S.S. 1988, in *IAU Sym. 132*, p. 253
- Vrba, F.J. et al. 1986, ApJ **306**, 199
- Vrba, F.J., Herbst, W., Booth, J.F. 1988, AJ **96**, 1032
- Vrba, F.J. et al. 1993, AJ **106**, 1608
- Walter, F.M., et al. 1980, ApJ **236**, 212
- Walter, F.M. 1987, PASP **99**, 31
- Walter, F.M., et al. 1988, AJ **96**, 297
- Weiler, E.J., Owen, F.N., Bopp, B.W. 1978, ApJ **225**, 919
- Weiler, E.J., Stencel, R.E. 1979, AJ **84**, 1372
- Weintraub, A.D., et al. 1989, ApJ **340**, L69
- Welty, A.D., Ramsey, L.W. 1995, AJ **110**, 336
- Wood, K., et al. 1996, ApJ **458**, L79
- Zappala, R.R. 1974, ApJ **187**, 257
- Zeilik, M., et al. 1988, ApJ **332**, 293
- Zeilik, M., et al. 1990, ApJ **354**, 352